U.S. Department of Transportation
Federal Aviation Administration

FINAL PROJECT REPORT

Form Approved:
O.M.B. No. 2120-0559
9/30/2013

PART I - PROJECT IDENTIFICATION INFORMATION

1. Institution and Address	2. FAA Program	3. FAA Award Number
University of Dayton Research Institute		13-C-AJFE-UD-4, 9, 10, 13, 17, 18, 24
Dayton, OH	4. Award Period From 2/20/2015 To 2/04/2023	5. Cumulative Award Amount $2,006,322.00

6. Project Title
National Jet Fuels Combustion Program – Area #7: Overall Program Integration and Analysis

PART II - SUMMARY OF COMPLETED PROJECT (For Public Use)

This project involved coordination between dozens of researchers and stakeholders from several different countries relating to the influence of jet fuel variation on sprays and combustion operability including ignition and lean blowout, and the models required to anticipate combustor performance. The models included chemical kinetic models of the combustion phenomenon, various models of spray involving different levels empirical input or model sophistication, and several sub-models employed within computational fluid dynamics simulations. A clear deliverable of the National Jet Fuels Combustion Program was to package the models developed under the program into applications that could be used by combustor design teams working at each of the major jet engine manufacturers, who were each represented on the team. Overall, the NJFCP resulted in hundreds of publications within archival sources, including six with authorship contribution from the principal of this project. The crowning document marking the achievement of this project was the book cited here.

Colket, M., & Heyne, J. (2021). Fuel effects on operability of aircraft gas turbine combustors. American Institute of Aeronautics and Astronautics. https://doi.org/10.2514/4.106040

PART III - TECHNICAL INFORMATION (For Program Management Uses)

1. **ITEM** (Check appropriate blocks)	NONE	ATTACHED	PREVIOUSLY FURNISHED	TO BE FURNISHED SEPARATELY TO PROGRAM	
				Check (X)	Approx. Date
a. Abstracts of Theses			✘		
b. Publication Citations		✘			
c. Data on Scientific Collaborators		✘			
d. Information on Inventions	✘				
e. Technical Description of Project and Results		✘			
f. Other (specify)					

2. Principal Investigator/Project Director Name (Typed)	3. Principal Investigator / Project Director Signature	4. Date
Joshua S Heyne		Aug 2023

FAA Form 9550-5 (03-03) Supersedes Previous Edition

INSTRUCTIONS FOR FINAL PROJECT REPORT

One copy of this report is due within 90 days after the expiration of the award. It should be submitted to the cognizant technical monitor in the FAA award letter.

INSTRUCTIONS FOR PART I

These identifying data items should be the same as on the award documents.

INSTRUCTIONS FOR PART II

The summary (about 200 words) must be self-contained and intelligible to a scientifically literate reader. Without restating the project title, it should begin with a topic sentence stating the project's major thesis. The summary should include, if pertinent to the project being described, the following items:

- The primary objectives and scope of the project. The techniques or approaches used
- (only to the degree necessary for comprehension). The findings and implications
- stated as concisely and informatively as possible.

FAA may disseminate the project report through the National Technical Information Service (NTIS) of the Department of Commerce. Authors should also be aware that the summary may be used to answer inquiries by nonscientists as to the nature and significance of the supported activity. Scientific jargon and abbreviations should be avoided.

INSTRUCTIONS FOR PART III

Items in Part III may, but need not, be submitted with this Final Project Report. Place a check mark in the appropriate block next to each item to indicate the status of your submission.

a. Self-explanatory.

b. For publications (published and planned) include title, journal or other reference, date, and authors. Provide two copies of any reprints as they become available.

c. Scientific Collaborators provide a list of co-investigators, research assistants and others associated with the project. Include title or status, e.g. associate professor, graduate student, etc.

d. Briefly describe any inventions which resulted from the project and the status of pending patent applications, if any.

e. Provide a technical summary of the activities and results. The information supplied in proposals for further support, updated as necessary, may be used to fulfill this requirement.

f. Include any additional material, either specifically required in the award instrument (e.g. special technical reports or products such as films, books, studies) or which are considered to be useful to the Foundation.

PAPERWORK REDUCTION ACT

ASCENT Project 34

Project Information

Project Name	National Jet Fuels Combustion Program – Area #7: Overall Program Integration and Analysis
RH Display ID	10275
Funding Agreement	13-C-AJFE-UD, Amendments 4, 9, 10, 13, 17, 18, 24
Project Status	Completed
Period of Performance	2/20/2015 – 2/4/23
Funding Amount	$2,006,322.00
Managing Organization	Federal Aviation Administration
Program	Center of Excellence ASCENT
Performing Organization	University of Dayton Research Institute
Principal Investigator	Joshua S. Heyne, 0000-0002-1782-9056
Project URL	https://ascent.aero/project/overall-program-integration-and-analysis-area-7-2/
Abstract	This project involved coordination between dozens of researchers and stakeholders from several different countries relating to the influence of jet fuel variation on sprays and combustion operability including ignition and lean blowout, and the models required to anticipate combustor performance. The models included chemical kinetic models of the combustion phenomenon, various models of spray involving different levels empirical input or model sophistication, and several sub-models employed within computational fluid dynamics simulations. A clear deliverable of the National Jet Fuels Combustion Program was to package the models developed under the program into applications that could be used by combustor design teams working at each of the major jet engine manufacturers, who were each represented on the team. Overall, the NJFCP resulted in hundreds of publications within archival sources, including six with authorship contribution from the principal of this project. The crowning document marking the achievement of this project was the book cited here: Colket, M., & Heyne, J. (2021). Fuel effects on operability of aircraft gas turbine combustors. American Institute of Aeronautics and Astronautics. https://doi.org/10.2514/4.106040

Publication Information

Peer-reviewed journal publications

Boehm, R.C., Colborn, J. G., & Heyne, J. S. (2021). Comparing alternative jet fuel dependencies between combustors of different size and mixing approaches. Frontiers in Energy Research, 9, 701901. https://doi.org/10.3389/FENRG.2021.701901.

Colborn JG, Heyne JS, Stouffer SD, Hendershott TH, Corporan E. (2021) Chemical and physical effects on lean blowout in a swirl-stabilized single-cup combustor. Proc Combust Inst 38(4), 6309-6316. https://doi.org/10.1016/j.proci.2020.06.119

Colket, Meredith B., Joshua S. Heyne, Mark Rumizen, James T. Edwards, Mohan Gupta, William M. Roquemore, Jeffrey P. Moder, Julian M. Tishkoff, and Chiping Li. (2016). An Overview of the National Jet Fuels Combustion Program. AIAA Journal 55(4), 1087-1104. https://doi.org/10.2514/1.J055361

Heyne, J., Rauch, B., Le Clercq, P., & Colket, M. (2021). Sustainable aviation fuel prescreening tools and procedures. Fuel, *290*, 120004. https://doi.org/10.1016/j.fuel.2020.120004

Kramer, S., Andac, G., Heyne, J.; Ellsworth, J., Herzog, P., & Lewis, K. C. (2022) Perspectives on Fully Synthesized Sustainable Aviation Fuels: Direction and Opportunities. Frontiers in Energy Research, 9, 782823. https://doi.org/10.3389/fenrg.2021.782823

Peiffer, E.E., Heyne, J.S., & Colket, M. (2019). Sustainable aviation fuels approval streamlining: auxiliary power unit lean blowout testing. AIAA Journal, 57(11), 4854-4862. https://doi.org/10.2514/1.J058348

Ruan, H., Qin, Y., Heyne, J., Gieleciak, R., Feng, M., & Yang, B. (2019). Chemical compositions and properties of lignin-based jet fuel range hydrocarbons. Fuel 256, 115947, https://doi.org/10.1016/j.fuel.2019.115947

Yang, Zhibin, Robert Stachler, and Joshua S. Heyne. (2020). Orthogonal reference surrogate fuels for operability testing. Energies 13(8): 1948 https://doi.org/10.3390/en13081948

Published conference proceedings:

Bell DC, Heyne JS, Won S, Dryer FL. (2018). The Impact of Preferential Vaporization on Lean Blowout in a Referee Combustor at Figure of Merit Conditions. ASME. ASME Power Conference, *Volume 1: Fuels, Combustion, and Material Handling; Combustion Turbines Combined Cycles; Boilers and Heat Recovery Steam Generators; Virtual Plant and Cyber-Physical Systems; Plant Development and Construction; Renewable Energy Systems* ():V001T01A011. doi:10.1115/POWER2018-7432.

Colket, Meredith B., Joshua S. Heyne, Mark Rumizen, James T. Edwards, Mohan Gupta, William M. Roquemore, Jeffrey P. Moder, Julian M. Tishkoff, and Chiping Li. (2016). An Overview of the National Jet Fuels Combustion Program. In AIAA SciTech. AIAA SciTech. San Diego, CA: American Institute of Aeronautics and Astronautics. doi:doi:10.2514/6.2016-0177.

Heyne, J.S., Colket, M.B., Gupta, M., Jardines, A., Moder, J.P., Edwards, J.T., Roquemore, M., Li, C. and Rumizen, M. (2017). Year 2 of the National jet fuels combustion program: Towards a streamlined alternative jet fuels certification process. In *55th AIAA Aerospace Sciences Meeting* (p. 0145). https://doi.org/10.2514/6.2017-0145

Heyne, J., Peiffer, E., Colket, M., Jardines, A., Shaw, C., Moder, J., Roquemore, W. M., Edwards, J. T., Li, C., Rumizen, M., and Gupta, M. (2018) Year 3 of the National Jet Fuels Combustion Program: Practical and Scientific Impacts of Alternative Jet Fuel Research. 2018 AIAA Aerospace Sciences Meeting, AIAA SciTech Forum, (AIAA 2018-1667) https://doi.org/10.2514/6.2018-1667

Heyne, J., Opacich, K., Peiffer, E., & Colket, M. (2019). The effect of chemical and physical fuel properties on the approval and evaluation of alternative jet fuels. 11th U.S. National Combustion Meeting, Pasadena, CA

Opacich, K.C., Heyne, J.S., Peiffer, E., & Stouffer, S.D. (2019). Analyzing the relative impact of spray and volatile fuel properties on gas turbine combustor ignition in multiple rig geometries. AIAA SciTech, AIAA 2019-1434, San Diego, CA https://doi.org/10.2514/6.2019-1434

Peiffer, E.E., Heyne, J.S., & Colket, M. (2018) Characteristic Timescales for Lean Blowout of Alternative Jet Fuels. Joint Propulsion Conference. Cincinnati, Ohio: AIAA. https://doi.org/10.2514/6.2018-4914

Stachler, Robert D., Joshua S. Heyne, Scott D. Stouffer, Joseph D. Miller, and William M. Roquemore. (2017). Investigation of Combustion Emissions from Conventional and Alternative Aviation Fuels in a

Well-Stirred Reactor. 55th AIAA Aerospace Sciences Meeting. Grapevine, TX: American Institute of Aeronautics and Astronautics. https://doi.org/10.2514/6.2017-0382

Book publication

Colket, M., & Heyne, J. (2021). *Fuel effects on operability of aircraft gas turbine combustors*. American Institute of Aeronautics and Astronautics. https://doi.org/10.2514/4.106040

Book chapters

Colket, M., Heyne, J., Andac, G., Rumizen, M. (2021). Chapter I. Introduction. In T. C. Lieuwen (Ed.), *Fuel effects on operability of aircraft gas turbine combustors* (pp. 1-20). American Institute of Aeronautics and Astronautics.

Rock, N., Stouffer, S., Hendershott, T., Heyne, J., Blunck, D., Lukai, Z., Khandelwal, B., Emerson, B., Mastorakos, E., Colket, M. (2021). Chapter V. Lean blowout studies., In T. C. Lieuwen (Ed.), *Fuel effects on operability of aircraft gas turbine combustors* (pp. 143-196). American Institute of Aeronautics and Astronautics.

Heyne, J., Rauch, B., Hanson, R., Dooley, S., Blakey, S., Yang, Z., Ferris, A., Ure, A., Le Clercq, P., Boehm, R., Lewis, C., & Colket, M. Chapter XII. Prescreening of Sustainable Aviation Jet Fuels. In T. C. Lieuwen (Ed.), *Fuel effects on operability of aircraft gas turbine combustors* (pp. 487-523). American Institute of Aeronautics and Astronautics.

Heyne, J., Colket, M., Edwards, T., Moder, J., Rumizen, M., & Oldani, A. (2021). Chapter XIII. Summary. In T. C. Lieuwen (Ed.), *Fuel effects on operability of aircraft gas turbine combustors* (pp. 525-534). American Institute of Aeronautics and Astronautics.

Investigation Team

- Joshua Heyne (University of Dayton) was the project's lead investigator and was responsible for coordinating all NJFCP teams (both ASCENT and non-ASCENT efforts). 0000-0002-1782-9056
- Scott Stouffer (University of Dayton Research Institute) led the testing campaign on ignition of NJFCP fuels in the Referee Rig. 0000-0001-5421-6657
- Alejandro Briones (University of Dayton Research Institute) was the P.I. responsible for leading the common format routine software development.
- Vaidya Sankaran (UTRC) was sub-contracted to conduct the spray modeling of the Area 3 pressure atomizing spray injector.
- Bob Olding (University of Dayton Research Institute) was part of the team managed by Alejandro Briones to develop the common format routine software. Mr. Olding's main task was the Scheme GUI/TUI programing for later use by OEM CFD teams.
- Mike Hanchak (University of Dayton Research Institute) was part of the team managed by Alejandro Briones to develop the common format routine software. Mr. Hanchak's main task was the CFD and combustion programing for later use by OEM CFD teams.
- Robert Stachler (University of Dayton), a graduate student research assistant led the well-stirred reactor testing campaign, measuring lean blowout and emissions for several fuels.
- Tyler Hendershott (University of Dayton Research Institute) was part of the team working on the ignition of conventional and alternative jet fuels in the Referee Rig.
- Jeffery Monfort (University of Dayton Research Institute) was part of the team working on the ignition of conventional and alternative jet fuels in the Referee Rig.
- Erin Peiffer (University of Dayton), a graduate student research assistant linked experimental results across ASCENT and non-ASCENT teams.
- Jeremy Carson (University of Dayton), a graduate student research assistant linked experimental results across ASCENT and non-ASCENT teams.
- Katherine Opacich (University of Dayton) helped to document NJFCP activities and analyze ignition data across NJFCP teams as both an undergraduate and graduate student research assistant. 0009-0006-4845-6121
- Jen Colborn (University of Dayton) aided in the testing of fuels on the Referee Rig as both an undergraduate and graduate student research assistant. 0009-0002-0413-5693
- Shane Kosir (University of Dayton) analyzed LBO data as an undergraduate research assistant.

- Zhibin Yang (University of Dayton), a graduate student research assistant developed surrogates to match jet fuel properties, built the Tier Alpha fuel property prediction tool, and led Tier Beta fuel testing.
- David Bell (University of Dayton), a graduate student research assistant helped develop fuel surrogates
- Sherri Alexander (University of Dayton), an administrative assistant aided in the compilation of meeting minutes and setting up teleconference times.
- Randall Boehm (University of Dayton), a research engineer, combined the results from various combustor observations. 0000-0003-2983-1337

Project 034 National Jet Fuels Combustion Program – Area #7: Overall Program Integration and Analysis

University of Dayton

Project Lead Investigator

Joshua Heyne
Associate Professor
Mechanical Engineering
University of Dayton
300 College Park
Dayton, OH 45458
937 229-5319
Jheyne1@udayton.edu

University Participants

University of Dayton

- P.I.: Joshua Heyne
- FAA Award Number: 13-C-AJFE-UD (Amendment Nos. 9, 10, 13, 17, 18, and 24)
- Period of Performance: Sept. 18, 2015 to Feb 4, 2022
- Task:
    1. Integration and coordination of National Jet Fuel Combustion Program (NJFCP) teams
    2. Testing of NJFCP fuels in a well-stirred reactor
    3. Chemical effects in a toroidal jet stirred reactor
    4. Preferential vaporization effects on LBO in the referee rig
    5. Cross-experiment analysis
    6. Common format routine software development
    7. Spray modeling of area 3 pressure atomized spray injector
    8. Ignition and LBO testing of conventional and alternative jet fuels
    9. Development of operability surrogate fuels
    10. Investigation of chemical and physical effects on lean blowout (LBO)
    11. Investigation of alternative jet fuel dependencies between combustors of different sizes and mixing approaches

Project Funding Level

Amendment No. 9: $134,999.00 (September 18, 2015, to February 28, 2017)
Amendment No. 10: $249,330.00 (July 7, 2016, to December 31, 2017)
Amendment No. 13: $386,035.00 (August 30, 2016, to December 31, 2017)
Amendment No. 17: $192,997.00 (August 3, 2017, to September 30, 2018)
Amendment No. 18: $374,978.00 (December 7, 2017, to December 31, 2018)
Amendment No. 24: $582,983.00 (February 5, 2020, to February 4, 2022)
Cost share is from the University of Dayton, DLR Germany, Raytheon Technologies Research Center (RTRC), and the National Research Council (NRC) Canada.

Investigation Team

- Joshua Heyne (University of Dayton) was the project's lead investigator and was responsible for coordinating all NJFCP teams (both ASCENT and non-ASCENT efforts).
- Scott Stouffer (University of Dayton Research Institute) led the testing campaign on ignition of NJFCP fuels in the Referee Rig.

- Alejandro Briones (University of Dayton Research Institute) was the P.I. responsible for leading the common format routine software development.
- Vaidya Sankaran (UTRC) was sub-contracted to conduct the spray modeling of the Area 3 pressure atomizing spray injector.
- Bob Olding (University of Dayton Research Institute) was part of the team managed by Alejandro Briones to develop the common format routine software. Mr. Olding's main task was the Scheme GUI/TUI programing for later use by OEM CFD teams.
- Mike Hanchak (University of Dayton Research Institute) was part of the team managed by Alejandro Briones to develop the common format routine software. Mr. Hanchak's main task was the CFD and combustion programing for later use by OEM CFD teams.
- Robert Stachler (University of Dayton), a graduate student research assistant led the well-stirred reactor testing campaign, measuring lean blowout and emissions for several fuels.
- Tyler Hendershott (University of Dayton Research Institute) was part of the team working on the ignition of conventional and alternative jet fuels in the Referee Rig.
- Jeffery Monfort (University of Dayton Research Institute) was part of the team working on the ignition of conventional and alternative jet fuels in the Referee Rig.
- Erin Peiffer (University of Dayton), a graduate student research assistant linked experimental results across ASCENT and non-ASCENT teams.
- Jeremy Carson (University of Dayton), a graduate student research assistant linked experimental results across ASCENT and non-ASCENT teams.
- Katherine Opacich (University of Dayton) helped to document NJFCP activities and analyze ignition data across NJFCP teams as both an undergraduate and graduate student research assistant.
- Jen Colborn (University of Dayton) aided in the testing of fuels on the Referee Rig as both an undergraduate and graduate student research assistant.
- Shane Kosir (University of Dayton) analyzed LBO data as an undergraduate research assistant.
- Zhibin Yang (University of Dayton), a graduate student research assistant developed surrogates to match jet fuel properties, built the Tier Alpha fuel property prediction tool, and led Tier Beta fuel testing.
- David Bell (University of Dayton), a graduate student research assistant helped develop fuel surrogates
- Sherri Alexander (University of Dayton), an administrative assistant aided in the compilation of meeting minutes and setting up teleconference times.
- Randall Boehm (University of Dayton), a research engineer, combined the results from various combustor observations.

Project Overview

The NJFCP is composed of over two dozen member institutions that contribute information and data, including expert advice from gas turbine original equipment manufacturers (OEMs), federal agencies, and other ASCENT universities as well as corroborating experiments at the German Aerospace Center (DLR Germany), National Research Council Canada, and other international partners. This project involves coordinating and integrating research among these diverse program stakeholders and academic PIs; cross-analyzing results from other NJFCP areas; collecting data from a well-stirred reactor for modeling and fuel comparison purposes; conducting large eddy simulations of sprays for the Area 3 high-shear rig; and procuring additional swirler geometries for the NJFCP areas and allied partners while developing an interface for NJFCP modeling capabilities and OEM requirements. Work under this program consists of, but is not limited to:

- conducting meetings with member institutions to facilitate the consistency of testing and modeling,
- coordinating timely completion of program milestones,
- documenting results and procedures,
- creating documents critical for program processes (e.g., fuel down selection criteria),
- soliciting and incorporating program feedback from OEMs,
- reporting and presenting on behalf of the NJFCP at meetings and technical conferences,
- integrating state-of-the-art combustion and spray models into user-defined-functions (UDFs), and
- advising the program steering committee.

Project Summary

This project involved coordination between dozens of researchers and stakeholders from several different countries relating to the influence of jet fuel variation on sprays and combustion operability including ignition and lean blowout, and the models required to anticipate combustor performance. The models included chemical kinetic models of the combustion phenomenon, various models of spray involving different levels empirical input or model sophistication, and several sub-models employed within computational fluid dynamics simulations. A clear deliverable of the National Jet Fuels Combustion Program was to package the models developed under the program into applications that could be used by combustor design teams working at each of the major jet engine manufacturers, who were each represented on the team. Overall, the NJFCP resulted in hundreds of publications within archival sources, including six with authorship contribution from the principal of this project. The crowning document marking the achievement of this project was the book cited here.

Colket, M., & Heyne, J. (2021). Fuel effects on operability of aircraft gas turbine combustors. American Institute of Aeronautics and Astronautics. https://doi.org/10.2514/4.106040

Task 1 - Integration and Coordination of NJFCP Teams

University of Dayton

Objective(s)

The objective of this task is to integrate and coordinate all ASCENT and non-ASCENT team efforts by facilitating meetings, summarizing results, presenting results external to the NJFCP, communicating regularly with the steering committee, and performing other related activities.

Research Approach

The NJFCP is integrated and coordinated via two main techniques: (1) the structural combining of various teams into six topic areas; and (2) routine meetings and discussions both internal and external to individual topic areas. The topic areas are distinguished by the dominant physics associated with them (topics I and IV), the culmination of all relevant combustion physics (topics II, III, V), and the wrapping of all work into a single OEM graphical user interface package (topic VI). These six topic areas are as follows:

Topic I. Chemical kinetics: A chemical kinetic model, with the validation data to anchor modeling predictions, is foundational to any combustion model.
Topic II. Lean blowout (LBO): This topic covers data, screening, and validation, under relevant conditions, to statistically and theoretically anticipate the effects of fuel properties on this figure of merit (FOM).
Topic III. Ignition: Similar to Topic II, the focus of this topic is obtaining experimental screening and validation data for statistical and theoretical predictions.
Topic IV. Sprays: Historically, the dominant effect of fuel FOM behavior has been the spray character of the fuel relative to others. Experiments in this topic area focus on measuring the effects of fuel properties on spray behavior. Like Topic I, spray behavior is not a FOM (like Topics II and III), but it is critical to bounding the effects of physical properties on combustion behavior relative to other processes (i.e., chemical kinetics).
Topic V. Computational fluid dynamics (CFD) modeling. Complementary to the empirical Topics II, III, and IV, CFD modeling focuses on the theoretical prediction of measured data and facilitates the development of theoretical modeling approaches.
Topic VI. User-defined function development: Once the theoretical modeling approaches established in Topic V are validated, user-defined functions are developed for OEM evaluation of fuel performance in proprietary rigs.

The topic area teams meet and coordinate regularly. At minimum, NJFCP-wide meetings are held monthly, and topic area meetings typically occur every 2 to 3 weeks.

Introduction

Anthropogenic carbon emissions are increasingly being tied to deleterious environmental effects. To this end, various regulatory bodies are focusing on methods to minimize emissions of carbon in the transportation sector. The International Civil Aviation Organization (ICAO), for example, has established a Carbon Offsetting and Reduction Scheme for International Aviation (CORSIA), which sets voluntary carbon reduction standards during Phase 1 (through 2026) and mandatory standards during Phase 2 (2027 and beyond) (IATA, 2018). Sustainable aviation fuel (SAF) consumption will need to increase to >10%

of total jet fuel consumption by 2040 to meet ICAO commitments. On a global basis, this is more than the total volume of jet fuel consumed currently.

The key to the success of these goals is minimizing the barriers that inhibit the commercialization of novel SAFs to market. One of these critical barriers is the approval and evaluation process that SAFs must pass before commercialization. The approval of an SAF is contingent upon many factors, including bulk and trace fuel properties (ASTM D4054, Tiers 1 and 2) and the effect the fuel has on operability limits (ASTM D4054, Tiers 3 and 4). These later tests (Tiers 3 and 4) involve much larger fuel volumes and focus on testing three so-called FOMs. These FOMs, in turn, correspond to the most critical safety criteria required of fuel: the ability to stably hold a flame and to ignite under severe conditions.

Explicitly, the ability of a fuel to hold a flame stably is called the LBO limit of a fuel and it represents the lower operability limit of the stability loop. The other two key FOM behaviors are determined by the ease with which a fuel can ignite under cold atmospheric conditions (cold start) and cold-altitude conditions (altitude relight).

Over the last four years, the NJFCP has pursued advancements in understanding that could streamline the process of approving new alternative jet fuels for use in the aviation industry. Specifically, the program is focused on critical combustion-related safety aspects associated with the utilization of new fuels. The NJFCP is a joint effort among government, universities, engine manufacturers, and international partners. The program objectives have been described in detail (Colket et al., 2017), summaries of progress have been presented annually (Heyne et al., 2017; Heyne et al., 2018), and selective individual accomplishments have recently been presented or published (Bokhart et al., 2017; Hasti et al., 2018; Ma et al., 2019; Panchal et al., 2018; Rock et al., 2019; Wang et al., 2019). Major results have been in the areas of understanding the dependence of fuel properties on limits of LBO and of cold start and altitude relight. To explore these phenomena, new facilities and test procedures have been created, and science/technology related to fuel dependence (vaporized and spray) on chemical kinetics, spray phenomena, CFD simulations, ignition, and LBO have been tested both in controlled laboratory rigs and in engine-like hardware under realistic flow conditions.

One major and new conclusion of the program thus far is that LBO can depend *both* on the chemical nature and the physical properties of the fuel, based on hardware design and flow conditions of the rig and the fuel nozzle/swirler. The dependence on physical properties of the fuel has been known for decades (Lefebvre, 1983; Lefebvre & Ballal, 2010). However, the demonstration that LBO can be dependent on the derived cetane number (DCN), especially for combustors of modern design with new fuel injectors and intense fuel/air mixing is a relatively new observation and has been strongly validated under this program (Chtev et al., 2017; Stachler et al., 2017). A second major conclusion is the confirmation that ignition and altitude relight are most strongly correlated with fuel physical properties, in particular, density, volatility, viscosity, and surface tension. The relative dependency on each of these parameters and how they change with operating conditions and hardware is still under investigation.

Here, we report on the most recent cross-area analysis for two key FOM evaluation criteria as part of the approval and evaluation process for alternative jet fuel. Moreover, these cross-area analyses are articulated as a means to test a fuel formally as part of the ASTM D4054 approval process, informally as a prescreening process for potential jet fuel candidates, and for the prediction of deleterious operability. Combined, these tests and tools could facilitate the reduction of expensive and volume-intensive approval tests, enabling additional fuels to meet CORSIA requirements and faster approval and lower investment costs.

Methods/experiments

The NJFCP comprises multiple working groups each tasked with addressing specific problems. Combined, these working groups complement other aspects of the program by providing a greater level of experimental resolution on specific physics or adding a modeling accompaniment. The working groups include Kinetics, Sprays, LBO, Ignition, CFD, and Common Format Routine. This report focuses on combining and analyzing data from several teams within the LBO and Ignition working groups that have focused on quantifying fundamental FOM behavior under conditions identified by the NJFCP engine company advisory committee. The detailed methods used in these cross-area analyses have been documented previously (Heyne et al., 2018). Here, we report only the combined results from these works as well as the implications for ASTM approval and prescreening, while documenting fuels tested as well as recognizing key institutions and facilities.

Fuels

The fuels tested under the NJFCP have been documented extensively in previous publications (Edwards, 2017; Heyne et al., 2018). These fuels span properties associated with the range of conventional (Category A) fuels, and a wide breadth of

alternative and "test" fuels that stress the drop-in requirements; for example, Category C fuels. The operability sensitivity to conventional fuels is defined by the variance in the three Category A, or petroleum, fuels. The sensitivity to fuel effects from alternative fuels, then, is loosely bounded by the variance from the Category C fuels. Although the Category C fuel variance does not represent all possible alternative fuel property effects, the variance still captures many of the possible major contributions for fuel operability effects. Additional Category C fuels (C-7, C-8, and C-9) have been added to the NJFCP as new needs have developed. Table 1 and Figure 1 describe and illuminate the associated fuel property and compositional variance for the 12 NJFCP fuels.

Table 1. NJFCP Category A and C fuels. The Category A fuels represent the range of petroleum-derived fuels currently in use today; Category C fuels represent alternative jet fuels that have "extreme" properties that could affect figure of merit (FOM) operability limits.

Fuel	POSF Number	Composition, % volume	Description
A-1	10264	Petroleum JP-8 (w/high flash point and low viscosity and aromatics)	Low flash, viscosity, and aromatics
A-2	10325	Petroleum Jet A	Nominal jet fuel
A-3	10289	Petroleum JP-5	High flash, viscosity, and aromatics
C-1	11498, 12368, 12384	Gevo ATJ, Highly branched C12 and C16 alkanes	Low DCN, unusual boiling range
C-2	11813, 12223	16% *tri*-methylbenzene + 84% C14 *iso*-alkanes	Chemically asymmetric boiling range
C-3	12341, 12363	64% A-3 + 36% farnesane	High viscosity fuel, at viscosity limit for jet fuel at −20°C
C-4	12344, 12489	60% C9-12 *iso*-alkanes, 40% C-1	Low DCN, conventional, wide boiling range
C-5	12345, 12713, 12789, 12816	73% C10 *iso*-alkanes, 17% *tri*methylbenzene	Flat boiling range
C-6		High *cyclo*-alkane content	High *cyclo*-alkanes
C-7	12925	75% RP-2, 23% A-3, 2% decalin	High *cyclo*-alkanes
C-8	12923	Jet A + Exxon aromatic blend	High (maximum allowable) aromatics
C-9	12933	80% R-8 HEFA, 20% *n*-C12	High DCN

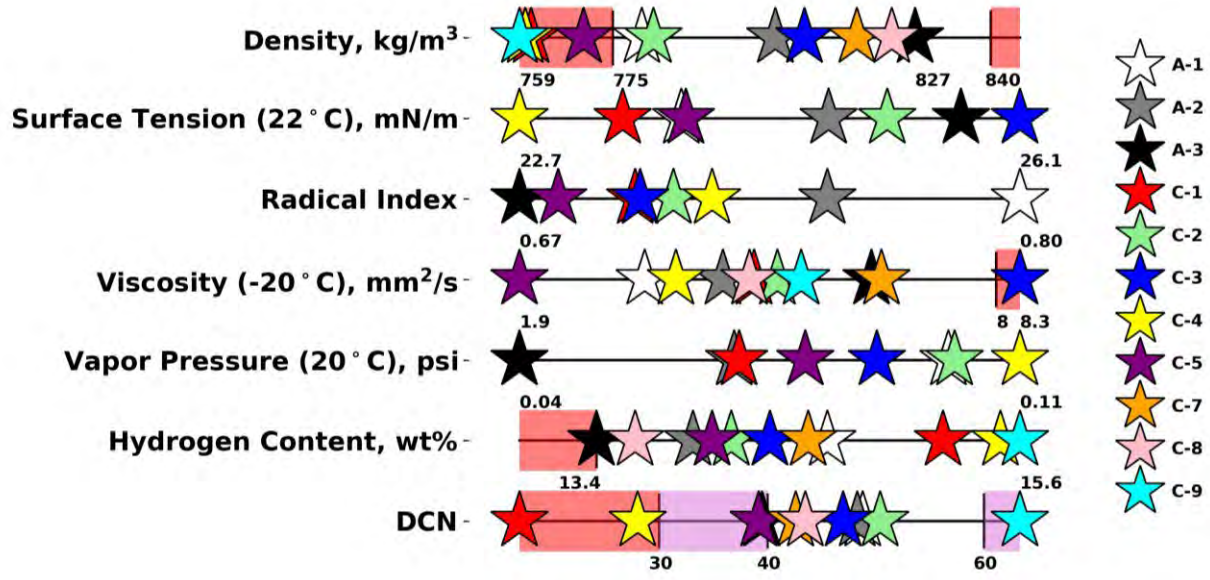

Figure 1. Category A and C range of fuel properties. Red regions represent established limits and purple areas represent proposed limits or areas to explore further. Category A fuels set the bounds of what is currently being used compared with the alternative jet fuel property ranges represented by the Category C fuels.

Institutions and experimental facilities

The NJFCP is composed of several working groups, each of which focuses on a given technical area relevant to the testing, evaluation, and modeling of an SAF. The focus of this paper is to highlight several key experimental facilities and their results as they directly relate to the SAF approval and evaluation process (ASTM D4054). The two most critical working groups evaluating operability limit sensitivity due to SAFs are the Ignition and LBO working groups. These groups have the most direct testing outcomes toward reducing the cost and time intensity of SAF approvals, because these are the two tests targeted in the high-volume Tier 3 and 4 tests. These working groups are composed of approximately 5 to 7 smaller research groups each. The details of many of these individual research groups can be found in dedicated papers, so we focus here on the most developed analyses and impactful results.

The major results from the LBO working group can be summarized via the variance observed in the data from an auxiliary power unit (APU) operated by Honeywell, a Tay combustor rig at the University of Sheffield, and the Referee Rig and toroidal jet-stirred reactor (TJSR), both at the Air Force Research Laboratory (AFRL)/University of Dayton Research Institute (UDRI). Combined, these groups span extremes in combustor geometries and test conditions, in terms of mixedness, atomization, and swirl stabilization. The Honeywell APU engine is characterized as being dominated by fuel physical properties for fuel operability limits and is one extreme of spray-atomization break-up dominance (Culbertson & Williams, 2017). The TJSR, being prevaporized and premixed, is at the other end of the spray-atomization break-up spectrum (Stachler et al., 2018). It has no spray character and, as a result, is dominated entirely by fuel chemical effects. The remaining rigs, the Referee Rig and the Tay combustor, could be dominated by either spray or chemical effects depending on thermodynamic and aerodynamic conditions (Khandelwal & Ahmed, 2017; Stouffer et al., 2017); both rigs utilize a pressure atomizer with an external co-axial swirler. The Ignition working group's major results will be highlighted only through results from one rig, the Honeywell APU (Culbertson & Williams, 2017). This rig is the only one with fully public results on ignition, although all other rigs show similar qualitative behavior.

Results and discussion

LBO

The LBO of a rig is contingent upon the competition of chemical, distillate, and physical properties in the determination of the limit. Under advantageous spray conditions, chemical properties will dominate the limit, whereas at lower temperatures

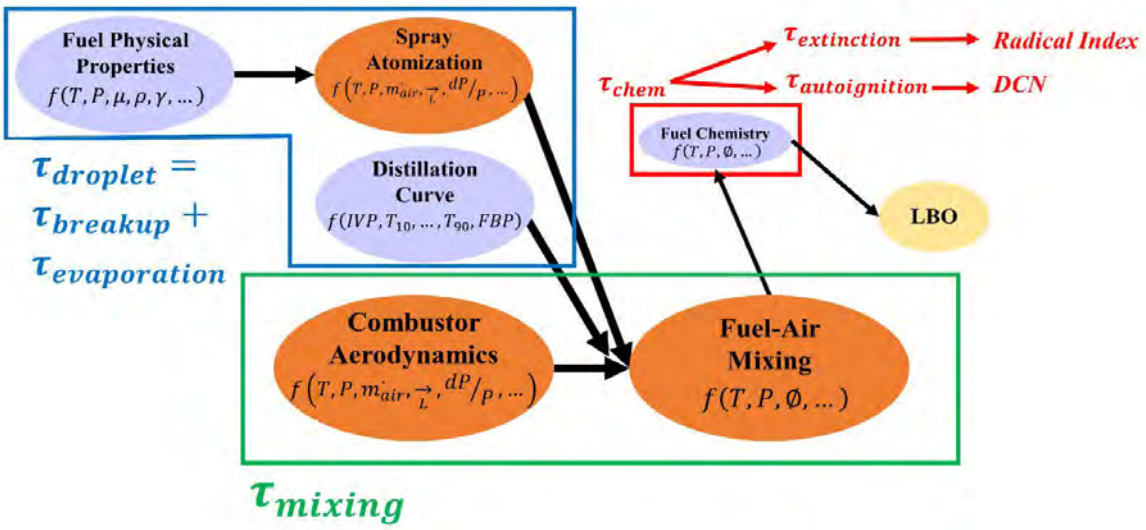

Figure 2. Generic physical phenomena controlling lean burnout (LBO) limits. Right-ward objects are dependent upon left-ward objects. Thus, spray properties can hinder later chemical reactions on the right side of the diagram. Purple objects correspond to fuel properties that can lead to engine operability sensitivity. The three bulk operability timescales identified are droplet, mixing, and chemical timescales. DCN, derived cetane number.

Figure 2 illustrates the dependency of cascading processes on the eventual global flame extinction at LBO. Moreover, any one of the three bulk properties associated with fuels can become the eventual bottleneck.

Figure 3 illustrates the relative sensitivity of these three bulk properties on LBO for previously reported NJFCP fuels. Sensitivities reported in Figure 3 were determined by random selection of orthogonal variables that could lead to LBO or represent the three fuel physical processes leading to LBO. For example, the 10%, 20%, or 50% distilled temperatures could all be representative of a fuel's distillate character. These temperatures are varied many times across the data regressions in parallel with other properties that could be important to other key processes, such as viscosity, surface tension, and density in the case of droplet break-up.

Results corroborate the physical and intuitive understanding of how each rig works. Physical and distillate properties dominate in the rig that has the least aggressive spray break-up mechanisms; see Figure 3a). Conversely, chemical properties dominate in the TJSR rig, as this rig is entirely premixed and prevaporized. The two rigs with swirlers exhibit some dependency on multiple properties. The Referee Rig, as before, is most directly influenced by the autoignition propensity of a fuel; that is, the DCN (Stouffer et al., 2017).

Combined, this analysis is carried out over hundreds of experimental observations, four rigs, and more than 11 fuels. The R^2 value was, at worst, 0.88 for one combination of properties in one rig, for which preferential vaporization has been discussed extensively (Bell et al., 2018). The implication, then, is that with this reduced-order regression, potential deleterious effects that might be discovered during Tier 3 and 4 testing can be mitigated by bounding properties similar to specification sheets. Fortunately, the properties used in this analysis are measured at earlier stages of fuel production scaling and Tier 1 and 2.

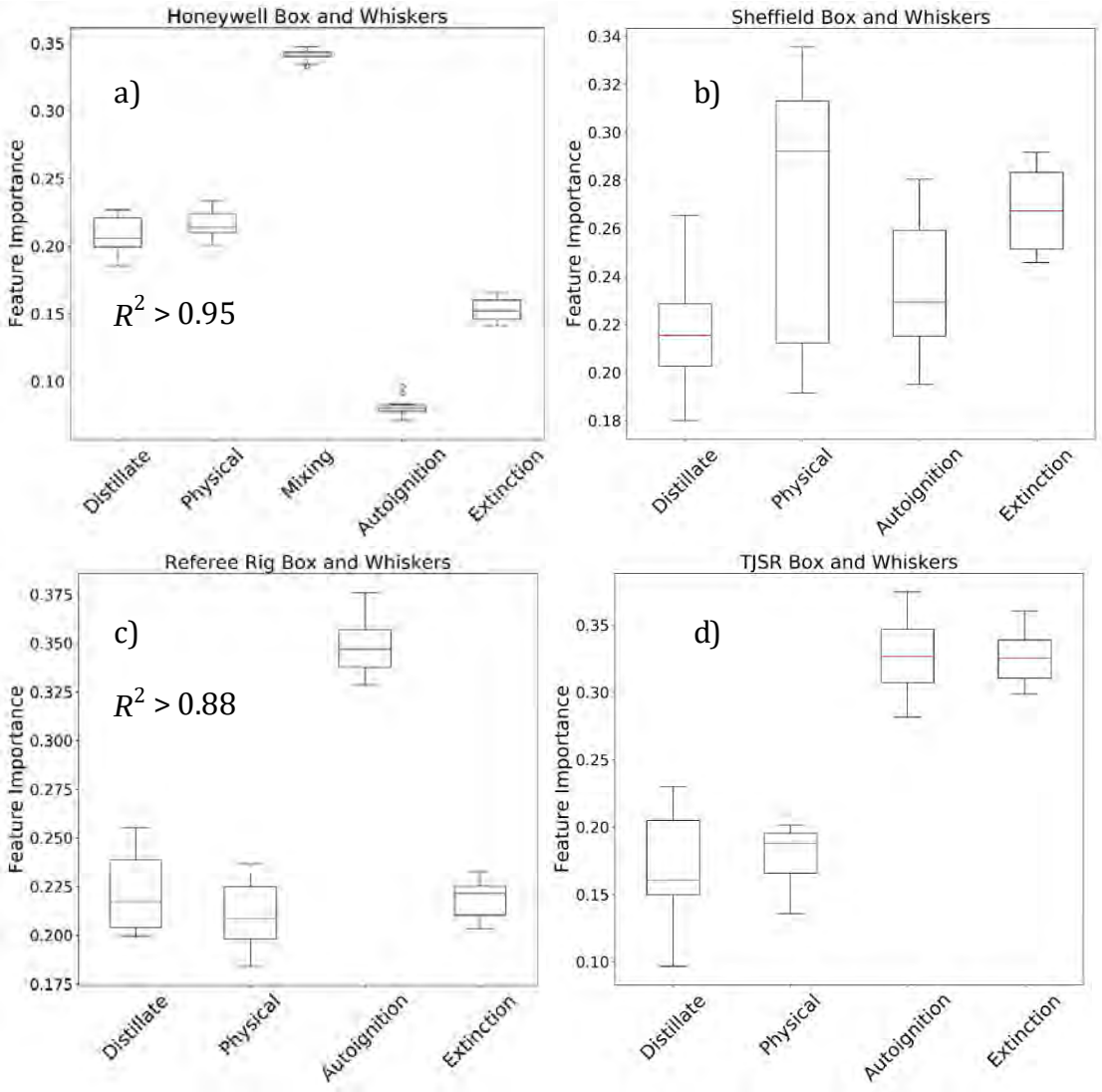

Figure 3. Box and whisker plots summarizing the analysis for the major contributions considered to lead to lean burnout (LBO) in four rigs of diverse architecture and conditions. Physical and distillate properties dominate the fuel effects in the Honeywell auxiliary power unit (APU; a) and the Sheffield rig (b). Chemical properties (autoignition and extinction) are strongly correlated with combustion phenomena in the Referee Rig (c) and the toroidal jet-stirred reactor (TJSR; d).

Ignition

Similar to the LBO flow path, the progression to ignition is illustrated in Figure 4. The critical fuel properties affecting successful ignition probability are shown in light purple; other ovals represent important categorical processes that are not directly tied to fuel effects. Thus far in the NJFCP, the effect of chemical properties is minimal for practical ignition probabilities. Sparse chemical effects have been reported in prevaporized, partially premixed combustion experiments.

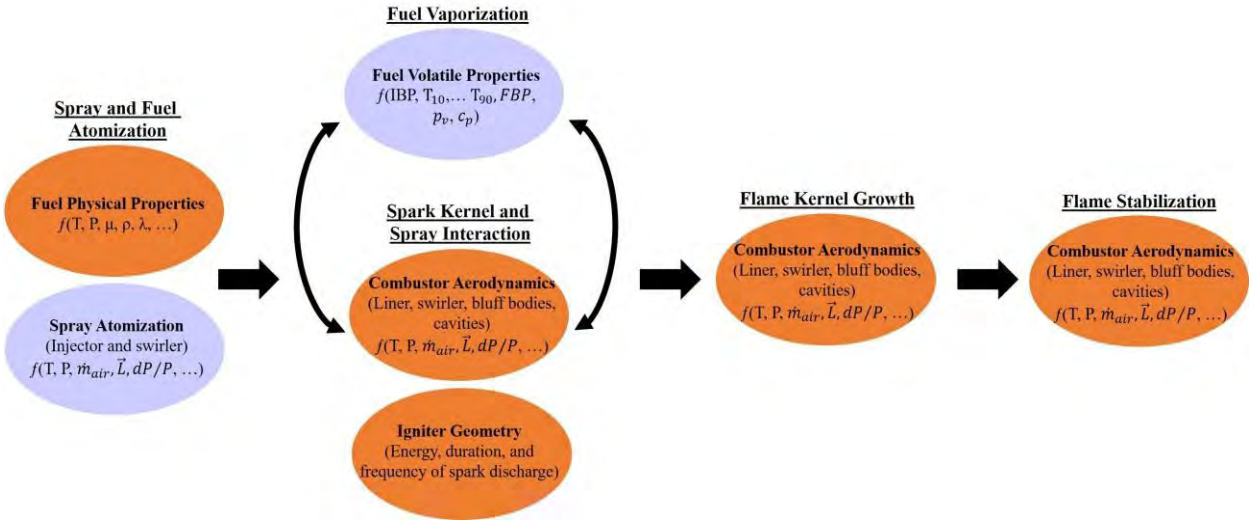

Figure 4. General flow diagram of physical processes for a stabilized flame from the injection of a plasma spark. Two of the five outlined processes involve potential fuel effects, and both of these fuel effects are common to the lean burnout (LBO) process outlined in Figure 2.

Ignition experiments analyzed here based on the data reported by Culbertson and Williams at Honeywell (Culbertson & Williams, 2017). This study (Culbertson & Williams, 2017) tested only 6 of the 11 NJFCP fuels. Previous analysis on these data showed competitive importance of surface tension and viscosity, depending upon the condition of the fuels (Opacich et al., 2019). Figures 5 and 6 report updated analyses for these data, with the updated analysis considering potential droplet temperature variance for chilled and heated fuels. This droplet temperature variance is intended to account for the potential droplet heat inductance due to spark kernel–droplet interactions. Thus, at higher levels of heat transfer to the droplet, surface temperatures and, in turn, vapor pressures will be higher.

Figure 5 illustrates the random forest regression analysis (RFRA) for the fuel property variables outlined in Figure 4. The RFRA is evaluated for fuel physical properties at the conditions reported (Culbertson & Williams, 2017). However, fuel vapor pressure for the RFRA is evaluated at the temperatures reported on the x-axis. This analysis is then repeated 100 times every 1°C. The apparent scatter in feature importance for each of the properties represents the randomness associated with each RFRA evaluation. These RFRA evaluations involved randomness introduced at both the variable and data set level. Figure 5 suggests that the ignition probability of a fuel is most directly related to the density and surface tension of a fuel. Variance in the viscosity is also strongly correlated with ignition probability. At 50°C, the feature importance of vapor pressure increases significantly, coincident with the inversion in the vapor pressure of A-1 and C-1 (Opacich et al., 2019).

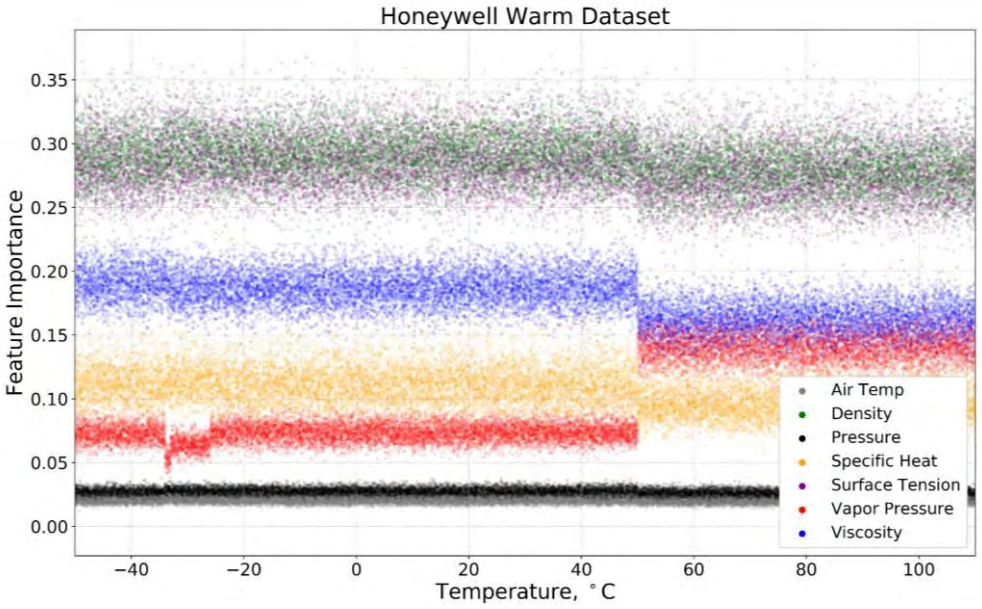

Figure 5. Feature importance concerning varying the droplet temperature for warm fuel tests in a Honeywell auxiliary power unit (APU). Vapor pressure has negligible importance for low temperatures but greater importance at high temperatures. The step change in the importance of vapor pressure represents the temperature at which C-1 has a higher vapor pressure than A-1. The noise in the plots represents the variance introduced by random selection of variables and subsets of data.

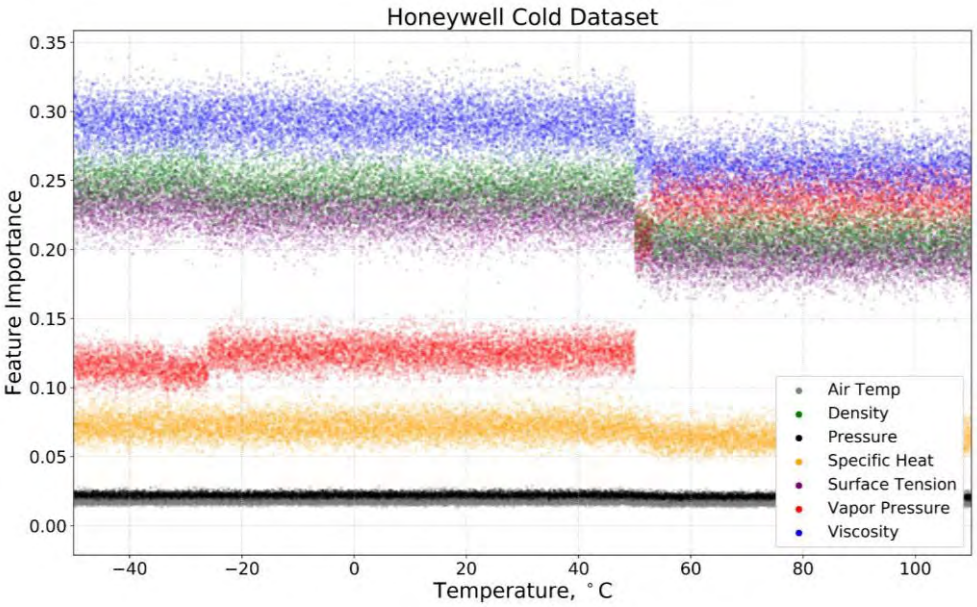

Figure 6. Feature importance for several critical properties in the ignition of a fuel. The cold fuel data analyzed here have more sensitivity to the viscosity of the fuel, which increases exponentially with decreasing temperature. Dependence of surface tension and density are nearly indistinguishable because of their nominal collinearity. The dramatic increase in the importance of the vapor pressure coincides with the inversion of the C-1 and A-1 vapor pressure curves.

Figure 6 shows a similar RFRA as that in Figure 5 for the cold fuel data of Culbertson and Williams. These analyses suggest that ignition probabilities are first affected by the viscosity of a fuel and second by the surface tension and density of a fuel at low droplet temperatures. However, as droplet temperature exceeds 50 °C, the vapor pressure of the fuel eclipses the feature importance of surface tension and density. Note that only at temperatures above 50 °C, are vapor pressures high enough to support combustion.

The feature importance effects between the warm and cold fuel cases appear counterintuitive. The cold fuel data are more sensitive to droplet temperatures exceeding 50 °C, and the probability of this occurring under the −37 to −19° C cold fuel condition is low compared with that under warm ambient fuel conditions. Although this observation is not conclusive, it is suggestive that additional analysis is needed.

Conclusions

LBO and ignition probability data from the four rigs were analyzed using orthogonal fuel properties and RFRA methods. LBO data from hundreds of data points, 11 fuels, many operating conditions, and four very different rigs and fuel injection approaches were analyzed. The results accounted for more than 89% of all variances. Fuel-dependent LBO effects depend on the chemical, physical, and distillate properties of a fuel, thermodynamic conditions, and geometrical bias of an experiment. DCN is an effective marker for autoignition reactivity of a fuel near LBO. Physical properties dominate cold ignition behavior and LBO in configurations with less intensive mixing-swirl stabilization and aggressive atomization methods. Distillate properties can affect evaporative timescales. Deleterious fuel effects are particularly apparent when chemical and distillate property effects are coupled in the case of preferential vaporization.

Combined, our observations offer an opportunity to not only screen fuels early in the approval process, before Tier 3, but also illuminate paths for prescreening of fuel properties. Prescreening fuel properties, as part of (or prior to) ASTM D4054 Tier 1 and 2 testing, would involve the evaluation or prediction of the properties listed above. Preliminary analysis suggests that with as little as several liters, most properties critical to LBO and cold ignition/altitude relight could be evaluated. These prescreening tests could also be done using predictive, low-volume fuel testing methods such as two-dimensional gas chromatography (GCxGC), nuclear magnetic resonance, and Fourier transform infrared spectroscopy.

References

Bell, D.C., Heyne, J.S., Won, S.H., & Dryer, F.L. (2018). The impact of preferential vaporization on lean blowout in a referee combustor at figure of merit conditions. ASME Power Conference.

Bokhart, A.J., Dongyun, S., Gejji, R., Buschhahen, T., Naik, S.V., Lucht, R.P., Gore, J.P., Sojka, P.E., & Meyer. S.E. (2017). AIAA Aerospace Sciences Meeting

Chtev, I., Rock, N., Ek, H., Emerson, B.L., Seitzman, J.M., Lieuwen, T.C., Noble, D.R., Mayhew, E., & Lee, T. (2017). Simultaneous high speed (5 kHz) Fuel-PLIE, OH-PLIF and stereo PIV imaging of pressurized swirl-stabilized flames using liquid fuels. 55th AIAA Aerospace Sciences Meeting

Colket, M.B., Heyne, J., Rumizen, M., Gupta, M., Edwards, T., & Roquemore, W.M. et al. (2017). An overview of the national jet fuels combustion program. AIAA J

Culbertson, B. & Williams, R. (2017). AFRL-RQ-WP-TR-2017-0047

Edwards, T. (2017). Reference jet fuels for combustion testing. 55th AIAA Aerospace Sciences Meeting. 1-58

Hasti, V.R., Kumar, G., Liu, S. Lucht, R.P., & Gore, J.P. (2018). Large eddy simulation of pilot stabilized turbulent premixed CH4+air jet flames. 2018 AIAA Aerospace Sciences Meeting

Heyne, J.S., Colket, M.B., Gupta, M., Jardines, A., Moder, J.P., & Edwards, J.T. et al. (2017). Year 2 of the national jet fuels combustion program: Towards a streamlined alternative jet fuels certification process. 55th AIAA Aerospace Science Meeting, 1-13

Heyne, J.S., Peiffer, E., Colket, M.B., Jardines, A., Shaw, C., & Moder, J.P. et al. (2018). Year 3 of the National Jet Fuels Combustion Program: Practical and scientific impacts of alternative jet fuel research. 56th AIAA Aerospace Science Meeting

IATA. (2018). Carbon Offsetting and Reduction Scheme for International Aviation (CORSIA): Fact sheet.

Lefebvre, A.H. (1983). Fuel effects on gas turbine combustion. Dayton, OH

Lefebvre, A. & Ballal, D. (2010). Gas turbine combustion alternative fuels and emissions. 3rd ed. Boca Raton: Taylor and Francis Group

Khandelwal, B. & Ahmed, I. (2017). Research report on lean blowout limit the university of Sheffield Department of Mechanical Engineering.

Ma, P.C., Wu, H., Labahn, J.W., Jaravel, T., & Ihme, M. (2019). Analysis of transient blow-out dynamics in a swirl-stabilized combustor using large-eddy simulations. Proceedings of the Combustion Institute. 37 5073–5082

Opacich, K.C., Heyne, J.S., Peiffer, E., & Stouffer, S.D. (2019). Analyzing the relative impact of spray and volatile fuel properties on gas turbine combustor ignition in multiple rig geometries. AIAA Scitech 2019 Forum

Panchal, A., Ranjan, R., & Menon, S. (2018). Effect of chemistry modeling on flame stabilization of a swirl spray combustor. 2018 Joint Propulsion Conference

Rock, N., Chterev, I., Emerson, B., Won, S.H., Seitzman, J., & Lieuwen, T. (2019). Liquid fuel property effects on lean blowout in an aircraft relevant combustor. J. Eng. Gas Turbines Power 141 71005–71013

Stachler, R.D., Heyne, J.S., Stouffer, J.S., Miller, J.D., & Roquemore, W.M. (2017). AIAA SciTech forum. 55th AIAA Aerospace Science Meeting

Stachler, R.D., Peiffer, E., Kosir, S.T., Heyne, J.S., Stouffer, S.D., & Miller, J.D. (2018). Lean blowoff and emissions of alternative and conventional fuels using a toroidal jet stirred reactor. AIAAJ. (in submission).

Stouffer, S.D., Hendershott, T.H., Monfort, J.R., Diemer, J., Corporan, E., Wrzesinski, P., & Caswell, A.W. (2017). Lean blowout and ignition characteristics of conventional and surrogate fuels measured in a swirl stabilized combustor. 55th AIAA Aerospace Science Meeting, 1–14

Wang, Y., Cao, Y., Wei, W., Davidson, D.F., & Hanson, R.K. (2019). A new method of estimating derived cetane number for hydrocarbon fuels. Fuel 241 319–326.

Milestone(s)

- Coordination of Biannual NJFCP meetings, 2016 - 2019
- NJFCP American Institute of Aeronautics and Astronautics (AIAA) Book was published.
- Developed Tier Alpha prescreening tool for novel sustainable aviation fuel (SAF) prescreening.

Major Accomplishments

- Edited, coordinated, and published an AIAA book documenting the lessons learned as a result of the NJFCP.
- Developed and published a Civil Aviation Alternative Fuels Initiative (CAAFI) R&D prescreening document to aid novel companies and producers in the refinement and development of fuels that can most easily eclipse the Tier 3 and 4 testing.
- Reported the alternative jet fuel dependencies between combustors of different sizes and mixing approaches.
- Experimental results from testing surrogate fuels can illustrate the maximum FOM sensitivity, aiding in the prescreening and formal evaluation of novel SAF.

Publications

Peer-reviewed journal publications

Colket, Meredith B., Joshua S. Heyne, Mark Rumizen, James T. Edwards, Mohan Gupta, William M. Roquemore, Jeffrey P. Moder, Julian M. Tishkoff, and Chiping Li. (2016). "An Overview of the National Jet Fuels Combustion Program." AIAA Journal 55(4), 1087-1104. https://doi.org/10.2514/1.J055361

Peiffer, E.E., Heyne, J.S., & Colket, M. (2019). Sustainable aviation fuels approval streamlining: auxiliary power unit lean blowout testing. AIAA Journal, pg. 1-9, https://doi.org/10.2514/1.J058348

Ruan, H., Qin, Y., Heyne, J., Gieleciak, R., Feng, M., & Yang, B. (2019). Chemical compositions and properties of lignin-based jet fuel range hydrocarbons. Fuel 256 115947, https://doi.org/10.1016/j.fuel.2019.115947

Colborn JG, Heyne JS, Stouffer SD, Hendershott TH, Corporan E. (2020) Chemical and physical effects on lean blowout in a swirl-stabilized single-cup combustor. Proc Combust Inst https://doi.org/10.1016/j.proci.2020.06.119

Heyne, J., Rauch, B., Le Clercq, P., & Colket, M. (2021). Sustainable aviation fuel prescreening tools and procedures. Fuel, *290*, 120004. https://doi.org/10.1016/j.fuel.2020.120004

Boehm, R.C., Colborn, J. G., & Heyne, J. S. (2021). Comparing alternative jet fuel dependencies between combustors of different size and mixing approaches. Frontiers in Energy Research, *13*. https://doi.org/10.3389/FENRG.2021.701901.

Kramer, S., Andac, G., Heyne, J.; Ellsworth, J., Herzog, P., & Lewis, K. C. (2022) Perspectives on Fully Synthesized Sustainable Aviation Fuels: Direction and Opportunities. Frontiers in Energy Research, 24. https://doi.org/10.3389/fenrg.2021.782823

Published conference proceedings:

Colket, Meredith B., Joshua S. Heyne, Mark Rumizen, James T. Edwards, Mohan Gupta, William M. Roquemore, Jeffrey P. Moder, Julian M. Tishkoff, and Chiping Li. (2016) "An Overview of the National Jet Fuels Combustion Program." In AIAA SciTech. AIAA SciTech. San Diego, CA: American Institute of Aeronautics and Astronautics. doi:doi:10.2514/6.2016-0177.

Heyne, J., Peiffer, E., Colket, M., Moder, J., Edwards, J. T., Roquemore, W. M., Shaw, C., Li, C., Rumizen, M., and Gupta, M. (2018) "Year 3 of the National Jet Fuels Combustion Program: Practical and Scientific Impacts," 56th AIAA Aerospace Sciences Meeting, Kissimmee, FL https://doi.org/10.2514/6.2018-1667

Heyne, J., Peiffer, E., Colket, M., Jardines, A., Shaw, C., Moder, J., Roquemore, W. M., Edwards, J. T., Li, C., Rumizen, M., and Gupta, M. (2018) "Year 3 of the National Jet Fuels Combustion Program: Practical and Scientific Impacts of Alternative Jet Fuel Research", 2018 AIAA Aerospace Sciences Meeting, AIAA SciTech Forum, (AIAA 2018-1667) https://doi.org/10.2514/6.2018-1667

Peiffer, E.E., Heyne, J.S., & Colket, M. (2018) Characteristic Timescales for Lean Blowout of Alternative Jet Fuels. Joint Propulsion Conference. Cincinnati, Ohio: AIAA. https://doi.org/10.2514/6.2018-4914

Heyne, J., Opacich, K., Peiffer, E., & Colket, M. (2019). The effect of chemical and physical fuel properties on the approval and evaluation of alternative jet fuels. 11th U.S. National Combustion Meeting, Pasadena, CA

Opacich, K.C., Heyne, J.S., Peiffer, E., & Stouffer, S.D. (2019). Analyzing the relative impact of spray and volatile fuel properties on gas turbine combustor ignition in multiple rig geometries. AIAA SciTech, AIAA 2019-1434, San Diego, CA https://doi.org/10.2514/6.2019-1434

Written reports

CAAFI R&D Committee. (2019). Prescreening of synthesized hydrocarbons intended for candidates as blending components for aviation turbine fuels. Commercial Alternative Aviation Fuel Initiative (CAAFI), CAAFI R&D Committee Publication

Book publication

Colket, M., & Heyne, J. (2021). *Fuel effects on operability of aircraft gas turbine combustors*. American Institute of Aeronautics and Astronautics. https://doi.org/10.2514/4.106040

Book chapters

Colket, M., Heyne, J., Andac, G., Rumizen, M. (2021). Chapter I. Introduction. In T. C. Lieuwen (Ed.), *Fuel effects on operability of aircraft gas turbine combustors* (pp. 1-20). American Institute of Aeronautics and Astronautics.

Rock, N., Stouffer, S., Hendershott, T., Heyne, J., Blunck, D., Lukai, Z., Khandelwal, B., Emerson, B., Mastorakos, E., Colket, M. (2021). Chapter V. Lean blowout studies., In T. C. Lieuwen (Ed.), *Fuel effects on operability of aircraft gas turbine combustors* (pp. 143–196). American Institute of Aeronautics and Astronautics.

Heyne, J., Rauch, B., Hanson, R., Dooley, S., Blakey, S., Yang, Z., Ferris, A., Ure, A., Le Clercq, P., Boehm, R., Lewis, C., & Colket, M. Chapter XII. Prescreening of Sustainable Aviation Jet Fuels. In T. C. Lieuwen (Ed.), *Fuel effects on operability of aircraft gas turbine combustors* (pp. 487–523). American Institute of Aeronautics and Astronautics.

Heyne, J., Colket, M., Edwards, T., Moder, J., Rumizen, M., & Oldani, A. (2021). Chapter XIII. Summary. In T. C. Lieuwen (Ed.), *Fuel effects on operability of aircraft gas turbine combustors* (pp. 525–534). American Institute of Aeronautics and Astronautics.

Outreach Efforts

Invited talks

- Heyne, Colket, Lee (2018) "An overview of ASCENT research efforts to improve our understanding of how fuel composition and characteristics determine performance," CAAFI Biennial General Meeting, December
- Heyne, J., Edwards, T. (2018) "What makes a Great Jet Fuel?" Keynote, Tri-Lateral US-Mexico-Canada Bio-Jet Workshop, Pacific Northwest National Laboratories, May
- Heyne, Colket, (2018) "Overview and Results from the National Jet Fuels Combustion Program," CAAFI SOAP-Jet Webinar, Jan.
- Colket, M. & Heyne, J. (2018). Early evaluation of alternative jet fuels based on NJFCP results. Advanced Bioeconomy Leadership Conference (ABLC), San Francisco, CA
- Colket, M. & Heyne, J. (2019). Major results from the National Jet fuels and Combustion Program. ASME TurboExpo, Phoenix, AZ
- Colket, M., Heyne, J., & Lee, T. (2018). An overview of ASCENT research efforts to improve our understanding of how fuel composition and characteristics determine performance. CAAFI Biennial General Meeting

- Colket, M., Heyne, J., & Lee, T. (2018). NJFCP update: Properties and modeling to FOM predictions. JetScreen Meeting, Paris, FR
- Edwards, T. & Heyne, J. (2019). Towards the minimization of ASTM D4054 tier 3 & 4 AJF approvals. 2019 CRC Aviation Committee Meetings, San Juan, PR
- Heyne, J. (2019). Drop-in high-performance fuels: From molecule selection to mission benefits. NREL IBRF Lab, Golden, CO
- Heyne, J. (2019). The approval and evaluation of alternative jet fuels, NJFCP learnings and high-performance fuels for operability and mission benefits. Rolls-Royce, Indianapolis, IN
- Heyne, J. (2020, November). High value drop-in aviation fuels: From molecule selection to mission benefits [Panel presentation]. Fuel Quality Matters, DOE BETO/PNNL HTL Workshop, Virtual meeting.
- Heyne, J. (2020, November). Prescreening of HTL SAFs: Rapid low-volume, low-cost testing. Sustainable Aviation Fuel Certification, DOE BETO/PNNL HTL Workshop, Virtual meeting.
- Heyne, J. (2020). Prescreening of sustainable aviation fuels. ACS Fall 2020 National Meeting & Exposition, San Francisco, CA
- Heyne J. (2021, May). Summative results of the national jet fuels combustion program [Panel presentation]. Properties and Emissions, CRC Aviation Fuels Meeting, Virtual meeting.
- Heyne, J. (2021, June). Prescreening of sustainable aviation fuels [Panel presentation]. CAAFI Virtual Mini-Symposium.
- Heyne, J. (2021, June 2). Sustainable aviation fuel prescreening, benefits, and a proposed streamlined evaluation process [Panel presentation]. National Academies, Transportation Research Board (AV030), Sustainable Aviation Fuels subcommittee midyear meeting.
- Heyne, J. (2021, August 17). Sustainable aviation fuel: Properties, compositions, and qualification requirements [Sponsored seminar]. Sandia National Laboratory.
- Heyne, J., (2021, August 17). Sustainable aviation fuel property needs and some solid waste candidates [Panel presentation]. Seminar on Hydrothermal Liquefaction: biocrudes and advances towards drop-in fuel potential, Aalborg University, Denmark.
- Heyne, J. (2021, November). Sustainable aviation fuel: Properties, compositions, and qualification requirements [Sponsored travel]. Center for Multiphase Flow Research and Education, Iowa State University.

Conference presentations

Heyne, J. (2016-2017) CRC Aviation Meeting, AIAA SciTech Meeting, Dayton Engineering Sciences Symposium ASME (DESS)

Heyne, J., Erin Peiffer, Meredith B. Colket, Aniel Jardines, Cecilia Shaw, Jeffrey P. Moder, William M. Roquemore, James T. Edwards, Chiping Li, Mark Rumizen, and Mohan Gupta (2018) "Year 3 of the National Jet Fuels Combustion Program: Practical and Scientific Impacts of Alternative Jet Fuel Research", 2018 AIAA Aerospace Sciences Meeting, AIAA SciTech Forum, (AIAA 2018-1667)

Opacich, K., Heyne, J.S., Peiffer, E., & Stouffer, S.D. (2018). Analyzing the relative impact of spray and volatile fuel properties on gas turbine combustor ignition. DESS2018-019, 14th Dayton Engineering Sciences Symposium, Wright State University

Peiffer, Erin, Heyne, Joshua (2018) "Combustor Rig Sensitivity to Derived Cetane Number for Lean Blowout and Ignition Results from Year Three of the National Jet Fuels Combustion Program." Dayton-Cincinnati Aerospace Sciences Symposium. Dayton, Ohio: ASME.

Peiffer, Erin, Heyne, Joshua, Colket, Meredith (2018) "Characteristic Timescales for Lean Blowout of Alternative Jet Fuels." Joint Propulsion Conference. Cincinnati, Ohio: AIAA.

Stachler, R., Heyne, J., Peiffer, E., Stouffer, S., & Miller, J. (2018). Assessment of lean blowoff in a toroidal jet stirred reactor. Dess2018-055, 14th Dayton Engineering Sciences Symposium, Wright State University

Yang Z., Heyne J. (2018). A GCxGC Tier Alpha and Combustor Figure-of-Merit Approach on Sustainable Aviation Fuels Prescreening 2018:1–6. Eastern States Section of the Combustion Institute. University of South Carolina

Stouffer, S., Heyne, J., Boehm, R., Mayhew, E., Lee, T., & Canteenwalla, P. (2019). Ignition WG update and 4-year summary. NJFCP 2019 Review Meeting. OAI, Cleveland, OH

Funded program review presentations

Heyne, J. ASCENT Spring and Fall 2016-2019

Heyne, J. & Colket, M. (2019). AIAA Book and year 5 - next steps and action item review. NJFCP 2019 Review Meeting, OAI, Cleveland, OH

Heyne, J. & Colket, M. (2019). Highlights of NJFCP achievements - overall impact of program tiers and HPF. NJFCP 2019 Review Meeting, OAI, Cleveland, OH

Heyne, J., Colket, M., Moder, J., & Shaw, C. (2018). NJFCP status update. FAA ASCENT, Alexandria, VA

Heyne, J., Emerson, B., Lieuwen, T., Stouffer, S., Blunck, D., Corporan, E., Mastorakas, N., & de Oliveira, P. (2019). LBO WG update and 4 year summary. NJFCP 2019 Review Meeting, OAI, Cleveland, OH
Stouffer, S., Heyne, J., Boehm, R., Mayhew, E., Lee, T., & Canteenwalla, P. (2019). Ignition WG update and 4 year summary. NJFCP 2019 Review Meeting. OAI, Cleveland, OH

Articles/press

Heyne, J., Wang, H., & Kalman, J. (2018). Safely improving jet, rocket fuels. Aerospace America, 2018 Year in Review, Propellants and Combustion Technical, Committee Contribution

Awards

Joshua Heyne

- 2016 SOCHE Faculty Excellence Award, University of Dayton
- 2018 Outstanding Service Award, ASME Dayton Section
- 2019 Blavatnik National Awards for Young Scientists, Nominee, University of Dayton
- 2021 Net Good Summit on Sustainable Travel, honored guest
- 2021 US Frontiers of Engineering Symposium, National Academies of Engineering, selected participant
- 2021 Vision Award for Excellence in Scholarship, School of Eng., University of Dayton

Jeremy Carson

- 2016 Best presentation Dayton Engineering Sciences Symposium
- 2017 Best presentation Dayton-Cincinnati Aerospace Sciences Symposium

Katherine Opacich:

- The Martin C. Kuntz, 1912, Award of Excellence to the Outstanding Junior in Mechanical Engineering, 2018
- Ohio Space Grant Consortium Master's Fellowship, 2019

Shane Kosir:

- Ohio Space Grant Consortium Master's Fellowship, 2019
- Class of 1902 Award of Excellence for Outstanding Mechanical Engineering Achievement, 2019

Student Involvement

Jeremy Carson, graduate student research assistant, 2015 – 2017
Erin Peiffer, graduate student research assistant, 2017 - 2018
Jennifer Colborn contributed as both an undergraduate and graduate student research assistant, 2016 – 2020
Katherine Opacich contributed as both an undergraduate and graduate student research assistant, 2017 – 2020
Zhibin (Harrison) Yang, Ph.D. student 2018 ff
Shane Kosir, undergraduate research assistant, 2018 - 2020

Task 2 - Testing of NJFCP Fuels in a Well-Stirred Reactor

University of Dayton

Objective(s)

We aim to measure the Lean Blowout (LBO) limit and emissions/speciation characteristics for NJFCP fuels within the program.

Research Approach

In response to legislative orders, industrial and governmental organizations are actively pursuing strategies to promote alternative energy fuels in gas turbine combustors, and to reduce pollutant emissions. Emissions tend to be of importance because of the adverse effects they have on air quality, health and the environment. Gaseous emissions of interest include nitrogen oxides (NO and NO_2), sulfur oxides (SO_x), carbon monoxide (CO), carbon dioxide (CO_2) and unburned hydrocarbons (UHC). The International Civil Aviation Organization (ICAO) currently regulates the total amount of UHC among NO_x, CO, and particulate (smoke number) emissions for aircraft, but the concentration of these emissions, whether unburned hydrocarbons or carbon monoxide, etc., have seen to have a local effect on areas around airports or flight lines (Anneken et al. 2014; D. L. Blunck et al. 2015; FAA 2012; Colket et al. 2016). Because of these effects and these initiatives, it is important to understand the emissions footprints of fuels for aviation for not only a sustainable future, but for better aircraft performance towards a carbon neutral future.

The National Jet Fuels Combustion Program (NJFCP) aims in streamlining the alternative jet fuel research and evaluation process, which is a major R&D directive covered in the Federal Alternative Jet Fuels Research and Development Strategy(AJF-IWG 2016; Colket et al. 2016). Use of specialized laboratory scale rigs are used in this program to determine fuel performance of a candidate alternative jet fuel while minimizing the use of multiple combustor rig tests. These rigs evaluate the impact of engine operability Figures of Merit (FOMs) such as lean blow off (LBO, high altitude relight, and cold start. These FOMs have a strong impact on aircraft safety or engine hardware and are likely impacted by fuel variation, whether due to the physical or chemical properties of the fuel. Performance and operability are also studied via emissions, combustor fuel coking and effects of temperature through pattern factors, radiation, and flame structure, all of which are secondary FOMs (Colket et al. 2016). It is imperative to investigate and pursue novel strategies and balance the combustor design characteristics with emissions reduction. Understanding performance and emissions with varying fuel composition provides the opportunity for use of potential alternative fuels in legacy and future aircraft and guidance to the quality and quantity of aircraft emissions produced.

Well-Stirred Reactor (WSR) experiments provide a simplified combustion environment to investigate chemical kinetic effects, among other parameters, such as combustion efficiency and LBO in the absence of physical property effects from the fuels. The lean premixed, prevaporized fuel and air mixtures used in these experiments remove physical effects such as droplet injection, evaporation, and atomization in addition to molecular mixing and transient and chemistry interaction of which is seen in typical gas-turbine combustors. With removing these physical effects, we also eliminate the physical complications native to modeling practical diffusion flame combustors such as, multi-dimensional flow, multi-phase fuel, and transient fluid dynamic and chemistry interactions. Use of this fundamental combustor experiment provides insight into LBO and emissions, a primary and secondary FOM in the NJFCP program, respectively, under relevant residence times and temperatures typically seen in practical gas-turbine-combustor environments(Colket et al. 2016).

We report the investigation of emissions and LBO of surrogate, conventional, and alternative fuel mixtures as lean combustion limits are approached in the WSR as funded by the FAA in relation the NJFCP. The WSR has provided considerable knowledge toward understanding lean and rich blow off limits, pollutant and particulate formation, kinetics of gaseous and liquid fuel combustion and combustion stability (D. Blunck et al. 2012; J. Blust, Ballal, and Sturgess 1997; S. D. Stouffer et al. 2005; J. W. Blust, Ballal, and Sturgess 1999; S Stouffer et al. 2002; Manzello et al. 2007; Vijlee 2014; Scott Stouffer et al. 2007; Nenniger et al. 1984; Zelina 1995; Karalus 2013; D. L. Blunck et al. 2015). Knowledge of the emissions and LBO provides the opportunity to investigate the controlling chemical kinetics and relating chemical properties among the fuels. Here we report a statistically significant correlation between LBO, derived cetane number, and radical index, yielding insight to the controlling chemical effects experienced in typical gas turbine combustors near LBO.

I. Experimental Details and Methodology

A. Well-Stirred Reactor

LBO and emissions experiments were performed in the well-stirred reactor (WSR) facility at the Air Force Research Laboratory in Dayton, OH. The toroidal WSR design was derived from the work of Nenniger et al.(Nenniger et al. 1984), Zelina (Zelina 1995), and Stouffer (S Stouffer et al. 2002) and approximates a zero-dimensional perfectly stirred reactor, *i.e.*, homogeneous in both space and time. The reactor, shown during operation in Fig. 1 a and b, comprises an Inconel jet ring, upper and lower ceramic reactor hemispheres, flow straightener, and exhaust stack. A representative cross section drawing of the reactor is shown in Fig. 1b. Premixed prevaporized fuel and air enter the jet ring through two opposed inlets to ensure equal flow around the reactor.

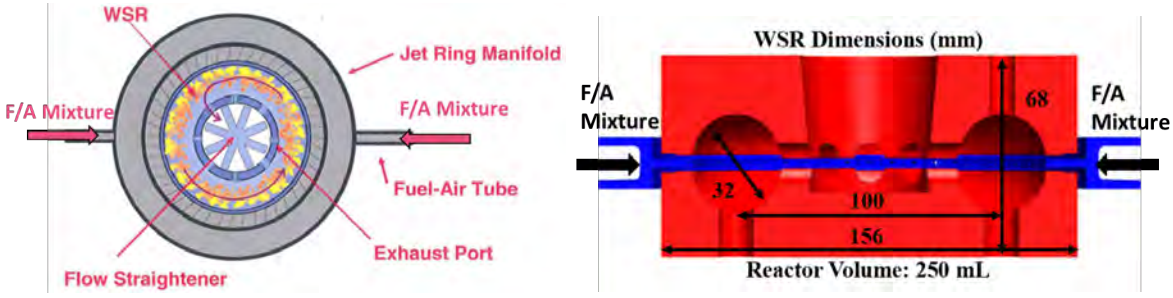

(a) (b)

Figure 1. (a) Cross-section of the WSR, top view (S. D. Stouffer et al. 2005; Scott Stouffer et al. 2007). Premixed, prevaporized fuel and air enters the jet ring via the two opposed inlets. The angled jets (20 degrees from the radius of the torus) inject the mixture into the reactor, where bulk recirculation and flow occurs around the reactor. Burned products exit towards the inner diameter of the toroid through the exhaust ports, the flow straightener, and exhaust stack. (b) Cross-section of the WSR, side view. Fuel an air enter the toroidal reactor through the jet ring in blue.

In the current work, a fused silica reactor (Rescor 750, SiO_2) was utilized and sealed using spring loaded sections.(S Stouffer et al. 2002; D. Blunck et al. 2012) This reactor material was chosen due to its low thermal conductivity, resistance to thermal cracking from fast transients, and reduction in the active cooling necessary around the reactor yielding reduced heat loss. An Inconel jet ring with 48 fuel/air jets at 1mm diameter was sealed between the reactor components. A ceramic paper gasket seal (Cotronics 390, 1/8" thickness) was placed between the upper reactor halve and jet ring while a mica gasket (0.064" thickness) was placed between the jet ring and bottom half to seal the reactor under fuel-lean operating conditions. Figure 2 highlights the construction of the WSR with the ceramic components in red and the jet ring in blue.

The feed jets in the jet ring inject the premixed fuel/air at an angle 20 degrees off the radius of the torus causing the bulk flow to move circumferentially around the reactor (S. D. Stouffer et al. 2005; S Stouffer et al. 2002; Vijlee 2014; Scott Stouffer et al. 2007; Nenniger et al. 1984). The sonic velocity and angle from the jets provides for recirculation zones around the upper and lower half of the toroid in addition to around the toroid. The high rate of continuous mixing between the unburned reactants and burned products is an additional characteristic that separates the WSR from other premixed combustions systems (Briones et al. 2008; D. L. Blunck et al. 2015; D. Blunck et al. 2012; S. D. Stouffer et al. 2005; Scott Stouffer et al. 2007). Previous work using numerical modeling has been performed to show that the WSR operates in the well-stirred turbulent regime (Briones et al. 2008). Products from combustion exit the reactor via 8 radial ports at the toroid inner diameter and through a 5-cm-diameter ceramic stack above the WSR. In this region, recirculation zones and bulk flow are reduced via the use of an alumina flow straightener, rested at the end of the exhaust and base of the stack(D. L. Blunck et al. 2015).

Liquid fuel is delivered to the vaporizer by two syringe pumps (Isco 500 D) operated in continuous flow mode. The piston flow meter accuracy is +/- 0.5%. The liquid fuel passes through a swirler and enters a heat exchanger, where the fuel reaches a temperature of 473 K at the inlet of the vaporizer. Heated fuel is introduced in the vaporizer with 10-20% of the total combustion air via an air-swirled atomizer nozzle containing heated air at 400 K and mass flow of 60 standard liters per minute (slpm). Remaining air at 489 K and mass flow of 440 slpm is added in the vaporizer as a coaxial stream(Scott Stouffer et al. 2007). Prior to entering the vaporizer, the airlines are filtered and monitored along with being controlled using two mass flow controllers, one rated at 1000 slpm and one rated at 75 slpm (Brooks Instruments) (S Stouffer et al. 2002). The accuracy for the mass flow controllers is rated at +/- 1% full scale and a repeatability of 0.25% of the flow rate. The flow controllers were measured and calibrated using sonic nozzles to allow for a more accurate measurement of the air flow rate. Electric, PID-controlled heaters preheat the incoming fuel and air streams. Flow rates of the fuel and air, paired with the temperature control of each, are used to control the incoming fuel-air mixture to the reactor. These flow rates ensure turbulent mixing and sonic velocities from the jets into the reactor (Vijlee 2014). The vaporizer used for the atmospheric WSR has been used in previous tests and was shown to safely and successfully mix the fuel with the air(S. D. Stouffer et al. 2005; Scott Stouffer et al. 2007). This strategy, using premixed and pre-vaporized fuel, eliminated physical complications associated with droplet combustion and established an ideal premixed combustion environment without physical complication.

A fixed custom spark igniter within the reactor initiates combustion. When testing with liquid fuel, the reactor was first brought to a stable thermal condition using a gaseous fuel (usually ethylene). Gaseous fuel flowrate into the WSR was controlled with a series of pressure regulators, to slowly reduce pressure, and mass flow controllers (Brooks Instruments). Introducing gaseous fuel before the liquid fuel allowed the reactor to effectively preheat for prevention of fuel condensation within the small jet ring passages. After operational temperatures were reached, the fuel was transitioned smoothly from the gaseous fuel to the given liquid fuel (Scott Stouffer et al. 2007).

B. Fuels

Four fuels tested in the current work are part of the National Jet Fuels Combustion Program (NJFCP). The NJFCP focus is to streamline the certification process for alternative jet fuels. Here the focus is to study the fundamental fuel kinetics and investigate the impact of alternative fuels on engine operability FOMs relative to reference fuels (Colket et al. 2016), enabling the process to be streamlined. FOMs such as cold start, altitude relight and LBO are key parameters considered in these fuels studies (Colket et al. 2016). The WSR is aimed to focus on the LBO FOM of engine operability in addition to determining the emissions footprint of the fuels in similar gas turbine combustor environments. The test fuels and their properties are shown in Table 1. These test fuels were characterized from the Combustion Rules and Tools for the Characterization of Alternative Fuels (CRATCAF) program and defined previously by OEMs (Colket et al. 2016). The category A fuels are intended to represent current jet fuels over a range of properties seen in current practice. Previous work has shown that flash point, aromatic content, and viscosity are of most impact for combustion behavior (Colket et al. 2016). A-2 and A-3 are fuels which exhibit 'average'/'worst' physical and chemical properties such as flash point, viscosity, aromatics, density, and derived cetane number respectively, giving an expectation envelope for conventional fuel combustion properties as they map to combustion behavior. C-1 and C-5 are alternative test fuels down selected by the NJFCP committee in 2015 from a total of six alternative jet fuel solvents (Colket et al. 2016). These fuel blends were selected to have properties near or exceed the limits acceptable jet fuels (i.e. viscosity, distillation curve, and chemical composition) (Colket et al. 2016). C-1 is composed of highly branched iso-paraffinic molecules with 12 and 16 carbon atoms, which have a low reactivity as exhibited by a derived cetane number of 17.1 (Colket et al. 2016). C-5 is a test fuel composed of two components, an isoparaffinic 10 carbon molecule and 1,3,5 trimethyl-benzene, which results in a flat boiling temperature/distillation curve (Colket et al. 2016). These two test fuels, C-1 and C-5, were intended to investigate effects of low cetane and narrow vaporization range of fuels on these combustor FOMs (Colket et al. 2016).

Table 1. Properties of the NJFCP Fuels Used for Testing in the WSR.

Fuel ID	A-2	A-3	C-1	C-5
POSF	10325	10289	12368	12345
Empirical Formula	$C_{11.4}H_{22.1}$	$C_{11.9}H_{22.6}$	$C_{12.6}H_{27.2}$	$C_{9.7}H_{18.7}$
AMW (g/mole)*	159	166	178	135
H/C Ratio	1.939	1.899	2.159	1.928
Stoichiometric Fuel/Air	0.0685	0.0687	0.0671	0.0686
Heat of Combustion (MJ/kg)	43.3	43	43.9	42.8
Density (g/cc)**	0.803	0.827	0.759	0.770
Derived Cetane Number (DCN)***	48.3	48.8	17.1	39.6

*Average molecular weight (AMW) measured using GCxGC
**Density measured using ASTM 4052, 15°C (kg/L)
***DCN measured using ASTM D5890(Colket et al. 2016)

Additional fuel surrogates were studied to investigate the effects of chemical structure on combustion performance and emissions and compared against current conventional fuels and fuel solvents. The surrogate fuels were chosen from the Strategic Environmental Research and Development Program (SERDP) aimed at studying the science of emissions of

alternative fuels. *n*-Dodecane was used as a base fuel, and commonly used as a second-generation fuel surrogate, emulating JP-8 flame speed. This surrogate provides a better representation of the n-alkane content in jet fuels. *m*-Xylene was chosen as an additive to the base surrogate fuel to study the effects of aromatic content and was chosen as 25% by volume to emulate the aromatic limit of JP-8. Molar carbon for the additive was kept constant to the aromatic content in the *n*-dodecane mixture, establishing a baseline for comparing surrogate performance. This fuel surrogate represents the *iso*-alkane hydrocarbon structure in jet fuels, and typically found in gas-to-liquid and FT fuels. Methylcyclohexane is used as the fuel surrogate for the cycloparaffins found in coal derived fuels. *n*-heptane is a straight chained hydrocarbon that mimics the light hydrocarbons in jet fuel and represents straight chain alkanes for a gasoline fuel surrogate. All surrogate mixtures in this paper were formulated to preserve the same carbon mole fraction as the *m*-xylene additive. Table 2 contains a list of relevant fuel properties pertaining to the WSR. Derived cetane number (DCN) for S-1, S-2, S-4, and S-5 were measured using the same ASTM standard as the NJFCP fuels. The DCN for S-3 was calculated using the summation of the volume fraction of the given fuel multiplied by its corresponding cetane number(Yanowitz et al. 2004).

Table 2. Properties of the Surrogate Fuels Used for Testing in the WSR.

Surrogate Blends	*n*-dodecane (61.8 mol%) / *m*-Xylene (38.2 mol%)	*n*-dodecane (61.8 mol %) / *iso*-Octane (38.2 mol%)	*n*-dodecane	*n*-dodecane (58.6 mol%) / Methyl-cyclohexane (41.4 mol%)	*n*-dodecane (58.6 mol%) / *n*-heptane (41.4 mol%)
Fuel ID	S-1	S-2	S-3	S-4	S-5
Empirical Formula	$C_{10.47}H_{19.9}$	$C_{10.49}H_{22.98}$	$C_{12}H_{26}$	$C_{9.93}H_{21.03}$	$C_{9.93}H_{21.86}$
H/C Ratio	1.900	2.191	2.167	2.118	2.201
Stoichiometric Fuel/air	0.0687	0.0669	0.0670	0.0673	0.0668
MW	145.84	149.12	170.31	140.45	141.28
Density (g/cc)	0.778	0.737	0.750	0.758	0.734
Derived Cetane* Number (DCN)	57.47	60.91	78.5	54.05	67.46

*DCN for S-1, S-2, S-4, S-5 measured using ASTM D5890(Colket et al. 2016)

C. Emissions and Instrumentation

A bare, linear-tracking, custom, type-B thermocouple (0.2mm diameter, platinum – 6% rhodium, platinum – 30% rhodium) without coating was used to measure reactor temperature. Measurements for temperature were taken at 0.25" from the outer wall of the reactor and were not corrected for radiation and other heat losses. Therefore, the gas temperature readings may not be accurate in an absolute sense, yielding lower temperatures than expected, but enable relative comparisons between conditions. The thermocouple location is within the uniform temperature region in the WSR and the temperature can therefore be taken as the average temperature in the reactor. A 0-5 psia pressure transducer was used to monitor the slight pressure increase in the reactor during operation. A maximum pressure of 5.5 kPa above ambient conditions was experienced during testing.

Exhaust samples were extracted using an oil-cooled probe (420 K) through a 1.4-mm-diameter orifice. The samples were passed through the probe which quenches the reactions, similar to quenching in a typical combustor (D. Blunck et al. 2012). The probe rested 5 mm above the wall of the lower toroid and is 90 degrees around the axis of the toroid from the thermocouple. Temperatures of the oil were kept constant at 420 K while sampling to minimize condensation in the sampling line.

Gaseous emissions were transported through a heated line containing a pump, filter and oven before entering the Fourier Transform Infrared (FTIR) analyzer. The heated lines and oven were maintained at 420 K by PID controllers. Flow entered and exited the FTIR at a constant temperature of 463 K where it was exhausted or sampled via charcoal tubes and gas bags. A sketch of the sampling methodology is shown in Fig. 3.

The FTIR system utilized in the current work was a MKS 2030 High Speed (5Hz) gas analyzer with a gas cell path length of 5.11 m and was used to measure the emissions from the WSR. This FTIR system allows major gaseous species to be detected online, while saving the spectra for later detailed investigation. The Gasoline Ethanol method, within the MKS software package, was employed to analyze the IR spectra and calculate emission concentration values. Measurement accuracy using this FTIR is +/- 2%. Carbon monoxide (CO), carbon dioxide (CO_2), water (H_2O), nitrogen oxide (NO), nitrogen dioxide (NO2), acetylene (C_2H_2), ethylene (C_2H_4), and formaldehyde (CH_2O) are among the many emissions that absorb infrared radiation and can be quantified using the method employed in the FTIR.

Following the FTIR was a valve to capture bag samples and enable offline measurement of C1-C12 species, primarily for C1-C4 hydrocarbons. An Agilent 6890/5973 GC-FID-MS (Gas Chromatography-Flame Ionization Detector-Mass Spectrometry) and Gas Pro Column was utilized to analyze emissions from the extracted samples. Capturing exhaust emissions through charcoal tubes was also employed as a sampling technique to obtain heavy hydrocarbon species, generally above C4 species. Another valve following the FTIR was used to draw these samples. A pump drew 1-liter exhaust emission samples at a rate of 1 liter per minute. Remaining gases pulled through the pump were exhausted through the hood where the WSR operates. Previous work has been performed using this method to extract hydrocarbons from jet-fuel emissions (Anneken et al. 2014). The tube was later extracted with carbon disulfide and the mass of each component was measured using an Agilent 7890 GC-FID and Gas Pro Column.

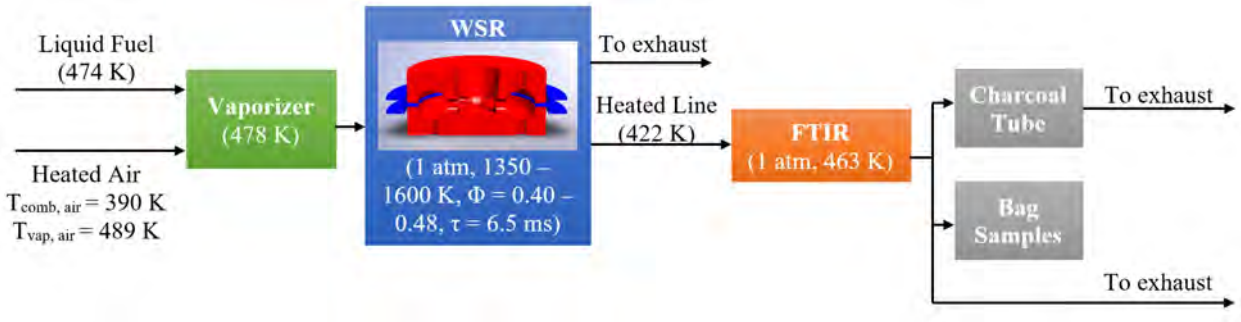

Figure 3. Experimental Schematic for WSR Emission Studies. A heated line takes the sample from the reaction region in the WSR to the FTIR. Charcoal tube and bag samples are taken after the FTIR before being exhausted.

During testing, online concentration measurements of various species were made using an FTIR. Roughly 95% of the carbon containing species were recovered by the FTIR at the higher equivalence ratios, reducing to roughly 92% near LBO as shown in Figure 4. The ~5% carbon deficit can be attributed primarily to FTIR measurement uncertainties. In addition, insufficient quenching during extractive sampling from the WSR can contribute to the uncertainty as sampled could react in the sampling lines and measurements are not representative of the actual combusting environment. The high percent of carbon recovered provides confidence as to the quantitative fidelity of species measured and the relative species concentration between fuels.

II. Experimental Conditions

The equivalence ratio was set by varying fuel flow rate. Each LBO measurement was initiated at an equivalence ratio of >0.48 where formaldehyde levels dropped below the detection limit (≈0 ppm). Equivalence ratios were reduced by keeping air constant and decreasing fuel flow until LBO where the flame extinguished. Heat loss at LBO conditions becomes too large and combustion is unstable and is not sustained. A drop in reactor temperature and change in noise generated by the reactor corresponded to a LBO(Scott Stouffer et al. 2007).

Temperatures at these conditions were well below the maximum operating temperature of the ceramic. This enabled durability for testing with a single build of the reactor and prevented cracking. Premixed fuel and air coming into the jet ring was held at a constant temperature of 460 K, which is in the typical combustor range of 200-900 K (McAllister, Chen, and Fernandez-Pello 2011; Colket et al. 2016). Reactor temperatures during the test varied between 1350 K and 1500 K based on the heat of combustion of each fuel and heat loss from the system. The heat loss from the system was estimated at 5%

using the ceramic reactor (J. Blust, Ballal, and Sturgess 1997). The health of the ceramic reactor was monitored by measuring the temperature of the jet ring. When a crack formed, a large asymmetric temperature profile was observed in the jet ring.

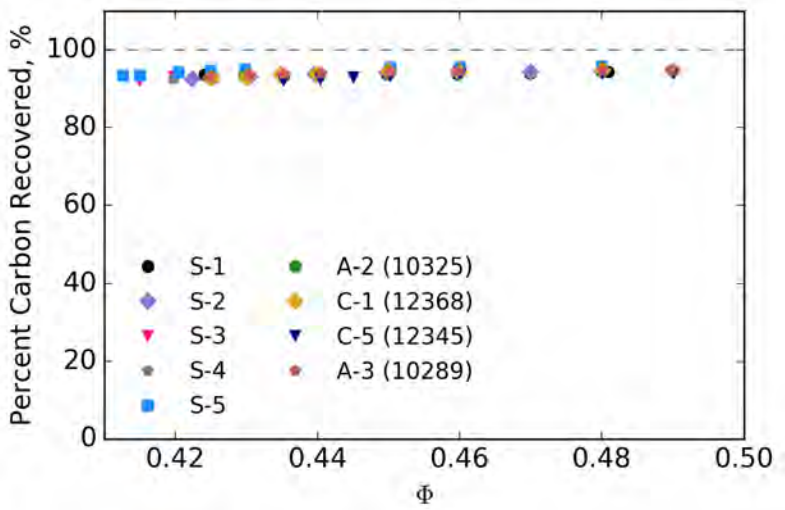

Figure 4. Carbon recovery from the species captured via online FTIR sampling. A decrease in percent carbon recovered is seen as equivalence ratio (Φ) is decreased. This signifies that intermediate species are produced and some are not recovered using this emissions measurement technique. The high percentage of carbon recovered provides confidence that this method captures emissions adequately to yield quantitative results.

Towards leaner conditions, the jet ring temperature profile varied a maximum of approximately 2% (10 K) peak-to-peak, indicating the ceramic reactor remained free from cracks.

Global reacting residence time for the experiments was 6-7 ms. Bulk residence time was calculated using the volume of the reactor, the flow rates of the fuel and air, and the density of the mixture under reacting conditions. Variations in residence time were primarily a result of changes in reactor temperature and fuel mass flow since change in reactor pressure and molecular weight are small(Scott Stouffer et al. 2007). At most points throughout each experiment, the reactor was allowed to reach a thermal steady state and then held at constant flow and thermal conditions for more than 12 minutes. Non-emission data was captured from a running average of approximately 12 seconds every 3 minutes.

FTIR measurements, recorded continuously at 5 Hz, were averaged over the 12 second running average period for each sample, while gas bags and charcoal tubes were taken at the last point of the sampling process for each equivalence ratio. This holistic sampling process captured major and minor species throughout the duration of the experiment, while ensuring steady state conditions for the bag and charcoal tube samples.

For points at or near LBO, the reactor could not be held constant for 12 minutes because of the tendency to blow off. At these near-LBO conditions, a non-steady-state condition between the wall and gas temperatures may be responsible for some scatter in the WSR temperature data. Once blow off occurred, the reactor was re-ignited by reducing air and fuel flow rates. Once steady state conditions were reached at the start of the blow off test, a second test was conducted in a similar fashion. As experienced in previous experiments, hysteresis does exist in approaching LBO if there is insufficient time for the reactor to reach a steady-state temperature at each condition. Leaner conditions can be reached if the reactor walls are relatively hot, resulting from a rapid decrease in equivalence ratio. If LBO is approached more slowly, the walls have sufficient time to cool to the local gas temperature and, therefore, LBO is experienced at higher equivalence ratios(Vijlee 2014). Increments were small while decreasing the fuel flow, thus reducing the chance for hysteresis. Previous literature showed variance in blow off temperature of +/- 50 K(Vijlee 2014) and uncertainty of blow off equivalence ratio near 2% (D. L. Blunck et al. 2015). Based on the sonic nozzle calibration and the self-consistency between the two or more LBO tests per fuel, the uncertainty in equivalence ratio was estimated as Φ +/- ~0.0025. The primary parameter controlling the uncertainty was the repeatability of the air mass flow controllers based on the operating conditions.

Table 3. Operating conditions using the WSR

Pressure (atm)	1
Inlet Temperature (K)	460
Reactor Temperature (K)	1350 – 1600
Bulk Residence Time (ms)	6 – 7
Mass Flow Air (g/min)	600
Equivalence Ratio	0.425 – 0.49

III. Results and Discussion

D. LBO

LBO occurs when the flame cannot be sustained because of either fluid dynamic or chemical processes. In the WSR, LBO is most sensitive to chemical processes associated with heat release, and ideally insensitive to mixing and fluid processes. Experimental results are shown in the figures below for the four NJFCP fuels and the five surrogate mixtures. Figure 6 shows the effect of lowering the fuel flow, hence lowering the equivalence ratio. The reactor trends to decrease linearly with leaner conditions. C-1 shows to have the least resistance to LBO, having the highest Φ at LBO, while the S-3 and S-5 straight chained alkane surrogates trended to have the most resistance to LBO. LBO occurs at the lowest recorded equivalence ratio of roughly 0.414, In contrast, the C-1 fuel exhibits LBO at the highest recorded equivalence ratio.

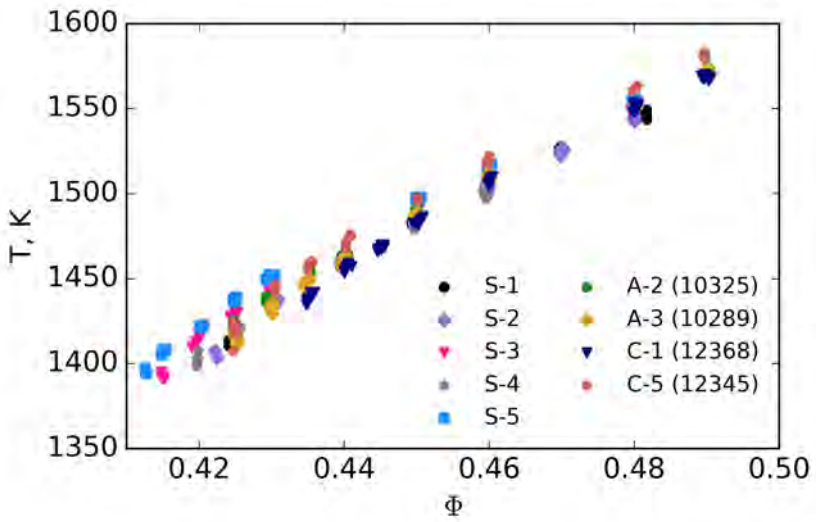

Figure 6. Reactor temperature (K) as a function of Φ for the fuels. Points represent the samples taken at each equivalence ratio tested. As leaner conditions are approached, the reactor temperature lowers linearly to the point where combustion cannot be sustained, corresponding to LBO. C-1 has the least resistance to LBO, having the highest Φ at LBO, while S-3 and S-5, straight chain alkane blends, trended to have the most resistance to LBO.

Since the WSR is operating in a lean, premixed, prevaporized combustion environment, the combustion property targets (CPTs) can be investigated as it relates to LBO. These CPTs, H/C ratio, MW, Threshold Sooting Index (TSI), and derived cetane number (DCN), have shown to sufficiently match combustion behaviors in pre-vaporized environments for petroleum-derived and synthetic jet fuels(Won, Veloo, Santner, Ju, Dryer, et al., n.d.). H/C ratio is used as it relates energy density of a particular fuel, as well as describes the composition and the distribution of radicals produced form combustion processes.(Won, Veloo, Santner, Ju, Dryer, et al., n.d.) LBO is shown below in Figure 7 as a function of H/C ratio. For each fuel, the last sampled condition immediately preceding LBO was averaged for both runs. If LBO occurred during sampling, the mean LBO was calculated using the average of those samples with the previous full sample preceding LBO. The uncertainty bars represent the uncertainty based on the air and mass flow rates. Towards the left of Fig. 7, mean LBO was nearly identical at ~0.425.

This is a result of the roughly 0.005 (~1%) step size in equivalence ratio, used to obtain stable points for emissions capture near LBO. The mean Φ represents roughly the last point captured for emissions data before blow-off occurs. However, based on the given fuels and their LBO conditions, there exists a distribution of fuels which lie outside the bounds of the uncertainty estimated and are statistically significant. Based on the current distribution of data, there doesn't exist a correlation of LBO for the given fuels with varying H/C ratios. Molecular weight was also plotted as a function of Φ for the fuels. This property corresponds to the reactivity of the fuel via the normal and branched alkanes in the fuel and also does not correlate with LBO, as shown in Figure 8.

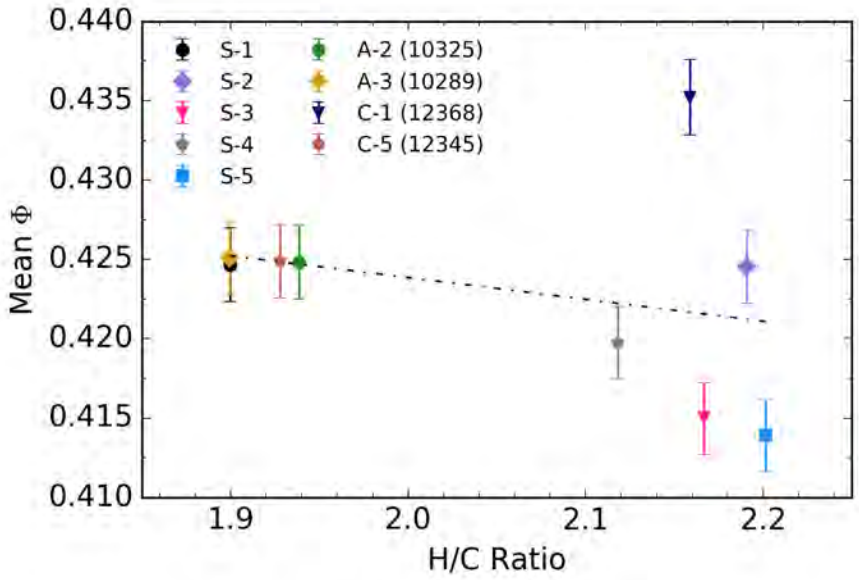

Figure 7. Mean Φ as a function of H/C Ratio. Points represent the average of the data at each equivalence ratio, while the error bars represent the uncertainty of the measured and averaged Φ. (Eq. -0.01374x+0.45134 = y, R^2 = 0.0849).

TSI, another CPT, correlates the competition of aromatic molecules and highly-branched alkanes with the radical pool and is important as it describes the sooting tendency of a fuel(Won, Veloo, Santner, Ju, Dryer, et al., n.d.). This correlation of reactivity of a fuel varies inversely with TSI, using this methodology(Won, Veloo, Santner, Ju, Dryer, et al., n.d.). Values were estimated for the given surrogate fuels using linear combination of each mole percent of components by their corresponding TSI.(Mensch 2009) Based on Fig. 9 below, there doesn't exist to show a correlation among the TSI and LBO. Although there is no apparent correlation, the effect of aromatic content in S-1 shows to have an effect on increasing the TSI, where further investigation on determining the TSI of the conventional and alternative fuels would be useful.

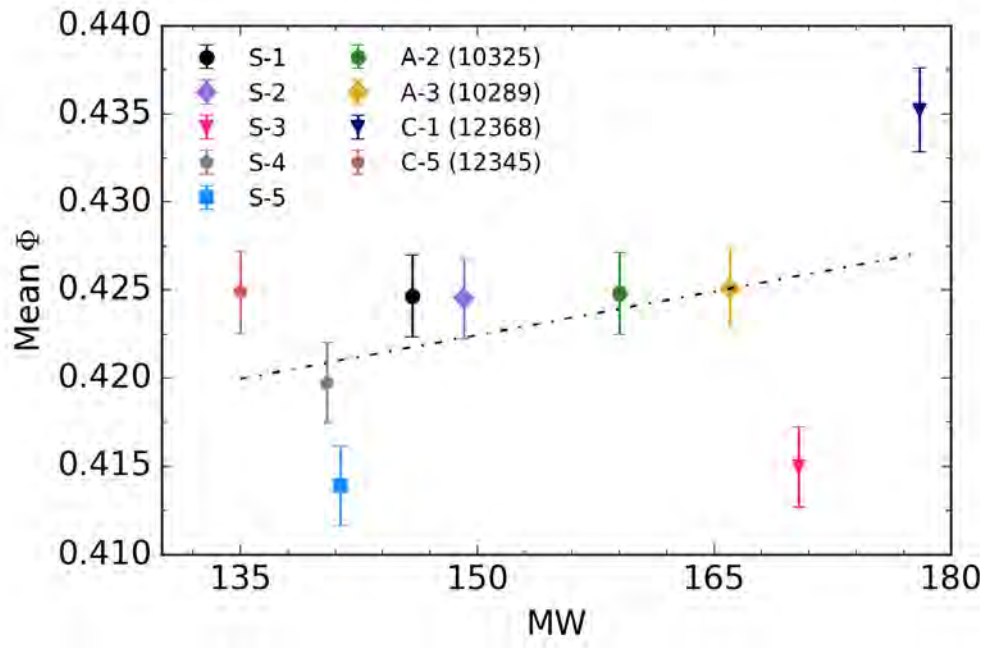

Figure 8. Mean Φ as a function of molecular weight. Points represent the average of the data at each equivalence ratio, while the error bars represent the uncertainty of the measured and averaged Φ. (Eq. 1.652E-04x+0.0.3977 = y, R^2 = 0.1527).

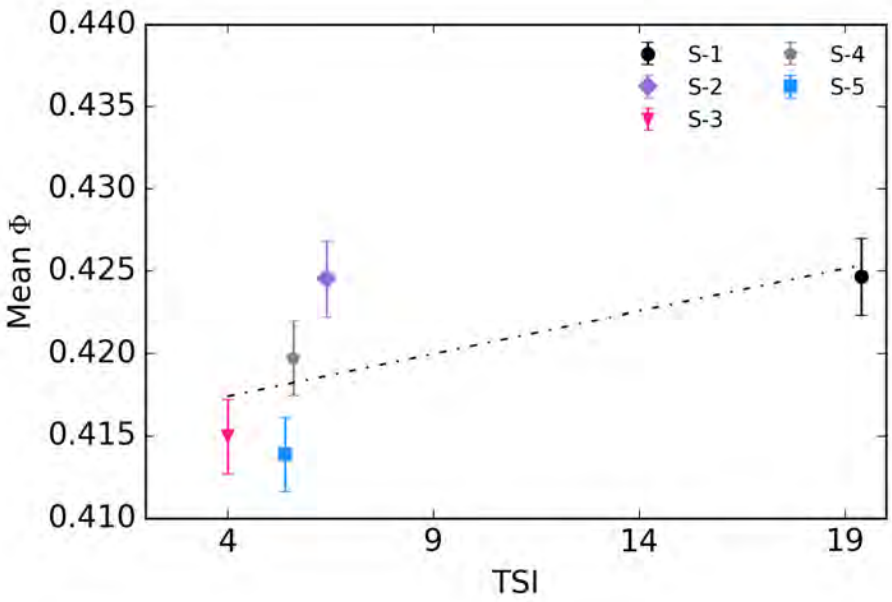

Figure 9. Mean Φ as a function of TSI. Points represent the average of the data at each equivalence ratio, while the error bars represent the uncertainty of the measured and averaged Φ. (Eq. 5.158E-04x+0.41536= y, R^2 = 0.41134).

Figures 10 and 11 display the effects of LBO with DCN and radical index, respectively. Based on the given data set and Fig. 10 below, there appears to be a functional dependence on cetane number of the fuel when comparing to LBO. Low derived cetane numbers correspond to a longer ignition delay, which is a potential attribute to the LBO difference seen in the given fuels set. This trend can yield understand towards this parameter and potential implications in gas turbine combustors. Also, the tested data only contains two emissions profiles per fuel, yielding some additional uncertainty.

Radical indices were approximated from literature (Won, Veloo, Santner, Ju, and Dryer, n.d.; Won, Dooley, et al., n.d.). S-1 and S-2 were estimated using the radical indices of the surrogate mixture components multiplied by the corresponding mole percentage. The radical index for *m*-xylene was approximated between toluene and 135TMB assuming a linear correlation(Won, Dooley, et al., n.d.). S-3 and S-5 mixture was approximated at 1, being of n-paraffinic structure, where A-2 and C-1 were assumed to be similar to JP-8 and IPK, respectively(Won, Veloo, Santner, Ju, and Dryer, n.d.). A-3 was assumed to be of JP8(Won, Veloo, Santner, Ju, and Dryer, n.d.), even though A-3 contains more iso-paraffins. The radical indices for *iso*-octane and JP8 were near identical and used as a rough estimate to investigate potential correlations of LBO with radical index. A radical index for m-xylene was approximated between the values of toluene and 135TMB, assuming a linear relationship between the values. These preliminary approximations show a correlation with LBO as seen in Fig. 8. The higher radical index indicates a larger radical pool in which the radicals aid in sustaining combustion, tending to blow out at leaner conditions. Towards the left portion of Fig. 8, C-1 trends to blow out at a higher equivalence ratio, where it has the lowest assumed radical index. Behavior experienced in Figure 10 and 11 show a similar trend with LBO and indicate dependence on DCN and on radical index. This knowledge, along with the ability to create surrogates to vary one of the characteristics (DCN or RI), can assist in further understanding the extinction and LBO behavior of a given fuel.

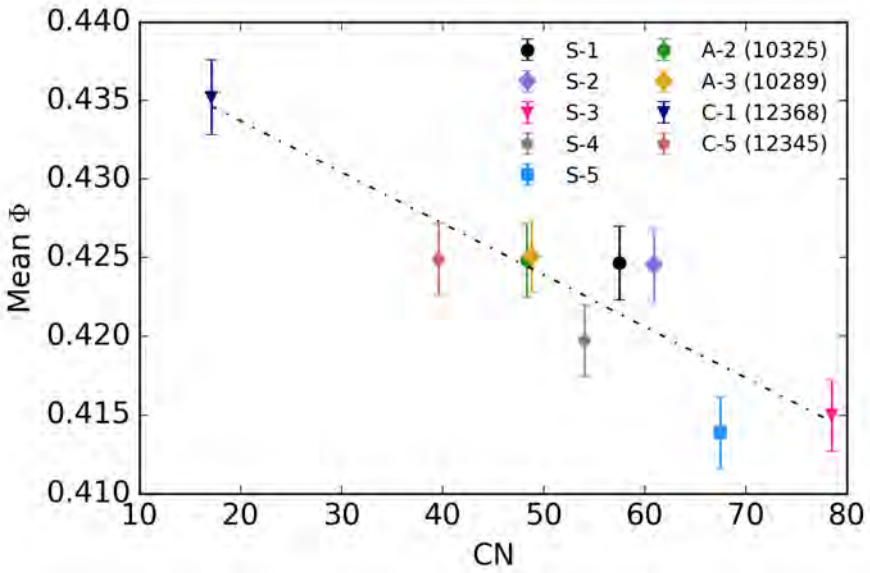

Figure 10. Mean Φ as a function of DCN. Points represent the average of the data at each equivalence ratio, while the error bars represent the uncertainty of the measured and averaged Φ. (Eq. -3.268E-4x+0.44023 = y, R^2 = 0.8097). Percent Difference in Φ from S-5 to C-1 is ~5%.

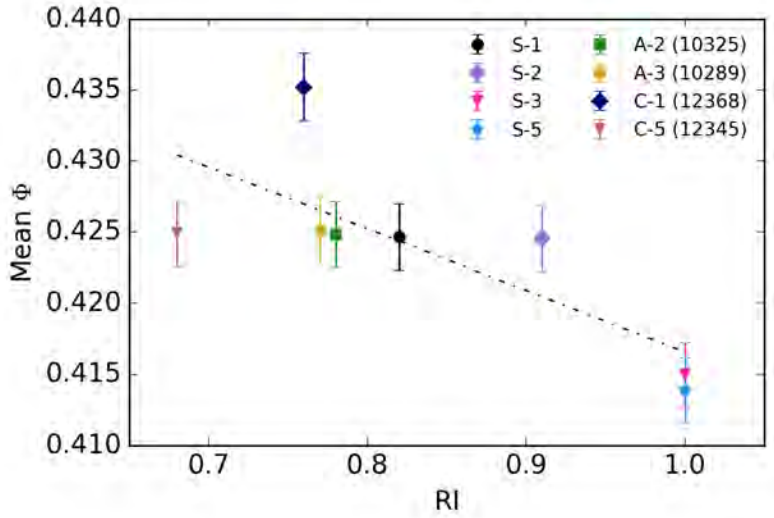

Figure 11. Mean Φ as a function of Radical Index. Points represent the average of the data at each equivalence ratio, while the error bars represent the uncertainty of the measured and averaged Φ. (Eq. -0.04328x+0.4599= y, R^2 = 0.585)

E. Emissions Profile

As described in the previous section, the fuel chemistry can play an important role in LBO. For instance, surrogate fuels may have a similar heat of combustion and derived cetane number, S-1 and S-2, but different radical index, 0.82 and 0.91 respectively. This difference in radical index can be caused by the presence of radical-promoting reactions and/or radical-trapping reactions that occur as a result of the fuel chemistry, in this case aromatic or iso-alkane content. The WSR is specifically designed to provide relevant information on the effects of fuel chemistry on combustion emissions and stability under conditions similar to those in typical combustors, specifically the primary and secondary zones. This approach enables fuel-specific emissions fingerprints to be generated while approaching LBO. The species produced under these conditions are highly sensitive to the specific fuel chemistry and, therefore, provide a sensitive metric for developing reduced-order chemical mechanisms. These emissions profiles can also be utilized along with the DCN, radical index, H/C ratio, MW, and TSI to determine the chemical property dependencies driving LBO in various experimental arrangements.

Figure 12 shows the major carbon-containing combustion products, as a function of equivalence ratio, produced during testing of the WSR. CO and CO_2 compose approximately 99.9% and 99% of the total carbon count in the sampled emissions at the areas of higher equivalence ratios and towards the leanest conditions, respectively. As the fuel rate decreases to leaner conditions, less CO_2 is produced allowing for intermediate species to be formed as a result of incomplete combustion and thus incomplete conversion to CO_2. As observed in Figure 12(a), CO_2 produced from the C-1 fuel and the S-2 surrogate mixture are similar yet follow a distinctly different curve towards LBO relative to the other fuels, although C-1 LBO occurs at a higher equivalence ratio. In contrast, CO is increased as LBO is approached for all fuels. The two bounding fuels are S-5 which produced the most CO_2 and least CO and C-1 which produced the least CO_2 and most CO for a given equivalence ratio.

Although the carbon deficit in the CO_2 production between C-1 and S-5 was primarily recovered in the form of CO, the total carbon count for the six largest carbon containing species is shown in Figure 13. It is clear that at Φ = 0.435, C-1 produces an order of magnitude more formaldehyde than any other fuel, in addition to increased concentrations of ethylene, acetylene, methane, and isobutene.

Formaldehyde production as a function of equivalence ratio is displayed in Figure 14 for all fuels. This species is particularly important as it is a key intermediate species in the oxidation of hydrocarbons and can significantly shorten the ignition delay time of fuel/air mixtures. Specifically, previous work has shown that many hydrocarbon species can be linearly related to formaldehyde production, regardless of fuel type(D. L. Blunck et al. 2015), although C-1 tends to be the outlier. Methane recorded from the FTIR is seen to exhibit that linear relationship as a function of formaldehyde, as observed in the same figure. For this reason, species production in all subsequent figures are plotted against both equivalence ratio and formaldehyde.

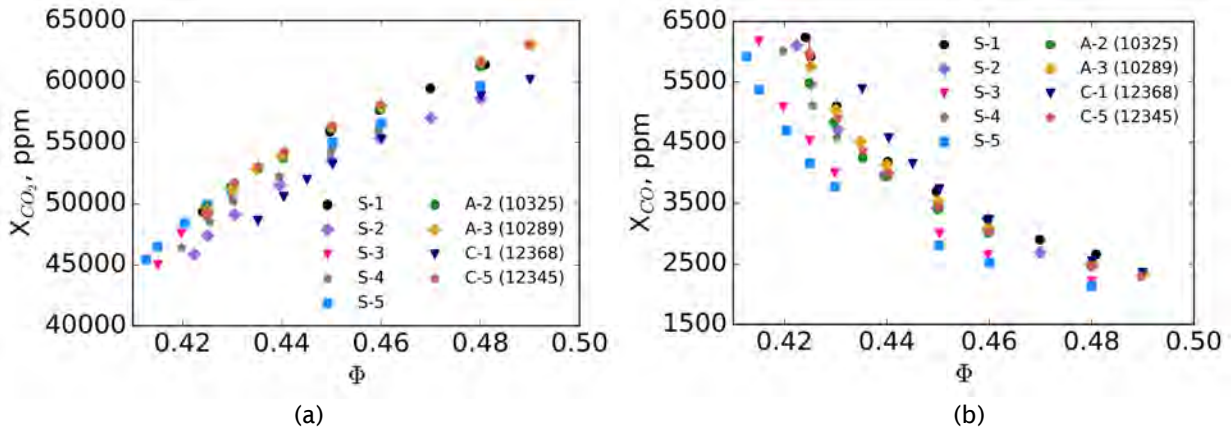

Figure 12. CO_2 (a) and CO (b) as a function of equivalence ratio (Φ). Points represent the average of the data at each equivalence ratio, while the error bars represent one standard deviation. Trends in decreasing CO_2 and increasing CO while approaching leaner conditions is expected, signifying losses in combustion efficiency towards LBO.

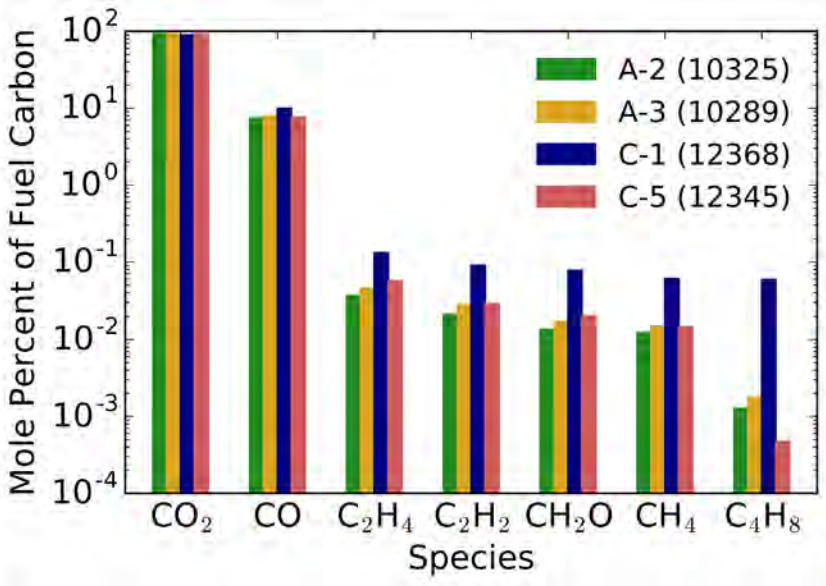

Figure 13. Mole percent of fuel carbon on the given species at Φ = 0.435. C-1 appears to be most distinguished, as it is at the leanest condition before LBO, producing more intermediate species.

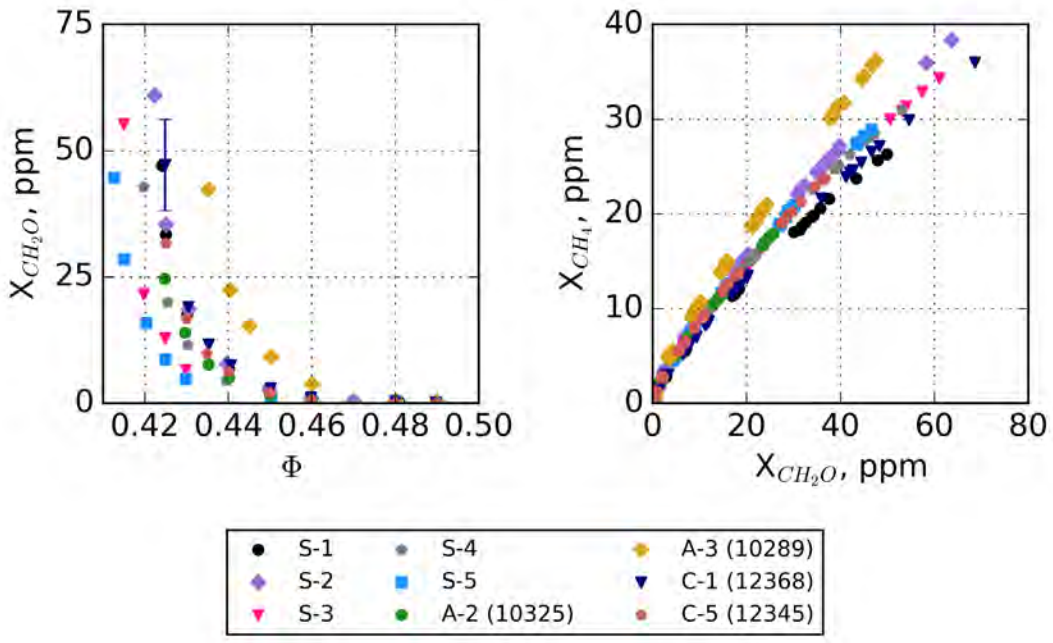

(a) (b)

Figure 14. Formaldehyde (CH_2O) as a function of equivalence ratio (Φ) and methane (CH_4) as a function of formaldhyde production. Points represent the average of the data at each equivalence ratio, while the error bars represent the maximum standard deviation in the reported set.

Figure 15 and 16 displays ethylene and acetylene production towards lean low off conditions using the online FTIR method, respectively. Figures 17 and 18 show the isobutene production using both the FTIR and charcoal tube methodologies of capturing emissions.

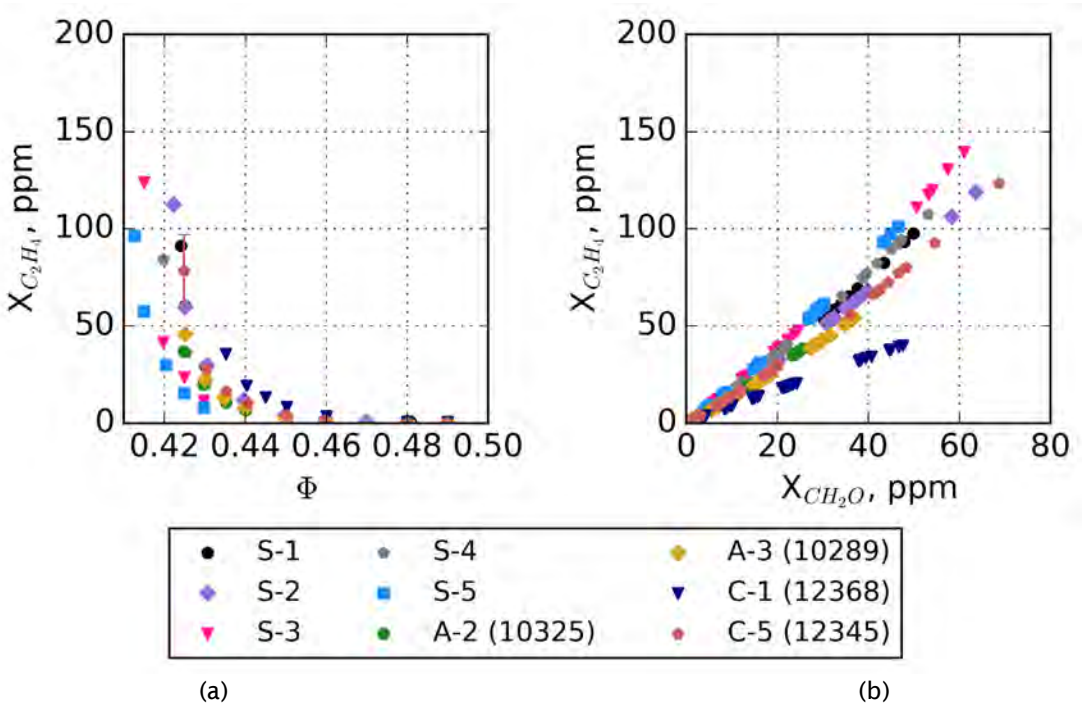

Figure 15. Ethylene (C_2H_4) as a function of equivalence ratio (Φ) sampled from the FTIR. (a) Points represent the average of the data at each equivalence ratio, while the error bars represent the maximum standard deviation in the reported set. (b) Points represent the all the sampled data as a function of formaldehyde.

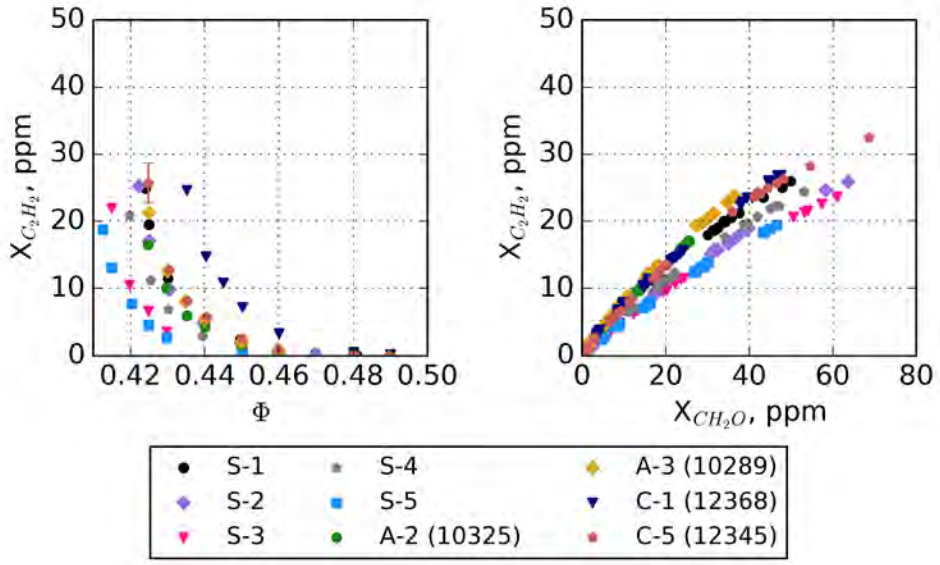

(a) (b)

Figure 16. Acetylene (C_2H_2) as a function of equivalence ratio (Φ) sampled from the FTIR. (a) Points represent the average of the data at each equivalence ratio, while the error bars represent the maximum standard deviation in the reported set. (b) Points represent the all the sampled data as a function of formaldehyde.

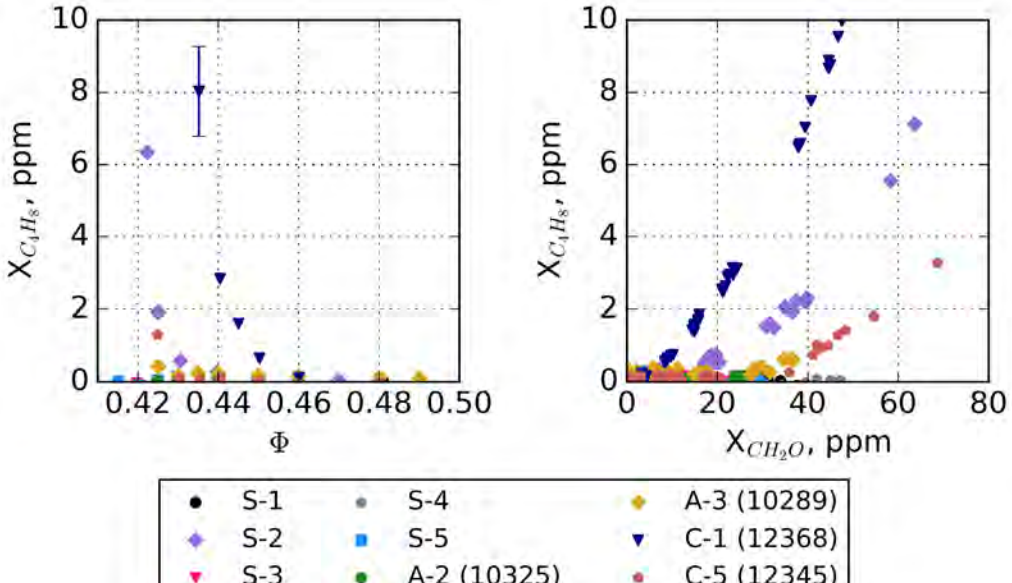

(a) (b)

Figure 17. Isobutene (C_4H_8) as a function of equivalence ratio (Φ) sampled from the FTIR. (a) Points represent the average of the data at each equivalence ratio, while the error bars represent the maximum standard deviation in the reported set. (b) Points represent the all the sampled data as a function of formaldehyde.

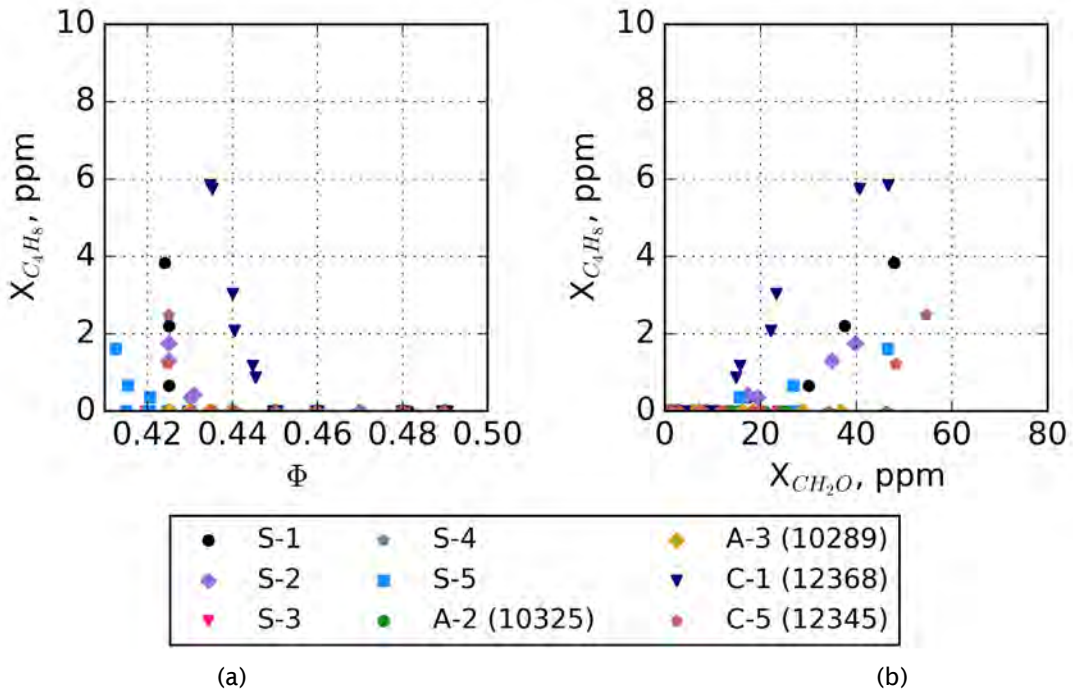

Figure 18. Isobutene (C_4H_8) as a function of equivalence ratio (Φ) from the charcoal tube methodology. (a) Points and samples taken during testing at the end of each condition as a function of equivalence ratio. (b) Points and samples taken during testing at the end of each condition as a function of formaldehyde.

Additional efforts were made with the Well-Stirred Reactor to refine the LBO measurements. The previous procedure towards LBO provided the ability to obtain steady state emissions measurements within the WSR approaching LBO. A new technique was integrated into the data acquisition system to decrease the fuel flow rate automatically, keeping the air flow rate constant, as in previous experiments. This procedure allows for multiple LBO measurements to be made within a single test run per fuel. The fuels tested with this new approach were selected to stress-test the DCN hypothesis.

Table 4. Fuels tested in the WSR using the new LBO procedure (*S-1 from Won, et. al. 2017).

Name	DCN	Nomenclature
Dodecane (n-C12)	74	C_{12}
Surrogate Fuel 1*	50.4	S-1
NJFCP A-2	48.3	A-2
NJFCP C-4	28	C-4
75.5% 135 TMB, 24.5% n-C12	19.08	J-1
NJFCP C-1	17.1	C-1

Dodecane was selected on the upper bound of the DCN that was tested, where C-1 was the lower bound to the DCN. Additional fuels tested as part of the NJFCP program include A-2 and C-4. A surrogate fuel to emulate the characteristics of NJFCP A-2 and given combustion property targets was additionally selected, named S-1 (Won, et. al., 2017). An additional fuel, J-1, comprised of 1,3,5 trimethylbenzene (135 TMB) and dodecane, was added to investigate the effect of radical index at a lower DCN to investigate radical pooling effects towards extinction, as previously discussed. Number of ramp rates performed with LBO testing was 13 for the fuels except Dodecane (5 samples for Dodecane). A lean equivalence ratio usually around 0.45, above the extinction limit, was established before decreasing the equivalence ratio 0.001 (~0.05 mL/min using

the Isco pumps for the fuel) every 4 seconds. This ramp rate was chosen to reduce wall effects on LBO that are around the outer surface of the reactor and to establish a steady decrease in reactor temperature as minimizing transient effects are optimal. LBO is reached when there exists a significant temperature drop from the previous value. The tradeoff with this approach is that emissions sampling was reduced to only the FTIR online sampling, as the duration of capturing the emissions using the gas bags and charcoal tube measurements takes longer than the ramp rate utilized in the experiment. Data acquisition from the 5Hz online MKS 2030 HS gas analyzer was averaged and matched to the time histories of the other experimental data captured (0.5 Hz). The gas analyzer was the same as previously used in the other experiments.

LBO and emissions towards LBO are presented in the figures below. Fig. 17 shows the linear correlation between the LBO and DCN of the corresponding fuels. Error bars on the figure represent the standard deviation of the LBO J-1 and C-1 both yield similar LBO values, although the chemical compositions are vastly different, and their radical index is different. High percentages of aromatics as seen in the J-1 fuel also decreases the resistance to LBO, whereas the C-1 fuel is comprised of the iso-paraffinic compounds. S-1 and A-2 have been observed to have similar LBO values, as expected. Dodecane is also seen to have the lowest LBO value and having the highest DCN value. Emissions profiles for ethylene and isobutene are plotted as functions of equivalence ratio and formaldehyde. An exponential increase in emissions is seen similarly to the other experiment performed in the WSR. As leaner conditions are approached towards LBO, there is a reduction in combustion efficiency, where incomplete reactions are occurring, not converting the fuel to the CO2 and H2O and is seen in the figures. S-1 emissions trends yield similarity to A-2, further establishing similarity between a surrogate fuel mixture comprised of 3 compounds to a jet-fuel comprised of multiple components. Emissions as a function of formaldehyde has been presented as formaldehyde is a marker for the incomplete combustion and for other pollutant emissions to be generated. Non-linearity is presented towards higher amounts of formaldehyde production and shows the instability towards the extinction process.

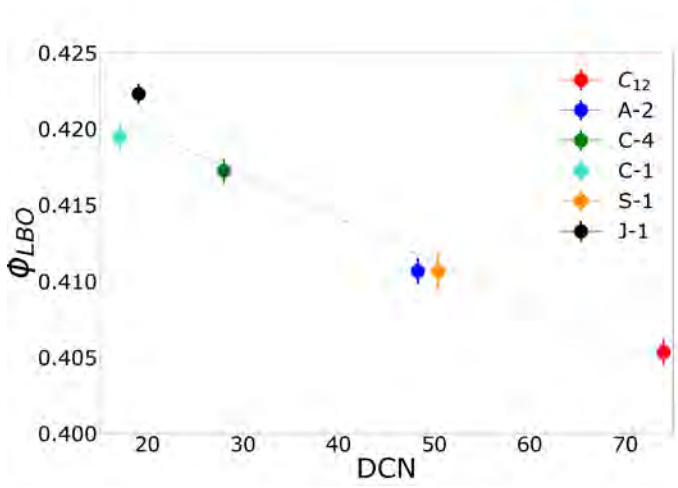

Figure 19. LBO as a function of DCN. The R^2 value based off a linear fit is 0.9581 (-2.8466E-04*DCN + 0.42552 = ϕ_{LBO}).

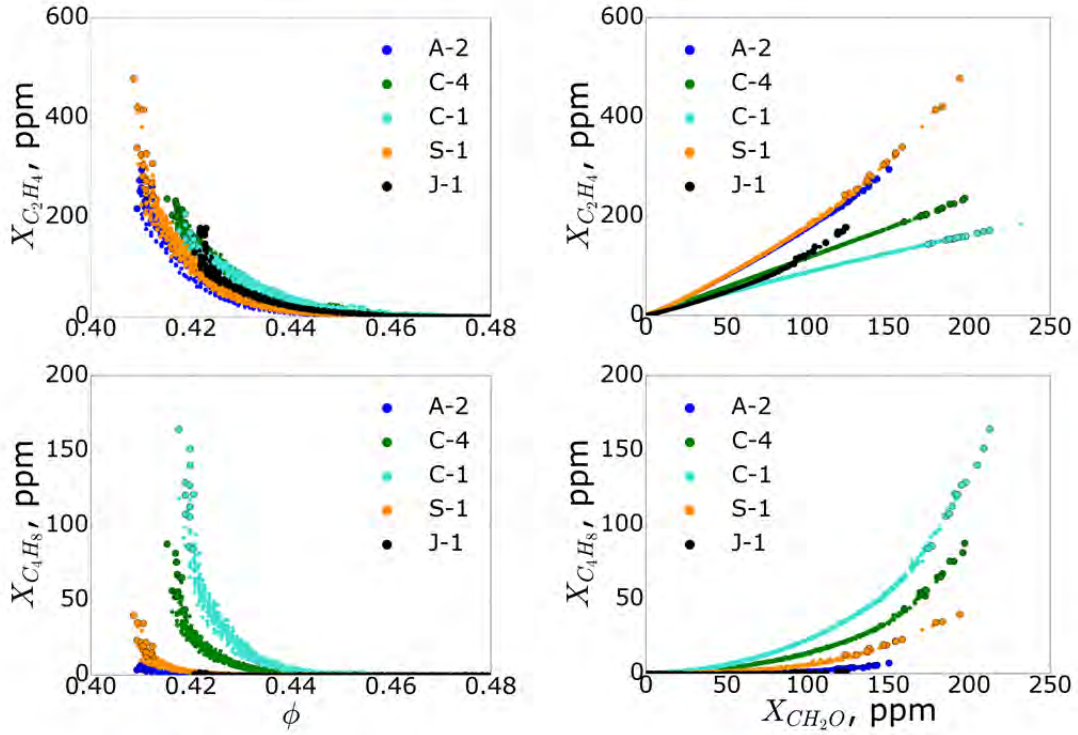

Figure 20. Emissions v. ϕ_{LBO} for the WSR. (R side) Emissions v. CH_2O for the WSR. A-2 and S-1 data trends similarly with each other.

IV. Conclusions

A WSR operating under fuel-lean conditions was utilized to measure performance and gaseous emissions characteristics of conventional and alternative aviation fuels. LBO was also explored under the same loading condition to determine the difference in LBO with different fuels. The experiment showed:

1. Recovery of carbon captured is favorable from the FTIR and can provide encouraging results with the current species captured.
2. The C-1 test fuel is least resistant to LBO as the conditions for which it occurs happens at a higher equivalence ratio and at a higher reactor temperature than the other tested fuels.
3. LBO shows a strong correlation with derived cetane number, which describes a need for investigating fuel dependency on combustor design.
4. As conditions approach LBO, intermediate species are produced that have a correlation between formaldehyde productions. These conditions towards LBO signify decreased combustion efficiency as more intermediate species are seen.
5. S-1 yielded similar performance characteristics in the WSR as A-2.

Continued analysis will enable investigation of chemical kinetic pathways specific to each fuel, which then establishes an understanding of the chemical effects in a lean, premixed, pre-vaporized environment, a relevant area of interest for future gas turbine combustor design. The WSR represents an ideal, premixed, pre-vaporized combustor. It is used to study fuel chemistry effects on emissions and LBO. Thus, we believe the knowledge gained from the fuel effects in our LBO and emissions studies have relevance to current and future combustion systems.

References

AJF-IWG. 2016. "Federal Alternative Jet Fuels Research and Development Strategy." OSTP.

Anneken, David, Richard Striebich, Matthew J. DeWitt, Christopher Klingshirn, and Edwin Corporan. 2014. "Development of Methodologies for Identification and Quantification of Hazardous Air Pollutants from Turbine Engine Emissions." Journal of the Air & Waste Management Association 65 (3): 336–46. doi:10.1080/10962247.2014.991855.

Blunck, D, J Cain, Rc Striebich, Sz Vijlee, Sd Stouffer, and Wm Roquemore. 2012. "Fuel-Rich Combustion Products from a Well-Stirred Reactor Operated Using Traditional and Alternative Fuels." Central States Combustion Meeting, 1–8.

Blunck, David L., Steven Zeppieri, Justin T. Gross, Scott Stouffer, and Meredith B. Colket. 2015. "Hydrocarbon Emissions from a WSR Near Lean Blow-Off." In 53rd AIAA Aerospace Sciences Meeting, 1–12. Kissimmee, FL: American Institute of Aeronautics and Astronautics. doi:10.2514/6.2015-0415.

Blust, J., D. Ballal, and G. Sturgess. 1997. "Emissions Characteristics of Liquid Hydrocarbons in a Well Stirred Reactor." In 33rd AIAA/ASME/SAE/ASEE Joint Propulsion Conference & Exhibit, 1–18. Seattle, WA: AIAA. doi:10.2514/6.1997-2710.

Blust, J. W., D R Ballal, and G J Sturgess. 1999. "Fuel Effects on Lean Blowout and Emissions from a Well-Stirred Reactor." Journal of Propulsion and Power 15 (2): 216–23. doi:10.2514/2.5444.

Briones, AM, B Sekar, J Zelina, R Pawlik, and SD Stouffer. 2008. "Numerical Modeling of Combustion Performance for a Well-Stirred Reactor for Aviation Hydrocarbon Fuels (AIAA-2008-4565)." In 44th AIAA/ASME/SAE/ASEE Joint Propulsion Conference & Exhibit, 1–19. Hartford, CT: AIAA. doi:doi:10.2514/6.2008-4565.

Colket, Meredith B., Joshua S. Heyne, Mark Rumizen, James T. Edwards, Mohan Gupta, William M. Roquemore, Jeffrey P. Moder, Julian M. Tishkoff, and Chiping Li. 2016. "An Overview of the National Jet Fuels Combustion Program." In AIAA SciTech. AIAA SciTech. San Diego, CA: American Institute of Aeronautics and Astronautics. doi:doi:10.2514/6.2016-0177.

FAA. 2012. "U.S. Aviation Greenhouse Gas Emissions Reduction Plan," no. June: 1–16.

Karalus, Megan. 2013. "An Investigation of Lean Blowout of Gaseous Fuel Alternatives to Natural Gas." University of Washington.

Manzello, Samuel L., David B. Lenhert, Ahmet Yozgatligil, Michael T. Donovan, George W. Mulholland, Michael R. Zachariah, and Wing Tsang. 2007. "Soot Particle Size Distributions in a Well-Stirred Reactor/plug Flow Reactor." Proceedings of the Combustion Institute 31 (1): 675–83. doi:10.1016/j.proci.2006.07.013.

McAllister, Sara, Jyh-Yuan Chen, and A. Carlos Fernandez-Pello. 2011. Fundamentals of Combustion Processes. Mechanical Engineering Series. New York, NY: Springer New York. doi:10.1007/978-1-4419-7943-8.

Mensch, Amy. 2009. "A Study on the Sooting Tendency of Jet Fuel Surrogates Using the Threshold Soot Index." M.S. Thesis. The Pennsylvania State University.

Nenniger, J.E., A. Kridiotis, J. Chomiak, J.P. Longwell, and A.F. Sarofim. 1984. "Characterization of a Toroidal Well Stirred Reactor." Twentieth Symposium (International) on Combustion. The Combustion Institute, 473–79.

Stouffer, S, R C Striebich, C W Frayne, and J Zelina. 2002. "Combustion Particulates Mitigation Investigation Using a Well-Stirred Reactor." In 38th AIAA/ASME/SAE/ASEE Joint Propulsion Conference and Exhibit, 1–11. Indianapolis, IN: American Institute of Aeronautics and Astronautics. doi:10.2514/6.2002-3723.

Stouffer, Scott D, Dilip R Ballal, Joseph Zelina, Dale T Shouse, Robert D Hancock, and Hukam C Mongia. 2005. "Development and Combustion Performance of High Pressure WSR and TAPS Combustor." In 43rd AIAA Aerospace Sciences Meeting and Exhibit, 1–9. Reno, NV: American Institute of Aeronautics and Astronautics. doi:10.2514/6.2005-1416.

Stouffer, Scott, Robert Pawlik, Garth Justinger, Joshua Heyne, Joseph Zelina, and Dilip Ballal. 2007. "Combustion Performance and Emissions Characteristics for a Well Stirred Reactor for Low Volatility Hydrocarbon Fuels." In 43rd AIAA/ASME/SAE/ASEE Joint Propulsion Conference and Exhibit, 1–12. Cincinnati, OH: American Institute of Aeronautics and Astronautics. doi:10.2514/6.2007-5663.

Vijlee, Shazib Z. 2014. "Effects of Fuel Composition on Combustion Stability and NOX Emissions for Traditional and Alternative Jet Fuels." University of Washington.

Won, Sang Hee, Stephen Dooley, Frederick L Dryer, and Yiguang Ju. n.d. "Radical Index on Extinction Limits of Diffusion Flames for Large Hydrocabon Fuels." doi:10.2514/6.2011-318.

Won, Sang Hee, Peter S Veloo, Jeffrey Santner, Yiguang Ju, and Frederick L Dryer. n.d. "Comparative Evaluation of Global Combustion Properties of Alternative Jet Fuels." doi:10.2514/6.2013-156.

Won, Sang Hee, Peter S Veloo, Jeffrey Santner, Yiguang Ju, Frederick L Dryer, and Stephen Dooley. n.d. "Characterization of Global Combustion Properties with Simple Fuel Property Measurements for Alternative Jet Fuels." doi:10.2514/6.2014-3469.

Won, S. H., Haas, F. M., Dooley, S., Edwards, T., and Dryer, F. L., "Reconstruction of chemical structure of real fuel by surrogate formulation based upon combustion property targets," Combustion and Flame, vol. 183, Sep. 2017, pp. 39–49.

Wordland, Justin. 2015. "What to Know About the Historic 'Paris Agreement' on Climate Change."

Yanowitz, J, Ecoengineering M A Ratcliff, R L Mccormick, J D Taylor, and M J Murphy. 2004. "Compendium of Experimental Cetane Numbers."

Zelina, Joseph. 1995. "Combustion Studies in a Well-Stirred Reactor." University of Dayton.

Major Accomplishments

Determined and reported LBO equivalence ratios in WSR for four NJFCP fuels.

Publications

Conference Proceedings:

Stachler, Robert D., Joshua S. Heyne, Scott D. Stouffer, Joseph D. Miller, and William M. Roquemore. 2017. "Investigation of Combustion Emissions from Conventional and Alternative Aviation Fuels in a Well-Stirred Reactor." In 55th AIAA Aerospace Sciences Meeting. Grapevine, TX: American Institute of Aeronautics and Astronautics.

Outreach Efforts

Conference presentations:

Stachler, Robert D., Joshua S. Heyne, Scott D. Stouffer, Joseph D. Miller, and William M. Roquemore. 2017. "Investigation of Combustion Emissions from Conventional and Alternative Aviation Fuels in a Well-Stirred Reactor." 55th AIAA Aerospace Sciences Meeting. Grapevine, TX: American Institute of Aeronautics and Astronautics. https://doi.org/10.2514/6.2017-0382

Stachler, Robert D., Joshua S. Heyne, Scott D. Stouffer, Joseph D. Miller, and William M. Roquemore. 2016. "Investigation of Combustion Emissions from Conventional and Alternative Aviation Fuels in a Well-Stirred Reactor." 12th Annual Dayton Engineering Sciences Symposium. Dayton, OH: ASME.

Awards

Joshua Heyne – SOCHE Faculty Excellence Award, 2016
Robert Stachler – ASME Outstanding Young Engineer, 2016

Student Involvement

Robert Stachler, Ph.D. student, led this effort.

Task 3 - Chemical Effects in a Toroidal Jet Stirred Reactor

University of Dayton

Objective(s)

Measure the Lean Blowout (LBO) limit and emissions/speciation characteristics for NJFCP fuels within the program.

Research Approach

Introduction

Due to increasing global concern about climate change resulting from anthropocentric carbon emissions, the aviation sector has identified alternative jet fuels (AJFs) to have major potential for carbon mitigation. As alternative modes of transportation are seeking the usage of alternative fuel sources for the near and long term (e.g., fuel cells, batteries), power density is critical for the aviation sector resulting in hydrocarbon dependencies for years to come. Additionally, fuel costs for commercial airliners is large, accounting for roughly 27% of operating expenses with slight increases in the crude oil price resulting in millions of dollars of additional expenses [1,2]. Jet fuel made from alternative feedstocks has the opportunity to increase national security by reducing country dependence on foreign oil, reduce impacts of oil industry cost fluctuations, and create jobs. [1]. Use of bioderived jet fuels requires alternative pathways into the market as large capital cost paired with other economic and technological barriers exist in transition promising AJFs to market.

The National Jet Fuels Combustion Program (NJFCP) was created to streamline certification pathways of AJFs by minimizing the barrier of increased cost and testing in full scale combustor testing rigs [3]. Fuel properties to be studied against Combustor Figures of Merit (FOMs) include high altitude relight, cold start ignition, and lean blowout (LBO) [3,4]. Tests on these FOMs provide a scope of fuel performance among a variety of aviation gas turbine engine operating conditions.

LBO occurs when the flame extinguishes, which requires re-ignition of the given combustor cups or cans, during operation presenting potential safety concerns [3]. Chemical effects are shown to yield importance as lean flammability limits are being approached signifying the relevance of LBO as a FOM [3]. Target conditions for temperature and pressure, referenced to the inlet of the combustor, are 400-450 K and 2-4 atm., respectively [3]. Prior experiments with the Referee Rig and Toroidal Jet-Stirred Reactor (TJSR) have shown a first order correlation with derived cetane number (DCN) and LBO, assessed via equivalence ratio [3,5–7]. Identification of DCN, a metric seldom considered in initial fuel screening processes, illuminates the importance of fuel autoignition capabilities in these combustors near LBO.

Lefebvre, Mellor, and later Burger developed a phenomenological explanation of LBO behavior, relating it to the evaporation, chemical and mixing timescales shown in Equation 1 and Figure 1 [8–11]. Burger was able to integrate the use of non-conventional fuels into this timescale analysis to describe the competition between chemistry and evaporation in the fuels as it pertains to combustor performance. The time associated with fuel atomization and evaporation correlates to the evaporative timescale. Mixing timescales are primarily a function of combustor design, and effects of pressure, temperature, air flow rate, and recirculation within the device. Chemical timescales are influenced by the fuel, at the supplied temperature and pressure. The recent findings concerning LBO and DCN imply that the chemical timescales largely correspond to autoignition timescales. A common measure of autoignition timescales is ignition delay, which is indirectly how DCN is calculated per ASTM D6890, which will be leveraged in the subsequent analysis [12].

$$\phi(LBO) \sim \left(\frac{1}{\tau_{chem}} + \frac{1}{\tau_{evap}} + \frac{1}{\tau_{mix}} \right)^{-1} \quad (1)$$

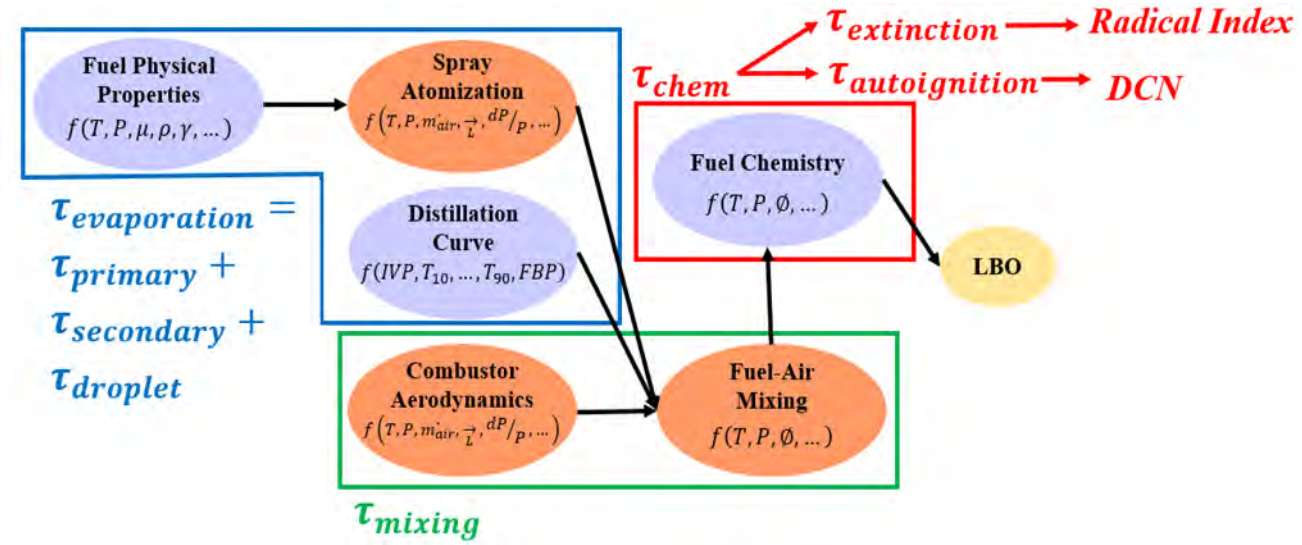

Figure 1. Relevant timescales driving LBO performance and the parameters influencing those associated timescales. Purple circles correspond to the fuel effects whereas orange circles are influenced by the combustor design.

A previous random forest regression analysis for the TJSR LBO data, including physical and chemical properties commonly measured for jet fuel performance, suggests radical index is a key predictor for LBO. Radical index (RI), a value used to measure the role of kinetics in extinction strain rate for counterflow diffusion flames, could effectively describe the effects of extinction within the TJSR [13]. Both DCN and RI are metrics that can lead to the fundamental timescales associated with autoignition and extinction, respectively. The relevant pathways to understand the competition between these timescales as they relate to the chemical timescale are shown below:

$$\tau_{extinction} \rightarrow Radical\ Index \rightarrow Extinction\ Strain\ Rate\ (a_e)$$

$$\tau_{autoignition} \rightarrow DCN \rightarrow Ignition\ Delay$$

The TJSR, an applied combustion device, has been previously used to investigate soot inception, emissions, and lean/rich blowout stability limits while operating in the well-stirred regime [14–20]. This well-stirred regime allows for reduced order physics to a 0-D system, synonymous to a perfectly-stirred reactor (PSR) with modeling efforts, where concentration, temperature, and flow fields are homogeneous with space and steady state. Minimal gradient effects exist near the wall of the TJSR, but temperature and species concentrations have yielded near constant profiles in prior experiments [15]. Using a premixed, prevaporized fuel-air mixture allows for assessment of fuels on a gas phase basis allowing for isolation of exclusively the chemical effects, as opposed to other combustion devices which study LBO in a multiphase environment where physical and chemical effects are coupled represented, in addition, by the evaporative timescale. Atomized fuel and air near the primary recirculation zone has been modeled previously as a PSR or an array of PSRs due to the 0-D nature in space and time with the reduced conservation equations associated to them. Development and implementation of a device operating near a well-stirred regime allows for the observation of chemistry effects of alternative fuels to be studied in an environment similar to that of typical gas turbine combustors, where a device to assess performance in this regime does not exist. The TJSR uses multiple jets injecting premixed, prevaporized fuel and air into the 250-mL reactor volume at temperatures and pressures near 458 K and 1 atm, respectively, and bulk fluid residence times of around 6-7 ms. LBO performance vs fuel type was assessed at high temperatures using fused silica (Rescor 750) reactor hemispheres with an Inconel jet-ring manifold and an absence of dilution. Experimental conditions for the TJSR are relatively similar to that of typical gas turbine combustors [3,18]. The influence of the chemical timescale will be discussed relative to the competition of extinction timescales and autoignition timescales.

Methods/ Experimental

TJSR Information and Instrumentation

LBO testing was performed in the TJSR where lean, premixed, prevaporized fuel and air enter the reactor via jets located on the outer diameter of the toroid. Fuel is vaporized and mixed with air upstream of the reactor, where it is then exhausted

through exhaust ports located within the center of the toroid. Diagrams and additional reactor information are in Stachler, et. al., 2017 [7].

Four diagnostic ports are located within the bottom hemisphere of the TJSR. A linear tracking, bare, type B thermocouple (0.2 mm diameter, platinum – 6% rhodium, platinum – 30% rhodium) surrounded by alumina was used to measure the temperature within the reactor. Measurements were assessed approximately 0.25" from the bottom of the reactor and were not corrected for radiation and other heat losses. A custom igniter which was located flush with the reactor wall. Pressure fluctuations within the TJSR were measured using a high speed 0-5 psid pressure transducer, and it was found that pressure fluctuations were limited to +/- 5.5 kPa. Exhaust gas samples were extracted within the reactor using a 1.4 mm OD oil-cooled (420 K) probe. Measurements were taken as the probe rested approximately 5 mm from the lower wall of the toroid, situated 90 degrees relative to the thermocouple.

Fuels Tested

Various fuel/solvent mixtures were used for assessment of LBO in the TJSR that span a wide range of chemical and physical properties. These fuels are shown in Table 1, where additional fuel property information can be found in Edwards, 2017 [4]. DCN, a chemical property of fuels which is measured using ASTM D6890, varied from 17 to 74, outside of the 40 to 60 range that current aviation fuels exhibit [5,12]. RI values were estimated for A-2, C-1, and C-4 using previously published results, whereas the radical indices of the 1-3 species mixtures (nC12, S-1, and J-1) were calculated using the sum of mole fractions of the fuel multiplied by their respective radical index value [13].

A-2 is the nominal jet fuel, containing average values in flash point, viscosity, and aromatic content among the Jet-A fuels. C-1 and C-4 fuels have lower DCN values than that of conventional jet fuels and have an unusual and broad boiling range, respectively [3,4]. S-1, a surrogate fuel, was formulated to stress key combustion properties including DCN, molecular weight, H/C ratio, and threshold sooting index while emulating Jet-A fuel performance in prevaporized fuel-air environments [4,21]. The single species *n*-dodecane is a common fuel surrogate utilized for the contribution of n-alkanes in petroleum derived jet fuels [7,21]. Lastly, J-1, which has a similar DCN to C-1, was designed to stress the importance of RI to gain understanding of the kinetic influence in the progress to LBO. This 2-species fuel mixture contains a high mole fraction of aromatics to effectively lower RI without the presence of any *iso*-paraffins.

Table 1. Fuels tested within the TJSR for LBO testing. Additional fuel properties for A-2, C-1, C-4, and S-1 are in Edwards, 2017 [4]. Other 1-3 component fuel / solvent mixtures values were estimated using traditional blending methods [22,23].

Fuel / Solvent Mixture Nomenclature	Composition (% vol)	Fuel / Solvent Mixture Chemical Composition C_mH_n	Derived Cetane Number (DCN)	Radical Index (RI)
nC12	*n*-dodecane	$C_{12}H_{26}$	74.0	1.000
A-2	Petroleum Jet A	$C_{11.4}H_{22.1}$	48.3	0.750
S-1	59.3% *n*-dodecane, 18.4% *iso*-octane, 22.2% 1,3,5-*tri*-methylbenzene	$C_{10.3}H_{20.1}$	50.4	0.745
C-4	60% C9-12 *iso*-paraffins, 40% C-1	$C_{11.4}H_{24.8}$	28.0	0.720
C-1	Highly branched C12 & C16 paraffins	$C_{12.6}H_{27.2}$	19.08	0.700
J-1	75.5% 1,3,5-*tri*-methylbenzene, 24.5% *n*-dodecane	$C_{9.5}H_{14.3}$	17.01	0.466

Operating Conditions and Procedure

Liquid fuel is delivered using two syringe pumps (Teledyne Isco 500 D), where the fuel passes a swirler and heat exchanger to elevate the temperature to 473 K prior to being introduced in the vaporizer. Uncertainty in the liquid flow measurement with calibration is estimated to be +/-1.4%, where the piston flow meter accuracy is +/- 0.5%. The heated fuel is introduced with 10-20% of the air flow in the beginning of the vaporizer via an air-swirled atomizer and air at 400 K. The remainder of air is introduced coaxially throughout the length of the vaporizer at 489 K. The air lines are filtered, monitored, and controlled upstream of the vaporizer using mass flow controllers (Brooks Instruments 5851i and 5853). Uncertainty for the mass flow controllers is +/- 1.5% FSO. PID-controlled electric heaters were used to establish consistent temperatures in the heated fuel and air streams. Total air flow rate was held constant at around 600 g/min, adjusting fuel flow rate to attain the desired equivalence ratio. The constant air flow rates establish a near constant residence time and constant turbulence intensities.

Measurements of pressure, temperature, and fuel and air mass flow rates were monitored and controlled via LABVIEW software. Calculations for other relevant parameters (equivalence ratio, bulk residence time, mass flow) were performed in real time with this software as well. Global residence time for the experiment was around 6-7 ms and varied slightly with temperature differences and reduction in overall mass flow due to fuel flow rate [15]. Inlet temperatures were held constant around 458K and were measured prior the fuel-air mixture to the jet ring manifold.

Initial operation of the TJSR uses a gaseous fuel (ethylene) to allow the initial warmup of the reactor and jet ring to avoid condensation of low volatility fuels in the small passages of the jet ring. Once operational temperatures are established, and the reactor is thermally stable, fuel usage was transitioned to the liquid fuel. Thermal conditions are stabilized again before LBO testing. The ethylene was controlled using a series of pressure regulators and a mass flow controller (MKS Instruments M100B).

Each LBO test was initiated at an equivalence ratio (ϕ) of 0.48, where temperatures within the reactor were below the maximum allowable temperature for the fused silica reactor. Equivalence ratios were reduced by reducing fuel flow rate until LBO. This limiting condition occurs when the heat loss becomes large enough to where combustion becomes unstable and is not sustained. A change in operating noise and a sharp decrease in reactor temperature correspond to LBO [15]. The fuel flow rate was automated to decrease at approximately 0.05 mL/min ($\phi \sim 0.001$) every 4 seconds to LBO conditions to minimize hysteresis effects of the LBO values, e.g. hotter temperatures sustaining LBO to leaner conditions. Automation of decreasing fuel flow rate is similar to the methodology presented for the Referee Rig and their subsequent LBO testing [6]. This ramp rate for fuel flow provides for use of a singular fuel pump throughout the duration of the LBO test and minimizes transitional effects between operation of the two syringe pumps. To minimize fuel contamination between LBO testing of different fuels and dead volume associated with the syringe pumps, the pumps were flushed out with the new fuel approximately 4 times prior to the liquid fuel being introduced for testing. Also, as the WSR was approaching stable thermal conditions, the fuel lines experienced proper flushing of previous fuel to minimize contamination. Once LBO occurs, reignition of the fuel and air mixture occurs, where thermal equilibrium is achieved at $\phi = 0.48$ and LBO process begins again. Thirteen (13) LBO points were taken for all fuels except nC12. Only five LBO points were taken for nC12.

Computational Methods

Ignition delay estimations were calculated using Cantera and a constant volume ideal gas reactor [24]. Initial temperatures and pressures of 700-1500 K and 1 atm, respectively, were selected to emulate the TJSR experimental conditions. Simulations stepped through time using internal stepping to minimize gradients and increase computational efficiency. A 965-species model from Dooley, et. al. was employed as the mechanism in this work as it consisted of models for the species components in the fuels tested [25]. The time at which OH concentration reached a maximum was interpreted in this work is the ignition delay time.

Perfectly stirred reactor (PSR) modeling with Cantera was also explored using an ideal gas reactor, introducing mass flow aligning with the experimental conditions at a volume of 250 mL and a bulk residence time of 7.1 ms. Mass fractions of the fuel-air mixture and temperature were extracted at steady state conditions and at equivalence ratios at LBO. Equilibrium temperatures were also calculated using the experimental conditions (T=458K, P=1atm, ϕ=ϕ_{LBO}).

Results and Discussion

Lean blowout was measured using six fuels in the TJSR, which span a wide DCN range, to investigate the first-order dependence on DCN in a premixed, prevaporized configuration. Fuel flow rate was lowered, lowering the reactor temperature, until a large drop (> 20 K) in temperature occurred, at LBO. Figure 2 illuminates this trend as the different fuels blowout at different equivalence ratios, as shown in the larger symbols. Points beyond LBO are included to illustrate the rapid decrease in temperature that occurs once LBO is experienced

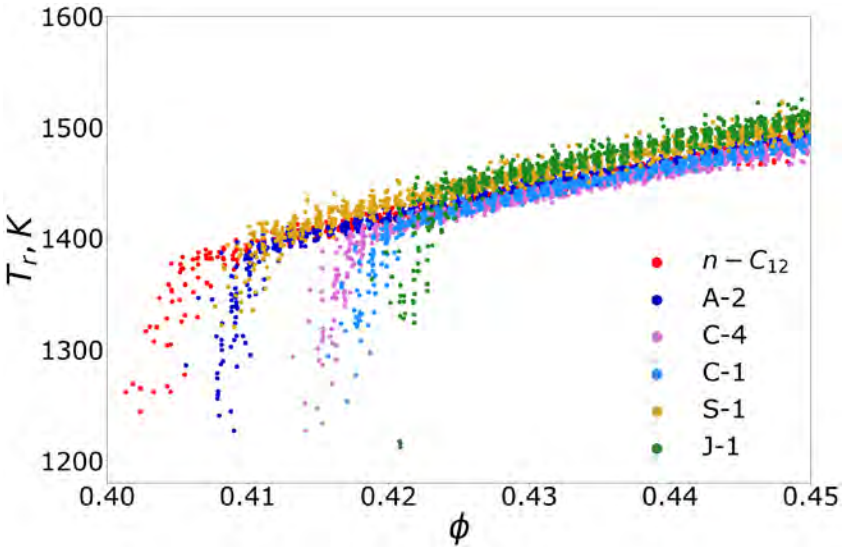

Figure 2. Reactor Temperature (K) as a function of ϕ in the TJSR. TJSR experimental conditions: P=~1atm, T_o=458K, τ = 6-7 ms.

The LBO values were then normalized relative to the LBO values of A-2, where a random forest regression analysis was utilized. This analysis, shown in Figure 3, provides a method to assess the relative important factors from the ranging physical and chemical properties among the different fuels and fuel mixtures. DCN and RI are among the top feature importances of the data set. Normalized fuel property regression results yield the same top feature importances, but to a lesser degree than the results shown in Figure 3. Chemical properties, like iso-paraffins and n-paraffins, correlate with the next important factors, being DCN and RI. The importance of DCN and RI are both fuel property values that can influence the timescales of autoignition and extinction within the TJSR.

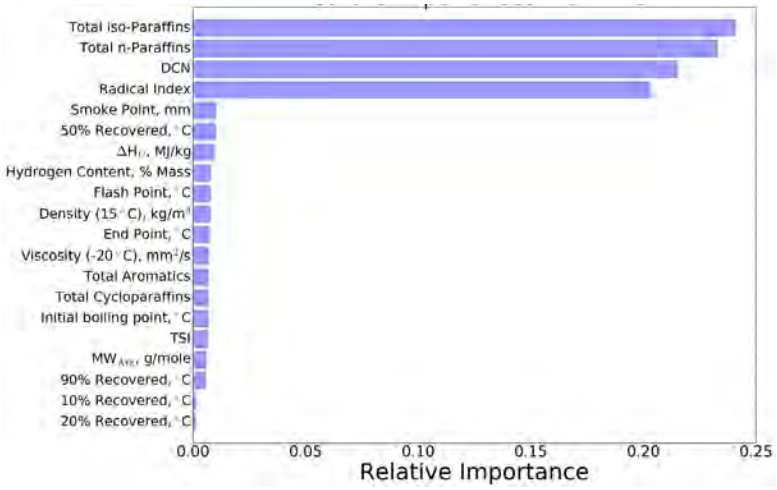

Figure 3. Relative feature importances using random forest regression analysis on the TJSR LBO data.

Figure 4 illuminates a first order correlation to LBO recorded using the TJSR. Although the LBO values are narrow with ~4% between max and min values, the statistical uncertainty with the testing performed still show a relative performance difference among the fuels and contains a moderate R^2 value. LBO for A-2 and S-1 yield consistent results in a premixed, prevaporized fuel-air environment, as with other experiments [6,21]. C-1 also exhibited an extended stability limit compared to J-1, although the fuels had similar DCN values (17.1 v. 19.08). It is also shown that the highest radical index value - 1 for nC12 - has the most resistance to LBO. Moderate radical index fuels span the gap between the two extremes of LBO

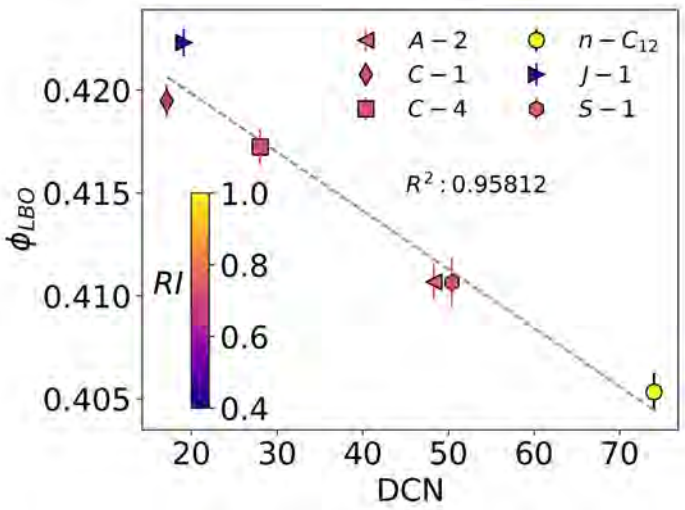

Figure 4. ϕ_{LBO} as a function of DCN in a TJSR. TJSR experimental conditions: P=~1atm, T_o=458K, τ = 6-7 ms. Error bars correspond to 1σ of the statistical uncertainty between measured LBO. RI values are included in figure as colors, indicated via the color bar. Gray dotted lines correspond to the line of best fit, with the given R^2 value provided in the figure.

Radical index aids in estimation of extinction strain rate values and toward an extinction timescale. Extinction strain rate values were calculated using the equation provided in Figure 5 from S.H. Won, et. al., 2012 [13], which is shown below for brevity. Fuel concentration represented by [Fuel] was estimated given the equivalence ratio at LBO. ΔH_c corresponds to the heat of combustion of the given fuel, where MW_{fuel} and $MW_{nitrogen}$ correspond to the molecular weights of the fuel and nitrogen, respectively.

$$a_e\left[\frac{1}{s}\right] = 230\, RI\, [Fuel]\Delta H_c\left(\frac{MW_{fuel}}{MW_{nitrogen}}\right)^{-\frac{1}{2}} - 54 \quad (2)$$

Previous counterflow diffusion flame efforts were made to study the kinetic effect of extinction strain rate for varying fuel species and components. A correlation was established, collapsing the experimental and simulated data on a line. This was accomplished via RI and transport weighted enthalpy [13]. Values of RI, fuel used, and equivalence ratio allowed for relative comparison amongst the fuels and their LBO values. Figure 5 displays LBO as a function of the calculated extinction strain rate. Fuels with large n-alkane content show increased extinction had high strain rate values whereas the lower DCN fuels had smaller strain rate values. Surrogate mixtures with large amounts of aromatics tend to have lower extinction strain rates as the radical indices are smaller than that of the other components. A linear trend of increased strain rate to decreased LBO is additionally seen in the figure with a lower R^2 value than that of Figure 4. Inverses of strain rate yields values in the 1.5-2 ms range. However, it is not determined if an inverse of the strain rate, with a unit of time, is adequate as the higher extinction strain rate values result in lower time values.

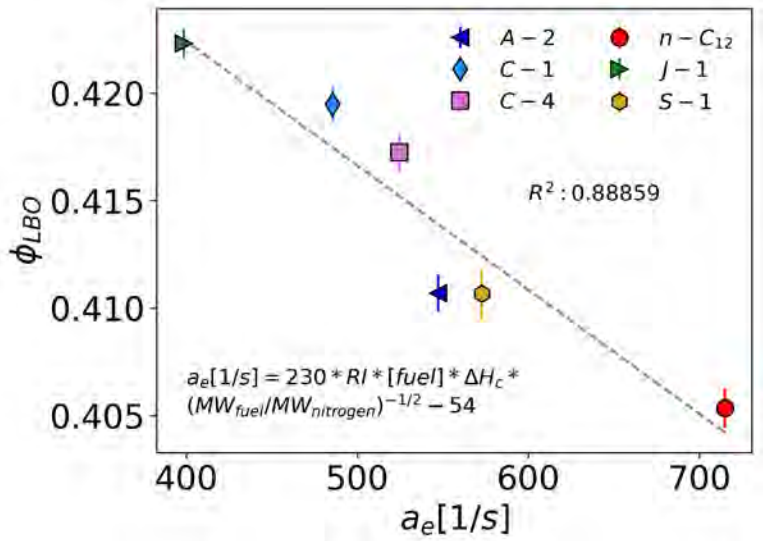

Figure 5. ϕ_{LBO} as a function of extinction strain rate (a_e) in a TJSR. TJSR experimental conditions: P=~1 atm, T_o=458K, τ=6-7 ms. Error bars correspond to 1σ of the statistical uncertainty between measured LBO. Gray dotted lines correspond to the line of best fit, with the given R^2 value provided in the figure.

Correlations with DCN and the TJSR indicate autoignition as an important characteristic when approaching LBO conditions. Ignition delay allows for investigation in the effect of autoignition and comparison of those timescales relative to other timescales that may exist. In Figure 6, ignition delay was estimated via simulation with Cantera using *n*-dodecane and *iso*-octane, the latter of which is utilized in this effort because the DCN value is very similar to that of C-1 [26]. Because of this assumption, the experimental temperature in the plot where *iso*-octane is located is the temperature at which LBO occurred for C-1. To illuminate the effects of recirculation of burned exhaust products to fresh reactants, burned mass fractions of products, expressed as a percentage, were incorporated into the lines provided in the figures. The remaining percentage was multiplied by the respective mass fractions of fresh reactants at the given equivalence ratio. Burned mass fractions were extracted using a PSR simulation at the given LBO value. Figure 6 displays ignition delay for different percentages of burned products incorporated within the overall mixture. A green line on both figures indicates the bulk residence time. Toward the reactor temperature limits, ignition delay is roughly two orders of magnitude less than that of the bulk residence time, but drastically approaches the bulk residence time around ~ 1111 K. Even among the two fuels presented in the figure, these small differences between *n*-dodecane and *iso*-octane impact the ability to autoignite in adequate time for a given gas turbine combustor.

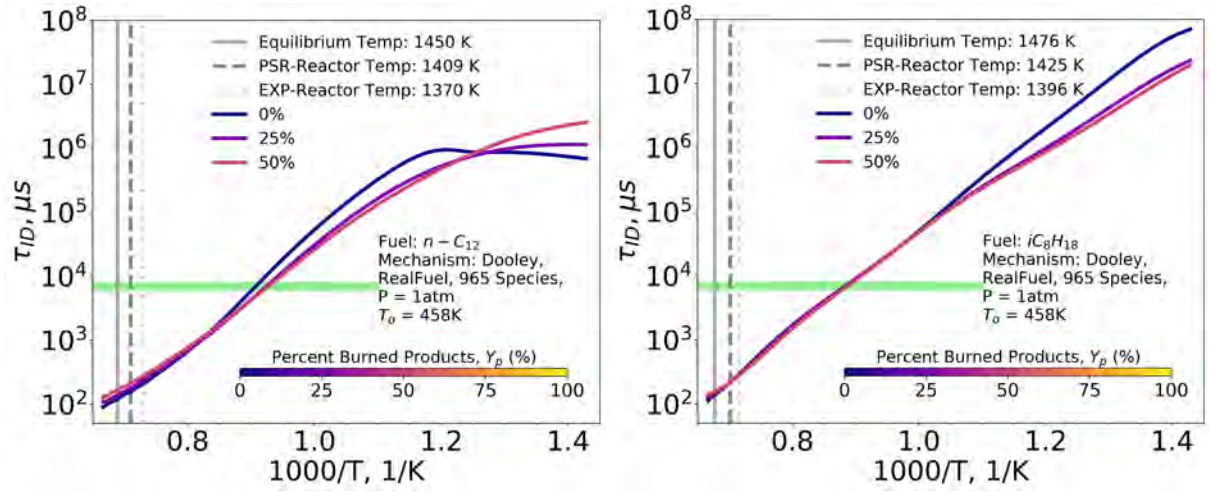

Figure 6. Ignition delay plots for *n*-dodecane and *iso*-octane for various mass percentages of burned products introduced in initial conditions. Equilibrium, PSR, and experimental temperatures are plotted in gray with the values provided in the legend. The experimental temperature for C-1 was assumed as the experimental value for *iso*-octane. The green bar on the plot signifies the order of magnitude of the bulk residence time relative to the other ignition delay times estimated from the simulation.

Conclusions

Lean blowout (LBO), a common combustor performance metric to assess alternative fuels, was assessed in a toroidal jet-stirred reactor (TJSR) with a variety of fuels spanning derived cetane numbers (DCN). This device operates in a premixed, prevaporized environment, under relevant gas turbine combustor conditions, where other combustor devices offer limited insight into experiments near perfectly stirred reactor environments. Key findings of this work include:

- LBO contains a first-order effect with DCN, which is additionally elucidated in other practical and applied combustor experiments.
- Radical index was identified as a feature importance in predicting LBO in this experimental configuration, emphasizing extinction timescales as a driving factor for LBO in a TJSR, which can be investigated using extinction strain rate.
- A competition between autoignition and extinction timescales exists on the approach to LBO, and this affects the overall chemical timescale as it relates to the bulk residence time of the reactor.

References

[1] Alternative Aviation Fuels: Overview of Challenges, Opportunities, and Next Steps, US DOE, 2016.
[2] W-C. Wang, L. Tao, J. Markham, Y. Zhang, E. Tan, L. Batan, E. Warner, M. Biddy. Review of Biojet Fuel Conversion Technologies, Report No TP-5100-66291, NREL, 2016.
[3] M. Colket, J. Heyne, M. Rumizen, M. Gupta, T. Edwards, W.M. Roquemore, G. Andac, R. Boehm, J. Lovett, R. Williams, J. Condevaux, D. Turner, N. Rizk, J. Tishkoff, C. Li, J. Moder, D. Friend, V. Sankaran, AIAA J. 55 (2017) 1087–1104.
[4] J.T. Edwards, Reference Jet Fuels for Combustion Testing. 55th AIAA Aerosp. Sci. Meet., AIAA, 2017.
[5] J. Heyne, E. Peiffer, M. Colket, J. Moder, J.T. Edwards, W.M. Roquemore, C. Shaw, C. Li, M. Rumizen, M. Gupta, Year 3 of the National Jet Fuels Combustion Program: Practical and Scientific Impacts, 2018 AIAA Aerosp. Sci. Meet., AIAA, 2018.
[6] S. Stouffer, T. Hendershott, J. Monfort, J. Diemer, E. Corporan, P. Wrzesinski, A. Caswell, Lean Blowout and Ignition Characteristics of Conventional and Surrogate Fuels Measured in a Swirl Stabilized Combustor, 55th AIAA Aerosp. Sci. Meet., AIAA, 2017.
[7] R.D. Stachler, J.S. Heyne, S. Stouffer, J.D. Miller, W.M. Roquemore, Investigation of Combustion Emissions from Conventional and Alternative Aviation Fuels in a Well-Stirred Reactor, 55th AIAA Aerosp. Sci. Meet., AIAA, 2017.
[8] A.H. Lefebvre, D.R. Ballal. Gas Turbine Combustion: Alternative Fuels and Emissions. 3rd ed. CRC Press, Boca Raton, FL, USA, 2010.
[9] A.H. Lefebvre, Int. J. Heat Fluid Flow 107 (1985) 24-37.

[10] S.L. Plee, A.M. Mellor, Combust. Flame. 31 (1979) 61–80.
[11] V. Burger, The Influence of Fuel Properties on Threshold Combustion in Aviation Gas Turbine Engines. 2017.
[12] A Standard Test Method for Determination of Ignition Delay and Derived Cetane Number (DCN) of Diesel Fuel Oils by Combustion in a Constant Volume Chamber, D6890-16e1, ASTM Int., 2016.
[13] S.H. Won, S. Dooley, F.L. Dryer, Y. Ju, Combust. Flame 159 (2012) 541–551.
[14] S.D. Stouffer, D.R. Ballal, J. Zelina, D.T. Shouse, R.D. Hancock, H.C. Mongia. Development and Combustion Performance of High Pressure WSR and TAPS Combustor. 43rd AIAA Aerosp. Sci. Meet. Exhib., AIAA, 2005.
[15] S. Stouffer, R. Pawlik, G. Justinger, J. Heyne, J. Zelina, D. Ballal, Combustion Performance and Emissions Characteristics for a Well Stirred Reactor for Low Volatility Hydrocarbon Fuels. 43rd AIAA/ASME/SAE/ASEE Jt. Propuls. Conf. Exhib., AIAA, 2007.
[16] D. Blunck, J. Cain, R.C. Striebich, S.Z. Vijlee, S.D. Stouffer, W.M. Roquemore, Fuel-rich Combustion Products from a Well-Stirred Reactor Operated using Traditional and Alternative Fuels. Cent. States Combust. Meet., The Combustion Institute, 2012.
[17] S.Z. Vijlee, Effects of Fuel Composition on Combustion Stability and NOX Emissions for Traditional and Alternative Jet Fuels. University of Washington, 2014.
[18] J. Zelina, D.R. Ballal, J. Eng. Gas Turbines Power 119 (1997) 70–75.
[19] A. Briones, B. Sekar, J. Zelina, R. Pawlik, S. Stouffer, Numerical Modeling of Combustion Performance for a Well-Stirred Reactor for Aviation Hydrocarbon Fuels, 44th AIAA/ASME/SAE/ASEE Jt. Propuls. Conf. Exhib., AIAA, 2008.
[20] J.E. Nenniger, A. Kridiotis, J. Chomiak, J.P. Longwell JP, A.F. Sarofim, Proc. Comb. Inst. 20 (1984) 473–479.
[21] S.H. Won, F.M. Haas, S. Dooley, T. Edwards, F.L. Dryer, Combust. Flame 183 (2017) 39–49.
[22] S. McAllister, J-Y. Chen, A.C. Fernandez-Pello, Fundamentals of Combustion Processes. Springer New York, New York, NY, 2011.
[23] B.E. Poling, J.M. Prausnitz, J.P. O'Connell, The Properties of Gases & Liquids. vol. 1. 5th ed. The McGraw-Hill Companies, Inc., 2001.
[24] D.G. Goodwin, H.K. Moffat, R.L. Speth, Cantera: An Object-oriented Software Toolkit for Chemical Kinetics, Thermodynamics, and Transport Processes, 2017.
[25] S. Dooley, F. Dryer, S.H. Won, T. Farouk, Reduced Kinetic Models for the Combustion of Jet Propulsion Fuels, 51st AIAA Aerosp. Sci. Meet. Incl. New Horizons Forum Aerosp. Expo, AIAA, 2013.
[26] J. Yanowitz, M.A. Ratcliff, R.L. Mccormick, J.D. Taylor, M.J. Murphy. Compendium of Experimental Cetane Numbers, Report No. TP-5400-67585, NREL, 2017.

Milestone(s)

- Measured LBO, a Figure of Merit in the NJFCP, for four fuels. Results are consistent with the more complicated Area 6 Referee Rig. LBO trends with both DCN and Radical Index, chemical properties that correspond to autoignition and extinction phenomena, respectively.
- Emissions were additionally recorded, and trends for a surrogate fuel, S-1, are similar to that of A-2, a conventional jet fuel.

Major Accomplishments

Determined and reported LBO equivalence ratios for four NJFCP fuels in a Toroidal Jet-Stirred Reactor.

Publications

Conference Proceedings

Stachler, R., Peiffer, E., Kosir, S., Heyne, J., and Stouffer, S., "A Study into the Chemical Timescale for a Toroidal Jet-Stirred Reactor (TJSR)," Central States Section of The Combustion Institute, Minneapolis: 2018, https://doi.org/10.2514/6.2018-4914

Outreach Efforts

Conference presentations

Stachler, R., Peiffer, E., Kosir, S., Heyne, J., and Stouffer, S., "A Study into the Chemical Timescale for a Toroidal Jet-Stirred Reactor (TJSR)," Central States Section of The Combustion Institute, Minneapolis: 2018, https://doi.org/10.2514/6.2018-4914

Awards

Robert Stachler, Ph.D. student, 2018 Outstanding Research Award – Mechanical Engineering, University of Dayton

Student Involvement

Robert Stachler, Ph.D. student, led this effort.

Task 4 - Preferential Vaporization Effects on LBO in the Referee Rig

University of Dayton

Objective(s)

Explain Lean blowout (LBO) results from the Referee Rig, including NJFCP and non-NJFCP fuels. Some of these fuels exhibited non-monotomic behavior at LBO.

Research Approach

The certification process for non-conventional jet fuels historically has required significant time and financial resources, as full-scale engine tests for multiple engine geometries have been used in the past to evaluate fuel effects. (These large-scale tests then jeopardize the plausibility of a new fuel's implementation.) Not only does this restrict the development and deployment of biotechnological research and results, but also it fosters a non-sustainable, longer-term dependence on fossil fuels which are contributing to climate change. Jet fuel certification rightfully errs to the side of caution as system failure in flight will likely result in catastrophic results. For non-conventional fuels this caution is amplified, as these fuels often contain unique molecular compositions resulting in different chemical and physical properties from conventional fuel sources. Thus, paramount to the decarbonization of aviation transportation and the certification of alternative jet fuels is the mapping of unique chemical and physical properties to the fit-for purpose performance and safety criteria for conventional fuels.

The National Jet Fuels Combustion Program (NJFCP) was formulated with the mission of reducing the costs and time of the jet fuel certification process [1,2]. The NJFCP's method for accomplishing this task is to map the performance of extreme alternative fuel properties to three so called Figures of Merit: cold start ignition, altitude relight, and lean blowout (LBO). These areas were selected because of their implications on safety and because of their sensitivity to fuel properties [2]. In the context of the NJFCP, significant progress has been made toward the evaluation of alternative fuel effects on LBO, with significant progress toward ignition sensitivity only occurring very recently [3]. The NJFCP tests a wide variety of fuels on multiple different experimental rigs with different geometries to evaluate Figure of Merit performance in diverse geometries [4].

A keystone of the experimental NJFCP work is the development of a combustor rig capable of capturing fuel sensitivity typical of a swirl stabilized rich-quench-lean geometry with effusion cooling. This combustor rig, in theory, would be able to capture fuel effects in an aircraft main engine by screening the fuel, which would either reduce or eliminate subsequent and costly large-scale tests. The motivation to develop this rig has led to the development of the Referee Rig at AFRL/UDRI. Previous LBO work reported on the Referee Rig has shown that fuels with conventional fuel properties exhibit an LBO first order dependency on the fuel DCN. That is, fuels with a higher DCN exhibited greater stability limits than fuels with a lower DCN. These results, and detailed measurements reported by Chtev et al.[5] , suggest that the LBO limit of a fuel in a swirl stabilized rig is limited to first order by the ability of a fuel to autoignite, which has only very recently been suggested [2,4,6,7].

Fundamentally, LBO behavior will scale with evaporative, mixing, and chemical time scales. Both fuel properties and combustor design will have impacts on the significance of each of these relative time scales with LBO being limited by the longest relative time scale. A phenomenological description of LBO, based on these time scales, was developed by Mellor, where he hypothesized LBO will occur when combustion efficiency drops below a certain threshold [8,9]. The time scale behavior described is shown in Equation 1.

$$\eta_c = f\left((air\ flow\ rate)^{-1}\left(\frac{1}{\tau_{evap}}+\frac{1}{\tau_{mix}}+\frac{1}{\tau_{chem}}\right)^{-1}\right) \qquad (1)$$

The evaporative time scales will be determined by droplet spray and atomization behavior as well as by the volatility of the fuel. The mixing timescales will primarily be driven by combustor fluid dynamic properties. In turbulent combustion, mixing will be dominated by convection; combustor flow behavior will determine mixing time scales. The correlation found between LBO and DCN in the Referee Rig suggests the chemical time scales are at least in part determined by autoignition time scales as indicated by DCN. As DCN is a property describing a fuel's propensity to autoignite, the chemical time scales could be effectively ignition delay times. Regardless, the chemical timescales will also be a function of temperature, pressure, and

concentrations of the fuel and oxidizer. As the individual time scales increase in magnitude, the overall time scale of the process increases correspondingly. When the overall process exceeds the time available in the combustor, LBO will occur. Therefore, reducing any of these time scales will improve overall combustion stability.

Historically, fuel property effects on combustor performance have been studied by Lefebvre, Mellor, and more recently by Burger, whose work was initiated with altitude LBO experiments as part of the certification of a Fully-Synthetic-Jet-Fuel (FSJF) [7–11]. Lefebvre and Mellor's work focused on the variation of properties associated with conventional fuels and did not include as significant of variations of alternative fuel property effects as those within the NJFCP. Conventional fuels chemical properties do not vary significantly between fuels, obscuring the impact of chemical effects as they relate to LBO. Burger did consider the inclusion of non-conventional fuels in his work and leveraged Mellor's time scale analysis to explain the various trends in LBO data by the competing time scales for chemistry and evaporation. The inclusion of non-conventional fuels increased the range of chemical properties tested, highlighting the effects of the chemical time scales.

While much of the Referee Rig LBO data are consistent with the propensity of a fuel to autoignite, some of the data appear anomalous. This could be a result of second order effects from other time scales interfering with the autoignition correlation. Lefebvre and Mellor showed physical properties dominating fuel performance effects, and correspondingly their results have served as the primary fuel guidelines for certification. The identification of autoignition as a property of interest will also serve as important guidelines for new fuel certification. With added fuel property requirements, there will be more clarity on how future alternative fuels must be composed. New fuels will be able to be screened for certification/qualification using relatively inexpensive, small volume fuel property tests as opposed to expensive full-scale combustor tests.

The fuels tested for LBO on the Referee Rig are intentionally diverse in nature. With the goal to understand fuel effects on performance, fuels with diverse chemical and physical properties are utilized. Physical property variations will affect droplet atomization and vaporization, while chemical variations will affect combustion behavior. The fuels include conventional fuels, alternative fuels and fuel blends [12]. Real fuels used in applications generally contain many different species of diverse properties. Multi-species fuels vaporize differently from single species fuels [13–18]. Because future alternative fuels are expected to be multi-species in nature, understanding multi-species effects on combustion is of particular interest.

Here we propose three potential hypotheses explaining the previously reported anomalous Referee Rig LBO data by coupling droplet theory, distillation curve properties, and reactivity (via DCN). The possible explanations suggested here are: preferential vaporization (τ_{evap} and τ_{chem} coupling), extended droplet lifetimes (τ_{evap}), and local thermal quenching (τ_{evap} dilation via distillation and droplet time scale coupling). No single hypothesis is shown to explain all observed LBO behavior. Finally, fuel blends to test preferential vaporization are suggested for future work.

Methodology

Time Scale Approach to LBO Modeling

Similar to the previously reported work by Mellor and Burger, time scales can be assigned to the various competing phenomena and related to the three hypothesized criteria for deviation from DCN-LBO correlations. LBO thus can be interpreted to scale with the inverse sum of evaporative (τ_{evap}), chemical (τ_{chem}), and mixing (τ_{mix}) time scales.

$$\phi(LBO) \sim \left(\frac{1}{\tau_{chem}} + \frac{1}{\tau_{evap}} + \frac{1}{\tau_{mix}}\right)^{-1} \qquad (2)$$

Evaporative times scales are associated with the relative spray and evaporation time scales of a fuel. Mixing time scales are associated with the fluid dynamic primary recirculation time scales. Chemical time scales are best characterized by an autoignition time scale. Nominally, one can interpret the time scales to be independent, as in the prevaporized premixed toroidal jet-stirred reactor which could be considered a two time scale device (chemical and mixing) [6]. Results from the toroid stirred reactor were found to be largely consistent with the Referee Rig results with greater agreement with subtle variations that are still being investigated.

The agreement between the Referee Rig and the toroidal jet stirred reactor suggest the chemical time scales are a function DCN and equivalence ratio, ϕ, and not heat of combustion as implied with Lefebrve's correlation. DCN is a measure of the fuels autoignition propensity; this is consistent with the observation of the simultaneous extinction and ignition events as blowout is approached [19]. Although DCN is a measure of autoignition in the negative temperature coefficient regime, DCN

correlates accurately with ignition delays at high temperatures, which is the case in LBO [20]. From this, the significant chemical time scale could be proposed to be the ignition delay time. Regardless, the chemical time scale of significance can be described as,

$$\tau_{chem} = \tau_{chem}(DCN, \phi, T)$$

with the DCN being a function of the local (net species evolved/evaporated since droplet inception) or global (sum of total reactivity of the fuel.

Evaporation time scales can be interpreted as the algebraic sum of primary and secondary atomization (τ_{atom}) and droplet evaporation time ($\tau_{droplet}$) scales. Spray experiments on the same geometry and conditions as the Referee Rig have shown nominally similar Sauter Mean Diameters in the primary combustion region for fuels with significantly different fuel properties associated with primary and secondary atomization such as viscosity and surface tension[21]. These results imply similar primary and secondary atomization time scales.

$$\Rightarrow \tau_{atom} = \text{constant}$$

Droplet evaporation time scales ($\tau_{droplet}$) conventionally have been described by the d^2-law for a droplet of SMD [22]. The d^2-law assumes single species vaporization of a spherically symmetric, isolated droplet at steady state in a quiescent environment [23]. In the highly turbulent, multi-species vaporization of a spray, most of these assumptions are not met [24]; however the d^2-law is still generally used as an indicator of relative droplet evaporation times [25].

Initial droplet size, d_0, is a function of atomizer and physical properties of the fuel. Spray measurement experiments with the atomizer used in the Referee Rig have been made showing little variation in droplet distribution amongst fuels with variation amongst properties associated with spray quality [21].

The vaporization rate constant expression in the classic d^2-law, K_v, is a function of thermal conductivity, specific heat, heat of vaporization, fuel density, heat of combustion, air inlet temperatures and droplet surface temperature. All of these properties except for droplet surface temperature are approximately constant across fuels [12]. Droplet surface temperature will change throughout the vaporization process and is analogous to distillation temperatures in combustion applications.

Two fuels which with extreme distillate properties were tested, C-3 and C-5. C-3 distills between 183-256 ˚C and C-5 distills between 156-173 ˚C[12,26], with $\tau_{droplet}(\text{C5}) < \tau_{droplet}(\text{C3})$. Neither of these fuels performed abnormally according the LBO vs. DCN trend suggesting the absolute distillate temperatures didn't result in measurable differences. The surface temperature term in K_v does not have a significant impact on the overall value because the term is included as a temperature difference from the surrounding temperature; because the surrounding temperature is much greater than the vaporization temperatures, K_v is relatively insensitive to it. The coupling of the relatively constant droplet distribution and the relative vaporization rate constant suggest overall absolute evaporative time scales are either relatively constant or small as compared to the other timescales. And droplet time scales that followed the DCN-Law correlation follow the following relationship.

$$\tau_{droplet} \ll \tau_{mix} \text{ and/or } \tau_{chem}$$
$$\Rightarrow \quad \forall \text{ fuels with } \tau_{droplet} < \tau_{droplet}(\text{C3})$$

In a swirl stabilized combustor like the Referee Rig, mixing is primarily driven by convection (as opposed to diffusion). Because all of the fuels were tested in the same geometry with the same conditions, it is assumed mixing time scales are constant across all fuels.

$$\tau_{mix} \cong \text{constant}$$

Given these results, the divergence in the DCN-Law suggest performance variation could be explained by the eclipsing of chemical time scales by droplet time scales or a coupling of the chemical and droplet timescales. In the latter case, the time scales cannot be viewed as independent characteristics, but rather co-dependent as they progress simultaneously. In these LBO results, chemical time scales are to first order DCN dependent with droplet time scales being described with a d^2-law

accounting for distillation properties. The two hypothesized explanations both examine how the fuel vaporization could impact the chemical time scales and thus affect the stability of the fuel. Both explanations will assume vaporization and combustion follow the batch distillation limit. Each of these theories describe the vaporization of the entire spray as the vaporization of a single droplet.

Fuels

The fuel data considered in this study have been reported previously [4,12,27] and are for fuels that have been widely tested at a number of experimental facilities within the NJFCP. This suite of fuels is composed of three conventional fuels (a 'best,' average, and worse case jet fuel), five alternative fuels with fuel properties near those of jet fuel specifications, four conventional-alternative fuel blends, 2 single species fuels, and 9 blends of pure components. Two of the blended pure component (S-1 and S-2) surrogates were designed to mimic the fully prevaporized chemical combustion property targets of A-2, but have significantly differing physical properties than A-2. A full list of all fuels and their properties can be found in Table 1 and are detailed further by Edwards [12].

The listed fuel properties can be related to relative time scale estimates for each fuel. The evaporative time scale is most closely related to the distillation curve of a fuel and the fuel's effect on the spray/droplet character. High relative T_{10}, T_{50}, and T_{90} distillation properties are associated with lower vapor pressures, flash points, and increased heat transfer to the droplet surface to maintain a constant hydrocarbon vapor pressure. Higher relative viscosities, densities, and surface tensions are associated with poorer spray character as these properties inhibit atomization and mixing.

At the LBO conditions referenced here, negligible spray effects have been observed for fuels with varying properties associated with spray quality [21]. Thus, deviations in evaporative time scales are likely due to the relative distillation differences rather than spray effects based on these spray data. Additional support for this claim has been documented in reacting versus non-reacting spray data at AFRL/UDRI and Purdue respectively. These data show that for the non-reacting case very little variation is seen in the A-2 and C-5 fuels. However, very few small droplets were measured in the C-5 reacting case versus A-2 as C-5 has much lower distillation temperatures relative to A-2. The chemical time scales can be associated with the relative DCN of the fuels. A very wide range of DCNs for the fuels have been reported previously.

LBO Data Analyzed

Data used in this paper is reported in previously published literature, see [26,27]. Nominally, the LBO of a fuel is measured at a constant air mass flow rate (0.392 kg/sec), $\Delta P/P$ (3%), T (394/322 K air/fuel), and P (2 atm), with the LBO of a fuel being determined as the fuel mass flow rate limit in which extinction is global within the rig. The LBO conditions of these data are typical where LBO events at altitude occur. The LBO point as reported here is determined from multiple LBO events with uncertainties of the LBO point of approximately $+/-1.5\%$ the reported value. LBO data from 23 fuels are used in the reported analysis, see a description of these fuel in Table 1. Three conventional fuels associated with 'best' (A-1), 'average' (A-2), and 'worse' (A-3) combustion properties are used to determine stability limits of conventional fuels. While, 20 additional alternative fuels, alternative-conventional fuel blends, and solvent blends are used to approximate the 'best' and 'worse' case alternative fuel behavior for LBO by significantly varying their associated properties [4]. Fuels distinguished with a 'C' are fuels studied extensively in the NJFCP.

Table 1. Fuels tested for LBO on the Referee Rig. The fuels have diverse chemical, physical and distillate properties. The 2/3 species blends are shown in bold.

Fuel/Solvent Mixture	Composition, % volume
A-1	Petroleum JP-8 (w/high flash point and low viscosity and aromatics)
A-2	Petroleum Jet A
A-3	Petroleum JP-5
C-1	Highly branched C12 and C16 paraffins
C-2	16% *tri*-methylbenzene + 84% C14 *iso*-paraffins
C-3	64% A-3 + 36% farnesane
C-4	60% C9-12 *iso*-paraffins, 40% C-1
C-5	73% C10 *iso*-paraffins, 17% *tri*-methylbenzene
F-1	80/20 A-2/C-2
F-2	50/50 A-2/C-1
F-3	20/80 A-2/C-1
F-4	80/20 A-2/C-5
n-C12	*n*-C12
n-C12/n-C16 mix	**71.6% n-C12, 28.4% n-C16**
n-C12/M-xylene mix	**75% n-C12, 25% m-xylene**
n-C7	*n*-C7
n-C7/n-C12 mix	**31.2% n-C7, 68.8% n-C12**
n-C12/MCH mix	**71.6% n-C12, 28.4% MCH**
n-C7/n-C16 mix	**73.5% n-C7, 26.5% n-C16**
Sasol (IPK)	~88% *iso*-alkanes, 12% cycloalkanes, 0.4% aromatic
n-C12/i-C8 mix	**69.1% n-C12, 30.9% i-C8**
S-1	**59.3/18.4/22.2 *n*-dodecane/ *iso*-octane/ 1,3,5-*tri*-methylbenzene**
S-2	**52.6/25.1/22.2 *n*-hexadecane/ *iso*-octane/ 1,3,5-*tri*-methylbenzene**

LBO for these fuels are reported in Figure 1. The LBO points are plotted relative to the fuel's respective DCN. Blue symbols are fuels that do not include fuels composed of only 2/3 species, and the dashed line is a regression of $\phi(LBO)$ versus DCN for fuels excluding 2/3 species blends. All LBO measurements are found to be in agreement with the reported regression within their statistical uncertainty. Red symbols are fuels that are composed of only 2/3 species, and the solid black line is a DCN regression for all fuels plotted. Strong agreement between the non-2/3 species blends and the DCN was observed. There is a strong correlation of LBOs with DCN when the 2/3 species blends are excluded. Their correlation for all fuels is much weaker, especially in terms of correlative results for only the 2/3 species blends. Of particular note is the disparity of the S-2 fuel LBO (labeled with red text) from the strong correlation results, while the LBO data for A-2 lie very near the correlation. Recall that the S-2 mixture was derived by matching the fully pre-vaporized combustion property targets of A-2. Regression analysis, considering all fuel properties, continues to demonstrate that the DCN is still the leading order predictor for LBO behavior in the Referee Rig and 8 other rig geometries [4].

Fuels are distinguished by their apparent ability to stress the following three criteria:

- A lag in the relative mass evaporation rate of a droplet leading to local *thermal quenching*. Again, fuels with significant quantities of a light front distillate fraction and a heavy back distillate fraction, such as *n*-cetane, could

lead to lower mass evaporation rates after the light end of the droplet evaporates and before the heavy end of the droplet begins.

- The *relative lifetime of a droplet* (τ_{evap}) evaporating in the rig is substantially longer than other droplets. The longer droplet lifetime leads to incomplete combustion and, again, poorer stability limits at LBO. High concentrations of *n*-cetane, for example, could extend the lifetime of a droplet significantly, leading to lower combustion efficiencies that are associated with the onset of LBO [6].
- The ability of a droplet to have locally varying autoignition propensities as a function of evaporated droplet mass fraction, referred to as *preferential vaporization*. Fuels with non-reactive light components and highly reactive heavy components, such as S-2, could exhibit less stability as LBO is approached than a fuel of similar DCN but no evaporation-reactivity sensitivity [28].

Fuels composed of 2 or 3 components meet one or more of the above criteria and are distinguished as such in Figure 1. **It should be additionally noted that all the 2 and 3 component blends investigated here exhibited poorer stability than their corresponding DCN would predict.**

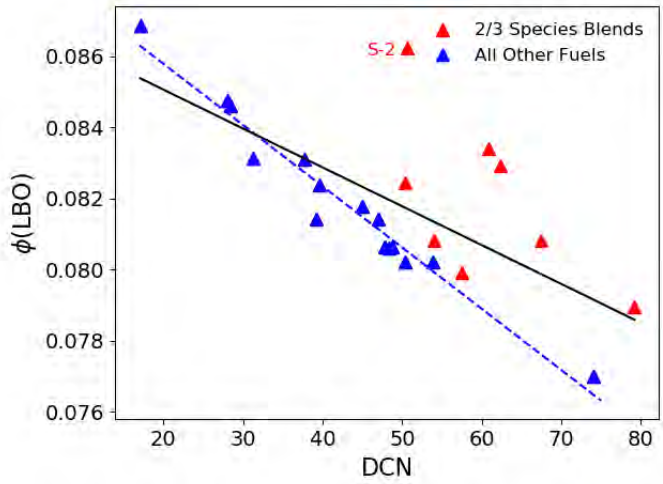

Figure 1. Experimental lean blowout as a function of DCN. The correlation is weak (R^2=0.40) until the 2 and 3 species blends are removed (R^2=0.97). The correlation with the 2 and 3 species blends removed represents the 'DCN-law.' "S-2" is labeled as it represents the greatest deviation from the d^2-law and is used as the representative fuel.

Results and Discussion

Thermal Quenching

The first explanation is the multi-species nature of the blends alone is causing the change in behavior. The explanation would support the theory of a 'DCN trend'. Each species has a unique volatility. If the species have significantly different volatilities, the species could vaporize in multiple phases divided by a heating phase in between. This concept has been observed experimentally in a heptane/cetane mixture [29]. Conventional fuels have a wide array of species and therefore volatilities. The distribution of volatilities causes the vaporization and by extension the combustion to occur at a relatively constant rate. Figure 2 shows how fuels with conventional distillation curves, like Jet A (A-2), have relatively constant vaporization rates similar to the d^2-law.

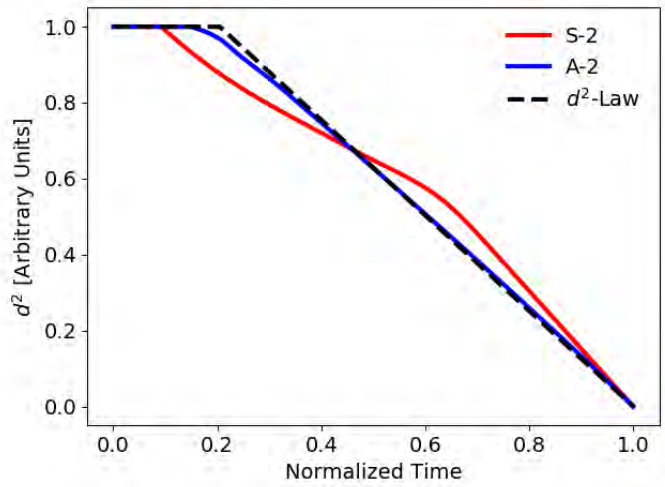

Figure 2. The relative normalized vaporization rates of a 3 species blend with bi-modal vaporization behavior, a conventional fuel, and the d^2-law. Conventional fuels with many species have a constant volatility distribution which causes them to follow similar behavior to the d^2-law.

It is unclear how multispecies blends would affect LBO behavior, however, there are multiple theories as to why this behavior could affect lean blowout. The first explanation is a concept called *thermal quenching*. Thermal quenching refers to the change in heat transfer behavior during the transition phase between the highly volatile and less volatile component. During the transition period, heat transfer continues to enter the droplet, but significantly less vapor is created per unit energy. Extinction and ignition phenomena are both highly temperature sensitive events. If at any point in the vaporization and combustion process extinction without reignition occurs, then blowout will occur. At each limit there is a balance of heat loss and energy generation which describes their limit. If during the transition phase, the heat entering into the droplet is viewed as heat loss, extinction and, correspondingly, lack of ignition could be described by the Semenov criterion. The Semenov criterion states that reactions will continue as long as heat generation exceeds heat losses. If heat generation is constant, then the increase in instantaneous heat losses could cause this limit to be reached.

Following the same assumption, during the transition phase the gaseous temperatures will decrease. Reduced gaseous temperatures will decrease flame speed which will lead to increased extinction probability. Simultaneously, reduction of the temperature of the vapor will have non-linear effects on ignition delay. If reignition is attempted at lower temperatures, it is highly unlikely it would occur and correspondingly no combustion would occur, signifying blowout.

The heat transfer into the droplet will be driven by the temperature of the flame and products. When these temperatures are high, increased amounts of heat are consequently lost to the walls and non-reacting air. If during the volatility transition this temperature decreases because of less mass combusting, the heat transfer into the droplet would decrease. Subsequently, a decrease in heat transfer would lead to further decrease in mass transfer, resulting in a negative feedback loop concluding with extinction.

Similar to thermal quenching, another theory is the volatility transition period has an effect on specifically mass transfer. During the transition, the reduction in mass vaporization rate would have an impact on instantaneous localized equivalence ratio. Chemical time scales will be significantly affected by reduced mass concentrations. Due to the turbulent environment, combustion occurs at fuel-to-air ratios other than stoichiometric. Because chemical time scales have been described as functions of equivalence ratio, potentially, the reduction in mass vaporization rate could have an impact on effective chemical time scales.

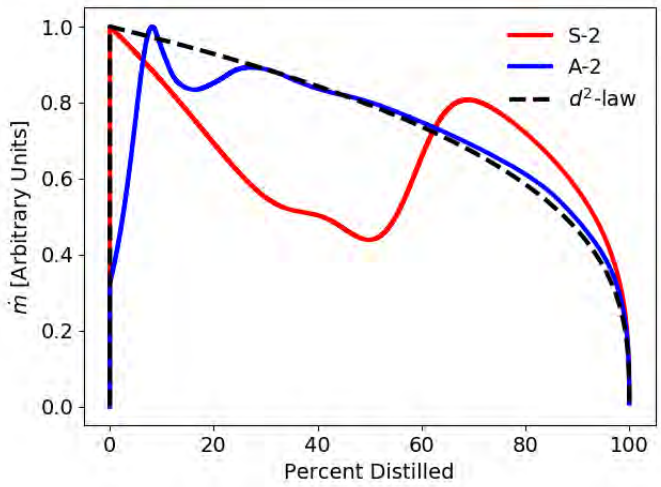

Figure 3. Mass vaporization/combustion rate as a function of volume combusted. Again, real fuels follow a similar trajectory to idealized fuels, but 2 and 3 species blends do not. Vaporization rates significantly slow down during the transition period.

During blowout testing, it was qualitatively observed that while testing S-2, unburned liquid particles were escaping the combustor [30]. This did not occur for other fuels. This supports the theory that the discontinuous volatility distribution of 2 and 3 species blends is causing the issue. Each of the explanations proposed suggest there is difficulty in advancing past the transition period to the less volatile component. Other fuels tested with comparably high final boiling points didn't show this behavior.

To stress test this theory, more 2/3 species blends need to be tested. The blends should be constructed of species with highly different volatilities. Ideally the concentrations of each species are close to equal as possible; this would maximize the distinctness between the different phases of distillation and highlight the effects.

Relative Lifetime of Droplets

The second explanation for the unique behavior of some of the fuels is that the time scale of vaporization is lower for the blends. Three of the greatest outliers include nC_{16} as a blending component. This molecule is among the least volatile molecules typically found in jet fuel. Inherently this increases vaporization time to some degree. If the more volatile component vaporizes first, the remaining non-volatile nC_{16} will be left with less surface area for heat transfer into the droplet, enhancing the effect of the high distillation temperatures. This is strongly influenced by the observation of liquid fuel escaping the combustor for the tests of the fuel S-2 [30]. This effect does not explain all of the outliers but could contribute to moving these points closer to the DCN trend line.

Preferential Vaporization

The third explanation of the unique behavior of the 2 and 3 species blends is preferential vaporization. Each of the 2 and 3 species blends tested were a blend of a more reactive, less volatile species with a less reactive volatile species. Preferential vaporization suggests that the species concentrations vaporizing as a function of time changes which, by extension, impacts combustion behavior. Preferential vaporization has been shown to occur in droplet vaporization [13,29]. Preferential vaporization has been shown to have an effect in both ignition and extinction experiments [31,32]. If this behavior is occurring in the Referee Rig, the bulk DCN may not be the chemical property of significance, but rather some intermediate DCN partially through the distillation process.

The more volatile species will be the first to vaporize. Once vaporized they will be present throughout the process either in the form their original molecule, intermediate species, or products with their corresponding heat. The species with the most time in vapor form have the most potential to impact combustion. If preferential vaporization is the behavior driving the

performance deviation between the 2 and 3 species blends from the DCN-law, then it would be possible to have a fuel that outperforms the DCN-law.

To validate a preferential vaporization model, the instantaneous property, in this case DCN, needs to be numerically estimated throughout the distillation process. Because of the variety of fuels tested to be compared, three different approximations are used: 1) a constant DCN throughout the distillation process, 2) a linear by volume blending rule of DCN and 3) a Quantitative Structure-Property Relation (QSPR) regression approximation. A constant DCN was approximated throughout the distillation process for fuels that were never blended before testing. This approximation is used for the conventional fuels. Although it is possible these fuels have variation in properties throughout the distillation process, these variations are approximated as negligible because of the relatively normal distribution of the different species types throughout the molecular weight (MW) distribution [12]. A linear by volume blending rule, in conjunction with an approximated blend distillation method, is used to approximate fuels which are blends of fuels with known properties [33,34]. QSPR regression combined with the Antoine Equation and vapor-liquid equilibrium is used to estimate DCN throughout the distillation of the fuels with known species and concentrations [28]. The methods used for each fuel is shown in Table 2

Table 2. The method used to estimate DCN as a function of percent distilled for each fuel. *=Methyl-cyclohexane could not be used in QSPR because it does not yet include cyclo-paraffin behavior.

Constant DCN	Linear by Volume	QSPR Regression
A-1, A-2, A-3, Sasol IPK	C-2, C-3, C-4, C-5, A-2/C-1 blends, A-2/C-5 blend, nC_{12}/MCH*	C-1, nC_{12}, nC_7, nC_{12}/M-Xylene, nC_{12}/iC_8, nC_{12}/nC_{16}, nC_7/nC_{12}, S-1, S-2

Using the methods described above, the DCNs throughout the distillation curve are calculated and power law regressions of LBO, as a function of the instantaneous DCN, are run to identify the optimal predictive value. In Figure 4, the R^2's of the regressions of LBO, with the calculated instantaneous DCN as the only indicator, are shown. The ideal predicator is found to be the DCN through 34% of the distillation process with a corresponding R^2 of 0.824. This result suggests that for the Referee Rig the first 34% of the fuel to vaporize are the species which will drive when blowout will occur. For different combustor designs, the physical time scales would vary and would thus have a different ideal predictive indicator. The predicted LBO will follow the regression shown in equation 4.

$$\frac{\phi(LBO_i)}{\phi(LBO_{A2})} = \left(\frac{DCN34_i}{DCN34_{A2}}\right)^{-0.069} \quad (4)$$

This analysis shows DCN through 34% of the distillation process is a better indicator than the overall DCN of a fuel, however the current data only contains fuels with more reactive, 'second halves' of the distillation process. Although this parameter does not predict the overall combustion perfectly, the predicted results from the chemistry alone are unbiased. Figure 5 shows the absence of bias between predicted and experimental results. The resulting error could potentially be explained by other chemical and physical properties.

None of the fuels tested have 'beat' the limiting 'DCN trend.' To show preferential vaporization has an effect, it needs to be shown preferential vaporization can be leveraged to improve a fuels performance and not only make it perform worse. The goal is to produce a fuel that will land in below the DCN-law line. If the partially vaporized DCN value appropriately captures the chemical-physical interaction in describing lean blowout, then designing a fuel to beat this trend should be possible.

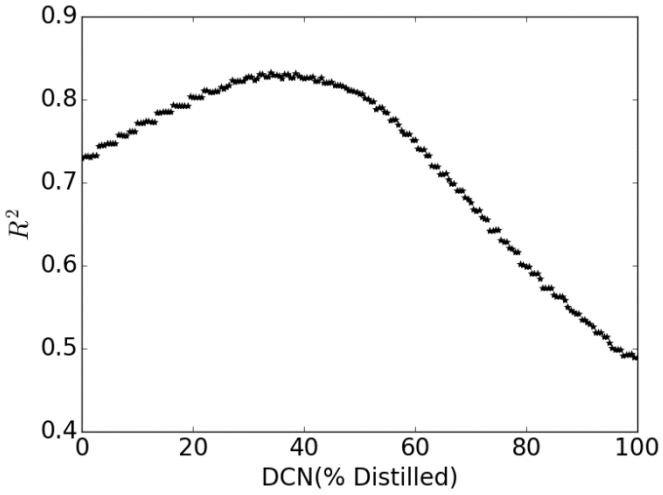

Figure 4. The R^2 of LBO vs instantaneous DCN, where DCN is a function of percent distilled. This result shows the optimal predictor of LBO for this experiment is the DCN at 34% distilled (R^2 = 0.824).

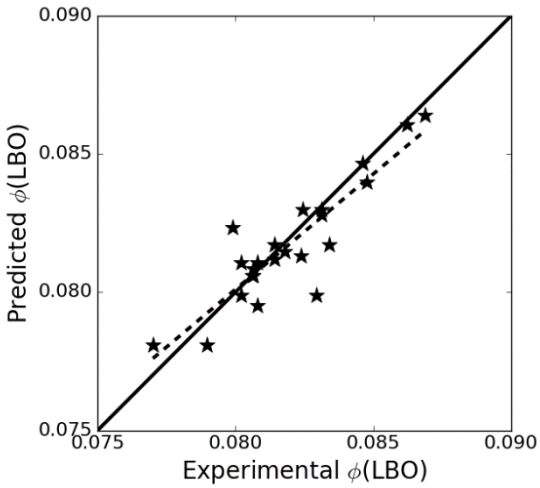

Figure 5. Predicted $\boldsymbol{\phi(LBO)}$ vs. Experimental $\boldsymbol{\phi(LBO)}$ for fuels reported in Table 1. The error associated with a prediction using Equation 4 is the distance from the solid line (R^2=0.824). The dashed line is a fit showing that there is consistency between experimental and predicted values.

Proposed Fuels

A fuel that will land below the DCN-law line needs to have a higher DCN at 34% vaporized than its overall DCN. To accomplish this, a fuel with high DCN and low molecular weight (MW), which corresponds with lower volatility, needs to be blended with a fuel with low DCN and high MW. Normal paraffins have the highest DCN among the different general molecular structures. Unfortunately, the normal paraffins with the highest DCN are the molecules with the highest MW. A range of *n*-paraffins are considered for use as the high DCN, low MW component in the blend. Low DCN, high MW fuels include large aromatics and large highly branched *iso*-paraffins. Highly branched *iso*-paraffins are preferred as the primary blending component because high concentrations of aromatics could have unforeseen effects as they less mimic previously tested fuels.

Fuel availability constraints lead us to a fuel which has already been tested, C-1. C-1 is a mix of almost exclusively *iso*-paraffins ranging from 5 to 20 carbons. It is heavily weighted towards highly branched *iso*-dodecane and *iso*-cetane [12]. For the purposes of this research, C-1 is approximated to be exclusively 80% by mole *iso*-dodecane and 20% by mole *iso*-cetane. *iso*-Cetane would be a near perfect candidate for the less reactive blending component due to its high MW and low DCN. In conventional jet fuels, there are very few molecules larger than 16 carbons, thus *iso*-cetane represents the upper bound for MW. *iso*-Cetane blends are considered as they represent an upper bound for maximizing preferential vaporization behavior.

The final fuel blend is selected as the blend that produces the highest difference between predicted LBOs by the DCN trend and the new 34% vaporized DCN regression in equation [2] (Figure 6). *n*-Paraffins between 7 carbons and 10 carbons are considered and blended with both C-1 and *iso*-cetane. Figure 7 shows the potential fuel blends and their respective differences between their predicted LBOs. The C-1 blended with *n*-heptane (nC_7) is the best option among C-1 blends offering a predicted difference of about 0.0022 in equivalence ratio at blowout with concentrations of 21% nC_7 and 79% C-1 by moles. The blend showing the greatest improvement with *iso*-cetane occurs similarly with *n*-octane (nC8) and *n*-nonane (nC9) offering a difference of about 0.0026 in equivalence ratio at blowout from the DCN-law line. This difference is achieved with 17% nC_8 and 83% *iso*-cetane as well as with 17% nC_9 and 83% *iso*-cetane.

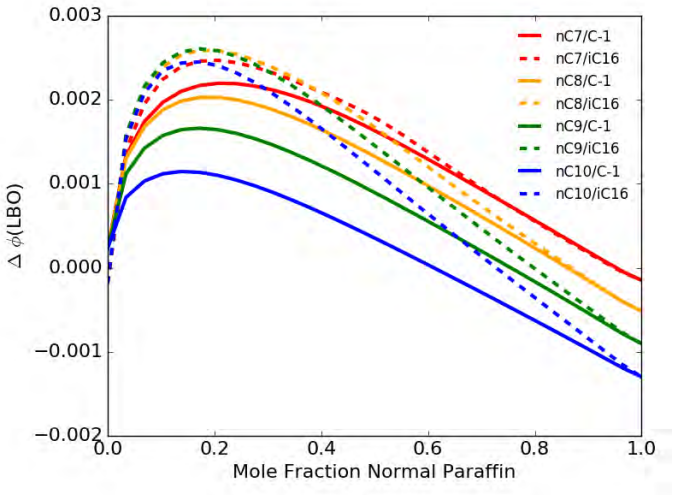

Figure 6. The difference between LBO predictions using DCN vs DCN through 34% of distillation. The difference is plotted for different blending ratios of n-paraffins mixed with C1 and Distilled C1. The peaks represent the ideal blending ratio for each blending combination.

The new blends as they are expected to perform are shown in Figure 8. Both the points for the generated fuels are in the target region, but not to the degree of the surrogates on the opposite side of the line. This is caused by physical limitations in the chemistry as low molecular weight species cannot have as high of DCN's as large molecular weight fuels. Each of the blends is shown as to their performance relative to the DCN trend line. Unfortunately, the predicted improvement below the DCN-law line is very close to the bounds of experimental error.

Both of the explanations for the outlier experimental results described above could be tested with one fuel. A 2-species blend fuel designed to test preferential vaporization would illuminate the impact of both effects if they are present. If the proposed fuels perform significantly worse than the DCN law line, then it would suggest it is not a chemical effect but rather a characteristic of 2 species blends. If the proposed fuels perform better than the DCN trend line, then it would be further evidence of preferential vaporization and its corresponding impact on chemistry, having an effect.

The Referee Rig, similar to other gas turbine combustors, requires a minimum amount of aromatics present in fuel to facilitate o-ring swelling. A large aromatic in relatively low concentrations can be added to the fuel and it should not significantly affect performance.

In theory, the effect of both of the described phenomenon would be enhanced in a low-pressure experiment. At lower pressures, individual species vaporize more ordinarily. Figure 8 shows the preferential distillation DCN values of S-2 at three different pressures. At 20 atm, the nC_{16} has higher relative partial vapor pressures resulting in higher molar concentrations to vaporize early in the process. This causes the partially distilled DCN to be higher at lower volumes distilled. At low pressures, a local minimum can be seen around 45% distilled. This is caused by the vaporization of the 1,3,5 TMB. At each of the pressures the final ~30% distilled is all nC_{16} vaporizing, resulting in similar paths.

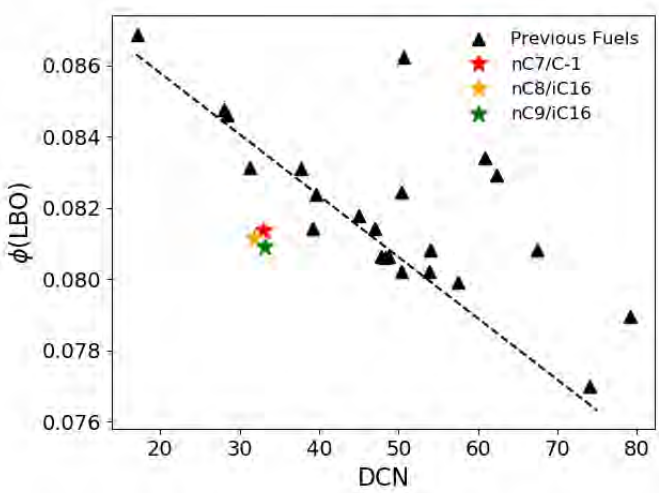

Figure 7. Shows the predicted LBO using preferential vaporization of the newly generated fuels. The new fuels would land below the current limiting bound.

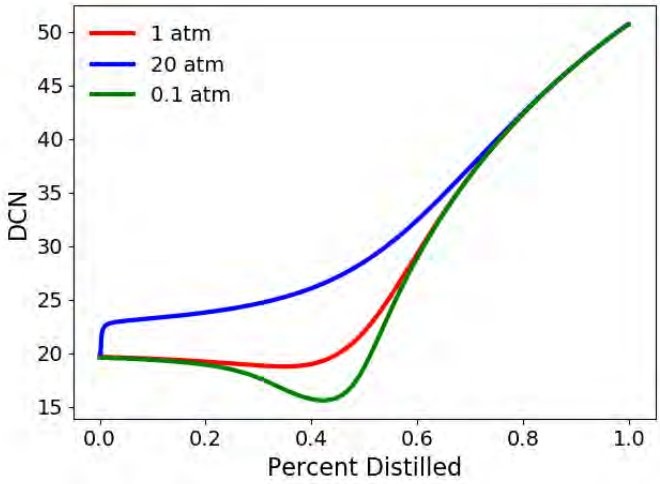

Figure 8. The DCN as a function of percent distilled of S-2 at various pressures. At high pressures, the species vaporize less ordinally. At 0.1 atm the decrease in DCN seen is the vaporization of 1,3,5 TMB. To maximize preferential distillation behavior, a low-pressure experiment is preferred.

It should be noted, tests at different pressures will significantly affect boiling points and correspondingly vaporization rates. This could have an unexpected impact on the overall behavior near lean blowout.

Conclusions

The time scales of evaporative, chemical, and chemical-evaporative have been discussed and developed into several hypothesis to explain LBO events anomalous to the previously reported DCN trend. This time scale analysis has been applied to LBO data reported on the Referee Rig at AFRL/UDRI. These analyses suggest that no single time scale analysis or coupling is sufficient to explain all the observation in the Referee Rig. Numerical analysis suggests that one developed hypothesis, preferential vaporization, has the possibility to explain much of the observed discrepancies versus the DCN trend. Additionally, fuel blend and compositions to test this hypothesis have been suggested to confirm or discredit this hypothesis (21% by mole *n*-heptane and 79% Gevo ATJ (C-1)). Finally, additional work is needed to explore in greater depth the quantitative effects of the other two hypothesis listed and discussed (thermal quenching and relative lifetime of a droplet).

References

[1] Colket, M. B., Heyne, J., Rumizen, M., Edwards, J. T., Gupta, M., Roquemore, W. M., Moder, J. P., Tishkoff, J. M., and Li, C., 2016, "An Overview of the National Jet Fuels Combustion Program," 54th AIAA Aerosp. Sci. Meet., (Jan), pp. 1–24.

[2] Heyne, J. S., Colket, M. B., Gupta, M., Jardines, A., Moder, J. P., Edwards, J. T., Roquemore, M., Li, C., and Rumizen, M., 2017, "Year 2 of the National Jet Fuels Combustion Program: Towards a Streamlined Alternative Jet Fuels Certification Process," *55th AIAA Aerospace Sciences Meeting*, p. 145.

[3] Hendershott, T. H., Stouffer, S. D., Monfort, J. R., Diemer, J., Corporan, E., Wrzesinski, P., and Caswell, A. W., 2018, "Ignition of Conventional and Alternative Fuel at Low Temperatures in a Single-Cup Swirl-Stabilized Combustor," *56th AIAA Aerospace Sciences Meeting*, American Institute of Aeronautics and Astronautics, Kissimmee, FL.

[4] Heyne, J. S., Peiffer, E., Colket, M., Shaw, C., Jardines, A., Moder, J., Edwards, J. T., Roquemore, W. M., Li, C., Rumizen, M., and Gupta, M., 2018, "Year 3 of the National Jet Fuels CombustionProgram: PRactical and Scientific Impacts of Alternative Jet Fuel Research," *56th AIAA Aerospace Sciences Meeting*.

[5] Chtev, I., Rock, N., Ek, H., Smith, T., Emerson, B., Nobel, D. R., Seitzman, J., Lieuwen, T., Mayhew, E., Lee, T., Jiang, N., and Roy, S., 2017, "Simultaneous High Speed (5 kHz) Fuel-PLIE, OH-PLIF and Stereo PIV Imaging of Pressurized Swirl-Stabilized Flames Using Liquid Fuels," *Submitted to the 55th AIAA Aerospace Sciences Meeting*, American Institute of Aeronautics and Astronautics, Grapevine.

[6] Stachler, R. D., Heyne, J. S., Stouffer, S. D., Miller, J. D., and Roquemore, W. M., 2017, "Investigation of Combustion Emissions from Conventional and Alternative Aviation Fuels in a Well-Stirred Reactor," *Submitted to the 55th AIAA Aerospace Sciences Meeting*, Grapevine, TX.

[7] Burger, V., 2017, "The Influence of Fuel Properties on Threshold Combustion in Aviation Gas Turbine Engines," (Feb).

[8] Plee, S. L., and Mellor, A. M., 1979, "Characteristic Time Correlation for Lean Blowoff of Bluff-Body-Stabilized Flames," Combust. Flame, **35**(C), pp. 61–80.

[9] Mellor, A. M., 1980, "Semi-Empirical Correlations for Gas Turbine Emissions, Ignition, and Flame Stabilization," Prog. Energy Combust. Sci., **6**(4), pp. 347–358.

[10] Lefebvre, A. H., and Ballal, D. R., 2010, "Gas Turbine Combustion," Book, **Third Edit**.

[11] Lefebvre, A. H., *Influence of Fuel Properties on Gas Turbine Combustion Performance*, West Lafayette, IN.

[12] Edwards, J. T., 2017, "Reference Jet Fuels for Combustion Testing," *Submitted to the 55th AIAA Aerospace Sciences Meeting*, American Institute of Aeronautics and Astronautics, Grapevine.

[13] Law, C. K., Prakesh, S., and Sirignano, W. A., 1981, "Theory of Transient Multicomponent Droplet Vaporization in a Convective Field," Symp. Combust., **18**(1), pp. 1365–1374.

[14] Yang, S., Ra, Y., and Reitz, R. D., 2010, "A Vaporization Model for Realistic Multi-Component Fuels," *Proceedings of the 22nd Annual Conference on on Liquid Atomization and Spray Systems*.

[15] Sirignano, W. A., 1983, "Fuel Droplet Vaporization and Spray Combustion Theory," Prog. Energy Combust. Sci., **9**(4), pp. 291–322.

[16] Clercq, P. Le, and Dou, N., 2009, "Validation of a Multicomponent-Fuel Model for Spray Computations *," 47th AIAA Aerosp. Sci. Meet., (January), p. 2009.

[17] Rauch, B., Le Clercq, P., Aigner, M., Rachner, M., Calabria, R., and Massoli, P., 2011, "Jet A-1 Fuel Spray Evaporation in a Turbulent Flow: Experimental Investigations and Validation of Numerical Models," *49th AIAA Aerospace Sciences Meeting*, Orlando, FL, pp. 1–13.

[18] Liu, Y. C., Savas, A. J., and Avedisian, C. T., 2012, "Surrogate Fuel Development Based on Droplet Combustion: Comparison of Multi-Component Mixtures with an Aviation Fuel," *50th AIAA Aerospace Sciences Meeting Including the New Horizons Forum and Aerospace Exposition*, Nashville, TN, pp. 1–8.

[19] Emerson, B., Lieuwen, T., and Juniper, M. P., 2017, "Local Stability Analysis and Eigenvalue Sensitivity of Reacting Bluff-Body Wakes," J. Fluid Mech, **788**, pp. 549–575.

[20] Hanson, R. K., "Personal Communication," December 2017.

[21] Bokhart, A. J., Shin, D., Rodrigues, N., Sojka, P., Gore, J., and Lucht, R. P., 2018, "Spray Characteristics at Lean Blowout

and Cold Start Conditions Using Phase Doppler Anemometry," *56th AIAA Aerospace Sciences Meeting*, Kissimmee, FL.
[22] Law, C. K., 2006, *Combustion Physics*, Cambridge University Press, New York.
[23] Law, C. K., 1982, "Recent Advances in Droplet Vaporization and Combustion," Prog. Energy Combust. Sci., **8**(3), pp. 171–201.
[24] Marti, F., Martinez, O., Mazo, D., Garman, J., and Dunn-Rankin, D., 2017, "Evaporation of a Droplet Larger than the Kolmogorov Length Scale Immersed in a Relative Mean Flow," Int. J. Multiph. Flow, **88**, pp. 63–68.
[25] Law, C. K., and Law, H. K., 1982, "A d2-Law for Multicomponent Droplet Vaporization and Combustion," AIAA J., **20**(4), pp. 522–527.
[26] Stouffer, S., Hendershott, T., Monfort, J. R., Diemer, J., Corporan, E., Wrzesinski, P., and Caswell, A. W., 2017, "Lean Blowout and Ignition Characteristics of Conventional and Surrogate Fuels Measured in a Swirl Stabilized Combustor," *55th AIAA Aerospace Sciences Meeting*, Grapevine, TX, pp. 1–14.
[27] Corporan, E., Edwards, J. T., Stouffer, S., DeWitt, M., West, Z., Klingshirn, C., and Bruening, C., 2017, "Impacts of Fuel Properties on Combustor Performance, Operability and Emissions Characteristics," *55th AIAA Aerospace Sciences Meeting*, pp. 1–19.
[28] Won, S. H., Haas, F. M., Dooley, S., Edwards, T., and Dryer, F. L., 2017, "Reconstruction of Chemical Structure of Real Fuel by Surrogate Formulation Based upon Combustion Property Targets," Combust. Flame, **183**, pp. 39–49.
[29] Wang, C. H., Liu, X. Q., and Law, C. K., 1984, "Combustion and Microexplosion of Freely Falling Multicomponent Droplets," Combust. Flame, **56**(2), pp. 175–197.
[30] Stouffer, S. D., "Personal Communication," Novemb. 2017.
[31] Stagni, A., Esclapez, L., Govindaraju, P., Cuoci, A., Faravelli, T., and Ihme, M., 2017, "The Role of Preferential Evaporation on the Ignition of Multicomponent Fuels in a Homogeneous Spray/air Mixture," Proc. Combust. Inst., **36**(2), pp. 2483–2491.
[32] Yi, F., and Axelbaum, R. L., 2014, "Utilizing Preferential Vaporization to Enhance the Stability of Spray Combustion for High Water Content Fuels," Combust. Flame, **161**(8), pp. 2008–2014.
[33] Bell, D., Heyne, J. S., Won, S. H., Dryer, F. L., Haas, F. M., and Dooley, S., 2017, "On the Development of General Surrogate Composition Calculations for Chemical and Physical Properties," *55th AIAA Aerospace Sciences Meeting*, American Institute of Aeronautics and Astronautics, Grapevine, TX.
[34] Lefkowitz, J. A., and Haas, F. M., 2017, "Distillation-Resolved Evolution of Key Combustion Properties," *10th U.S. National Combustion Meeting*, College Park, Maryland.

Major Accomplishments

- Explained observed LBO behavior, which had previously appeared to be anomalous.

Publications

Conference Proceedings:

Bell DC, Heyne JS, Won S, Dryer FL. The Impact of Preferential Vaporization on Lean Blowout in a Referee Combustor at Figure of Merit Conditions. ASME. ASME Power Conference, *Volume 1: Fuels, Combustion, and Material Handling; Combustion Turbines Combined Cycles; Boilers and Heat Recovery Steam Generators; Virtual Plant and Cyber-Physical Systems; Plant Development and Construction; Renewable Energy Systems* ():V001T01A011. doi:10.1115/POWER2018-7432.

Outreach Efforts

Conference presentations:

Bell DC, Heyne JS, Won S, Dryer FL. The Impact of Preferential Vaporization on Lean Blowout in a Referee Combustor at Figure of Merit Conditions. ASME. ASME Power Conference, *Volume 1: Fuels, Combustion, and Material Handling; Combustion Turbines Combined Cycles; Boilers and Heat Recovery Steam Generators; Virtual Plant and Cyber-Physical Systems; Plant Development and Construction; Renewable Energy Systems* ():V001T01A011. doi:10.1115/POWER2018-7432.

Awards

David Bell, 2018 Young Engineer of the Year- ASME Dayton Section Award

Student Involvement

David Bell led this project.

Task 5 - Cross-Experiment Analysis

University of Dayton

Objective(s)

The objective of this task is to link low-cost fundamental experiments to larger cost more complicated experiments internal to the NJFCP.

Research Approach

Methodology

The combustor rigs in the NJFCP aim to capture combustor variations found in actual gas turbine engines. In testing in the different combustors, rig sensitivity to fuel properties can be more fully realized. The Referee Rig, Georgia Tech, Sheffield, Cambridge, UTRC, and DLR rigs are all variations of traditional Rich-Quench-Lean combustors. The Honeywell rig is an Auxiliary Power Unit, a combustor that is used to start the main engines and provide emergency backup for electrical systems in the case of engine failure during flight. As such, this combustor is smaller than the other rigs in the program. The last rig in the program, the Well Stirred Reactor (WSR), is premixed and pre-vaporized. Although not currently used in gas turbine engines, the WSR is a useful research tool to evaluate the chemical fuel property effects on combustion. Table 1 provides a breakdown of the combustor rigs in the NJFCP including atomizer geometry and the operating conditions tested. An additional column, "Random Forest", was included to indicate the rigs that were used in the random forest regression results presented later.

The results discussed in this paper include conventional (Category A) and test (Category C) fuels, with the latter representing a large range of physical, volatile, and chemical properties. Category A fuels are conventional petroleum-derived fuels in use today that characterize the 'best' to 'worst' range of fuel properties while Category C fuels represent alternative jet fuels having extreme properties.

Figure 1 shows how the Category C fuel properties compare to the conventional Category A fuels. Notably, many of the Category C fuels fall outside the range of current experience, as depicted in the red regions on the plot, allowing for insight into how these fuels impact the key FOM.

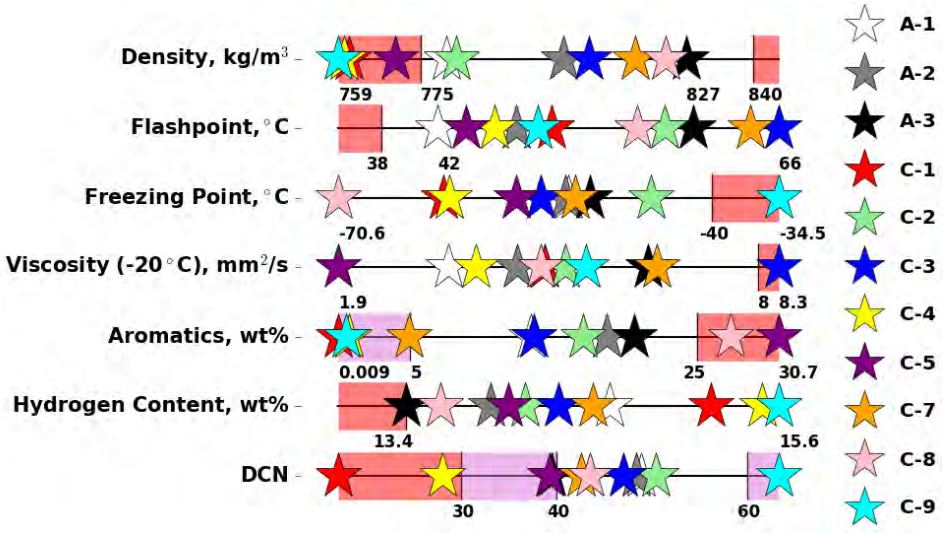

Figure 1. Category A and C range of fuel properties. The red regions represent current specification limits while the purple regions represent areas of interest to explore.

Table 1. NJFCP combustor rig descriptions and LBO test conditions for each institution. The DCN Slope column records the LBO vs DCN slope representing rig sensitivity to DCN. Rig data used in future Random Forest results are indicated here.

Rig Name	Geometry type (injector/swirler)	Secondary air jets	T_{air}, K	T_{fuel}, K	P, atm	DCN Slope	Institution	Random Forest
PA-GT	Pressure atomizer/ Pratt & Whitney Swirler	No	550, 450, 300	445-460	3.4	-0.194	Georgia Tech	
PA-HON	Pressure atomizer/ toroidal	No	324, 525, 557, 562, 394	288	1, 1.3, 1.4, 2, 3.3, 5.7	NA*	Honeywell	X
PA-RR	Pressure atomizer/ High-Swirl (P03)	Yes	239, 258, 400	239, 258, 320	2	-0.242	AFRL/ UDRI	X
PV-WSR	Prevaporized/ toroidal	No	450	450	1	-0.070	AFRL/UDRI	X
AA-SH	Airblast atomizer/ swirler stabilized/Rolls-Royce Tay Combustor	Yes	323, 373, 423		1	-0.273	Sheffield	X
PA-CAM	Pressure in bluff-body/	Yes	340	300	1	-0.254	Cambridge	
PA - UTRC	Pressure atomizer/ Pratt & Whitney Swirler	No	555, 494		8.64, 5.6	-0.153	UTRC	
PA-DLR	Pressure atomizer/ swirl stabilized	No	323, 373		1	-0.102	DLR Germany	

***HON data renormalized to protect proprietary rig information**

Tables 2 and 3 provide a summary of the fuels tested and included in the results for this paper. In addition to the A and C fuels included in Table 2, there are F fuels which are blends of the A and C fuels, and there are the surrogate (S) fuels which were designed to stress specific fuel properties. Detailed properties of the Category A and C fuels are provided by Edwards[13] and properties for other mixtures and blends were estimated using standard (linear) mixing rules. Radical indexes, a scaled determination of a fuels reactivity at strained extinction, for the A and C fuels were obtained from previously published literature[14] while surrogate values were calculated by the summation of mole fractions multiplied by their corresponding radical index[15].

Table 2. NJFCP category A and C fuels representing petroleum-derived and alternative fuels, respectively. The F fuels are blends consisting of both the A and C fuels. The S fuels are surrogates that were designed to stress certain fuel properties.

Fuel/Solvent Mixture	POSF Number	Composition, % volume	Description
A-1	10264	Petroleum JP-8	Low flash, viscosity, and aromatics
A-2	10325	Petroleum Jet A	Nominal jet fuel
A-3	10289	Petroleum JP-5	High flash, viscosity, and aromatics
C-1	11498, 12368, 12384	Gevo ATJ, Highly branched C12 and C16 paraffins	Low DCN, unusual boiling range
C-2	11813, 12223	16% *tri*-methylbenzene + 84% C14 *iso*-paraffins	Chemically-asymmetric boiling range
C-3	12341, 12363	64% A-3 + 36% farnesane	High viscosity fuel, at viscosity limit for jet fuel at -20˚C
C-4	12344, 12489	60% C9-12 *iso*-paraffins, 40% C-1	Low DCN, conventional, wide boiling range
C-5	12345, 12713, 12789, 12816	73% C10 *iso*-paraffins, 17% *tri*-methylbenzene	Flat boiling range
C-6		High cycloalkane content	High *cyclo*-paraffins
C-7	12925	75% RP-2, 23% A-3, 2% decalin	High *cyclo*-alkanes
C-8	12923	Jet A + Exxon aromatic blend	High (maximum allowable) aromatics
C-9	12933	80% R-8 HEFA, 20% *n*-C12	High DCN
F-1	NA	80/20 A-2/C-2	Blends
F-2	NA	50/50 A-2/C-1	Blends
F-3	NA	20/80 A-2/C-1	Blends
F-4	NA	80/20 A-2/C-5	Blends
J-1	NA	75.5% 1,3,5-tri-methylbenzene, 24.5% n-dodecane	Similar DCN to C-1 with low Radical Index
n-C12	NA	n-C12	High DCN
S-1	12765	59.3/18.4/22.2 vol% *n*-dodecane/ *iso*-octane/ 1,3,5-*tri*-methylbenzene	Similar to A-2, lower density and average molecular weight
S-2	12785	52.6/25.1/22.2 vol % *n*-hexadecane/ *iso*-octane/1,3,5-*tri*-methylbenzene	Similar to A-2, higher density and average molecular weight

Table 3. Fuels tested for LBO in each of the NJFCP rigs.

	A-1	A-2	A-3	C-1	C-2	C-3	C-4	C-5	F-1	F-2	F-3	F-4	S-1	S-2	nC12
GT	X	X	X	X	X	X	X	X	X	X	X		X	X	X
Honeywell	X	X	X	X	X			X							
Referee Rig	X	X	X	X	X	X	X	X	X	X	X	X	X	X	X
WSR		X	X	X			X								X
Sheffield	X	X	X	X		X	X	X							
Cambridge		X		X				X							
UTRC	Sasol IPK, F-76, L-210, JP-5, Jet-A, L-142, HRJ JP-5, Linpar 1416														
DLR	Crude-derived Jet A-1 ,Jet A-1 + 50% n-dodecane, FSJF (certification), FSJF (commercial), FSJF (commercial) + 1.5% HCPP, Experimental GTL kerosene, Synthetic paraffinic kerosene (SPK), Heavy naphtha refinery stream														

A methodological approach was taken to examine the observed differences in rig sensitivities, starting first with a statistical analysis of the LBO data from each rig using random forest regressions, as seen in Figure 4- Figure 7. Random forests, a machine learning technique, utilize a "forest" of decision trees to model complex sets of data without overfitting. A "forest" of regression trees, 500 in this case, is formed from the original data set by random sampling with replacement, also called bagging, which helps to de-correlate the trees and reduce bias. Each regression tree is then grown using Equation 2 where j is the splitting variable, s is the split point, R is the region, and c is the average y_i in the region. Trees are then modeled using Equation 3 where c_m is the average of $y_i|x_i \in Rm$.

$$\min_{j,s}\left[\min_{c_1}\sum_{x_i\in R_1(j,s)}(y_i-c_1)^2+\min_{c_2}\sum_{x_i\in R_2(j,s)}(y_i-c_2)^2\right] \tag{2}$$

$$f(x)=\sum_{}^{M}c_m I(x\in R_m) \tag{3}$$

For the regression, an additional level of randomness is added by randomly selecting m variables from p total variables at each node. The random forest predictor is then calculated using Equation 4 where B is the number of trees, $\{T(x;\Theta_b)\}_1^B$ is the actual trees in which $\Theta_b$describes the bth tree in terms of split variables, cut points, and terminal-node values. In this case, the tree continues to grow until the number of samples left at a given node is two.

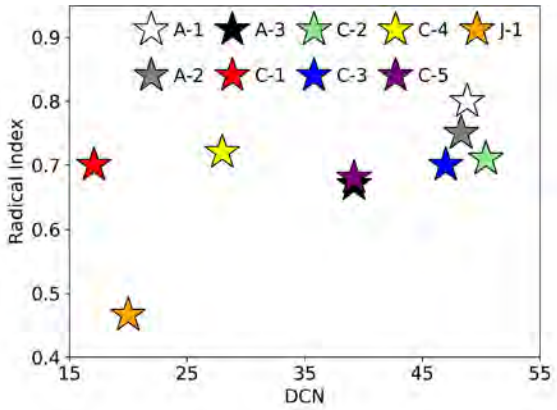

Figure 3. DCN versus Radical Index for the A and C fuels shows how high iso-octane fuels such as C-1 stress their correlation. The J-1 fuel was designed to further explore the importance of Radical Index relative to DCN.

$$\hat{f}_{rf}^{B}(x)=\frac{1}{B}\sum_{b=1}^{B}T(x;\ \Theta_b) \tag{4}$$

From the random forest predictor, features from the regression can be identified based on their importance to the model. These feature importance plots were used to understand the properties most impactful in LBO for each rig. For the LBO random forest regressions, the equivalence ratios (ϕ) at blowout for each fuel were normalized to A-2 to allow for equivalent comparison across rigs in combined regressions. This normalized phi value was used as the output of the regression while all other fuel characteristics, including volatile, physical, and chemical properties, along with test conditions (when relevant) were used as the predictors.

To better illuminate the importance of the characteristic timescales resulting in LBO, one fuel property was chosen to represent each of the timescales. The properties chosen in an attempt to maintain orthogonality, that is the variables (properties) are not correlated or covariate of each other. Twenty percent (20%) recovered, one measure of a fuel's volatility, was chosen to represent droplet evaporation. Viscosity was considered to represent the primary and secondary droplet breakup, but due to its high correlation with the distillate properties, density was chosen instead to characterize droplet break-up times.[16] Although DCN and radical index are highly correlated for fuels with high aromatic or n-alkane content, fuels with high *iso*-alkane content, such as C-1, break this correlation as seen in Figure 3. Additionally, the J-1 fuel was designed to have a DCN similar to C-1 with a lower radical index to stress the difference in the two fuel properties as explore by Stachler, et. al.[15] As such, DCN was used to represent the autoignition timescale while radical index was used to characterize the extinction timescale. Table 4 shows the breakdown of fuel property and corresponding timescale.

Table 4. Fuel properties were chosen to characterize each of the different timescales on the progression to LBO to orthogonalize the random forest results.

Fuel Property	Timescale
DCN	Autoignition
20% Recovered	Droplet Evaporation
Density	Primary and Secondary Droplet Breakup
Radical index	Extinction

Results

The results presented here focus on individual rig regressions as it was found that combined regressions were limited by the geometrically known properties of each rig. Of the nine rigs mentioned, only four are discussed here to show the range of rig physical property effects, where the WSR and Honeywell APU rig represent the extreme ends, and the Referee Rig and Sheffield rig represent real main engine effects. For the combined regressions to capture more variability in the data adequately, more detailed rig descriptions are needed. While past combined random forest regression results showed DCN as being the most important feature, interestingly, individual rig regressions show a wide range of results with additional fuel properties and test conditions appearing to have significant influence. As shown in Figure 4 the individual regression for the Referee Rig, when considering only the timescale representative fuel properties, shows DCN, or the autoignition timescale, as being the dominating timescale followed by droplet evaporation and droplet breakup. The extinction timescale, represented by radical index, was the least important timescale for this rig. The WSR, as seen in Figure 5 shows both the autoignition and extinction strain rate chemical timescales as being the most important in determining LBO, supporting past reported results. In contrast, for example to the WSR regression, the random forest regression for Honeywell shows DCN and radical index as the least important fuel properties in determining LBO while volatile and physical properties dominate, as seen in Figure 6[17]. Honeywell was able to test for LBO at a variety of inlet temperature and pressures unlike the other rigs discussed here, and as expected, these inlet conditions were among the top features important in determining LBO. Lastly, Sheffield, in Figure 7, showed droplet breakup and the autoignition timescales to be of near equal importance in the progression to LBO followed by droplet evaporation and extinction. Interestingly, using only four fuel properties representative of the various timescales in the progression to LBO yielded R-squared values comparable to the random forest regressions in which all fuel properties were included.

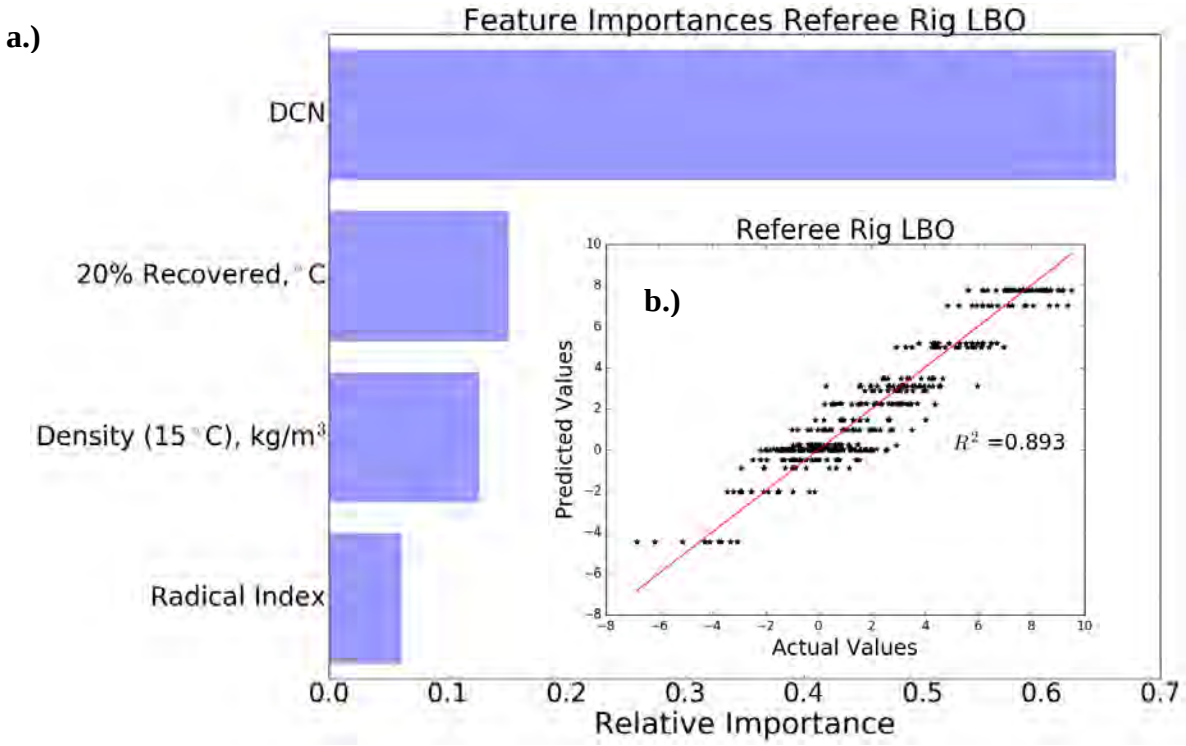

Figure 4. a.) Feature importances from the random forest regression for the Referee Rig show DCN as the most important fuel property representative of the autoignition timescale. b.) The predicted versus actual LBO data points are presented here.

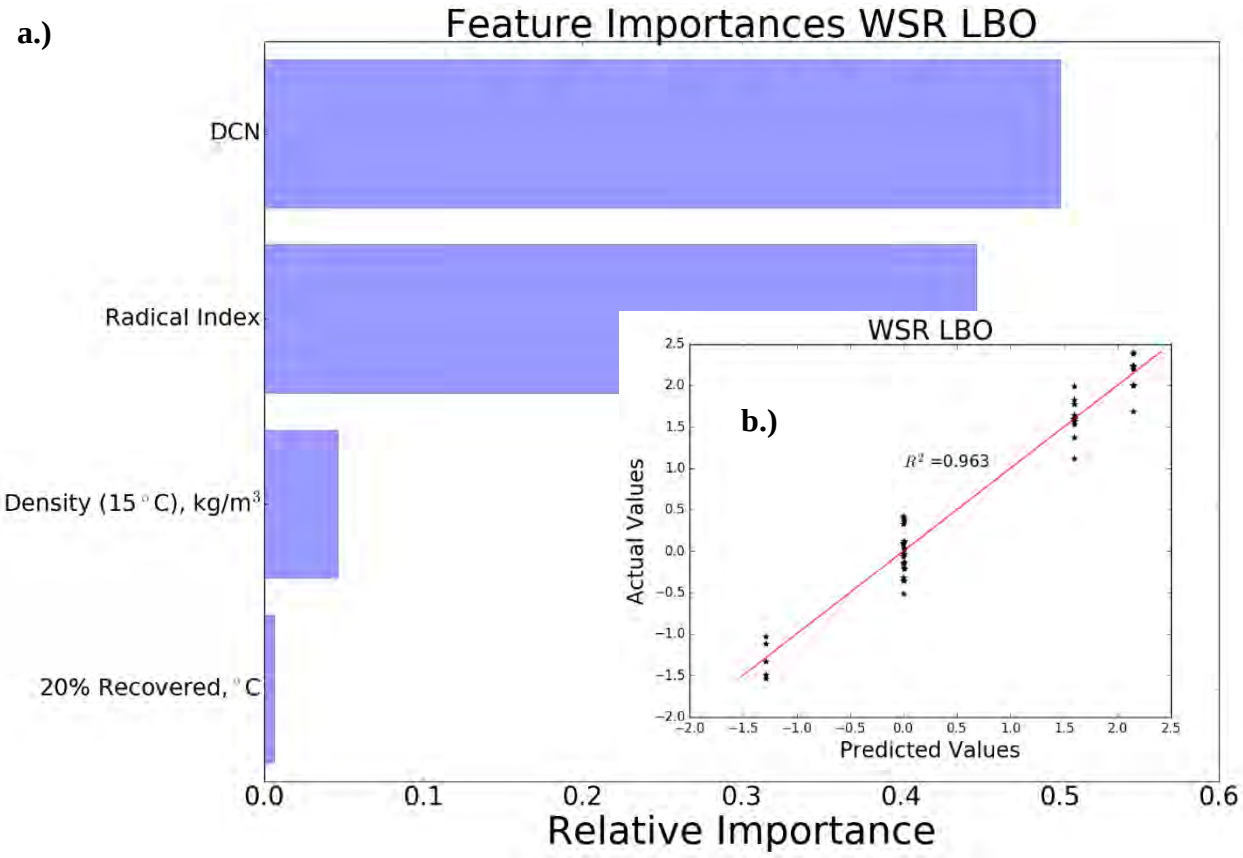

Figure 5. a.) Feature importances from the random forest regression for the Well-Stirred Reactor show the chemical timescales represented by DCN and radical index as being the most important features in determining LBO. Other properties such as distillate and physical properties show almost no statistical significance in the regression. b.) The predicted versus actual normalized LBO points are shown here.

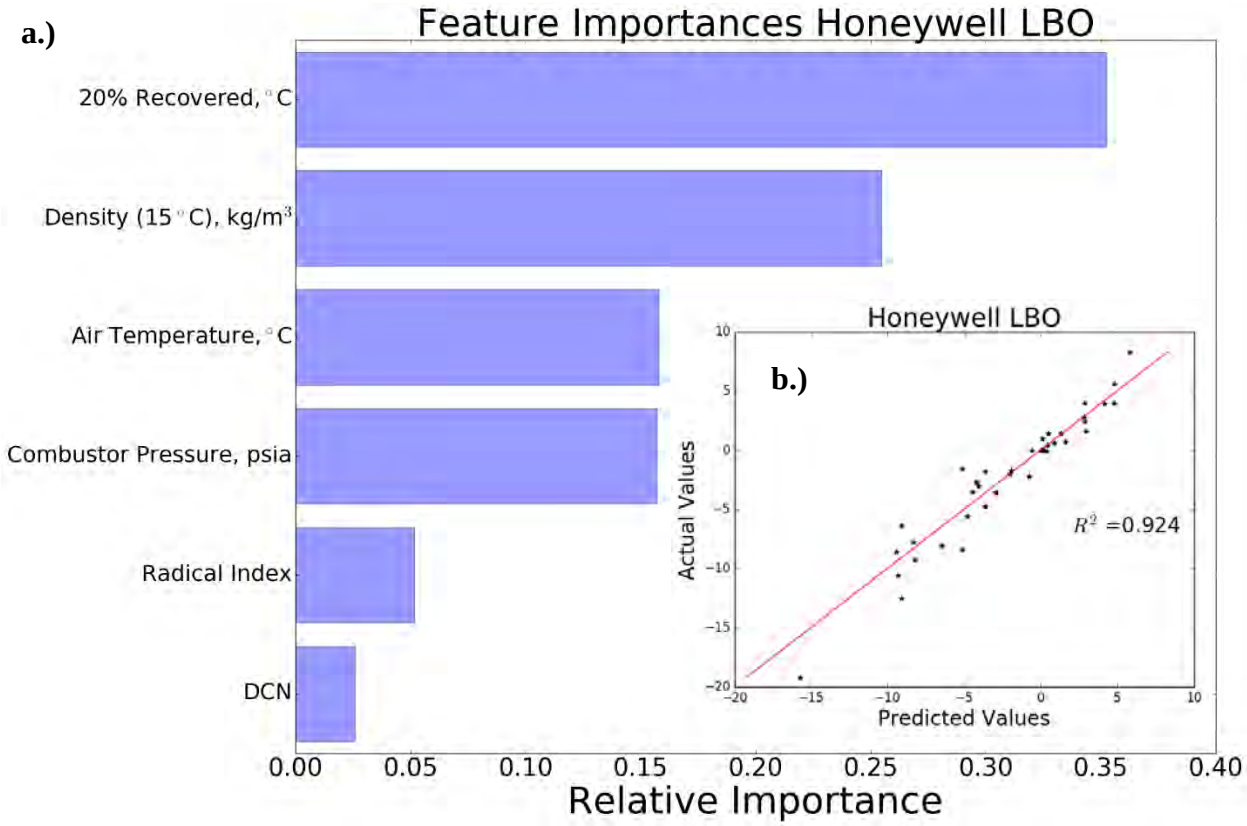

Figure 6. a.) Feature importances from the random forest regression for the Honeywell APU rig, the only rig in the NJFCP that does not show a dependency on DCN for predicting LBO. Distillate and density fuel properties, representative of droplet evaporation and breakup size, respectively, along with inlet temperature and pressure conditions were identified as the most import features for LBO for this rig. b.) Please note that the actual versus predicted values have been intentionally renormalized to protect proprietary information. Without the air temperature and combustor pressure parameters, the random forest regression only captures 61% of the variability in the data compared to the 92% presented here.

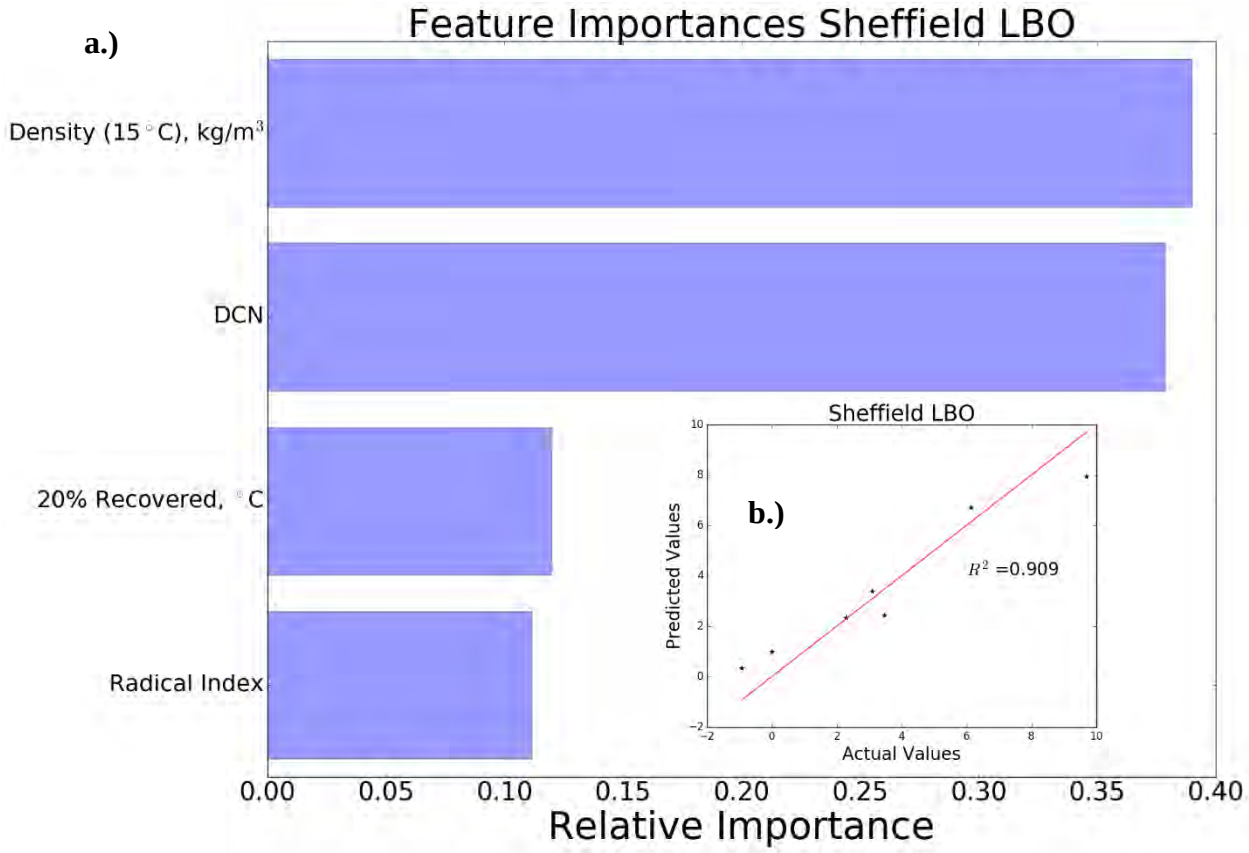

Figure 7. a.) Feature importances for the Sheffield rig show density, representative of droplet breakup, and DCN, representative of the autoignition timescale, as being of equal importance. b.) The predicted versus actual normalized LBO points are shown here.

Discussion

Although each rig expressed a different sensitivity to DCN, here we elaborate on a previously reported theory tying the observed sensitivity to experimental configuration of various rigs. Previously, a timescale analysis was suggested to account for preferential vaporization[18], spray-chemical reactivity timescales[4], and historical explanations of relative physical process times[3]. Figure 8 illustrates LBO as conceptual flow chart, beginning with fuel atomization and terminating with chemistry. LBO occurs when any of the six broad independent variables perturbe the system sufficiently that chemical heat release effectively terminates. Three of these broad physical variables revolve around fuel properties, and three physical variables revolve around geometrical and flow rate variables. Purple ovals represent fuel properties that can perturb stabile burning and coral ovals represent geometrical biases to the system. Fuel properties, purple ovals, are incorporated in the each of the previously reported random forest regressions. Geometrical variations across rigs, coral ovals, are only captured in combined random forest regressions, not reported here, through atomizer and rig geometry distinctions.

The six broad independent variable sets that can lead to LBO can additionally be described as three dependent times scales- referred to as evaporative, mixing, and chemical timescales. These timescales, therefore, are a combination of relevant fuel properties, geometrical biases, thermodynamic conditions, and rig flow rates. LBO occurs when a geometrically biased fuel property dependent timescale exceeds some other critical rig dependent timescale, such as primary recirculation or bulk rig residence times. Here the three dependent timescales are further explored and estimated to explain the relative fuel sensitivity differences across rigs.

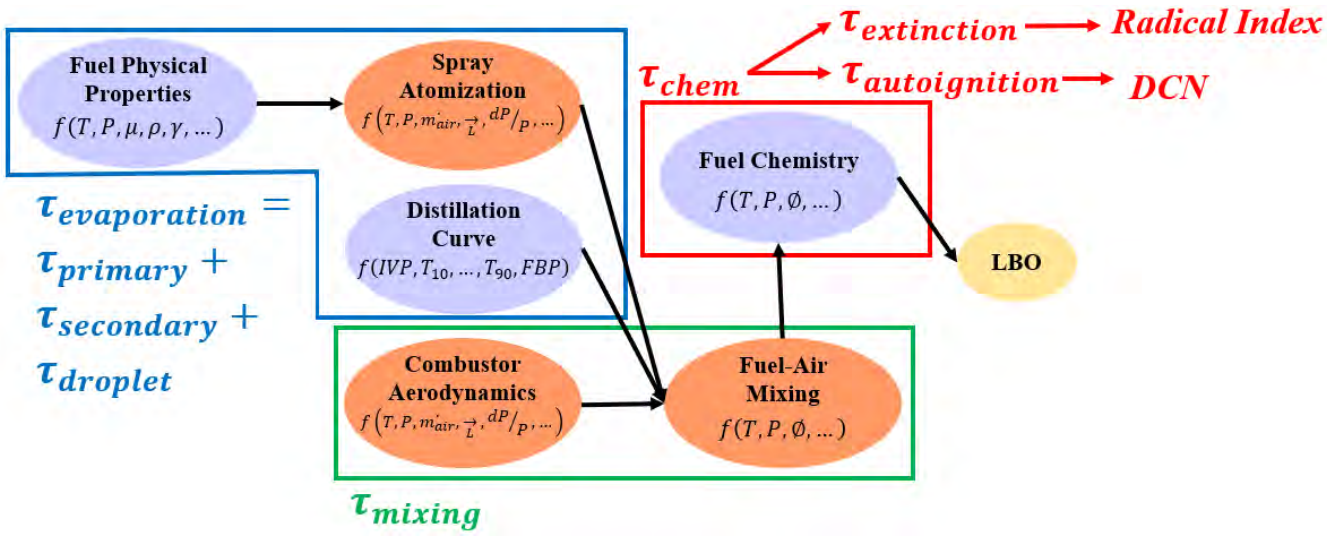

Figure 8. The pathways to LBO can be broken down into a conceptual flowchart. The purple ovals represent fuel properties while the orange ovals represent combustor characteristics. These pathways can be grouped to illustrate the evaporative, mixing, and chemical timescales that are factors in affecting blowout.

The evaporation timescale is a function of fuel physical properties, distillate properties, and atomizer characteristics for a given set of conditions. It can be approximated as the algebraic sum of primary atomization, secondary atomization, and droplet timescales. Primary and secondary atomization timescales increase with increasing fuel density, surface tension, and viscosity. Larger atomization timescales then result in larger droplets and longer evaporation times, and it should be noted that the atomization method has a significant effect on the primary and secondary atomization timescales. The droplet timescale of a fuel can be estimated with fuel volatility, as expressed through the distillation curve. Increases in the relative distillation temperatures of a fuel result in longer droplet timescales via larger characteristic heat capacities and lower vapor pressures. While all of the distillate properties are highly correlated, the 20% recovered temperature has been found to be the most influential in predicting LBO of the volatile properties for the rigs discussed here and thus was used in the earlier regressions.

The mixing timescale includes both combustor aerodynamics and fuel-air mixing, no fuel properties. Combustor aerodynamics is a function of combustor geometry ($\vec{L}$), temperature (T), pressure (P), mass flowrates of fuel and air ($\dot{m}$), relative pressure drop $\left(\frac{dP}{P}\right)$, along with other combustor operating conditions. The combustor timescale for mixing is assumed to be constant for a given rig at a given set of conditions.

Finally, the chemical timescale is a function of the fuel chemical properties and, similar to perfectly stirred reactor (PSR) theory, can be described as two timescales. PSR theory predicts an extinction and ignition timescale. Similarly, extinction and autoignition timescales have been observed[6] and speculated[15] from various NJFCP rigs reported here. Autoignition timescales are estimated from the DCN of a fuel, and extinction timescales can be approximated using radical indexes and extinction strain rates[15]. The relative concentrations of aromatics, *iso*-paraffins, *n*-paraffins, and cyclo-paraffins result in a fuel's radical index and DCN, which are derived directly from a fuel's chemical reaction pathways, specific energy [MJ/kg], and diffusivity [molecular weight, gm/mol]. Interestingly, autoignition timescales can be derived from both zero-dimensional simulations and measurements, but extinction timescales have been best approximated by one dimensional experiments.

Combined, these timescales can be used to illuminate dominate/controlling timescales/physics in each of the aforementioned rigs, which can be used to inform the ASTM alternative jet fuel evaluation and approval process. Figure 9 illustrates estimated (relative) timescale differences between the four rigs with the total time normalized to the same value. Evaporation timescale (blue) and chemical timescale (red) are estimated from the random forest regressions while the mixing timescale (green) is currently unquantified between the rigs (but is nearly constant for a rig across the fuels tested).

Collectively, the four rigs show chemical and evaporative dominated results as well as a rig with a competition between chemical and evaporative timescales.

Chemical timescales dominate for the Referee Rig and the WSR. The observed results for the WSR corroborate expectations, as the rig introduces prevaporized and premixed fuel into the reacting region. In the absence of any two-phase flow in the reactor, the evaporative timescale influence is anticipated to be zero. Similarly, Stachler et al. have shown in more detail that extinction strain rates (via radical indexes) are likely the controlling timescale for extinction strain rates. From the above regressions and past results, the WSR has demonstrated a dependence on DCN for predicting LBO. Alternatively, it can be argued that pure extinction is playing a much larger and limiting role than in the other combustor designs with strong recirculation.

The swirler and wide nozzle spray angle of the Referee Rig are anticipated to be the root causes for chemical timescale dominance in the Referee Rig. It is hypothesized that the strong recirculation zone, caused by the swirler, of the Referee Rig relative to the Honeywell APU elevates the probability of a reignition event in the region of primary recirculation. Additionally, the wide spray angle of the Referee Rig causes wetting on the surface of the swirler[7]. This wetting in turn enables an additional mechanism for atomization and spray break-up. Combined, it is hypothesized that the swirler and wide spray angle diminish the sensitivity of LBO to evaporative timescales.

Evaporative timescales are observed to dominate in the Honeywell APU, with chemical-evaporative timescales appearing to be in equilibrium in the Sheffield rig. Honeywell, in complete contrast to the WSR, showed almost no dependence on the chemical properties encompassing the chemical timescale in the progression to LBO[16]. Instead, the droplet breakup and evaporation are the dominating timescales. The Honeywell rig, in contrast to the WSR and Referee Rig, does not have a swirler, nor does it pre-vaporize or premix the fuel. Additionally, the Honeywell rig has a considerably smaller pressure atomizer. Pressure atomizers are known to more sensitive to atomization properties relative to air blast atomizers, with smaller pressure atomizers known to be even more sensitive to physical properties than larger pressure atomizers. This analysis, again, is consistent with existing/historical conceptual understandings of fuel spray effects.

The Sheffield rig shows an even split between the droplet breakup and autoignition timescale on the progression to LBO. As the Sheffield rig utilizes an airblast atomizer in contrast to the other pressure and pre-vaporized rigs, the larger dependence on density and other droplet breakup properties is well explained, although further analysis is needed to explain the autoignition timescale importance. The evaporative timescale and extinction timescale were found to be of lesser significance on the progression to LBO.

Of the seven rigs, the three most sensitive to DCN have secondary air jets which act to strengthen the primary recirculation zone. This would help to explain past results showing the DLR rig[4], a rig similar to the Referee Rig except without secondary air jets, having a much smaller sensitivity to DCN. This hypothesis could be confirmed through the acquisition of swirl numbers, a property than can be used to describe a combustor's primary recirculation zone strength. Additionally, continued LBO tests with varying secondary air jet configurations/strengths could confirm this hypothesis as well.

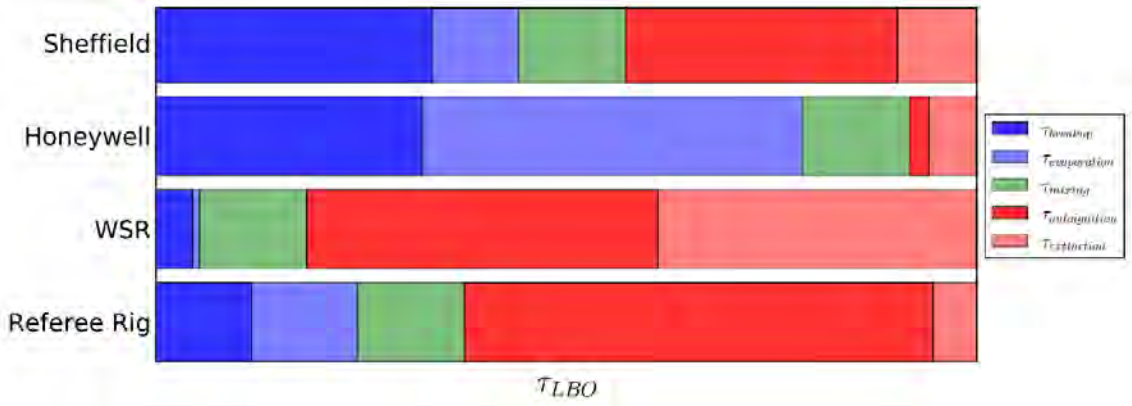

Figure 9. The LBO timescale, a summation of the evaporative (blue), mixing (green), and chemical (red) timescales, for the Referee Rig, Well-Stirred Reactor (WSR), and Honeywell based on feature importances from the random forest regressions. The mixing timescale was not captured in the regressions and thus the relative size of its timescale is unknown, represented here by two areas that suggest the true value could be larger or smaller than what is shown here.

Conclusion

The sensitivity of a combustor to fuel effects at LBO will remain a hurdle towards the certification of alternative jet fuel. This paper has sought to explain the differences in rig sensitivity at LBO for four down selected fuel properties. These down selected fuel properties are proposed to represent four fuel property dependent timescales near LBO. Random forest regressions with these four properties over four rigs were able to explain nearly 90% or better of all variance across all fuels considered. This analysis was extended to describe the relative timescales in each rig as LBO is approached.

Two rigs were shown to have chemical timescales dominate near LBO. Chemical timescales were dominate in the event of minimal spray importance via swirler recirculation, prevaporization, and rapid atomization as in the WSR and Referee Rig. The Honeywell APU, with its small pressure atomizer and lack of swirler, was shown to be dominated by evaporative timescales. The Sheffield rig was observed to have nearly equal evaporative and chemical timescale importance. Additional investigation into this rig is needed to fully explain the relative fuel effects in this rig. Future work will involve quantifying each timescale through modelling.

References

[1] Friedrich, C., and Robertson, P. A., "Hybrid-Electric Propulsion for Aircraft," *Journal of Aircraft*, vol. 52, 2015, pp. 176–189.

[2] Plee, S. L., and Mellor, A. M., "Characteristic time correlation for lean blowoff of bluff-body-stabilized flames," *Combustion and Flame*, vol. 35, 1979, pp. 61–80.

[3] Mellor, A. M., "Semi-empirical correlations for gas turbine emissions, ignition, and flame stabilization," *Progress in Energy and Combustion Science*, vol. 6, 1980, pp. 347–358.

[4] Burger, V., "The Influence of Fuel Properties on Threshold Combustion in Aviation Gas Turbine Engines," 2017.

[5] Heyne, J., Peiffer, E., Colket, M., Moder, J., Edwards, J. T., Roquemore, W. M., Shaw, C., Li, C., Rumizen, M., and Gupta, M., "Year 3 of the National Jet Fuels Combustion Program: Practical and Scientific Impacts," *56th AIAA Aerospace Sciences Meeting*, Kissimmee, FL: 2018.

[6] Chtev, I., Rock, N., Ek, H., Smith, T., Emerson, B., Nobel, D. R., Seitzman, J., Lieuwen, T., Mayhew, E., Lee, T., Jiang, N., and Roy, S., "Simultaneous High Speed (5 kHz) Fuel-PLIE, OH-PLIF and Stereo PIV Imaging of Pressurized Swirl-Stabilized Flames using Liquid Fuels," *Submitted to the 55th AIAA Aerospace Sciences Meeting*, Grapevine, TX: American Institute of Aeronautics and Astronautics, 2017.

[7] Stouffer, S., Hendershott, T., Monfort, J. R., Diemer, J., Corporan, E., Wrzesinski, P., and Caswell, A. W., "Lean Blowout and Ignition Characteristics of Conventional and Surrogate Fuels Measured in a Swirl Stabilized Combustor," *55th AIAA Aerospace Sciences Meeting*, 2017, pp. 1–14.

[8] Stachler, R. D., Heyne, J. S., Stouffer, S. D., Miller, J. D., and Roquemore, W. M., "Investigation of Combustion Emissions from Conventional and Alternative Aviation Fuels in a Well-Stirred Reactor," *Submitted to the 55th AIAA Aerospace*

Sciences Meeting, Grapevine, TX: American Institute of Aeronautics and Astronautics, 2017.
[9] Khandelwal, B., and Ahmed, I., "Research Report on Lean Blowout Limit The University of Sheffield Department of Mechanical Engineering," 2017.
[10] Allison, P. M., Sidney, J. A. M., and Mastorakos, E., "Forced Response of Kerosene Flames in a Bluff-body Stabilised Combustor," *55th AIAA Aerospace Sciences Meeting*, Grapevine, TX: American Institute of Aeronautics and Astronautics, 2017.
[11] Sidney, J. A. M., Allison, P. M., and Mastorakos, E., "The effect of fuel composition on swirling kerosene flames," *55th AIAA Aerospace Sciences Meeting*, Grapevine, TX: American Institute of Aeronautics and Astronautics, 2017.
[12] Colket, M., Zeppieri, S., Dai, Z., and Hautman, D., "Fuel Research at UTRC," *In Multi-Agency Coordinating Council for Combustion Research 5th Annual Fuel Research Meeting*, 2012.
[13] Edwards, T., "Reference Jet Fuels for Combustion Testing," *55th AIAA Aerospace Sciences Meeting*, Grapevine: American Institute of Aeronautics and Astronautics, 2017.
[14] Won, S. H., Dooley, S., Dryer, F. L., and Ju, Y., "A radical index for the determination of the chemical kinetic contribution to diffusion flame extinction of large hydrocarbon fuels," *Combustion and Flame*, vol. 159, Feb. 2012, pp. 541–551.
[15] Stachler, R., Peiffer, E., Kosir, S., Heyne, J., and Stouffer, S., "A Study into the Chemical Timescale for a Toroidal Jet-Stirred Reactor (TJSR)," *Central States Section of The Combustion Institute*, Minneapolis: 2018.
[16] Heyne, J. S., Peiffer, E., Colket, M. B., Jardines, A., Shaw, C., Moder, J. P., Roquemore, W. M., Edwards, J. T., Li, C., Rumizen, M., and Gupta, M., "Year 3 of the National Jet Fuels Combustion Program: Practical and Scientific Impacts of Alternative Jet Fuel Research," *2018 AIAA Aerospace Sciences Meeting*, Reston, Virginia: American Institute of Aeronautics and Astronautics, 2018.
[17] Culbertson, B., and Williams, R., *ALTERNATIVE AVIATION FUELS FOR USE IN MILITARY APUS AND ENGINES VERSATILE AFFORDABLE ADVANCED TURBINE ENGINE (VAATE), PHASE II AND III*, AFRL-RQ-WP-TR-2017-0047: 2017.
[18] Bell, D. C., Heyne, J. S., Won, S. H., and Dryer, F. L., "The Impact of Preferential Vaporization on Lean Blowout in a Referee Combustor at Figure of Merit Conditions," *ASME 2018 Power and Energy Conference*, Lake Buena Vista: 2018.

Major Accomplishments

We have shown strong evidence that LBO is most strongly predicted by the chemical property DCN across four experimental platforms in the NJFCP.

Outreach Efforts

Conference presentations:

Carson, Jeremy, Joshua S. Heyne, Scott D. Stouffer, and Tyler Hendershott. 2016. "On the Relative Importance of Fuel Properties on LBO Behavior." 12th Annual Dayton Engineering Sciences Symposium: ASME.

Carson, Jeremy and Joshua S. Heyne. 2017. "Updates on the Relative Importance of Fuel Properties on LBO Behavior." 42nd Dayton-Cincinnati Aerospace Sciences Symposium. Dayton, OH: AIAA.

Peiffer, Erin, Joshua S. Heyne. 2017. "LBO, Ignition, and Spray Feature Importances from Year 3 of the National Jet Fuels Combustion Program." 13th Annual Dayton Engineering Sciences Symposium. Dayton, Ohio: ASME.

Awards

Jeremy Carson – Best presentation DESS 2016, Best presentation DCASS 2017.

Student Involvement

Jeremy Carson, Graduate Research Assistant, 2015 – 2017
Erin Peiffer, Graduate Research Assistant, 2017
Jennifer Colborn, Undergraduate Research Assistant, 2016 – 2017
Katherine Opacich, Undergraduate Research Assistant, 2017

Task 6 - Common Format Routine Software Development

University of Dayton Research Institute

Objective(s)

We aim to develop a software package in which the OEMs can utilize the state-of-the-art models being developed by the other NJFCP modeling teams.

Research Approach

This work is motivated for the imperative necessity of expediting combustor rig evaluation process for ASTM D4054 through improved combustion modeling capabilities. This fuel certification entails three main figures of merit, lean blowout, ignition, and cold relight. Current fuel certification requires expensive and time-consuming experimental testing in gas turbine engines. State-of-the-art combustion models that could expedite this process are not readily available for original engine manufacturers (OEMs). The main objective of this work is to bridge the gap between state-of-the-art academic combustion models and industrial software. The second aspect of this project is to speed up the academic codes for reaching industrial grade software category. The third aspect of this project involves verification and validation of this common format routine (CFR) software.

Modeling and simulation of complex fuels in gas turbine combustors is not trivial. Gas turbine combustors are intricate devices with characteristic length scales varying from the sub-millimeter laminar flamelet thickness to the large centimeter-size dilution holes. Therefore, the mesh resolution for gas turbines combustors is in the order of millions to even hundreds of million cells. The time scales associated with combustion and turbulence in the combustor vary from microseconds for the Kolmogorov turbulent length scales and species reaction rates to milliseconds associated with the flow through-time of the combustor. The time steps and mesh requirements for modeling and simulating a combustor are nearly prohibitive. In order to mitigate some of the challenges associated with modeling and simulation of gas turbine combustors, the lower-dimensional manifold combustion (LDMC) models decouple the chemistry and chemistry-turbulence interaction from the complex turbulence computational fluid dynamics (CFD) calculations. The chemistry is computed *a priori* from one-dimensional stagnation flow equations and/or equilibrium calculation. The chemistry-turbulence interaction is computed by presuming probability density functions (PDFs). Transport equations for the moments of the mixture fraction (Z) and progress variable (C) are solved in the physical space. These values are then used to interpolate and to extract the thermo-chemical and transport information of the pre-tabulated table.

Commercial software such as Fluent [1,2] and Star-CCM+ already have built-in LDMC models. However, there are always limitations in terms of implementation. For instance, Fluent [1,2] pre-tabulates the table in a mixture fraction space directly. Hence, it does not solve for the one-dimensional equations. On the other hand, the CFR software presented in this paper uses a modified Cantera 2.3 [1] package. The CFR pre-tabulates chemical-turbulence interaction in the one-dimensional physical space. This allows the user to vary the transport coefficient formulation and investigated such effects on numerical predictions. Another difference between Fluent [1,2] and the CFR is that the latter can compute the three branches of the combustion phenomenon. The CFR is also more flexible because molecular properties are directly interpolated from the table. Fluent [1,2] does not offer this capability. However, other commercial software package such as Chemkin [1] offers flamelet calculations that include the three branches of combustion. This software is very robust, but does not offer the turbulence-chemistry convolution capability needed for computing turbulent flames. To the best of our knowledge there is no standalone software that offers the capability of performing turbulence-chemistry convolution of a flamelet library. In addition, the CFR software is designed in a manner that more modules and capability can be easily annexed providing more flexibility to the user.

The purpose of this paper are to document the development of the CFR as well as to prove that such software has been verified and validated. Subsequently, the software is introduced. Important definitions are formulations are illustrated and discussed. The verification and validation tests are then presented.

Common Format Routine (CFR) Software

In short, the CFR software can be sub-divided into two components, the pretabulator and the flamelet-based software, which is illustrated in Appendix Figure 1. The pretabulator is capable of tabulating thermo-chemical and transport data for laminar and turbulent flames. The pretabulator is based on a modified version of Cantera 2.3 [3]. Cantera is written in C++ and Python wrappers/codes were developed in order to include new capabilities in Cantera. This Python codes also interact with a C# GUI. This can currently tabulate flamelet prolongation of the intrinsic low-dimensional manifold (FPI) and flamelet

progress variable (FPV). The flamelet-based software can attach the pretabulated turbulence-chemistry interaction table to a CFD code. In this case the flamelet-based software was attached to Fluent [1,2]. The flamelet-based software machinery can perform bilinear, trilinear and tetralinear interpolation of this thermochemical table. This software is written in C and its GUI is written using C#. Now detailed description of the software is provided next.

A. Mixture Fraction Definition

Mixture fraction is a conserved scalar. This means that mixture fraction cannot be created or destroyed. Because atomic elements and enthalpy cannot be created or destroyed, mixture fractions is typically defined in this context. Here the mixture fraction is defined in terms of atomic elements and any combination of atomic elements is valid. However, the atomic composition needs to be chosen so that mixture fraction varies between zero and unity.

$$\mathrm{Z} = \sum_{i=1}^{N_{atomic\,selection}} \sum_{n=1}^{N_{species}} \frac{MW_i}{MW_n} Y_n \qquad (1)$$

The user selection of the mixture fraction definition is given by Appendix Figure 2.

B. Progress Variable Definition

The progress variable provides quantitative information of the combustion efficiency. The latter is equal to zero when the flame blows out and combustion efficiency is zero. The maximum value of the progress variable is a real number less than unity. The progress variable is defined in terms of species mass fractions. The equation below indicates that the mixture fraction is the summation of species mass fractions. Typically in the literature CO and CO_2 are selected to indicate the level of completeness of the combustion process. In addition, CO, CO_2, H_2 and H_2O are also chosen species to indicate the combustion efficiency (or completeness of the combustion process).

$$\mathrm{C} = \sum_{n=1}^{N_{species\,selected}} Y_n \qquad (2)$$

The user selection of the mixture fraction definition is given by Appendix Figure 3.

C. Progress Parameter Definition

For premixed and diffusion flamelets, the progress variable defined by Eq. (2) varies in the spatial direction. For a premixed flamelet C increases monotonically from the unburned reactants from zero to a maximum value downstream the flame front. For diffusion flamelets the behavior is non-monotonic and the maximum value of C occurs near stoichiometry and then its value decreases to zero towards the reactant inlets. Therefore, the progress variable definition is a function of mixture fraction, i.e. $C = \mathrm{C}(\mathrm{Z})$. Thereby, the progress parameter Λ is defined as a bijective, unique identifier that can be used to sort each flamelet. This definition is given below.

$$\Lambda = f(C, Z) \qquad (3)$$

This definition is particularly useful for modeling diffusion flamelets and has been implemented in the current software. In the CFR this conversion can be enable or disable.

D. Convoluted Thermochemical and Transport Variables

Once state relationships have been computed between thermochemical and transport properties and the lower dimensional manifold variables (i.e., Z and ϕ) these quantities need to be convoluted for the turbulence-chemistry interaction using the equation below. The probability density functions (PDF) in this equation reads as "the probability density function of Z as a function of $\tilde{Z}$ and $\widetilde{Z''^2}$." Then, all thermochemical and transport properties (ϕ) such as density (ρ), molecular weight (MW), temperature (T), specific heat capacity (c_p), dynamic viscosity (μ), thermal conductivity (k), species mass fractions (Y_i) and species reaction rates ($\dot{\omega}_i$) are a function of the transported lower-dimensional manifold variables ($\tilde{Z}, \widetilde{Z''^2}, \tilde{\Lambda}$ and $\widetilde{\Lambda''^2}$).

$$\widetilde{\phi}(\tilde{Z},\widetilde{Z''^2},\tilde{\Lambda},\widetilde{\Lambda''^2}) = \int_0^1\int_0^1 \phi(Z,\frac{\Lambda}{\Lambda_{max}})\, PDF(Z;\tilde{Z},\widetilde{Z''^2}) PDF(\frac{\Lambda}{\Lambda_{max}};\tilde{\Lambda},\widetilde{\Lambda''^2})\, dZd\Lambda \quad (4)$$

Importantly to note is that the above equation, the progress parameter requires normalization before integration.

E. Lower Dimensional Manifold Transported Variables For Laminar Flows

Equations (5) and (6) are mixture fraction (Z) and progress variable (C) transported equations. When solving for laminar flows convolutions such as that represented by (4) are not necessary. Both equations here contain a transient, a convective and a diffusive term. However, the progress variable in addition contains a source term $\dot{\Omega}_C$.

$$\frac{\partial(\rho Z)}{\partial t} + \frac{\partial(\rho Z u_j)}{\partial x_j} = \frac{\partial}{\partial x_j}\left(\frac{\lambda}{c_p}\frac{\partial Z}{\partial x_j}\right) \quad (5)$$

$$\frac{\partial(\rho C)}{\partial t} + \frac{\partial(\rho C u_j)}{\partial x_j} = \frac{\partial}{\partial x_j}\left(\frac{\lambda}{c_p}\frac{\partial C}{\partial x_j}\right) + \dot{\Omega}_C \quad (6)$$

The source term ($\dot{\Omega}_C$) is computed as follows,

$$\dot{\Omega}_C = \sum_{i=1}^{N_{species selected}} \dot{\Omega}_i \quad (7)$$

Hence, the definition of Eq. (7) has to be consistent with the definition of Eq. (2). Then, all thermochemical and transport properties such as density (ρ), molecular weight (MW), temperature (T), specific heat capacity (c_p), dynamic viscosity (μ), thermal conductivity (k), species mass fractions (Y_i) and species reaction rates ($\dot{\omega}_i$) are a function of the transported lower-dimensional manifold variables. The progress parameter can be obtained via Eq. (3).

F. Lower Dimensional Manifold Transported Variables For Turbulent Flows

The transport equations for the lower-dimensional manifold variables (i.e., mixture fraction ($\tilde{Z}$), mixture fraction variance ($\widetilde{Z''^2}$), and progress variable ($\tilde{C}$) are illustrated by equations (8)-(10)) in tensor notation (and in conservative form) in the context of either the unsteady Reynolds-Averaged Navier Stokes (URANS) or Large-eddy simulation (LES) turbulence model formulations. For the former formulation the dependent variable represents the Favre-weighted time-averaged variable whereas for the latter the dependent variable represents the Favre-weighted filtered variable. Equations (8) through (10), respectively, correspond to the mixture fraction ($\tilde{Z}$), mixture fraction variance ($\widetilde{Z''^2}$), and progress variable ($\tilde{C}$).

1. Transport Equations

The transported equations of the lower-dimensional manifold variables contain at least three terms, transient, convection and diffusion. The mixture fraction variance in addition contains a destruction and production of $\widetilde{Z''^2}$ represented by the last two terms of Eq. (9), respectively. The progress variable transport equation also contains a source term represented by the last term of Eq. (10).

$$\frac{\partial(\bar{\rho}\tilde{Z})}{\partial t} + \frac{\partial(\bar{\rho}\tilde{Z}\tilde{u}_j)}{\partial x_j} = \frac{\partial}{\partial x_j}\left(\left(\frac{\lambda}{c_p} + D_t\right)\frac{\partial \tilde{Z}}{\partial x_j}\right) \quad (8)$$

$$\frac{\partial\left(\bar{\rho}\widetilde{Z''^2}\right)}{\partial t} + \frac{\partial\left(\bar{\rho}\widetilde{Z''^2}\tilde{u}_j\right)}{\partial x_j} = \frac{\partial}{\partial x_j}\left(\left(\frac{\lambda}{c_p} + D_t\right)\frac{\partial \widetilde{Z''^2}}{\partial x_j}\right) - \bar{\rho}\widetilde{\chi_Z} + 2\bar{\rho}D_t\left(\frac{\partial \tilde{Z}}{\partial x_j}\right)^2 \quad (9)$$

$$\frac{\partial(\bar{\rho}\tilde{C})}{\partial t} + \frac{\partial(\bar{\rho}\tilde{C}\tilde{u}_j)}{\partial x_j} = \frac{\partial}{\partial x_j}\left(\left(\frac{\lambda}{c_p} + D_t\right)\frac{\partial \tilde{C}}{\partial x_j}\right) + \bar{\rho}\overline{\dot{\omega}_C} \quad (10)$$

2. Closure Models

For RANS, SAS, DES and LES models the scalar dissipation rate associated with the progress variable (C) is as computed as follows [5].

$$\widetilde{\chi_C} = \gamma_C \frac{\widetilde{Z''^2}}{\widetilde{C''^2}} \widetilde{\chi_Z} \tag{11}$$

The closure models for the RANS-based lower-dimensional manifold transported variable equations are given by the following equations [5].

$$D_t = \frac{\mu_t}{Sc_t} \tag{12}$$

$$\widetilde{\chi_Z} = 2.0 \frac{\varepsilon}{k} \widetilde{Z''^2} \tag{13}$$

The turbulent Schmidt number (Sc_t) is a constant that is typically chosen to be equal to 0.9. The closure models for the LES-based lower-dimensional manifold transported variable equations are given by the following equations [5].

$$D_t = C_\phi \Delta^2 |S| \tag{14}$$

$$\widetilde{\chi_Z} = 2.0 \frac{\mu_t}{Sc_t} \frac{1}{\Delta^2} \widetilde{Z''^2} \tag{15}$$

The constant C_ϕ is typically chosen to be equal to 0.4.

G. Low-Dimensional Manifold Combustion Models

The flamelet prolongation of ILDM (FPI) and the flamelet/progress variable (FPV) model utilize the one-dimensional stagnation flow equations for computing freely-propagating premixed flames and counterflow diffusion flames, respectively. The freely-propagating premixed flamelets of the FPI model are computed in the physical space and each flamelet is converted to the progress variable space (C) using Eq. (2). In turn, each premixed flamelet correspond to a mixture fraction (Z), which is directly related to an equivalence ratio. On the other hand, FPV model invokes the calculation of multiple diffusion flames. Each flame is computed in the physical space as well. The physical space can be converted to a mixture fraction state relationship (Z) following Eq. (1). Each flamelet correspond to a progress parameter (Λ). Therefore, calculations of multiple premixed and diffusion flamelets lead to a tabulation of thermochemical and transport properties as a function of mixture fraction (Z) and progress variable (C).

1. Transport Equations

The one-dimensional stagnation flow equations are presented above from Eqs. (16)-(21). In ascending order these equations represent the continuity, radial momentum, pressure curvature or strain rate eigenvalue, energy, species and a one-point or two-point dummy differential equation. The equations on the left of the table represent the original equations in Cantera 2.3 [3] for which the pressure curvature is the eigenvalue. The equations on the right represent the optional equations in a modified Cantera 2.3 in which strain rate (a) replaces the pressure curvature as the eigenvalue. The species and temperature

Table 1. Original and modified Cantera governing equations.

Equation	Cantera	Modified Cantera	
Continuity	$\frac{\partial \rho u}{\partial z} + 2\rho V = 0,\ V = \frac{v}{r}$	$\frac{\partial \rho u}{\partial z} + a\rho V = 0\ ,\ V = \frac{v}{v_e}$	(16)
Radial Momentum	$\rho u \frac{\partial V}{\partial z} + \rho V^2 = -\Xi + \frac{\partial}{\partial z}\left(\mu \frac{\partial V}{\partial z}\right)$	$\rho u \frac{\partial V}{\partial z} = \frac{\partial}{\partial z}\left(\mu \frac{\partial V}{\partial z}\right) + \Xi(\rho_F - \rho V^2)$	(17)
Pressure Curvature/Strain Rate	$\frac{d\Xi}{dz} = 0,\ \Xi = \frac{1}{r}\frac{\mathrm{dP}}{dr}$	$\frac{d\Xi}{dz} = 0,\ \Xi = a$	(18)
Energy	$\rho u c_p \frac{\partial T}{\partial z} = \frac{\partial}{\partial z}\left(\lambda \frac{\partial T}{\partial z}\right) - \sum_k j_k c_{p,k} \frac{\partial T}{\partial z} - \sum_k h_k W_k \dot{\omega}_k$		(19)
Species	$\rho u \frac{\partial Y_k}{\partial z} = -\frac{\partial j_k}{\partial z} + W_k \dot{\omega}_k$		(20)
One- or Two-point Control	$\frac{\mathrm{du}_o}{dz} = 0$		(21)

equations are not modified. However, an additional dummy Eq. () was added to the governing equations for when the flame control methods are activated.

2. Flamelet Prolongation of ILDM (FPI)

The FPI model computes premixed flamelets for each mixture fraction (Z). When the calculations do not converge because either the flamelets have exceeded the flammability limits or because the maximum temperature of the flamelet is higher than that of equilibrium, equilibrium calculations replace the freely-propagating premixed flamelets. The transport equations for the freely-propagating flamelets are given by Eqs. (22) – (26). The boundary conditions associated with the freely-propagating flamelets are shown in Table 2.

Table 2. Premixed flame boundary conditions.

Equation	Fuel Inlet	Oxidizer Inlet	
Continuity	-----	$\rho u = (\rho u)_O$	(22)
Radial Momentum	$V = V_F$	$V = V_O$	(23)
Pressure Curvature/ Strain Rate	$\rho u = (\rho u)_F$	-----	(24)
Energy	$T = T_F$	$T = T_O$	(25)
Species	$\rho u Y_k + \rho Y_k V_k = (\rho u Y_k)_F$	$\rho u Y_k + \rho Y_k V_k = (\rho u Y_k)_O$	(26)

Table 3. Nonpremixed flamelet boundary conditions.

Equation	Inlet B.C.	Internal B.C.	Outflow B.C.	
Continuity	-----	$T_{j=specified} = T_{fixed,specified}$	------	(27)
Radial Momentum	$V = V_0$	--------	$\frac{dV}{dz} = 0$	(28)
Pressure Curvature/ Strain Rate	$\Xi = 0$	--------	-----	(29)
Energy	$T = T_0$	--------	$\frac{dT}{dz} = 0$	(30)
Species	$\rho u Y_k + \rho Y_k V_k = (\rho u Y_k)_0$	--------	$\frac{dY_k}{dz} = 0$	(31)

3. Flamelet Progress/Variable

The FPV model computes diffusion flamelets for each progress parameter (Λ) along the S-curve. Multiple diffusion flamelets are necessary to build a table of thermochemical and transport properties. The first flamelet is computed at $\Lambda_{max}|Z$ and then the strain rate is increased by either increasing the inlet velocities, reducing the distance between the opposing jets, or by either the one-point or two point continuation. The computation of diffusion flamelets as a function of strain rates leads to the calculation of the S-curve containing two stable branches (strong and weak) and one unstable (middle) branch. Special continuations techniques are needed to compute the S-curve associated with the diffusion flamelets. This will be discussed in subsequent chapters. The boundary conditions associated with the counterflow flamelets are shown in Table 3.

H. Continuation Methods

Continuation techniques are now presented, zero-order, scaling rules, arc-length, and one- and two-point continuation techniques are presented. The zero-order continuation technique is used for FPI, whereas hybrid continuation techniques of zero-order, scaling rules, some features of arc-length continuation, and one- and two-point continuation techniques are used for the FPV model. The arc-length continuation technique was, however, fully utilized for perfectly-stirred reactors (PSRs) in order to progressively attain the now-used continuation technique for the FPV model. The arc-length continuation for PSR is only available in Python scripts and not through the GUI.

1. Zero Order Continuation

Zero-order continuation techniques can be applied to any flamelets. This technique only supposes that the previous solution is the initial solution to the current solution. This can be represented as $\boldsymbol{x}^* = \boldsymbol{x_0}$, where $\boldsymbol{x}$ refer to a vector solution with M grids points times N equations. This continuation methods can be applied to both FPI and FPV methods. For the former this is the only method available for continuation. For the latter the number of zero-order continuation can be selected from the Flame Control tab as illustrated in the Task 6 Appendix, Figure 4.

2. Scaling Rules

The scaling rules are ideal for computing the upper branch of S-curve. The scale factor proposed by Fiala and Sattelmayer [2] are suitable for the FPV model. These scaling factors are $u \sim a^{-1/2}$, $V \sim a$, $\dot{m}'' \sim a^{1/2}$, and $\Lambda \sim a^2$. The strain factor, which is the ratio of two sequential flame strain rates, can be entered by the user as illustrated in Appendix Figure 4.

3. Arc-Length Continuation

The system of nonlinear ODEs is represented by $\boldsymbol{F}(\boldsymbol{x}) = 0$. The solution is given by the vector $\boldsymbol{x}$. The results of these equations depend on the parameter λ. The extended solution is represented by $\boldsymbol{F}(\boldsymbol{x}(\lambda), \lambda) = 0$. The arc-length continuation [3] is a predictor-corrector continuation technique.

1. **Predictor:**

One such predictor is the forward Euler predictor given by:

$$\boldsymbol{x}^* = \boldsymbol{x_0} + \frac{\boldsymbol{dx}}{\boldsymbol{ds}} ds \qquad (32)$$

The gradient $\boldsymbol{dx/dF}$ can be either a tangent or a secant gradient. Here the former is used. The predicted solution $\boldsymbol{x}^*$ is the initial guess for computing the new flame. The solution vector $\boldsymbol{x}$ that lies on the path depends on the parameter λ and this, in turn, depends on arclength s.

2. **Corrector:**

The plane equation parameterized as a function of arclength, s, needs to correct the initial guess $\boldsymbol{x}^*$.

$$N\left(\boldsymbol{x}(\lambda(s)), \lambda(s)\right) \equiv \left\|\frac{\partial \boldsymbol{x}}{\partial s}\right\|_2^2 + \left(\frac{\partial \lambda}{\partial s}\right)^2 - 1 = 0 \qquad (33)$$

Now the augmented systems of equations is given by:

$$\begin{vmatrix} \boldsymbol{F}\left(\boldsymbol{x}(\lambda(s)), \lambda(s)\right) \\ N\left(\boldsymbol{x}(\lambda(s)), \lambda(s)\right) \end{vmatrix} = \begin{vmatrix} 0 \\ 0 \end{vmatrix} \qquad (34)$$

This new vector can also be written as $\mathrm{G}(\mathrm{F}(\mathrm{y}), \mathrm{N}(\mathrm{y})) = 0$. The augmented solution vector is given by $\mathrm{y} = \left(\mathrm{x}(\lambda(\mathrm{s})), \lambda(\mathrm{s})\right)$. The Jacobian matrix for the augmented system is represented by the following equation.

$$\boldsymbol{J} = \begin{vmatrix} \frac{\partial F}{\partial x} & \frac{\partial F}{\partial \lambda} \\ \frac{\partial N}{\partial x} & \frac{\partial N}{\partial \lambda} \end{vmatrix} \qquad (35)$$

The partial derivative of the plane equations needs to be determined from the plane equation:

$$N\left(\boldsymbol{x}(\lambda(s)), \lambda(s)\right) \equiv \left\|\frac{\partial \boldsymbol{x}}{\partial s}\right\| d\boldsymbol{x} + \frac{\partial \lambda}{\partial s} d\lambda - ds = 0 \qquad (36)$$

$$\frac{\partial N}{\partial x} = \left|\frac{\partial \boldsymbol{x}}{\partial s}\right|^T \qquad (37)$$

$$\frac{\partial N}{\partial \lambda} = \frac{\partial \lambda}{\partial s} \qquad (38)$$

After substituting the equations above into the Jacobian, the augmented Jacobian is now given by:

$$\boldsymbol{J} = \begin{vmatrix} \frac{\partial F}{\partial x} & \frac{\partial F}{\partial \lambda} \\ \left|\frac{\partial \boldsymbol{x}}{\partial s}\right|^{T} & \frac{\partial \lambda}{\partial s} \end{vmatrix} \qquad (39)$$

The augmented Jacobian and the residual equations are used in a Newton-Raphson type solver. The previous k solution is used to compute the new solution k+1.

$$\boldsymbol{y_{k+1}} = \boldsymbol{y_k} - \boldsymbol{J^{-1}G} \qquad (40)$$

The Newton-Raphson solver proceeds in this way. It computes the new change in the solution vector, $\Delta \boldsymbol{y_k}$. This change is added to the solution vector of the previous iteration. Note that k=0 the values of $y_0[0: N_{eqs} - 2]$ are equal to the values of $\boldsymbol{x}^*$.

$$\boldsymbol{J}\Delta \boldsymbol{y_k} = -\boldsymbol{G} \qquad (41)$$
$$\boldsymbol{y_{k+1}} = \boldsymbol{y_k} + \Delta \boldsymbol{y_k} \qquad (42)$$
$$if\ \Delta \boldsymbol{y_k} < \varepsilon \ \rightarrow \boldsymbol{y_n} = \boldsymbol{y_{k+1}} \qquad (43)$$

3. **Step-size Control:**

The user specifies an initial step size ds that is very large at first and the simulation proceeds. Near the turning points (bifurcations) the step size needs to become smaller in order to resolve the curve and avoid divergence of the Newton solver. Once the solution has passed the turning point the step size ds needs to increase again towards the other turning point. This is accomplished using the following step size control method.

$$\delta = N_{opt}/i_{Newton} \qquad (44)$$
$$if\ \delta < 0.5 \ \rightarrow \delta = 0.5 \qquad (45)$$
$$if\ \delta > 2.0 \ \rightarrow \delta = 2.0 \qquad (46)$$
$$ds = \delta \cdot ds \qquad (47)$$

This step size control technique works by allowing the user to specify the optimum number of Newton iterations, N_{opt}. If the number of Newton iterations i_{Newton} is below or above the N_{opt} the step size will increase or decrease, respectively. The multiplication factor δ is bounded between 0.5 and 2.0 in order to avoid very small step size or very large step sizes that would either get the simulation stagnant or diverging. The step size control can be accessed through the Flame Control tab.

Some verification calculations are shown in Figure 1 through Figure 3 with numerical results available in the literature. There is nearly perfect match between previously computed S-curve for perfectly-stirred reactors (PSRs) and those computed here. This demonstrates that homotopic calculations and step size control are appropriately programmed for later used in the FPV tabulation procedure.

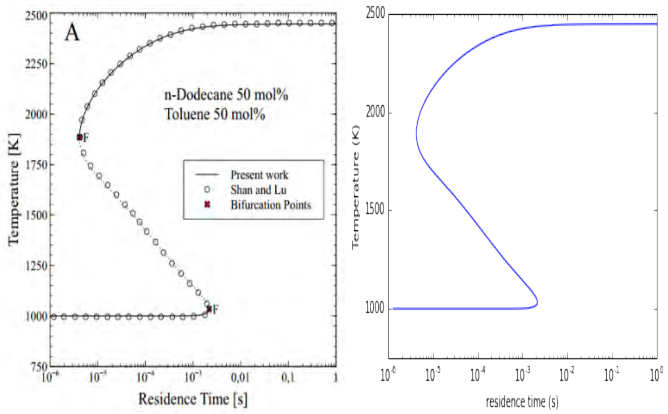

Figure 1. Comparison between Acampora and Marra [7] and in-house arc-length continuation for perfectly-stirred reactor (PSR). The inlet mass flow rate is the independent variable. Both temperature and residence time are output of the PSR. Reprinted from Computers and Chemical Engineering, 85, Acampora, L., Marra, F.S., A general study of counterflow diffusion flames at subcritical and supercritical conditions: Oxygen/hydrogen mixtures, with Permission from Elsevier.

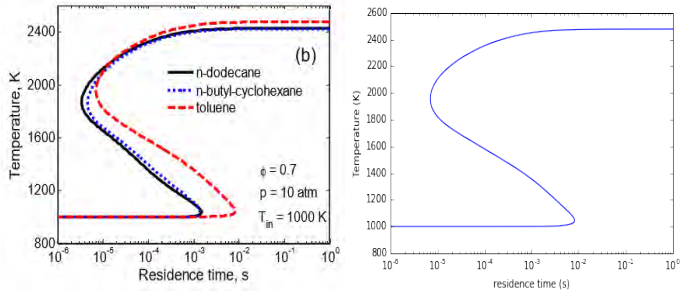

Figure 2. Comparison between Shan and Lu [1] and in-house arc-length continuation for perfectly-stirred reactor (PSR) burning Toluene. The inlet mixture temperature is the independent variable.

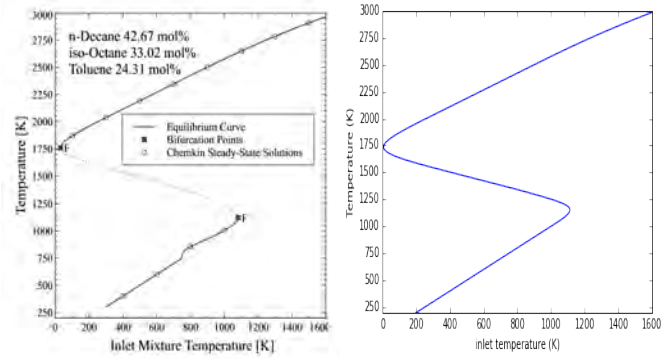

Figure 3. Comparison between Acampora and Marra [8] and in-house arc-length continuation for perfectly-stirred reactor (PSR). The inlet mixture temperature is the independent variable. Reprinted from Computers and Chemical Engineering, 85, Acampora, L., Marra, F.S., A general study of counterflow diffusion flames at subcritical and supercritical conditions: Oxygen/hydrogen mixtures, with Permission from Elsevier.

4. Flame Control Methods: One- and Two-Point

When the zero-order continuation and the scaling rules fail a flame control can be used to continue the bifurcation path of the S-curve. In the CFR this is automatically activated. The one- and two-point boundary conditions are based on the work of Nishioka et al. [8]. The boundary conditions for the pressure curvature or strain rate eigenvalue (Eq. (24)) is removed and replaced with an internal boundary condition (Eq. (48)) for the one-point continuation method. For the two-point continuation method the continuity equation boundary condition (Eq. (22)) is removed and a new internal boundary condition is added (Eq. (49)). For the one-point control method the oxidizer flux is specified as well as a fixed temperature on the fuel side. For the two-point control method neither the fuel nor the oxidizer flux are specified, but instead two fixed temperature location for the consecutive flamelet calculation at each side of the stagnation plane are prescribed.

Table 4. One- and two-point control boundary conditions.

Equation	Fuel Inlet	Internal B.C.	Internal B.C.	Oxid Inlet	
Pressure Curvature/ Strain Rate	-----	$T(j_{F,specified}) = T_{F,specified}$	-----	-----	(48)
Two-Point Control	------	-----	$T(j_{O,specified}) = T_{O,specified}$		(49)

Figure 4 shows the calculation of the S-curve for a more practical fuel used in gas turbine combustors.

Figure 5 clearly shows that upper and middle branches can be successfully calculated with the CFR at low and high pressure conditions. Figure 5 illustrates the effect of transport model on the S-curve. There is a slight change on the S-curve for hydrogen-oxygen combustion. This is important because it suggests that the inexpensive unity Lewis number computation is sufficient for PSR without having to invoke more computationally-expensive calculations such as mixture-averaged diffusivity. Figure 7 demonstrates that effect of varying the detailed chemistry. The same fuel-air composition is used with two different chemistry sets, but there is substantial change in the extinction strain rate.

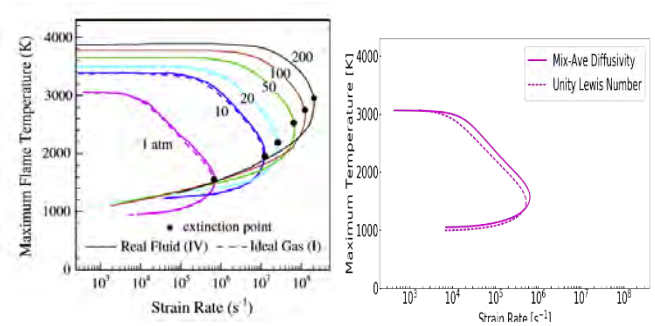

Figure 4. Comparison between mixture-averaged diffusivity and unity Lewis number. The mechanism used here is that of Burke et al. [13] Reprinted from Combustion and Flame, 161, Huo, H., Wang, X., Yang, V., A general study of counterflow diffusion flames at subcritical and supercritical conditions: Oxygen/hydrogen mixtures, with Permission from Elsevier.

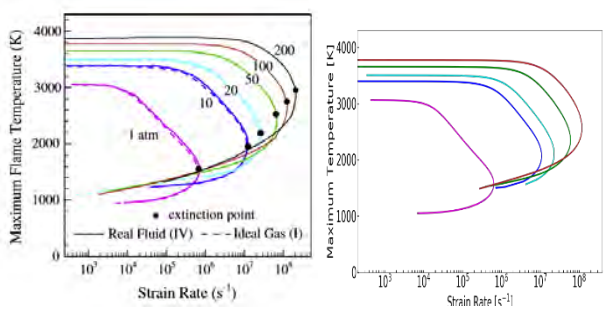

Figure 5. Comparison of strain rate vs. maximum flame temperature between Wang et al. [11] (left) and the in-house model (right). Wang et al. uses Li et al. [12] mechanism, whereas the in-house model uses Burke et al. [13] *Reprinted from Combustion and Flame, 161, Huo, H., Wang, X., Yang, V., A general study of counterflow diffusion flames at subcritical and supercritical conditions: Oxygen/hydrogen mixtures, with Permission from Elsevier.*

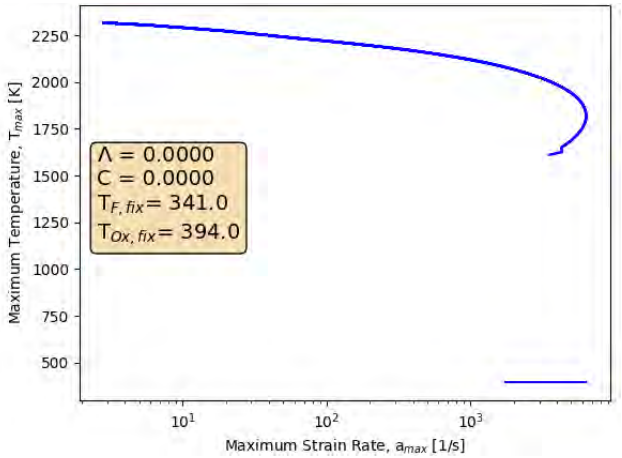

Figure 6. POSF10325-air diffusion flame s-curve.

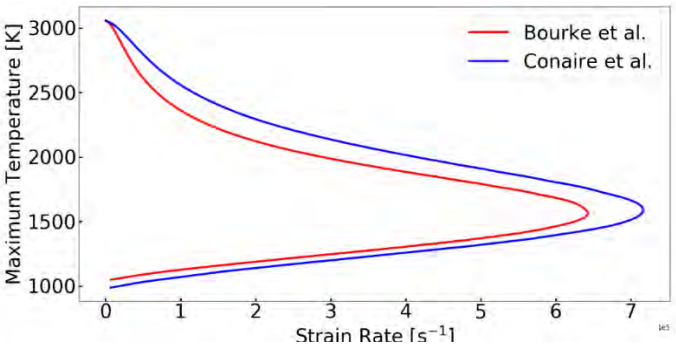

Figure 7. Comparison between Bourke et al. and Conaire et al. mechanisms for the H_2-O_2 flame at 1 atm and inlet temperatures of 300K.

I. Probability Density Functions

Here the Dirac-delta and Beta probability density functions (PDFs) are discussed here. These PDFs could be applied to either the lower-dimensional manifold variables. However, it has been proven that the Beta PDF is more suitable for mixture fraction (Z), whereas Dirac-delta or Beta PDF can be used for progress parameter (Λ).

1. Dirac Delta

The Dirac-delta probability density function is given by the equation below. Dirac-delta could be used for the progress parameter. Hence the x in the equation can be substituted by Λ.

$$\delta(x - x_0) = \begin{cases} 0, & x \neq x_0 \\ 1, & x = x_0 \end{cases} \tag{50}$$

2. Beta

The Beta probability density function is given by the equations below. The probability density function is appropriate for the mixture fraction (Z). Hence, the x in the equation can be substituted for the Z. This PDF could also be utilized to model the progress parameter and the x below would be substituted by Λ.

$$\beta\left(x; \tilde{x}, \widetilde{x''^2}\right) = \frac{\Gamma(a+b)}{\Gamma(a)\Gamma(b)} x^{a-1}(1-x)^{b-1} \tag{51}$$

$$a = \frac{\tilde{x}\left(\tilde{x} - \tilde{x}^2 - \widetilde{x''^2}\right)}{\widetilde{x''^2}} \tag{52}$$

$$b = \frac{(1-\tilde{x})\left(\tilde{x} - \tilde{x}^2 - \widetilde{x''^2}\right)}{\widetilde{x''^2}} \tag{53}$$

The demonstration of these convolutions are shown in Figure 8. The images correspond to a convoluted methane-air diffusion flame. Dirac-delta PDF was used for the progress variable. Note that the effect of turbulence-chemistry interaction represented by the variance of the mixture fraction (in this case) is to weaken the flame by lowering the peak temperature from ~2050 K to ~1750K. Similar the peak progress variable source term drops from ~500 to ~100 ks/m3s-1.

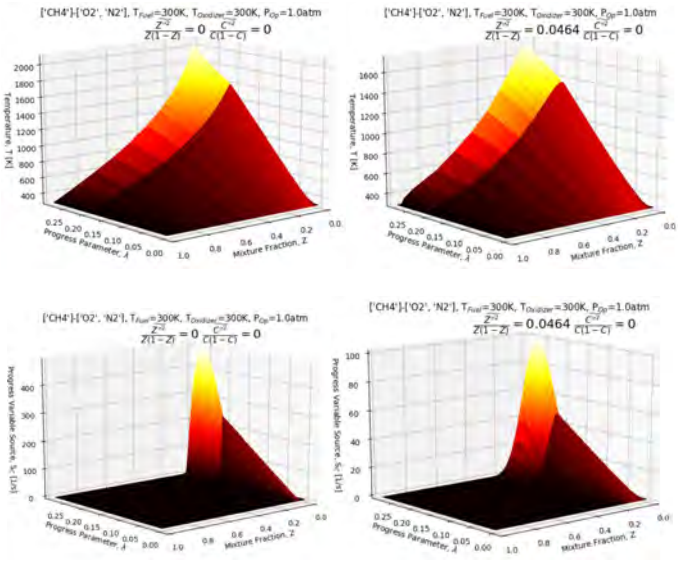

Figure 8. Sample images of a tabulated thermochemical transport tables for a CH_4-air diffusion flame. The top and bottom images illustrate temperature and progress variable source, respectively. The left images show the tabulated variables when both mixture fraction and progress variables are zero. The right images show the tabulated variables when the mixture fraction variance is non-zero.

J. Verification Tests

There are several verification and validation tests. A canonical laminar triple flame was computed using FPI or FPV models. The Sandia D piloted flame was also simulated using RANS/FPV and LES/FPV model. Finally, a single cup combustor rig was simulated using the LES/FPV model.

A. Simulations of a Canonical Triple Flame

Here is the verification test for the laminar formulation for the FPI model. Figure 9 indicates that both calculations are very similar in terms of temperature and CO mass fraction contours. Subtle difference can be attributed to the fact that Wu et al. [9] used FlameMaster solver [10], which computes the flamelets in mixture fraction space directly.

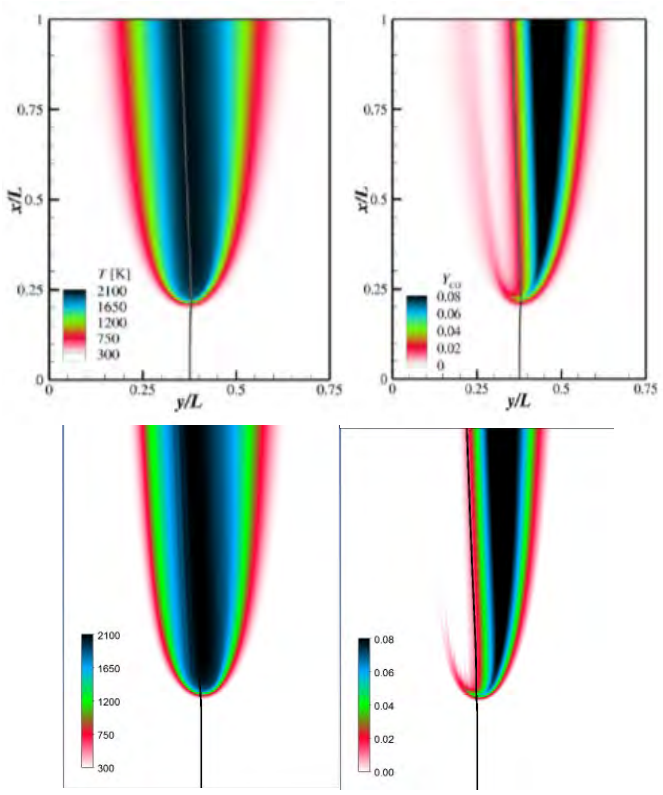

Figure 9. Comparison between (top) Wu et al. [15] and (bottom) CFR results of a laminar triple flame using FPI in terms of (left) temperature and (right) CO mass fractions.

B. Laminar Fpv Simulations For A Canonical Triple Flame

Here is the verification test for the laminar formulation for the FPV model. Figure 10 illustrates the verification step for computing the laminar version of the FPV combustion model of the CFR software.

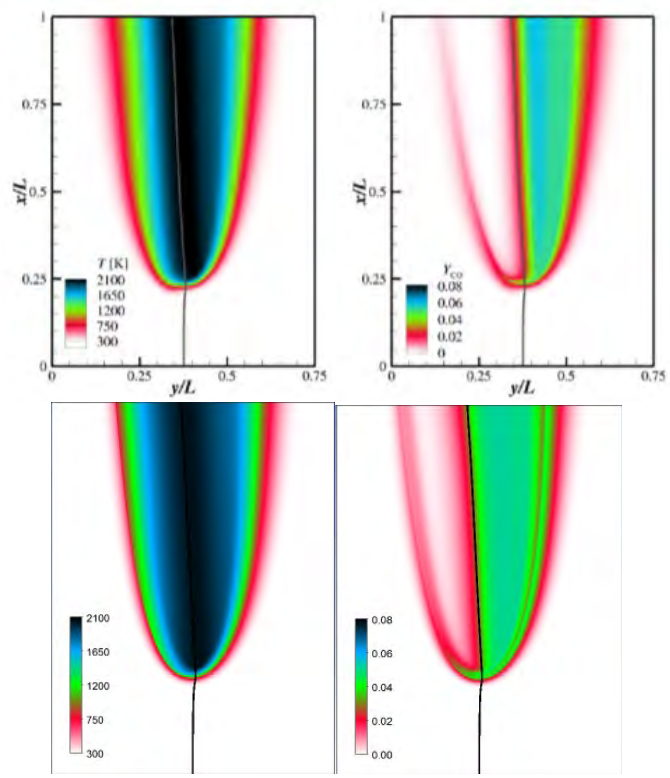

Figure 10. Comparison between (top) Wu et al. [15] and (bottom) CFR results of a laminar triple flame using FPV in terms of (left) temperature and (right) CO mass fractions.

C. Turbulent Simulations of Sandia D Flame

Here are the verification and validation tests for turbulent formulation of the FPV model. Figure 11 presents the experimental measurements against numerical predictions. Numerical simulations were performed only with Fluent [1,2] and with Fluent+CFR software. The k-ε and k-ω RANS version of FPV model were utilized. The Beta PDF is used for mixture fraction and Dirac-delta is used for progress variable. Generally, both the Fluent and Fluent+CFR results compared well with the experimental measurements in terms of temperature and species mass fractions. However, the Fluent+CFR outperforms the Fluent results, specifically, in terms of CO mass fraction. Both Fluent and Fluent+CFR results, nonetheless, underpredict the mixture fraction variance. In terms of RANS model, the k-ω better approximates the measurements.

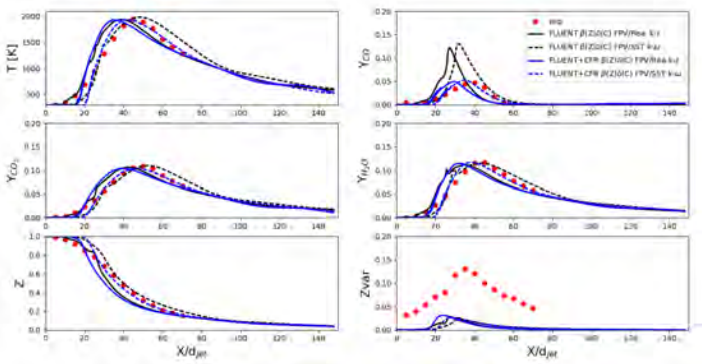

Figure 11. Centerline comparison between experiments and RANS simulations of the Sandia D turbulent flame.

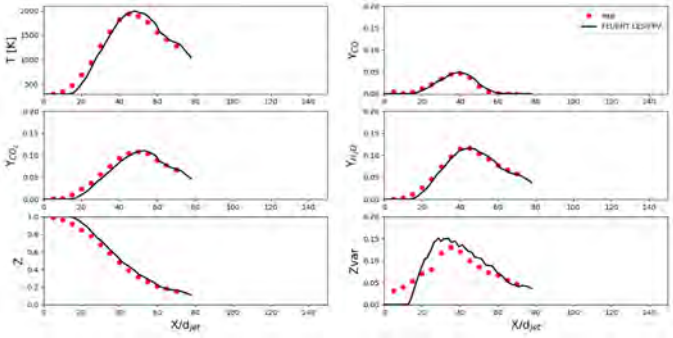

Figure 12. Centerline comparison between experiments and LES simulations of the Sandia D turbulent flame.

Conclusions

A common format routine (CFR) software for modeling combustion problems have been developed. This software is sub-divided into a thermochemical transport property pretabulator software and a flamelet-based software. The former can be used to create flamelet prolongation of the ILDM (FPI) or flamelet/progress variable (FPV) tables for either laminar or turbulent flames. The pretabulator allows for turbulence-chemistry interaction through either Beta or Dirac-delta probability density function (PDF) of the independent variables. The flamelet-based software can read, search and interpolate the table to extract thermochemical and transport composition based on lower-dimensional manifold transport variables (i.e., mixture fraction, mixture fraction variance and progress parameter). The k-□ and k-□ RANS, SAS, DES and LES turbulence model were coupled with the flamelet-based combustion models. A multiphase spray model successfully couples with the gas phase by exchanging mass. The CFR software was positively compared against laminar and turbulent flames in canonical configurations as well as in more practical single-swirler combustor rig. The developed software is reliable for modeling and simulation of complex combustion phenomena.

References

1. Ansys Inc., Fluent User's Guide, v18.0.
2. Ansys Inc., Fluent Theory Guide, v18.0.
3. Goodwin, D.G., Moffat, H.K., Speth, R.L., Cantera: An object – oriented software toolkit for chemical kinetics, thermodynamics, and transport properties," http://www.cantera.org, 2017, Version 2.3.0. doi:10.5281/zenodo.170284
4. ANSYS 18.0, Chemkin-Pro Theory Manual, ANSYS, Inc.: San Diego, 2017.
5. Ihme, M., Pitsch, H., "Prediction of extinction and reignition in nonpremixed turbulent flames using flamelet/progress variable model: 2. Application in LES of Sandia flames D and E," Combustion and Flame, 155, (1-2), pp. 90-107, 2008.

6. Fiala, T., Sattelmayer, T., "Nonpremixed Counterflow Flames: Scaling Rules for Batch Simulations," Journal of Combustion, 2014, 484372.
7. H. B. Keller, in Applications of bifurcation Theory, P. Rabinowithz, Ed. (Academic Press, New York, 1977).
8. Luigi Acampora and Francesco S. Marra, "Numerical Strategies for the Bifurcation Analysis of Perfectly Stirred Reactors with Detailed Combustion Mechanisms," Computers and Chemical Engineering 82 (2015) 273-282.
9. Ruiqin Shan, Tianfeng Lu, Effects of Surrogate Jet-Fuel Composition on Ignition and Extinction in High Temperature Applications, 8th U. S. National Combustion Meeting Organized by the Western States Section of the Combustion Institute and hosted by the University of Utah May 19-22, 2013.
10. Nishioka, M., Law, C., Takeno, T., "A flame controlling continuation method for generating S-curve responses with detailed chemistry," Combust. Flame 104 (3):328-342
11. Huo, H., Wang, X., Yang, V., "A general study of counterflow diffusion flames at subcritical and supercritical conditions: Oxygen/hydrogen mixtures," Combustion and Flames, 161, 2014.
12. J. Li, Z. Zhao, A. Kazakov, F.L. Dryer, "An updated comprehensive kinetic model of hydrogen combustion," Int. J. Chem. Kinetics, 36, 2004, 566-575.
13. Burke, M.P., Chaos, M., Ju, Y., Dryer, F.L., Klippenstein, S.J., "Comprehensive H2/O2 Kinetic Model for High-Pressure Combustion," Int. J. Chem. Kinet. (2011).
14. Connaire, M. O., Curran, H J., Simmie, J. M., Pitz, W. J. and Westbrook, C.K., "A Comprehensive Modeling Study of Hydrogen Oxidation", International Journal of Chemical Kinetics, 36:603-622, 2004.
15. Wu, H., See, Y.C., Wang, Q., and Ihme, M., "A Pareto-efficient combustion framework with submodel assignment for predicting complex flame configurations," 162(1), 2015, 4208-4230
16. Pitsch, H., FlameMaster v3.1, "A C++ computer program for 0D combustion and 1D laminar flame calculations," 1998.

Major Accomplishments

Developed and delivered to OEMs a stand-alone common format routine incorporating the latest theory from academic teams.

TASK 6 APPENDIX

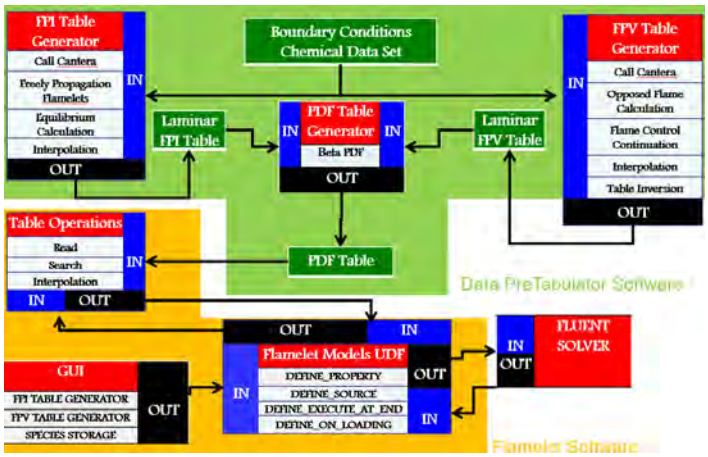

Appendix Figure 1. Schematic of the Common Format Routine (CFR) software. All the components with the green background correspond to the thermochemical and transport data pretabulator. All the components with the amber background corresponds to the flamelet-based software.

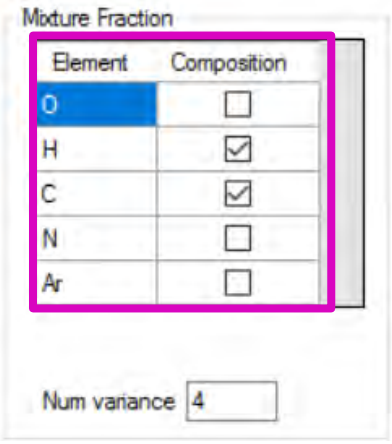

Appendix Figure 2. Pretabulator software selection of user's mixture fraction definition is indicated within the magenta-line box.

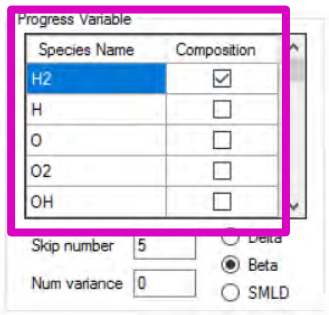

Appendix Figure 3. Pretabulator software selection of user's progress variable definition is indicated within the magenta line box.

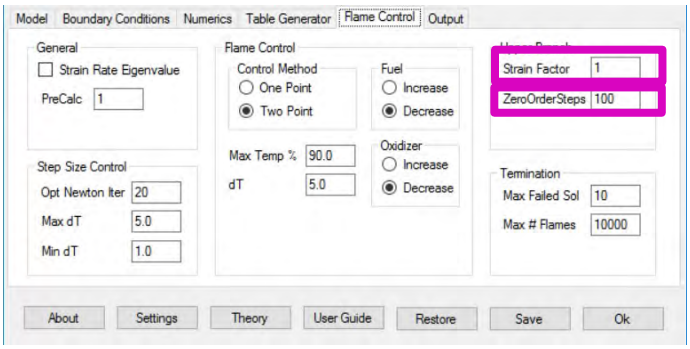

Appendix Figure 4. Pretabulator software selection of zero order continuation steps and strain factor are indicated in the magenta boxes.

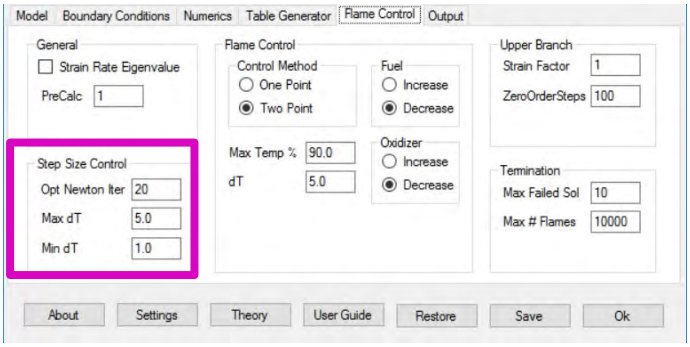

Appendix Figure 5. Pretabulator software selection of step size control is indicated in the magenta box.

Task 7 Spray Modeling of Area 3 Pressure Atomized Spray Injector

UTRC (Sub-contract)

Objective(s)

The objective of this task is to simulate the Area 3 High Sheer Rig pressure blast spray atomizer. Simulations of NJFCP experiments in the Area 3 High Sheer Rig will be done to explore the relative performance of simulations versus experiments and the relative spray and combustor character between the A-2, C-1, and C-5 fuels. These computational results will also illuminate the relative impact of a Pratt & Whitney swirler-injector geometry as compared to the other geometries in the program.

Research Approach

Research & Development Final Report 2018 Executive Summary

The objective of this effort is to develop, enhance and apply computational fluid dynamics-based models to simulate stable combustion and lean blowout behavior in a high shear rig combustor that was also experimentally studied at Georgia Institute of Technology. The goal is to understand if the models can predict the dependence of lean blowout (LBO) phenomena on fuel physical and chemical properties of the alternative jet fuels. A Large Eddy Simulation (LES) based modeling is employed to simulate the unsteady combustion phenomena for the stable and LBO conditions. Several sub-models for unsteady flow simulation, spray injection boundary conditions, spray evaporation models, wall heat flux boundary conditions and turbulent combustion models are required to correctly simulate the physical processes. Detailed description of the different submodels, along with validation or verification where possible, is presented as a part of this work. Simulation of lean blowout were performed upon completing the reacting LES for the two fuels at near blowout but stable conditions. To simulate lean blowout, fuel flow rate is reduced in discrete steps 6% (instantaneously instead of gradually) for three different values of fuel-flow rates. Each flow rate was held constant for 100 mill-seconds for the combustor to respond to the flow rate change and stabilize at the new condition. Overall, the two fuels show differences in evaporation rate and also commensurate differences in heat release rates. Both of the simulations show reduction in heat release rate as the flow rate is reduced but C1 seems to be dropping faster, relatively compared to A2. C1 fuels also shows increased evaporation rates compared to A2, however this leads to quick build of fuel vapor in a concentrated region and if the flow conditions in that region is not conducive in terms of residence time to complete the reaction, it contributes to even more accumulation of fuel vapor from the incomplete combustion. In the case of C1 fuel, this is hypothesized to be the mechanism for earlier flame blow out compared to the A2 fuel. Long combustor dimension coupled with very small time steps to resolve the flame structure, leads to excessive computational time at each flow rate for the combustion to reach a quasi-steady state. As a result, it was not possible to reduce the flow-rate all the way to the lean blowout value to demonstrate the lean blowout behavior. However, the qualitative trend observed from the three simulate fuel flow rate conditions seems to indicate that the models employed in this study have the ability to discriminate between the different fuel physical properties and its impact on the lean blow out behavior.

Research in Support of FAA-ASCENT Program & National Jet Fuels Combustion Program LES of High Shear Rig Combustor – Area 3 support

Introduction

Fuel cost, availability and environmental impact are main concerns that drive the search and use of alternative fuels (petroleum and non-petroleum derived) in commercial and military aviation. By understanding and establishing the properties of fuel and their impact on engine (combustor) performance, it may be possible to broaden the fuel specification and, in turn, broaden the available choice of economical and eco-friendly fuels for aviation engines. However, the introduction of fuels from alternative sources presents potential risks to aircraft engine operability, emissions and durability and hence requires a comprehensive understanding of the fuel properties and their potential impact on the systems and their performance. For instance, flame blowouts can occur during transient events in the flight envelope during rapid throttle movements. For example, during flight decent when the fuel flow-rates are typically low, the combustor fuel-air ratio may approach lean flammability limits that may result in a flame-out. This is typically known as the Lean Blow Out (LBO) and has obvious safety implications. During such highly transient events, fuel property variations have a large effect on the combustion processes. Since the fuel flow rates are low, physical properties of the fuel can alter the fuel spray atomization and vaporization processes, leading to a strong effect on combustion. In addition, fuel chemistry effects are presumed to be strongest at lean conditions, where chemical reaction rates are lowest and can therefore be coupled with the combustor aerodynamic stabilization processes. For these reasons, LBO is considered one of the most important operability metrics for evaluating alternative fuel effects. Other combustor performance metrics such as ignition at ground (cold start) and altitude conditions, gaseous and particulate emissions, liner temperature, radiation and durability, pattern/profile factor and combustion efficiency are all linked intimately to different physical and chemical properties of the fuel such as viscosity, surface tension, heating values, specific heats, boiling point distribution, vapor pressure, Cetane number etc. In general, there is some understanding of the impact of physical fuel properties on selective combustion behavior. However, the collective impact due to all or multiple properties (chemical and physical) is not well understood. Because the next-generation of combustors will be operating closer to stability limits they are more likely to exhibit stronger fuel sensitivity which warrants research to better understand the potential impacts of the new fuels on engines.

One of the important objectives of this research program is to develop modeling tools for predicting the performance of gas turbine combustors when using future alternative fuels. The success would enable a significant reduction in cost and effort when qualifying new fuels for use in aircraft engines. Computational Fluid Dynamics (CFD) simulations of the High Shear Combustor are being performed to develop and assess the ability of models to capture the impact of fuel properties on Lean Blow Out phenomena.

Experimental Facility

The high shear rig combustor is a canonical representation of an aviation combustor which was experimentally characterized by the teams at Georgia Institute of Technology. This rig was designed with optical access to enable non-intrusive diagnostics and for visualization of the flame. Data obtained include non-reacting and reacting PIV for the velocity fields at an equivalence ratio close to LBO where a stable flame configuration can be realized. PDPA measurements of the spray under non-reacting conditions close to the swirler/nozzle exit were also obtained in this configuration at UTRC. Temperature measurements at the combustor bulk-head were also obtained to characterize / quantify lean blowout phenomena.

Figure 1 shows the key components of this rig such as preconditioning air flow path, fuel supply, the optically accessible pressure vessel and liner and exhaust section. Compressed air at pressures up to 20 atm is heated to temperatures from 350 to 750 K. Following the heating process, a portion of the air is sent to the test section and the remainder is cooled to approximately 320 K in a heat exchanger. The secondary air flows around the liner and keeps the pressure vessel structure and windows cool. Hot combustion products mix with the cooling air downstream of the test section and exit through a water-cooled exhaust. A choked orifice plug of variable size is installed at the exhaust exit to maintain elevated pressure in the combustion chamber. Air mass flow rates and the air temperature were measured upstream of the dump plane and its value was continuously recorded during measurements.

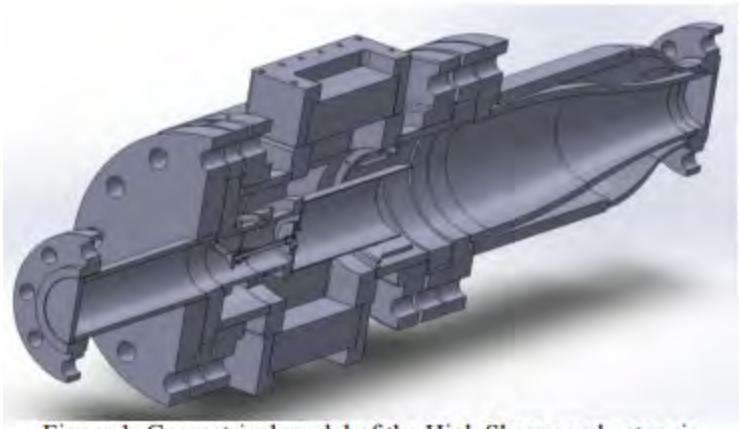

Figure 1. Geometrical model of the High Shear combustor rig

The combustor liner consists of a 30.5 cm long, 105 mm inner diameter quartz section. The front end of the combustor, called the bulkhead, is a stainless steel wall without secondary cooling passages. This bulkhead face contains four thermocouples situated flush with the surface for monitoring bulkhead temperature, a static pressure transducer, and an ignitor. The pressure vessel that houses the liner has optical access on all four sides and four quartz windows (Figure 1). The fuel nozzle uses a Pratt & Whitney proprietary swirler geometry, through which the pressurized preheated air passes through prior to entering the test section. The pressure atomizer is a commercially available McMaster-Carr misting nozzle (part number 3178K45) with a 0.51 mm orifice diameter and a flow number of 2.3.

Computational Models and Setup

The experimental setup of the high shear combustor rig was simulated using Large Eddy Simulations. Figure 2 shows a simple schematic diagram of the combustor. The simulation domain has an upstream plenum or air preconditioning flow path, from where the air enters the domain. Air mass flow rate is specified at the inflow boundary along with correct air temperature. This air passes through the swirler to enter into the combustor. A part of this air also flows on the outside of the combustor wall and enters the convergent section on the aft of the combustor to cool the hot gases that leave the cylindrical combustion chamber. Cooling air is specified at a surface near the exit of the combustion chamber using measured cooling mass flow that enters the convergent section.

Figure 2. Schematic diagram of the High Shear combustor rig simulated using LES

The long computational domain is needed to setup the correct exit boundary conditions even though it makes the simulation run time longer to obtain statistically steady solutions. Measurements of the wall temperatures on the bulkhead and secondary flow path were used to setup isothermal boundary conditions on these boundaries to simulate the heat transfer that happens at these walls. Before we present the results from this work, a brief summary of the CFD models are being provided here. LES solver used for this work is the fully compressible finite-volume based code LESLIE. It is a block-structured solver that uses a predictor-corrector scheme which is 2nd accurate in time and employs 2nd/4th order accurate spatial integration schemes. More details of the submodels are provided in Table 1. Computational domain was resolved with hexahedral cells with finest mesh of 0.1 mm near the swirler walls and coarsest mesh of 3mm in some plenum locations. Fine meshes were used in the vicinity of the swirler in the front end of the combustor to resolve the turbulent flow structures,

swirling flow and the flame anchoring in this region. The combustor region is resolved with nearly uniform sized cells to avoid dissipation errors. The total mesh count is little over 6 million cells.

Table 1. A comprehensive list of all the sub-models used in the current study

	Sub-Models
Solver Name	LESLIE
Spray Flame Modeling Approach	**Eulerian-Lagrangian (EL),**
Governing Equations	**Compressible multi-species Navier-Stokes with spray**
Grid Type	**Multi-block structured**
Solver Type	**Finite volume**
Spatial Discretization	**$2^{nd}/4^{th}$ order MacCormack,**
Time Integration	2^{nd} order explicit predictor-corrector **$2^{nd}/4^{th}$ order explicit Runge-Kutta for spray equations**
Boundary Conditions	**Characteristic boundary conditions**
Thermodynamics	Thermally perfect gas
Transport	Sutherland,
Chemical Kinetics	**Finite-rate (reduced/skeletal/detailed)**
Momentum Flux Closure	Boussinesq hypothesis. **Constant coefficient k^{sgs},**
Energy Flux Closure	**Gradient diffusion hypothesis**
Species Flux Closure	**Gradient diffusion hypothesis**
Reaction Rate Closure	**Quasi-laminar (QL),**
Dispersed Phase Physics	**Polydisperse with Evaporation**

Results and Discussion

Validation of non-reacting aerodynamic flow-fields

A series of step-by-step validation for the various sub-models used in this study was completed before performing the Lean Blowout simulations. As a first step, cold-flow validations were conducted to ensure the grids, boundary conditions and subgrid momentum closure models are adequate to simulate the non-reacting conditions.

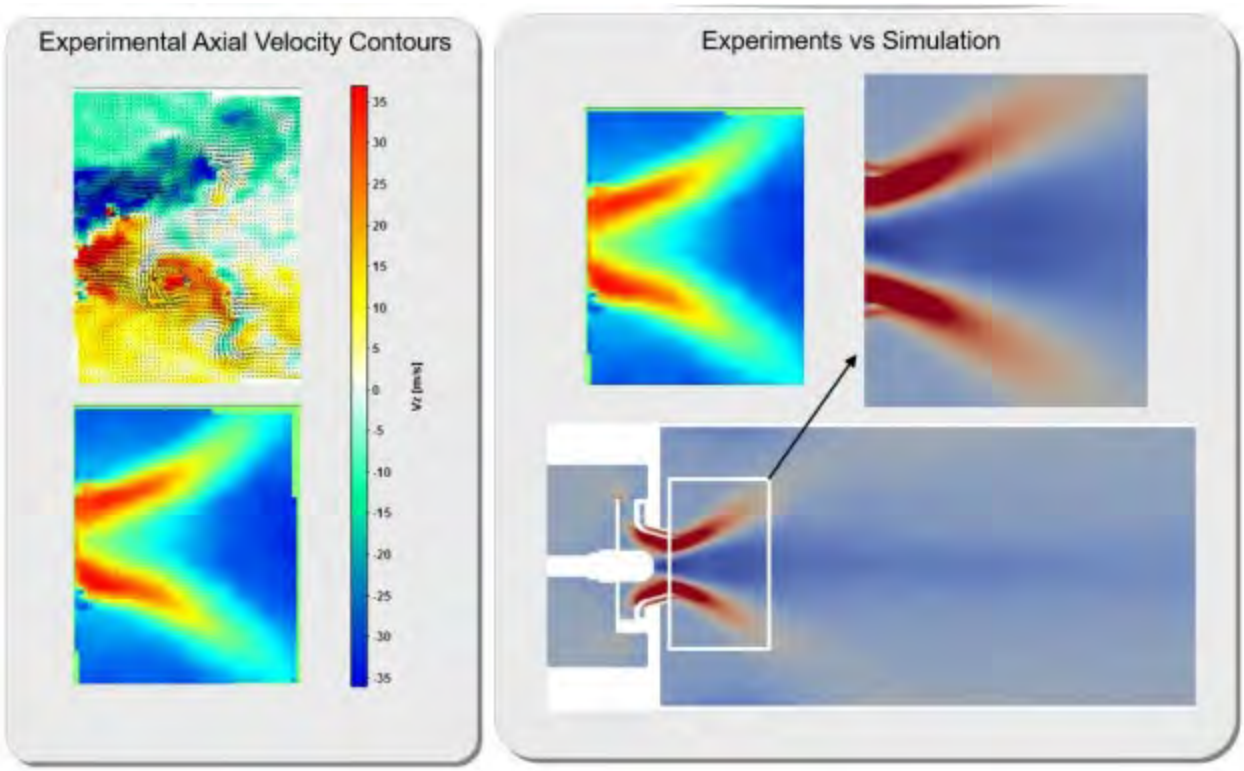

Figure 3. Time averaged contours of axial velocity from experiments (left panel) compared to simulations (right panel) from the central cross-sectional plane at non-reacting conditions in the High Shear Rig

Figure 3 shows the time-averaged contours of instantaneous and mean axial velocity obtained from PIV measurements on the left panel in the central cross-sectional plane of the combustor for non-reacting conditions. Flow through the radial and axial swirlers are clearly visible in this plot. As the flow enters the confining passages of the swirler from the preconditioning flow path, area reduction and continuity accelerates the flow significantly causing a high velocity annular jet to emanate out of the swirler. The tangential flow trajectory pushes the flow away from the center line of the swirler and hence a region of negative axial velocity or recirculation zones are created in the central sections of the combustor near the swirler exit. This recirculation region is intended for flame stabilization. Large velocity gradients near the swirler are also intended to help with better spray atomization. Overall, all the flow features are captured well in the simulation and are qualitatively in good agreement with the data. The spread angle, velocity magnitudes and the extent of the central recirculation regions were compared to be in good agreement with the measurements.

Figure 4 shows the time-averaged axial velocity field from the non-reacting experiments compared to non-reacting simulations in the high shear rig. Measurement data was obtained using stereo PIV. Overall, there is a reasonable agreement even though some particular discrepancies can be noticed. Simulations are over predicting the shear layer width especially in the near-field of the swirler. This could be attributed to the subgrid momentum closure models and the grid resolution. The mesh resolution near the solid wall in the swirler passages is usually inadequate as it would be prohibitively expensive to resolve the fine scales in the turbulent boundary layer. It is typical to use some specialized wall models or hybrid RANS-LES models to account for the lack of resolution near the wall. However, in this study no such models have been used. On the other hand, the measurements also report errors related to the inability of the stereo PIV technique to distinguish between the spray droplets and the PIV tracer particles. This can lead to systemic errors in the measurement data. Moreover, the measurements near the periphery of the optical windows have increased errors due to reflections and other issues related to light intensity. The swirling motion also causes flow perpendicular to the optical plane which also would introduce measurement errors. Considering all this, the overall qualitative and quantitative agreement between the experiments and

the simulation is reasonable to provide confidence in the mesh, subgrid momentum closure models and other boundary conditions used for nonreacting flow simulations.

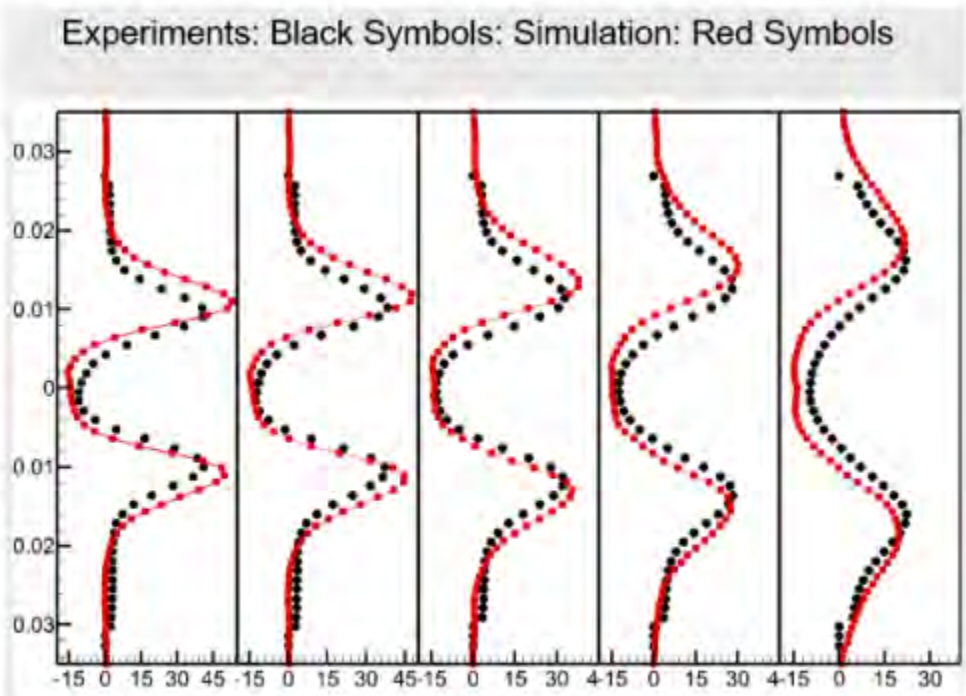

Figure 4. Time averaged contours of axial velocity from experiments (black dots) compared to simulations (red dots) at five axial stations showing the variation in radial directions for non-reacting conditions in the High Shear Rig

Validation of non-reacting spray boundary conditions and transport

Parametric study conducted for the spray initial conditions revealed that the spray evolution downstream and the flame location depends very strongly on the spray inlet boundary conditions such as the initial size distribution, position and velocity. Typically spray formation processes are not modeled in the reacting LES, due to the excessive modeling complexities and the computational cost required for simulating the atomization processes. Known empirical spray size distributions are prescribed as initial conditions (ignoring the primary break-up process). Log-normal and Rosin-Rammler are two popular spray size distributions that match experimentally measured spray size distributions for different injectors and flow conditions. But these correlations assume the same size distribution is valid across the entire fuel nozzle cross-section, which is known to be incorrect. Droplet velocity information is also not specified by these correlations and hence all droplets (regardless of their size) are assumed to be injected at the same velocity which can be another source of major error in the simulations. PDPA based measurement data can provide correlated spray size-position-velocity information, however, it is difficult to obtain such data very close to the injector and data is available only some distance downstream of the fuel injector. For this particular fuel injector and swirler configuration, UTRC conducted a testing campaign to obtain detailed PDPA data to simultaneously measure spray position, size and velocity for three different fuels at several flow conditions. The modeling team devised an approach to utilize the spray PDPA data measured downstream and specify boundary conditions close to the fuel injector. A snapshot image of the spray dispersing out of the fuel nozzle geometry is shown in Figure 5 below.

Our approach is based on geometric projection of the measured data, from the actual measurement plane to a plane close to the injector called the CFD injection plane. In Figure 5, the dashed red line shows the location of the measurement plane. Because the measurement planes are reasonably close to the swirler exit, it was assumed here that no significant evaporation would have occurred and that the droplet size obtained in the measurement is the result of atomization only. Based on this, we defined annular concentric strips at an arbitrary injection plane close to the injector face, as shown by the image in the middle of the panel in Figure 5. The number of strips corresponds to the number of radial locations at which the PDPA data

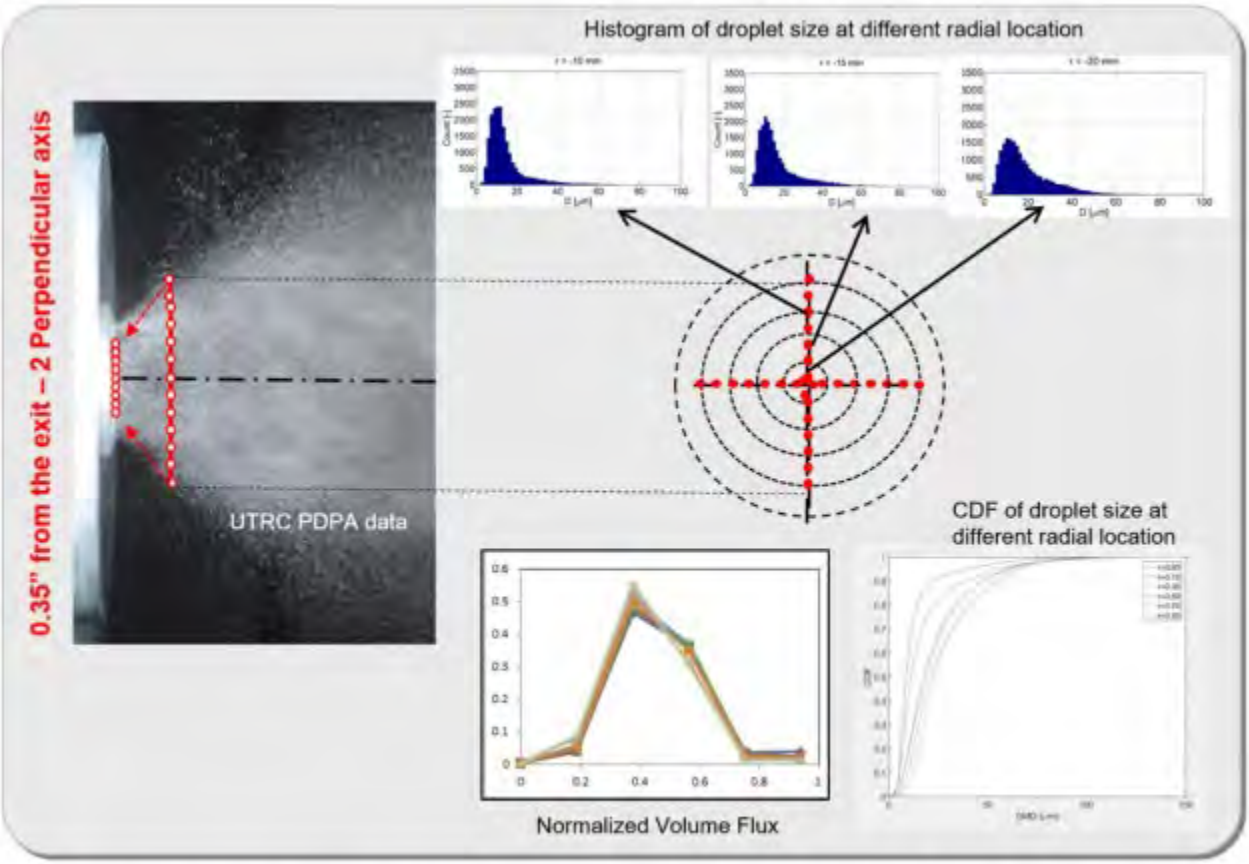

Figure 5. A snapshot of the spray injected out of the fuel nozzle and a conceptual image of the spray boundary conditions employed in the current work

Because PDPA gives correlated droplet size and velocity, one could also use the measured droplet size directly from the measurement as well. If all three components of the velocity are known from the measurement, then there is no need to specify spray cone angle. In the absence of component data, one could use the spray cone angle to obtain an estimate of the velocity components that is not available from the measurements. The key advantage of this approach is that joint PDF of drop-size-velocity and position can be specified in CFD. Droplets at different locations disperse to different positions based on their size and hence it is important to preserve the correlation between position, size and velocity to obtain the correct droplet dispersion. This would ensure that the correct size droplets disperse to the correct location which in turn would yield correct flame location and structure. Another major advantage of this approach comes from the use of measured data that is far enough from the injector face where secondary breakup and other atomization processes are nearly complete. By using such a data, one could avoid the need for secondary break-up models which further saves computational time. The major drawback of this approach is the implicit assumption that the droplet trajectories follow the geometrical projection from the injection plane to the measurement plane and that the evaporation between the CFD injection plane and the actual measurement plane is minimal. Therefore, validation of this approach is required to ensure that such approximations do not introduce unacceptable errors in the reacting flow simulation.

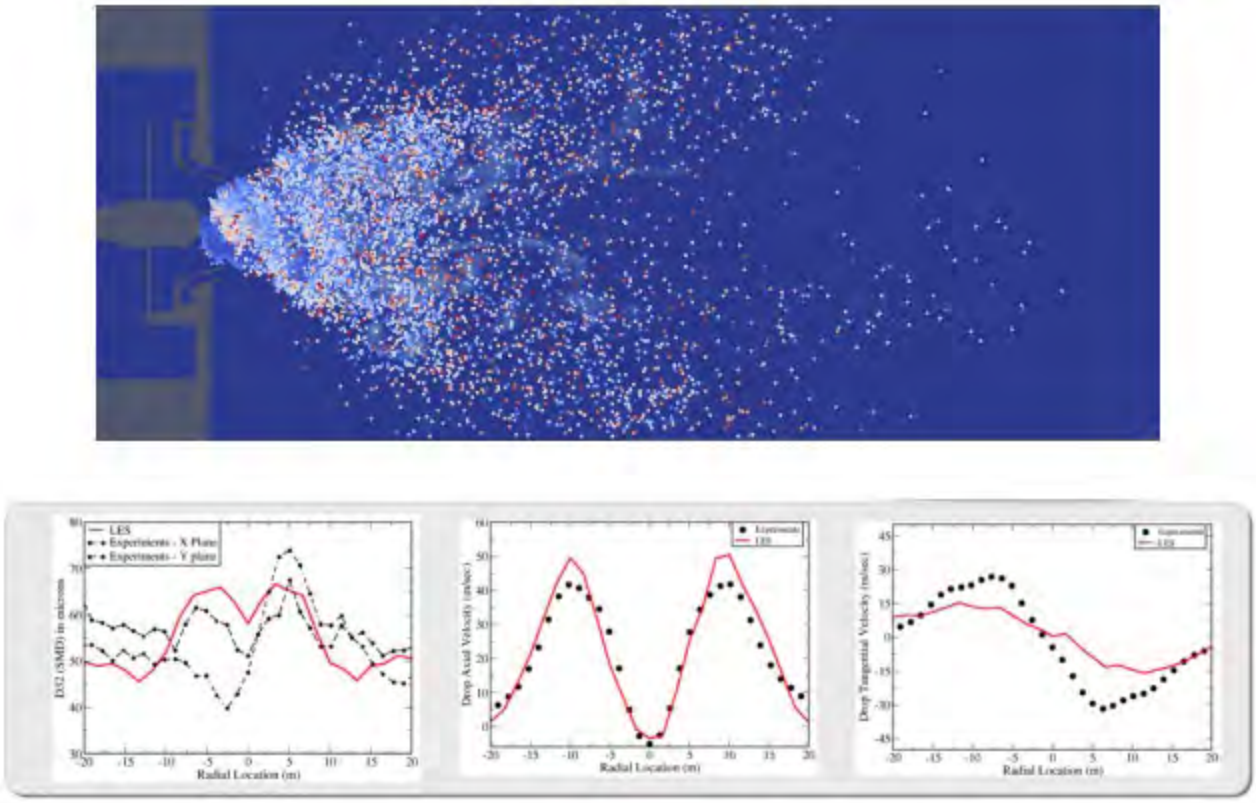

Figure 6. Top: Snapshot of spray dispersion in the high shear rig combustor (bottom) comparison of spray SMD, droplet axial and tangential velocity profiles between experiments (black dots) and simulations (red line).

Figure 6 (top image) shows the spray dispersion pattern from the spray boundary conditions described in this section. Experimental images and animations confirmed that the swirling air flow disperses the smaller sized drops in a swirling pattern and the simulated swirling spray pattern is in line with the expectation. In figure 6, (bottom image) compares the measured PDPA data with simulations. The image on the left-most side compares the Sauter mean diameter (D32) and the comparison is reasonable with differences less than 5 microns. The image in the middle of the panel compares the drop axial velocity and the agreement is excellent validating the supposition that the spray parcels follow the flow as assumed in the injection boundary conditions model. The image on the right side of the panel compares the droplet tangential velocity with data. The differences seen here are attributed to the lack of specification of tangential velocity boundary conditions for the droplets. Even though it is possible to specify the tangential component of droplet velocity, it was not used here intentionally due to the supposition that the swirling carrier gas flow would impart the momentum to the droplets and enable the droplets to achieve the correct velocity. As it can be observed from the simulation data, the droplets have picked up a tangential component and this can be further improved by specifying the tangential component of droplet velocity. Overall, the agreement in spray size, velocity and position demonstrates the potential of the proposed boundary conditions and also serves as a validation of this relatively easier and affordable methodology.

Multi-component evaporation models

Jet fuels are multi-component in nature with 100s of species. Liquid fuel vaporization depends on many thermo-physical properties such as its density, heat capacity, latent heat of evaporation, vapor pressure etc. Since these properties are functions of local temperature, pressure and composition, a good evaporation model is important to capture the correct evaporation behavior and the correct spatial distribution of fuel-air mixture which in turn impacts flame-stabilization and blowout. UTRC developed a multi-component evaporation model based on the distillation curve (under a different contract

in NJFCP) and validated with partial data from the AFRL. This model provides all thermo-physical properties for the liquid fuel based on a surrogate representation of the liquid that matches the distillation curve constrained by liquid-vapor thermodynamic equilibrium. An ab initio equilibrium calculator (SuperTrapp) from NIST that uses the corresponding state theory (the cubic equations of state which take into account the molecular potential energy interaction between different hydrocarbons) was utilized to compute the equilibrium fluid properties of the mixture. The distillation curve calculator was derived from the equilibrium library of SuperTrapp to simulate the ASTM distillation process. This method is designed to track the changes in the composition in the liquid (and gas) during the evaporation process. The distillation curve computed for a given surrogate fuel is then compared with the experimentally obtained distillation curve, overall molecular weight, and density and other fuel properties, such as viscosity, surface tension etc. The surrogate model is adjusted until it provides a good match to available data and meeting other constraints such as the overall C to H ratio and average molecular weight. This process of adjustment is based on the properties of each component; for example, increasing the composition of a cyclic compound while decreasing an aliphatic compound of the same carbon number will change the density of the mixture while keeping all other properties constant. The surrogate model thus found was then utilized to predict all fuel properties during the evaporation process. This way, we are basically deriving fuel properties from first principles using a representative set of hydrocarbons found in a specific fuel sample with fuel physical properties that are valid for a wide range of temperature and pressure. This model assumes that as a droplet evaporates, it follows the distillation curve and hence the volume recovery fraction is a one-to-one function of temperature. This way one can construct a look-up table for all fluid properties using temperature as the independent variable. For temperatures below the starting temperature of the distillation curve, we evaluate the liquid properties along the curve defined by the loci of the bubble point.

Figure 7 shows the distillation curves and liquid density variation as a function of temperature predicted by the surrogate model of JetA, JP8 and JP5 fuel at 1Bar. The modeling results compared with experimental data (from AFRL) show very good agreement and is also in good agreement with Jet A distillation curve data found in the CRC handbook.

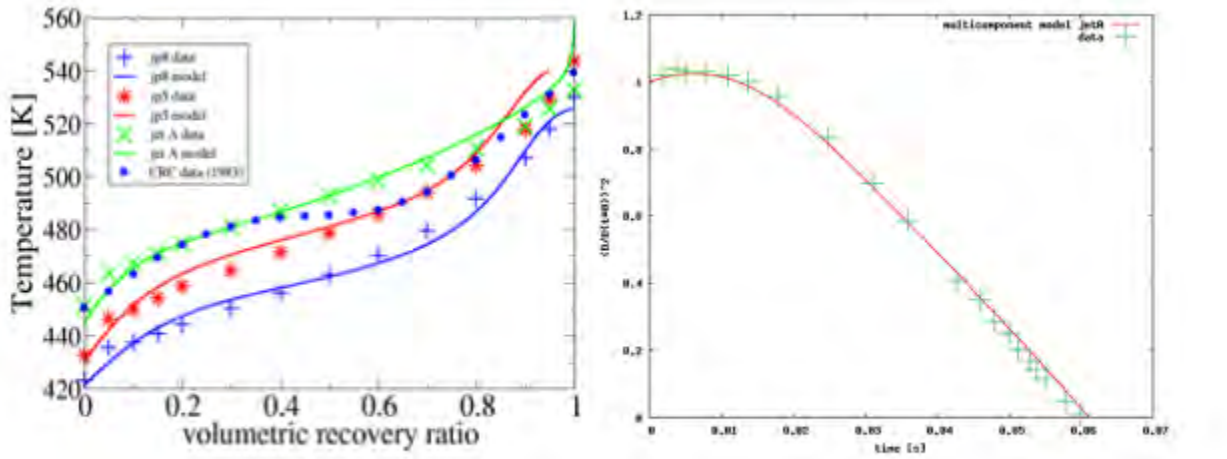

Figure 7: (left) Comparison of distillation curve predicted using data from AFRL and UTRC multicomponent evaporation model (right) comparison of single droplet evaporation time using the evaporation model

The properties needed for droplet evaporation simulation, computed using our surrogate models, are all tabulated and implemented into the reacting LES CFD code. Standard equations for droplet momentum, heat and mass transport equations are solved with classical correlations for drag and other inter-phase exchange terms. Another validation of the model was performed by simulating a single droplet evaporation. An isolated droplet of size 100 microns at an initial liquid fuel temperature of 300K embedded in ambient conditions of 1 bar and 800K was simulated for the reference Jet A fuel. Figure 7 (right) compares the D2 variation with time for Jet A as a function of time at 1 bar pressure and compares with the results from Burger et al exhibiting a very good level of agreement. Figure 8 shows the fuel physical properties for a range of temperatures and for 3 different pressures. Data at 1 atm is used for comparison with the models and data at 2 atm and 3 atm are used for LES simulations of referee rig (which operates at 2 atm) and high shear combustor rig (which operates at 3 atm), respectively. Overall the model captures the physical property variation for a wide range of conditions.

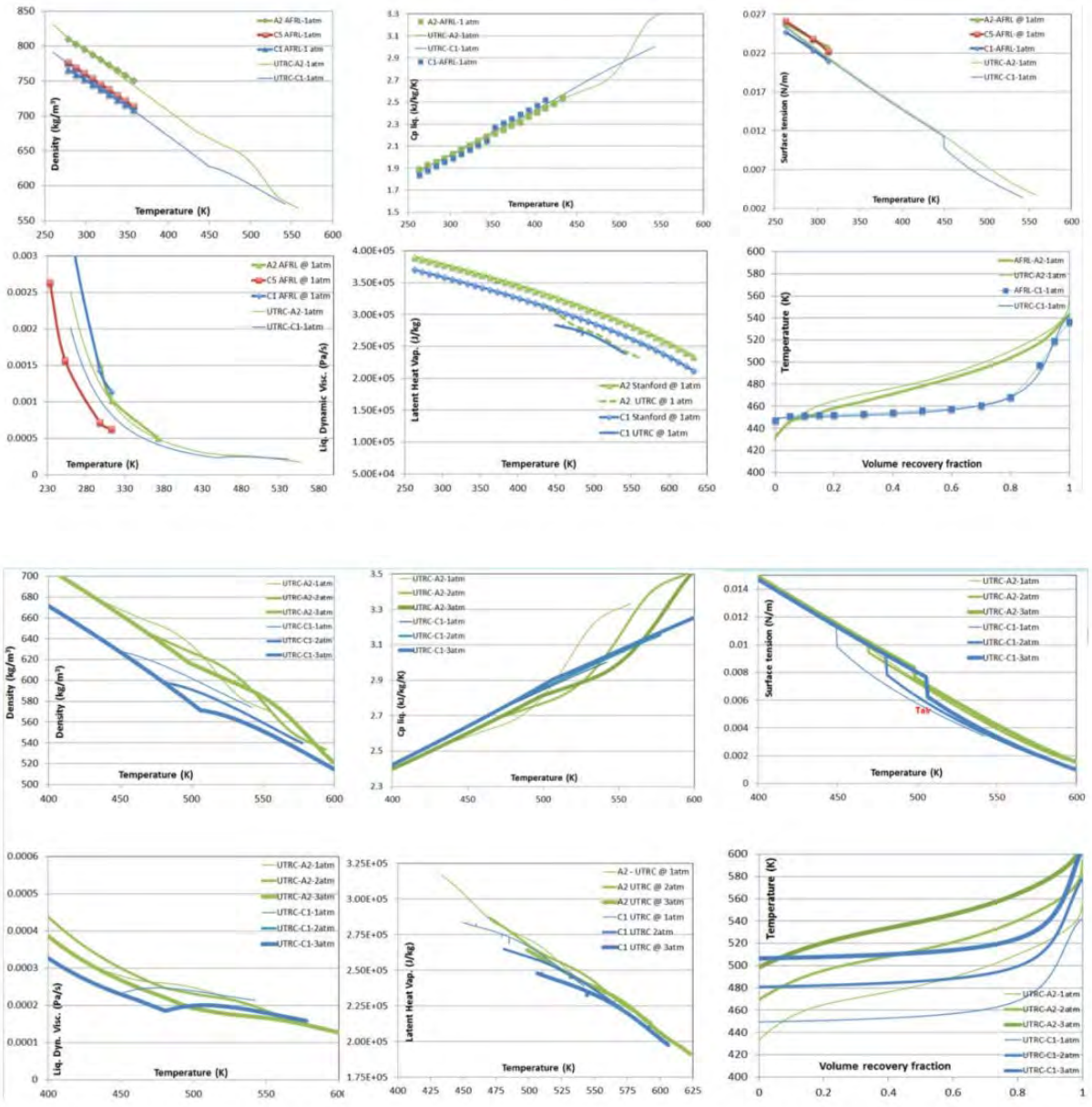

Figure 8: Prediction of fuel physical properties from the multi-component evaporation model. The top two rows (six figures) show comparison of density, specific heat surface tension, viscosity, vapor pressure and distillation curve at 1 atm and comparison to available data from AFRL. The bottom two rows of six figures shows the same properties at three different pressures.

Combustion Chemistry Mechanisms

As a part of the National Jet Fuels Combustion Program (NJFCP) teams from Stanford University developed a version of HyChem model for combustion chemistry or chemical kinetic mechanisms for A2, C1 and C5 fuels. The detailed chemical

mechanism was calibrated and validated using species yields measured from flow reactor experiments. Research teams from the University of Connecticut developed skeletal and reduced mechanisms using Directed Graph Approach and verified these mechanisms by matching with combustion target properties like flame- speed, ignition delay, extinction strain rate, etc. These mechanisms consists of over 30 species and 100s of reaction steps and hence would be expensive to use in reacting LES of high shear rig combustor. As a compromise, we devised a single step chemistry with 5 species as shown below:

$$C_cH_h + \left(c + \frac{h}{4}\right)(O_2 + 3.76N_2) \rightarrow cCO_2 + \left(\frac{h}{2}\right)H_2O + \left(c + \frac{h}{4}\right)3.76N_2$$

The reaction rate expression was chosen to mimic the Westbrook and Dryer single step chemistry and an empirical Pre-exponential factor (AFAC in the expression shown below) was introduced to account for the changes in the reaction rate as the local equivalence ratio varies in an evaporating spray combustion environment.

$$\mathrm{k} = AFAC * 5.1e^{11} \exp\left(-\frac{15098}{T}\right) Fuel^{0.25} O_2^{1.5}$$

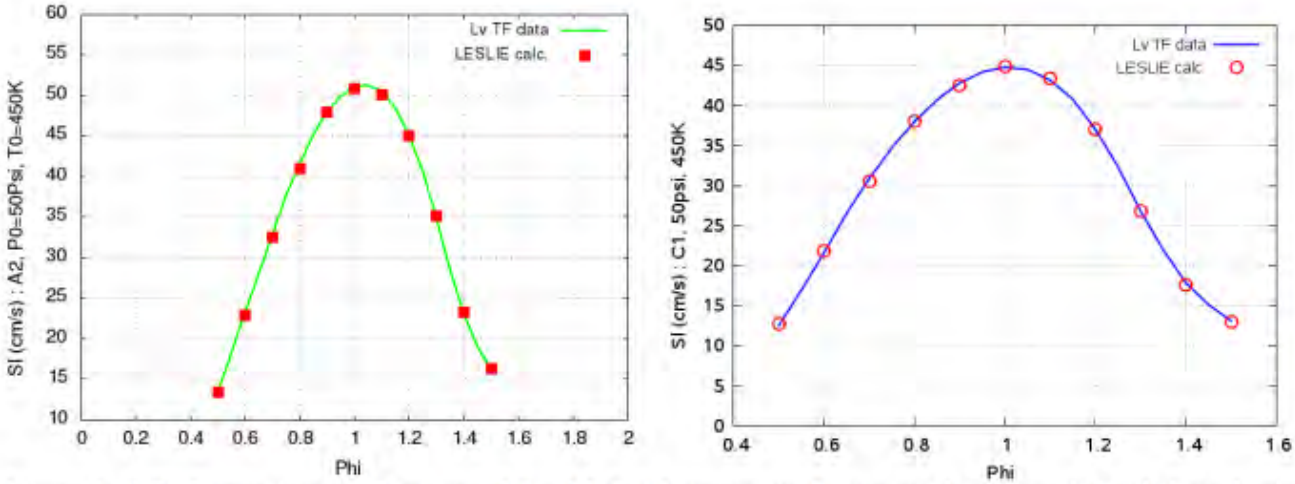

Figure 9: (left) Comparison of flame-speed for A2 fuel between single-step mechanism and detailed mechanism based on HyChem V2 chemistry model. (Right) Comparison of flame-speed for C1 fuel between current single-step mechanism and detailed mechanism based on HyChem V2 chemistry model

We simulated a one-dimensional freely-propagating premixed flame for different values of equivalence ratio (ϕ). For each value of ϕ, the AFAC term was changed until the mechanism yielded the correct flame-speed compared to the detailed mechanisms. By repeating this exercise for different values of ϕ, a correlation for AFAC as a function of ϕ was obtained that would be used in the reacting LES simulation of the high shear rig. Figure 9 shows the comparison of flame-speed obtained from the single-step mechanism for A2 and C1 fuels at inlet temperature and pressure corresponding to the high shear rig experiments. Overall an excellent agreement is obtained using this simple but empirical approach for deriving combustion chemistry models for complex LES simulations

Turbulent Combustion Models

The final sub-model that is needed for performing reacting LES is a turbulent combustion model. Even though different turbulent combustion models are available in the current CFD solver, a simple direct laminar closure model was used in this study. This model assumes that most of the turbulent mixing is resolved by the grid and hence the subgrid turbulent mixing can be ignored. As a result, the resolved species mass fractions, temperature, density and pressure can be used directly in the reaction rate expressions. The validity of the model is a function of how well the fine scale turbulent mixing is resolved by the underlying computational meshes used in this study.

In the next section, results from the simulations of high shear rig at near blow out but stable conditions will be presented for A2 and C1 fuels. Qualitative and quantitative comparisons of the contours and line plots will be presented to highlight any similarities and differences in the flow-field and flame structure for the two different fuels used here.

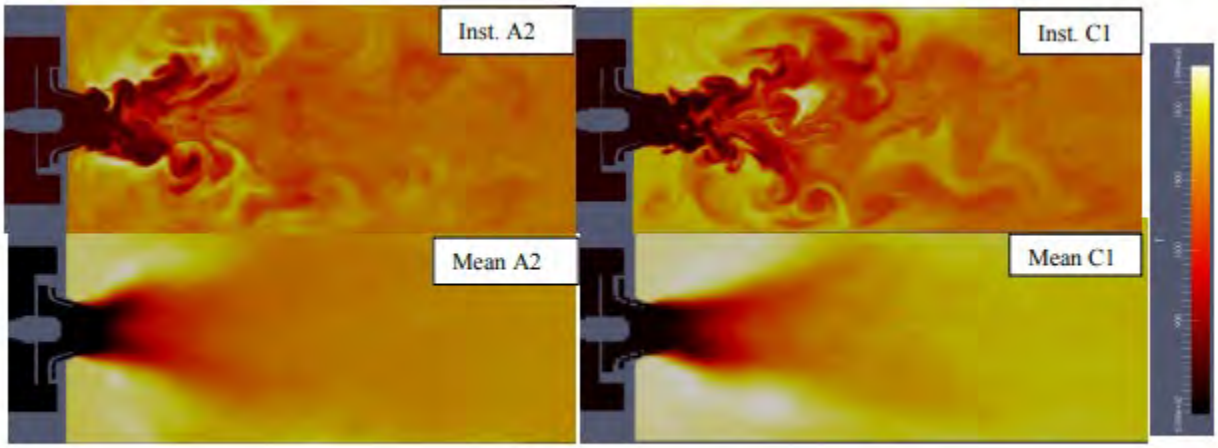

Figure 10: Contours of temperature from reacting LES of high shear rig combustor (top row) Instantaneous temperature contours (bottom row) mean or time-averaged temperature contours in central plane

Figure 10 shows the contours of temperature from the reacting simulations using the A2 and C1 fuels at near blowout (but stable) condition. The top row shows an instantaneous snapshot of the temperature contours at a particular instant and the bottom row shows time-averaged temperature contours for the same setup. Simulations were run for approximately 100 milli-seconds before averaging. To obtain mean or time-averaged data, simulation results were run for another 100 milli-seconds due to the lengthy combustor dimension. Darker regions near the swirler indicate colder air and it appears like a lifted flame is realized in this setup. The outer or corner recirculation zones bring in partially burnt hot products and mix them with the fresh air and evaporating fuel spray near the shear layers at the swirler exit. This creates a lifted flame that is stabilized between the shear layers and the central recirculation zones. It should be noted however that neither the instantaneous images nor time-averaged images show any visually significant differences for the two fuels simulated in this study.

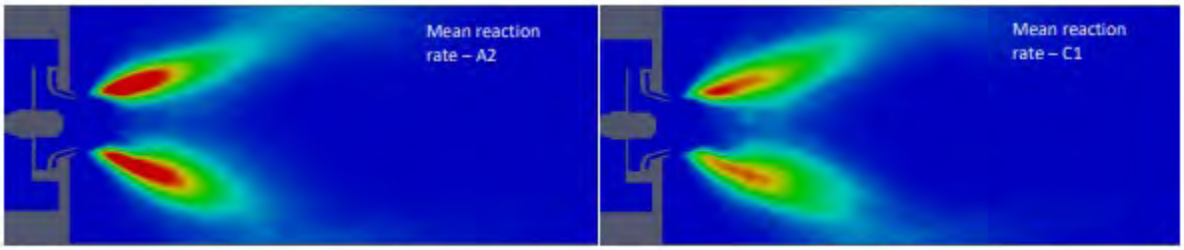

Figure 11: Contours of time-averaged fuel reaction rate obtained from reacting LES of high shear rig combustor (left) for A2 fuel (right) for C1 fuel

Figure 11 shows the contours of time-averaged fuel species reaction rate from the simulations of the stable conditions using A2 and C1 fuels. It can be observed that the flame structure, flame angle, anchoring locations are very similar for the two fuels. However, the magnitudes are noticeably different. A2 flame seems to have higher values of time-averaged reaction rates compared to C1 which is an indication that the A2 flames more robust and stable compared to the C1 flames, even though the C1 fuel has higher volatility compared to A2 fuels. This counterintuitive behavior is associated with the fact that all liquid fuel components in C1 fuel evaporate nearly at the same boiling temperature and hence in a very small region. Locally the mixture can be rich and has very little time for premixing. On the other hand the distillation curve for A2 fuel is gradual (see fig. 7) and different liquid fuel component evaporate at different boiling temperature. Hence, all the fuel vapor

are not dumped in a small region but instead smoothly spread over a wide area which gives it time for premixing and combustion. This observation is consistent with the experimental observation under stable and lean blow out conditions.

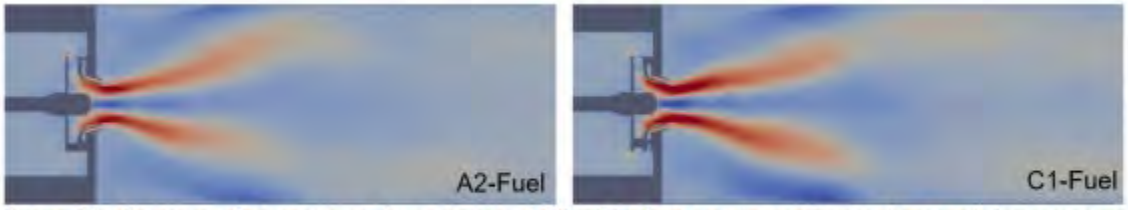

Figure 12: Contours of temperature from reacting LES of high shear rig combustor (top row) Instantaneous temperature contours (bottom row) mean or time-averaged temperature contours in central plane

Figure 12 shows contours of time-averaged axial velocity fields obtained from the reacting simulations using A2 and C1 fuels in the high shear rig. Consistent with the temperature contours, very little differences can be observed in the velocity fields. However, notable differences can be seen in comparison to the non-reacting velocity fields (Figure. 3). The angle of the annular swirling jet that comes out of the swirler in the reacting flow is shallower than the non-reacting flow field. This is an indication of a reduction in swirling or tangential component of the velocity due to combustion related flow acceleration in the axial direction. The magnitude of the axial velocity was also higher than the non-reacting flow field. The combined effect of the reduction in angle and increase in velocity leads to a more coherent or lengthy annular jet which will have an impact on the flame stabilization.

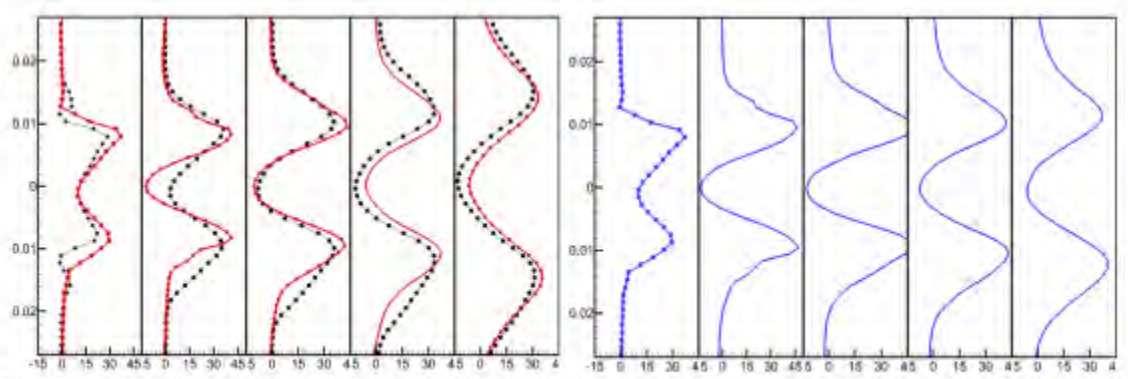

Figure 13: Radial profiles of axial velocity at five different axial stations for the A2 fuel (left) and for the C1 fuel (right). For the A2 fuel black dots represent the measurements and the red lines are from the simulation. For the C1 fuel measurements are not shown due to unavailability of the data at the time of comparison

Figure 13 shows the radial profiles of axial velocity at five different axial stations from the reacting simulations using A2 and C1 fuel. For the A2 fuel, comparison is also shown with measured data. For C1, fuel measurement data were not available for comparison with simulations. While some differences can be seen relative to the measurements, the agreement is still reasonable. As before, no significant differences can be observed between the two cases for these conditions. The lack of differences in the velocity fields between the two fuels indicate that the flames see/encounter similar level of turbulence and mixing and any notable differences in the lean blow out behavior would be due to evaporation and or chemistry effects.

Lean Blow Out Simulations

Upon completion of the reacting LES for the two fuels at near blowout but stable condition, simulations were performed to understand the capability of the tools to predict observed lean blow out trends for the two fuels considered in this study. Starting from the near blowout simulations, fuel flow rate was reduced in steps of 6% and held constant for 100 milli seconds before reducing the fuel flow rate again. This was continued until the flame blow-out was observed. It was empirically determined based on the simulation that it takes approximately 100 milliseconds for the combustor to respond to the flow rate change and stabilize at the new condition. Based on the experiments, the near blowout fuel flow rate was set at 11.40

pph. Figure 14 shows the variation of liquid fuel evaporation rate as a function of time that was observed in the simulations for A2 and C1 fuels. It can be observed that for the A2 fuel, it takes approximately 100 milli-seconds (black line) to reach ~94% evaporation efficiency (defined as evaporation rate/injected fuel flow rate). It is hypothesized that the isothermal heat transfer boundary condition employed in this study does not accurately reflect the true heat transfer magnitudes and location from the experiments and therefore, could be over-predicting the heat loss, which in turn reduces the evaporation efficiency in the simulations. However, in the absence of accurate wall temperature measurements from the tests, this approximate boundary conditions is a compromise between the accuracy and simulation cost. It is also possible if the simulations were continued further, the evaporation efficiency may increase and reach 100%. However in the interest of getting to the lean blow out conditions, it was empirically assumed to be the steady state and the fuel flow rate was reduced at this point. At this stage, the fuel flow rate was reduced instantaneously to 10.72 pph (6% lower than the near blowout condition), and the simulation was continued for another 100 milli-seconds (red line). With the fuel flow rate reduction, a slight increase in evaporation rate was observed for a brief period before it begins to reduce and approach a mean steady value of ~10.3 pph. Again this is approximately 93-94% of the liquid fuel flow rate and similar to the previous flow rate complete evaporation was not achieved. At this state, the fuel flow rate was further reduced instantaneously to 10 pph (green line) and the simulations were continued for another 100 milliseconds. The evaporation rate further decreased and appears to reach a steady state for which ~95% evaporation efficiency was predicted. Figure 14 (right image) shows the evaporation rate for C1 fuel. At a flow rate of 11.40 pph (black line) an improved evaporation rate for C1 compared to A2 fuel. Approximately 98% of the fuel evaporates after 100 mil-seconds. This is in in line with the expected better vaporization characteristics of the C1 fuel. As the fuel flow rate was further reduced to 10.72 pph, the evaporation rate decreased after a brief period and reaches a near stable state evaporating 98% of the injected fuel. As the flow rate was reduced to 10 pph, initially the evaporation rate decreased to ~88% and then it increases and reaches a near steady value of 96%. This is an indication of some unsteadiness as the fuel flow is approaches the lean blowout range (~9 pph) but not a conclusive evidence of the tool's ability to discriminate the effect of fuel property on the LBO behavior.

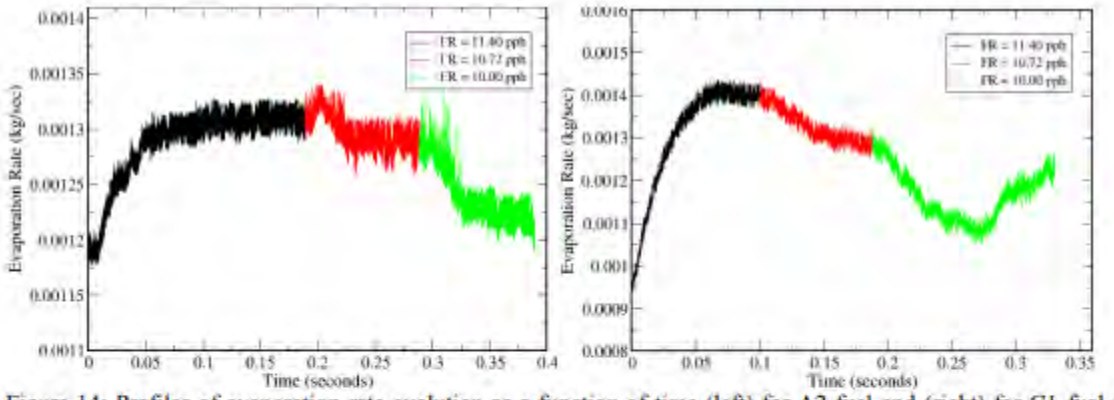

Figure 14: Profiles of evaporation rate evolution as a function of time (left) for A2 fuel and (right) for C1 fuel at three different flow rate conditions identified in the legend box

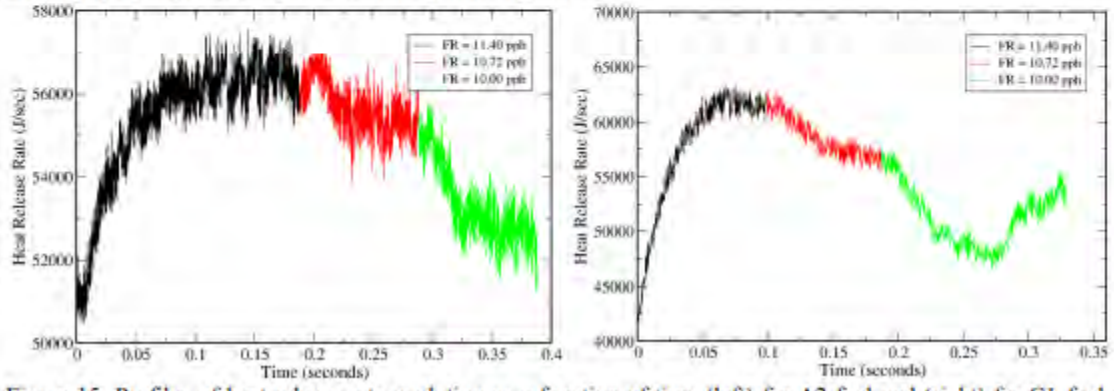

Figure 15: Profiles of heat release rate evolution as a function of time (left) for A2 fuel and (right) for C1 fuel at three different flow rate conditions identified in the legend box

Figure 15 shows corresponding profiles of heat release rate for the two fuels as the fuel flow rate was decreased systematically from the near blow out condition. Similar to the evaporation rate profiles, the heat release rate also decreases as the flow rate is reduced. In alignment with evaporation rate, heat release also shows relatively higher fluctuation levels for A2 fuel compared to C1 fuel. While the lower heating values of the two fuels are nearly the same (~43 MJ/kg) slightly lower levels of evaporation observed in the A2 fuel simulation leads to a slightly lower values of heat release rates predicted for A2 fuel. Overall, the two fuels show differences in evaporation rate and also commensurate differences in heat release rates. Both the simulations show reduction in heat release rate as the flow rate is reduced but C1 seems to be dropping faster, relatively compared to A2. The experimental work indicates that the blowout for both the fuels was a sharper event unlike the referee rig combustor. Even though the current simulations show reduction in evaporation rate and heat-release rate, it is hard to infer the propensity of one fuel to blowout compared to the other unless the simulations were continued to fuel flow rates lower than the experimentally observed LBO flow rates. Unfortunately, these simulations take significantly long execution times due to small time-step, and long combustor length. For instance, each 100 mill-seconds of simulation requires 2.5 million steps of calculation and assuming discrete steps of fuel flow rate reduction, it requires 15 million time-step simulation for each fuel. The steady state at near blowout was run for significantly longer times. As a result of this long simulation times, we could only simulate three different flow rate reduction and use the results to extrapolate the model behavior.

Figures 16 and 17 shows the contours of temperature and fuel mass fraction contours for the simulations using A2 fuel at five different time instants during the simulation. Qualitative behavior of the flame can be inferred from such snap-shots and are usually helpful in providing insights about the driving mechanisms responsible for a particular physics. It can be observed from the temperature plots that the outer recirculation zones near the bulkhead are effective in mixing the hot products and the incoming fresh mixture of fuel vapor and air. Due to the increased residence time available in this area, the gas temperature in these locations are always hotter. Also, due to good turbulent mixing at shear layer, the flame anchors in this location. As the flow moves downstream, the mixing and chemistry gets enough time for combustion and relatively higher temperatures can be observed. At lower fuel flow rates, with a globally lean mixture, the temperatures go down. Relatively cooler combustion products get pulled into the corner recirculation zones and the temperature in these locations begin to reduce as seen by darker contours of temperature. At the lowest flow rate simulated, much cooler temperatures were observed downstream to the exit of the combustors. Even though the global equivalence ratio reduces, the local equivalence ratio may not be as lean and hence in regions around the shear layers, robust flame structure can still be seen as one moves from one flow rate to the other. It is hypothesized here that the corner recirculation zone controls the lean blow out in this combustor. Reduction of fuel flow rate reduces the overall temperature of the hot products in the corner recirculation zone, which will be further reduced by the incoming cold air at the shear layers. If the resulting temperature is below the ignition temperature, then chemical reaction cannot be completed on time and it would be blown away. On occasion, local hot pocket from the corner recirculation zone may successfully burn a local fuel vapor-air mixture and hence re-ignition events may be possible in this combustor as observed in the experiments. A2 fuel having a wide distillation range, would be able to provide a spatially smoother fuel vapor distribution and hence has a better chance to reignite or sustain combustion for a longer time. Figure 17 shows the fuel vapor mass fraction contours at the corresponding time instants and it can be seen that higher values of fuel vapor (purple color) can be seen in the corner recirculation zone as the fuel flow rate is reduced due to the decrease in temperature and decrease in reaction rates which results in incomplete combustion of the reactants.

Figures 18 and 19 show the contours of temperature and fuel mass fraction contours for the simulations using C1 fuel at five different time instants during the simulation. Even though the same physics of shear layer mixing of reactants with hot products from the corner-recirculation zone applies in this scenario, evaporation rates are different for these two fuels. As a result, increased values of fuel mass fraction is seen both near the injector and also inside the combustor. While increased vaporization rates are beneficial, it also leads to quick build of fuel vapor in a concentrated region and if the flow conditions in that region is not conducive in terms of residence time for completing the reaction, then it would result in even more accumulation of fuel vapor from the incomplete combustion. In the case of C1 fuel, this is hypothesized to be the mechanism for earlier flame blow out compared to the A2 fuel. While our simulations do not conclusively show this, the qualitative trend seems to indicate that the models have the ability to discriminate between the different fuel physical properties and its impact on the lean blow out behavior.

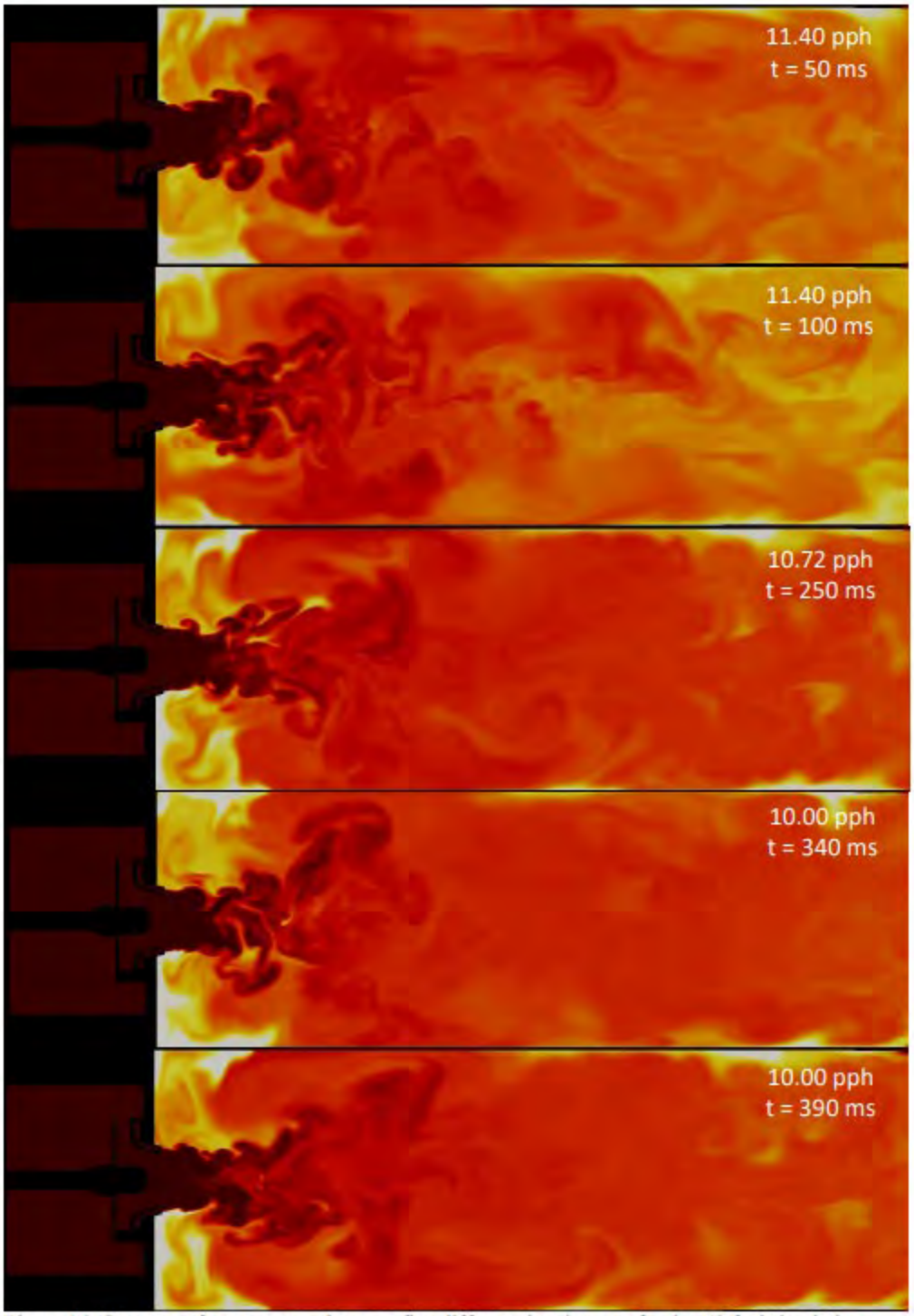

Figure 16: Contours of temperature shown at five different time instants for the A2 fuel simulation

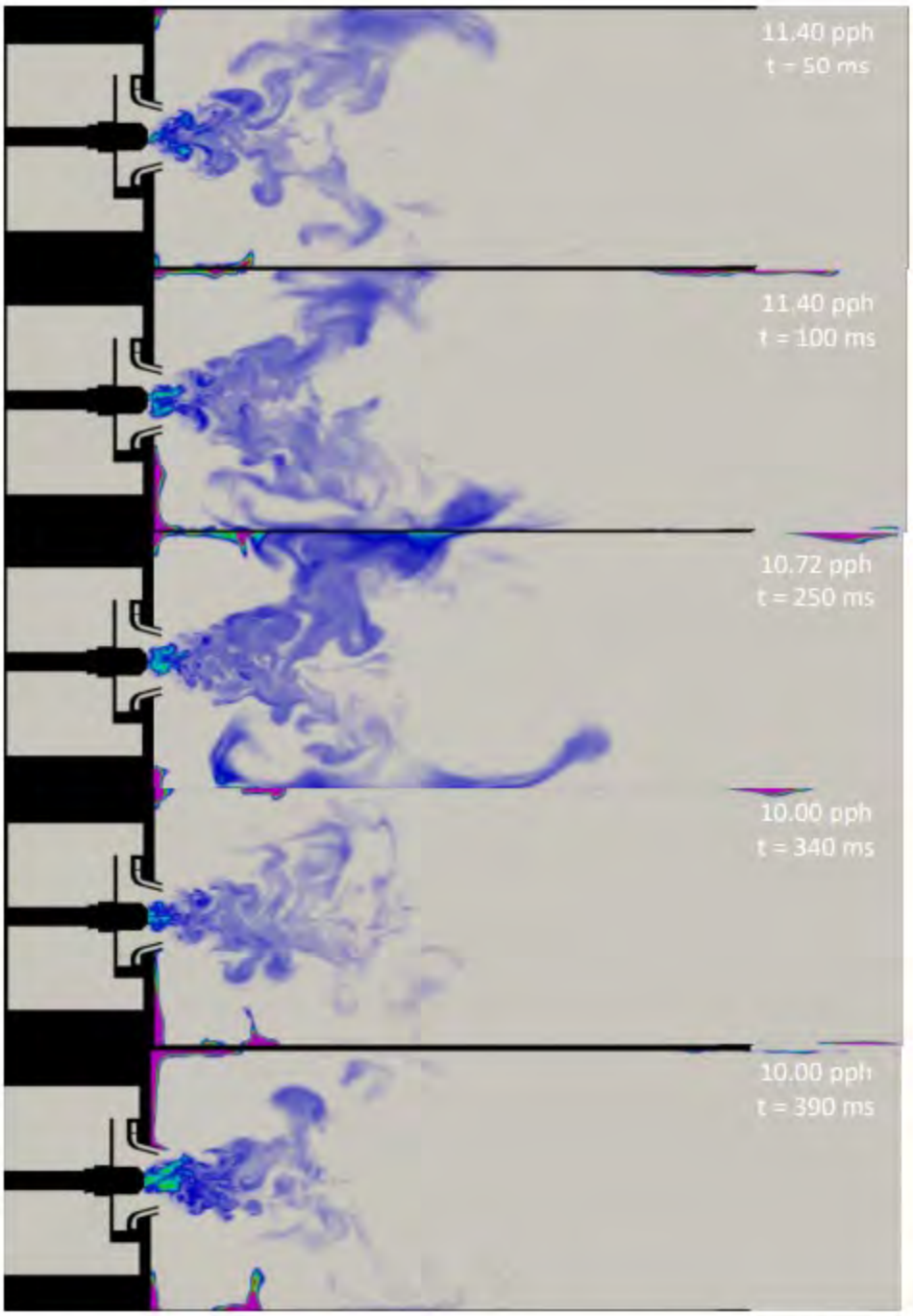

Figure 17: Contours of fuel mas fraction shown at five different time instants for the A2 fuel simulation

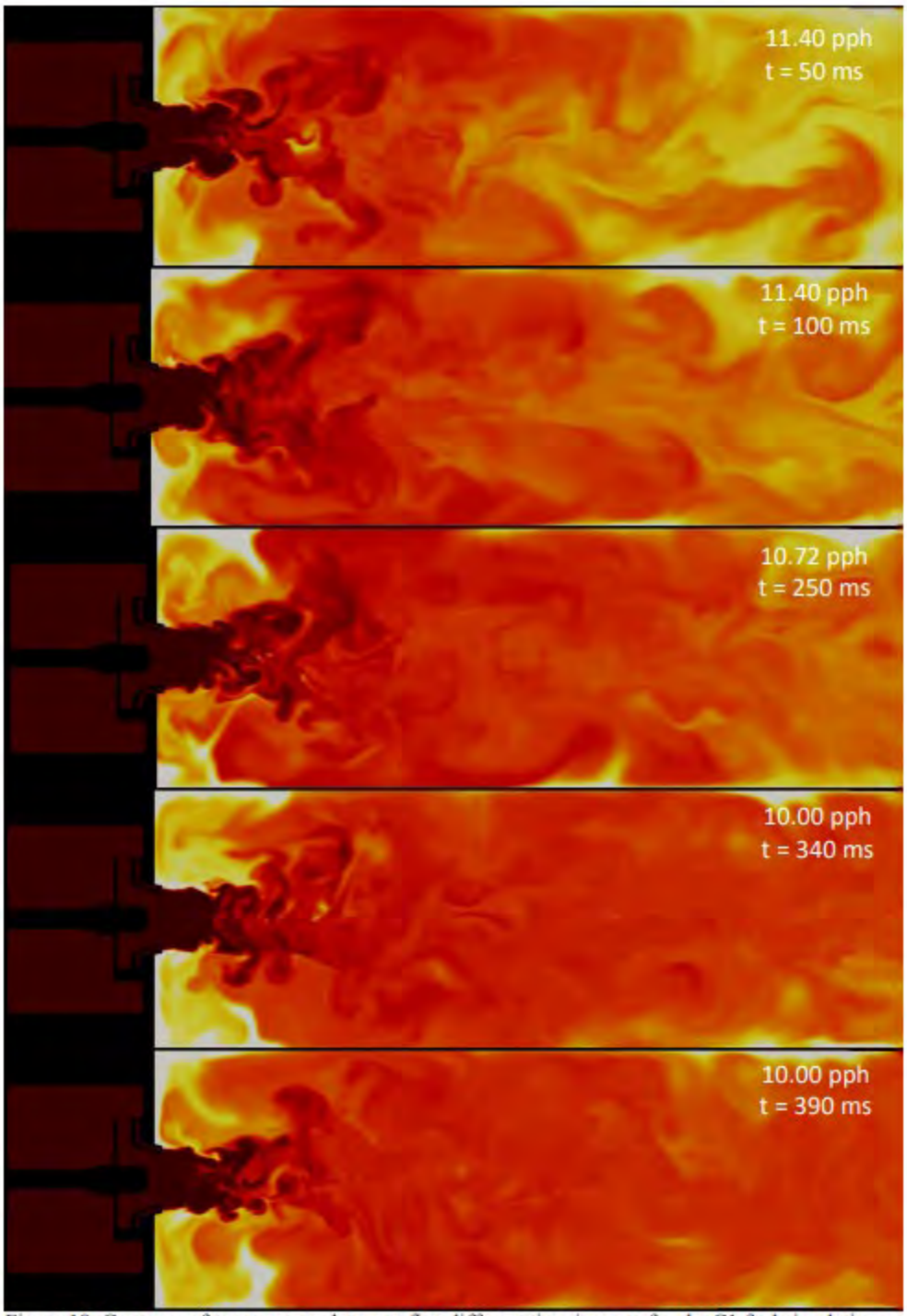

Figure 18: Contours of temperature shown at five different time instants for the C1 fuel simulation

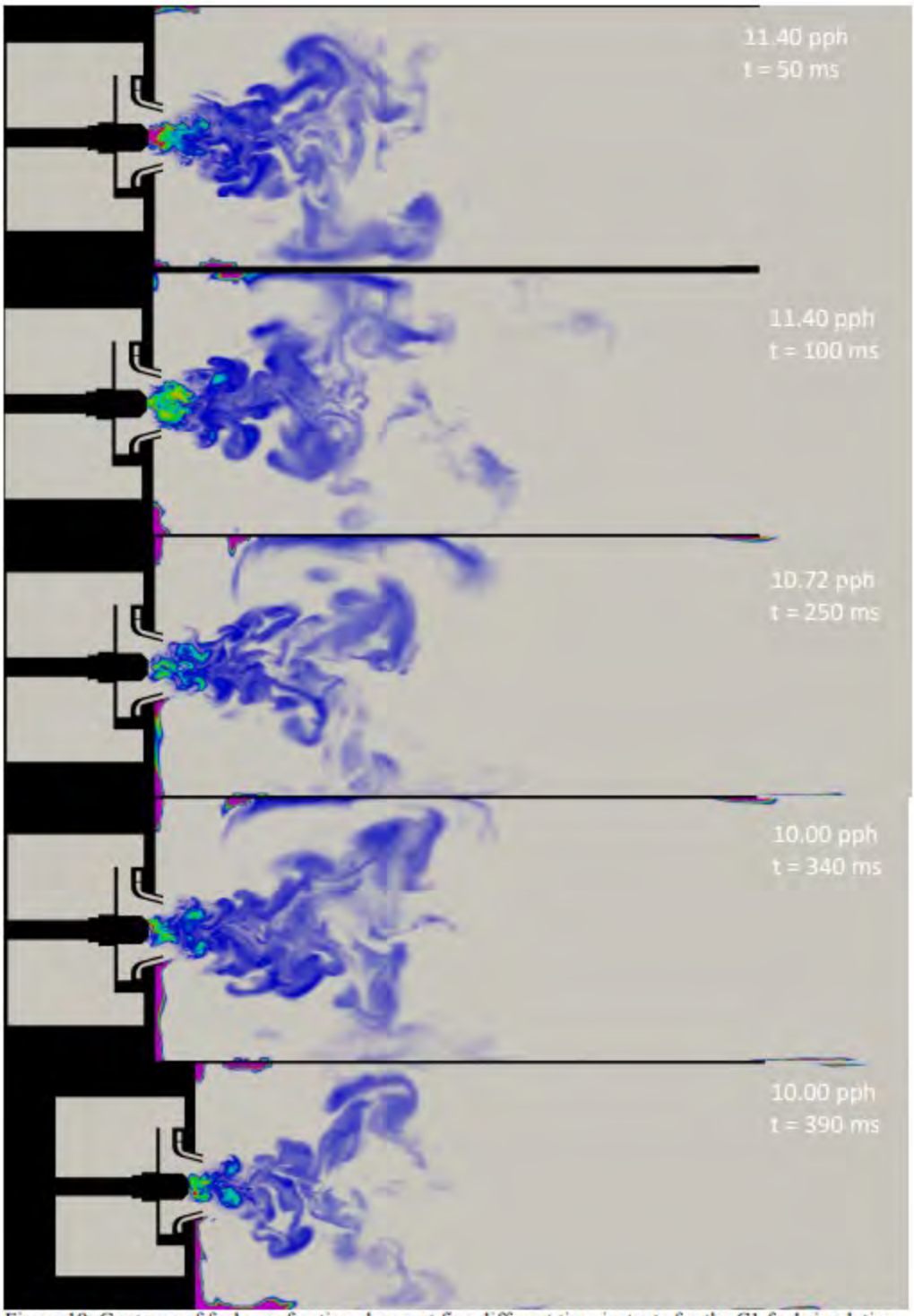

Figure 19: Contours of fuel mas fraction shown at five different time instants for the C1 fuel simulation

Conclusions

A Large Eddy Simulation-based analysis of the high shear rig combustor that was experimentally studied at Georgia Institute of Technology was performed in this study. The objective of this effort is to develop, enhance and apply computational fluid dynamics-based models to simulate stable combustion and lean blowout behavior in a high shear rig combustor. The goal is to understand if the models can predict the dependence of lean blowout phenomena on the physical and chemical properties of the alternative jet fuels. Several sub-models for unsteady flow simulation, spray injection boundary conditions, spray evaporation models, wall heat flux boundary conditions and turbulent combustion models are required to correctly simulate the physical processes. In this report we presented a description of different sub models, along with validation or verification where possible. Upon completion of the reacting LES for the two fuels at near blo out but stable condition, simulations of the lean blowout were performed by instantaneously reducing the fuel flow rate in steps of 6% for three different values of fuel-flow rates. Each flow rate was held constant for 100 mill-seconds for the combustor to respond to the flow rate change and stabilize at the new condition. Overall, the two fuels show differences in evaporation rate and also commensurate differences in heat release rates. Both of the simulations show reduction in heat release rate as the flow rate is reduced but C1 seems to be dropping faster, relatively compared to A2. C1 fuels also shows increase evaporation rates compared to A2, however this leads to quick build of fuel vapor in a concentrated region and if the flow conditions in that region is not conducive in terms of residence time to complete the reaction, it contributes to even more accumulation of fuel vapor from the incomplete combustion. In the case of C1 fuel, this is hypothesized to be the mechanism for earlier flame blow out compared to the A2 fuel. Long combustor dimension coupled with very small time steps to resolve the flame structure, leads to excessive computational time at each flow rate for the combustion to reach a quasi-steady state. As a result, it was not possible to reduce the flow-rate all the way to the lean blow out value to demonstrate the lean blow out behavior. However, the qualitative trend observed from the three simulate fuel flow rate conditions seems to indicate that the models employed in this study have the ability to discriminate between the different fuel physical properties and its impact on the lean blow out behavior.

Major Accomplishments

Simulation of multiple fuels for the swirler and nozzle configuration at Georgia Tech

Task 8 - Ignition and LBO Testing of Conventional and Alternative Jet Fuels

University of Dayton Research Institute

Research Approach

A. *Atmospheric Cold Start*

A study of atmospheric cold start ignition was completed for nine NJFCP fuels in the Referee Combustor Rig. The conditions for the study near atmospheric pressure, in the combustor, and fuel and air temperatures ranging from 239K to 258K (-30 to +5 ℉) with a pressure drop across the dome of 2 or 3.5%. For all of the experiments, the fuel temperature was controlled to match the air temperature.

The controlled cooling of the fuel and air temperatures was accomplished using a system designed around two recirculating fluid process chillers and five heat exchangers. A schematic and image of the cooling system are shown in Figure 1. The air is cooled in two stages, via four heat exchangers, with the heat transfer fluid supplied from two different chillers. To achieve air temperatures of -30 ℉, the air first passes through two parallel heat exchangers to cool the air down to -10 ℉. The air then flows through a second stage of heat exchangers, also arranged in parallel, cooled by the fluid circulated by a second chiller, to finish the cooling process and supply air at target temperature at the combustor. Control of the air temperature was accomplished by PID control of the temperature from both chillers and by controlling the fraction of coolant from the lower temperature chiller that was supplied to the air heat exchangers.

For all of the ignition experiments, the igniter current and voltage were measured and computed a delivered energy (to the igniter plug). The measurements of the spark energy provided a check on the consistency of the delivered energy for each spark as well as an early detector of excessive igniter plug erosion. The combustor pressure before ignition for the cold experiments was approximately 1 atm and the fuel and air were controlled to the same temperature ($T_{air} = T_{fuel}$ = -30 ℉ or 5 ℉). For each combination of fuel type and flow conditions (ΔP, P_{cmb}, T_{air}, T_{fuel}) at least five volume flow rates were selected which resulted in between high and low ignition probabilities, at each fuel flow rate there were ten ignition attempts which consisted

up to 40 sparks occurring at a frequency of ~3.5 Hz. After a successful ignition attempt was confirmed by video of the combustor, the spark sequence was stopped, and the fuel flow was stopped to end the ignition attempt. If ignition did not occur with 40 sparks the ignition attempt was halted for safety to avoid filling the downstream rig exhaust with large quantities of unlit fuel.

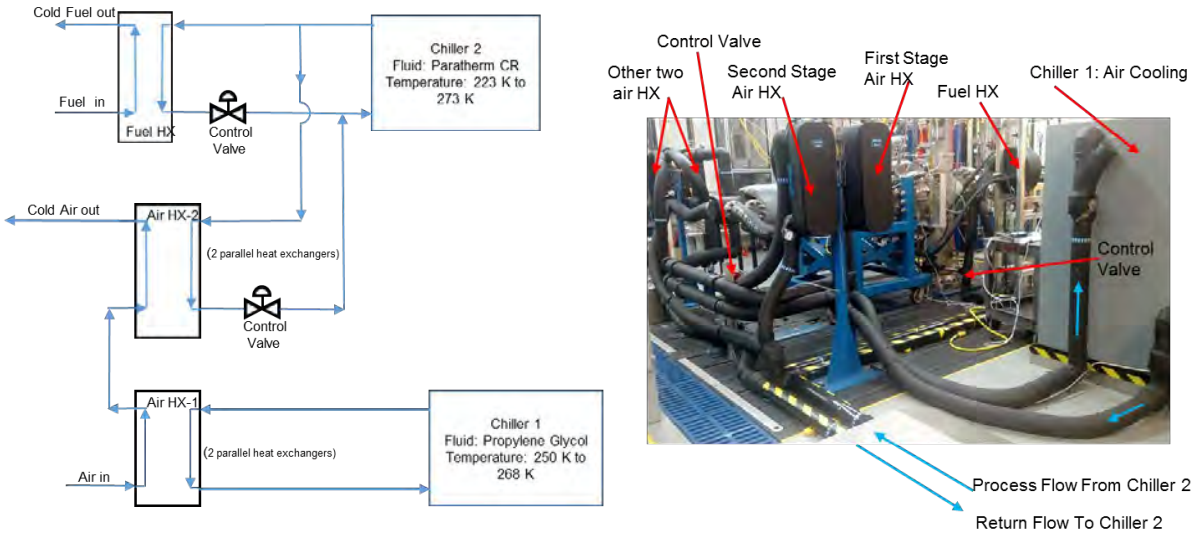

Figure 1. Schematic and Image of the Air and Fuel Cooling System

Each individual spark resulted in either a successful ignition, determined by spreading of the visible flame upstream of the spark ignitor and across the combustor, or an ignition failure. The successful ignition was determined from the photodiode traces as a continuous elevated signal above the threshold extending in time past the next spark. Figure 2 shows a bar chart for each set of combustor conditions noting the number of successful and unsuccessful sparks for each fuel. A total of 23,548 sparks were attempted, resulting in 1438 successful ignitions.

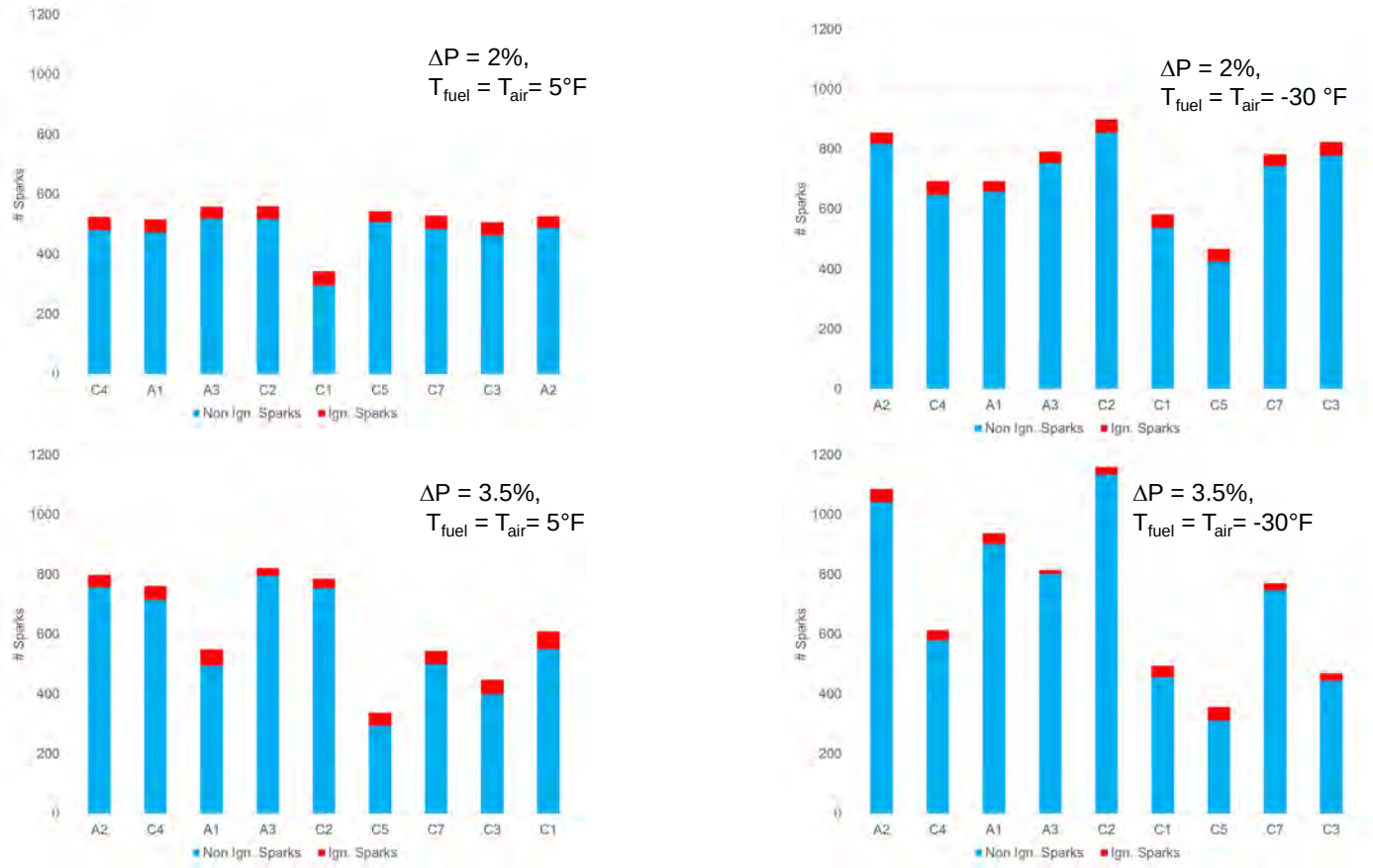

Figure 2. Summary of Sparks Resulting in Ignition and Non-Ignition for the Atmospheric Ignition Experiment. 23548 Sparks total, 1438 Successful Ignitions

The results from each spark were used to calculate ignition probabilities, with the sparks counted using the photodiode and characterized as either a 1 for ignition or a 0 for non-ignition. At low values of equivalence ratio the probability of ignition is essentially zero, whereas at higher equivalence ratios the probability approaches one. In between these two extremes there is a region where the successful and non-successful ignition results overlap. Binomial logistic regression was used with the logistic function to reduce the 0's and 1's into a probability curve vs the equivalence ratio.

Ignition probability curves are plotted in Figure 3 and Figure 4 for 3.5% ΔP cases. The data is shown as a regression line for each case and fuel plotted up to the maximum equivalence ratio ϕ tested. Each curve increases in ignition probability as ϕ increases. For all fuels and pressure drop conditions, raising the temperature increased the ignition probability at a given ϕ. The rankings of the ignition performance for all of the fuels remained consistent as the imposed external conditions (T_{fuel}, T_{air} and ΔP) changed, with the only exception being the performance of C1 and A1 relative to each other.

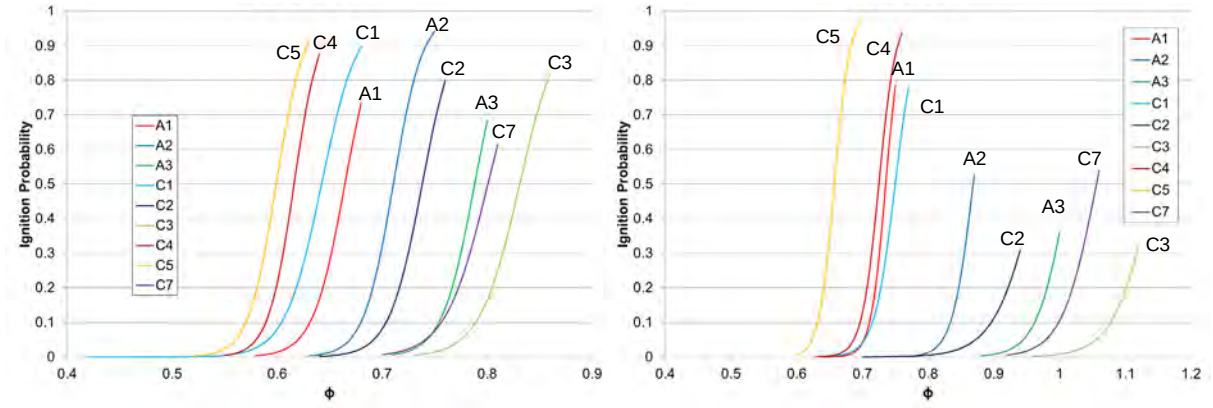

(a) (b)

Figure 3. Ignition Probability vs ϕ for cases with ΔP = 2%, Pcomb = 1 atm. (a) $T_{air} = T_{fuel}$ = 5˚F, (b) Tair = T_{fuel} = -30˚F

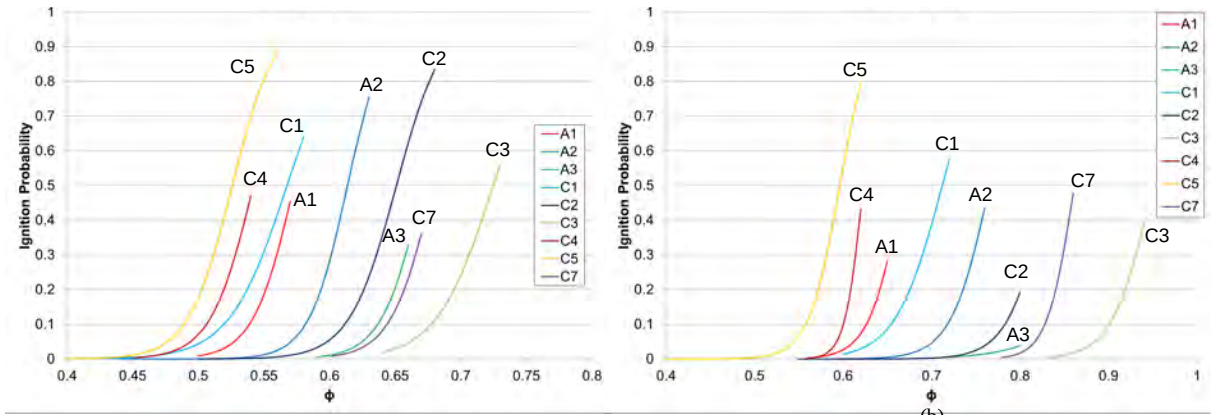

(a) (b)

Figure 4. Ignition Probability vs ϕ for cases with ΔP = 3.5%, P_{comb} = 1 atm. (a) $T_{air} = T_{fuel}$ = 5˚F, (b) $T_{air} = T_{fuel}$ = -30˚F

The effect of the physical properties on the ignition performance of the fuels was considered and partial results are shown in Figure 5 - Figure 7. Strong correlations are shown with the atomization, surface tension, & viscosity, and distillation properties (T10, and T 20). Further efforts are underway to better understand the relationship to of ignition to properties through advanced regression analysis. Further details from the cold start ignition experiments were presented at the AIAA SCITECH conference [1].

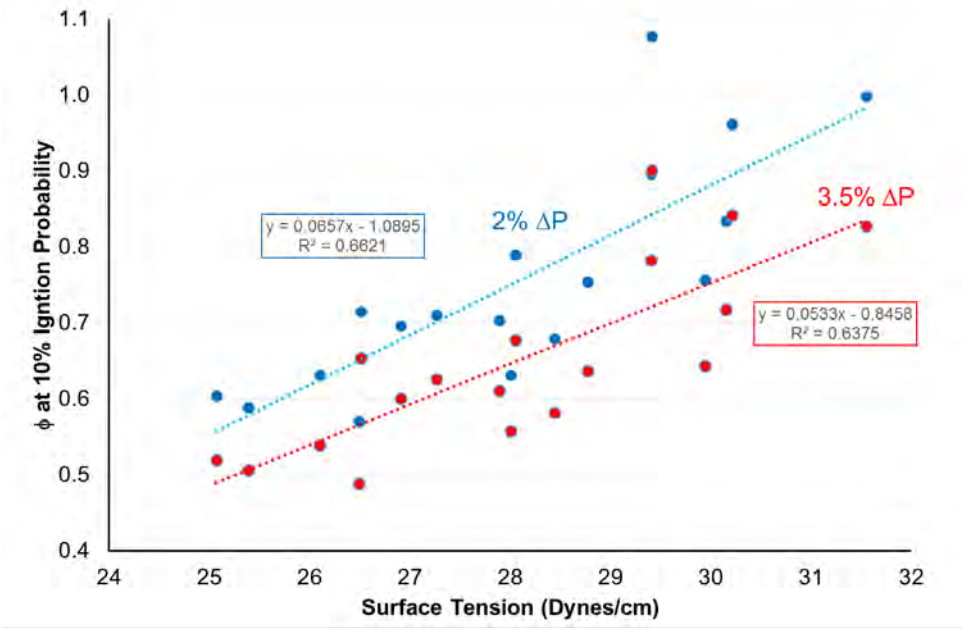

Figure 5. Equivalence Ratio at 10% probability vs Surface Tension for Atmospheric Cold Start Tests

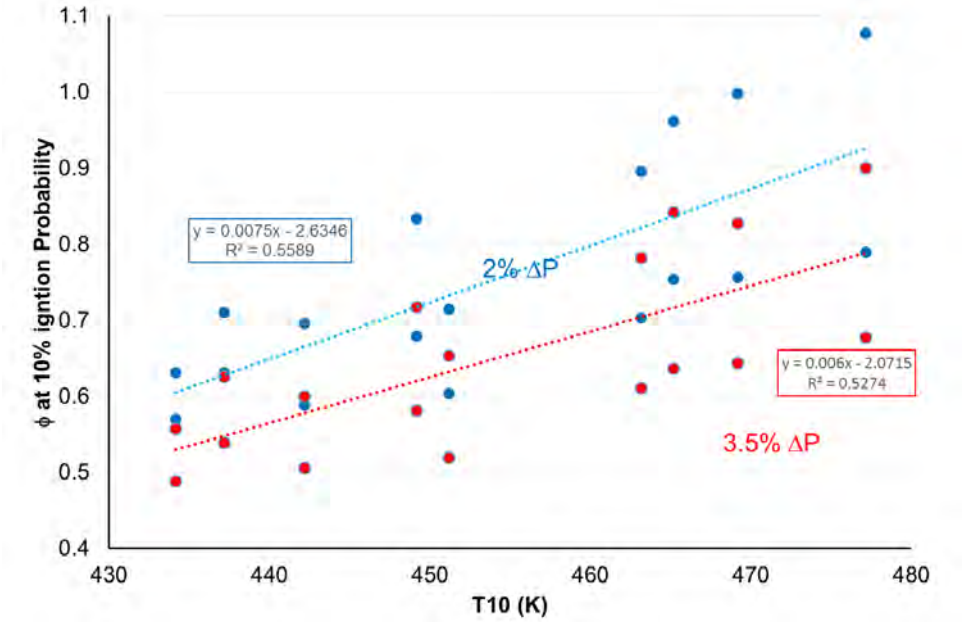

Figure 6. Equivalence Ratio at 10% probability vs T10 for Atmospheric Cold Start Tests

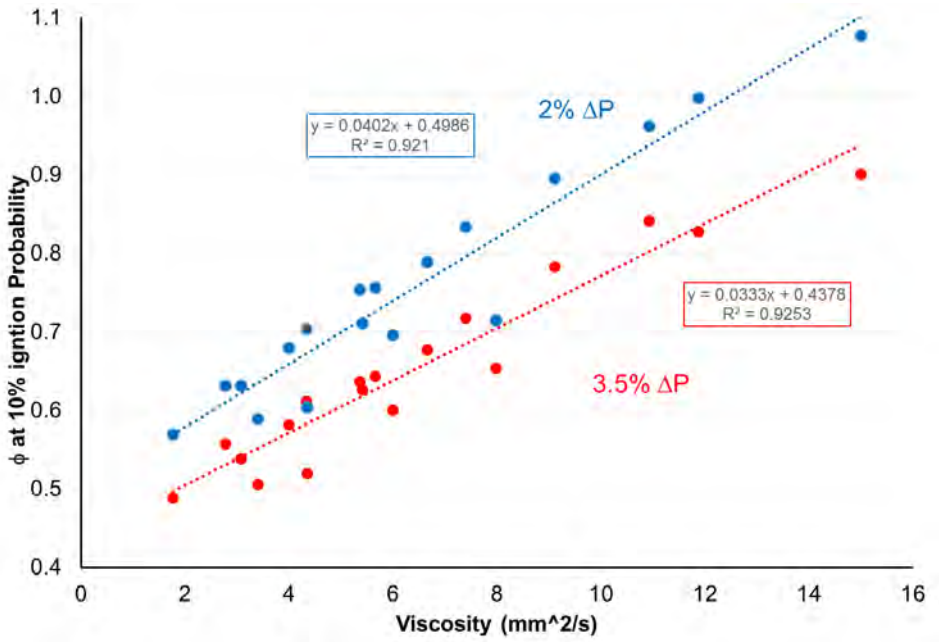

Figure 7. Equivalence Ratio at 10% probability vs Viscosity for Atmospheric Cold Start Tests

B. Cold Lean Blowout Experiments

Lean Blowout data was also obtained from form a subset of the tests cold start tests. The conditions represented during the LBO are not strictly conditions that show up in operation of the normal operation but represent a stressed, low pressure, low temperature condition. The motivation for this test came from the OEM committee involved with the project, with the rationale of "as long as we are lighting the combustor we may as well get data during blowout."

Several practical testing issues made these tests challenging and time consuming. The normal LBO experiments, conducted previously at high temperatures and pressures, were conducted over a time period of ~5 minutes per LBO attempt, and the hardware downstream of the combustor was water-cooled. The cold flow experiments precluded the use of water cooling because of the difficulties of using water as a coolant at air temperatures 25 to 65 ℉ below the freezing temperature of the water. Therefore, the experimental method used was a quick LBO approach in which the ramp rate was greatly increased to allow LBO to occur within 20 seconds of light off and rely on heat sink to cool the rig. This compromise approach worked, but required an additional 7-10 minutes, with the internal flow of cold air to cool the combustor back down to the baseline temperature, between ignition attempts.

Results for the cold LBO experiments taken at combustor pressures of ~1 atm are shown in Figure 8 along with previous results at 2 atm and T_{air} =250˚F. It can be seen that the decrease in temperature decreases the magnitude of the phi at LBO. Previous results for LBO at high temperatures showed that the LBO results correlated strongly with Derived Cetane Number (DCN) and showed little correlation with atomization and evaporation parameters (Density, surface tension, viscosity) implying that the chemistry is important for LBO at normal conditions seen during LBO. For the cold LBO tests the opposite was observed. DCN showed little correlation to the LBO results and the LBO correlated best with viscosity and T50. Linear correlations of the LBO ϕ normalized by the LBO ϕ for A2 with viscosity and T50 are shown in Figure 9.

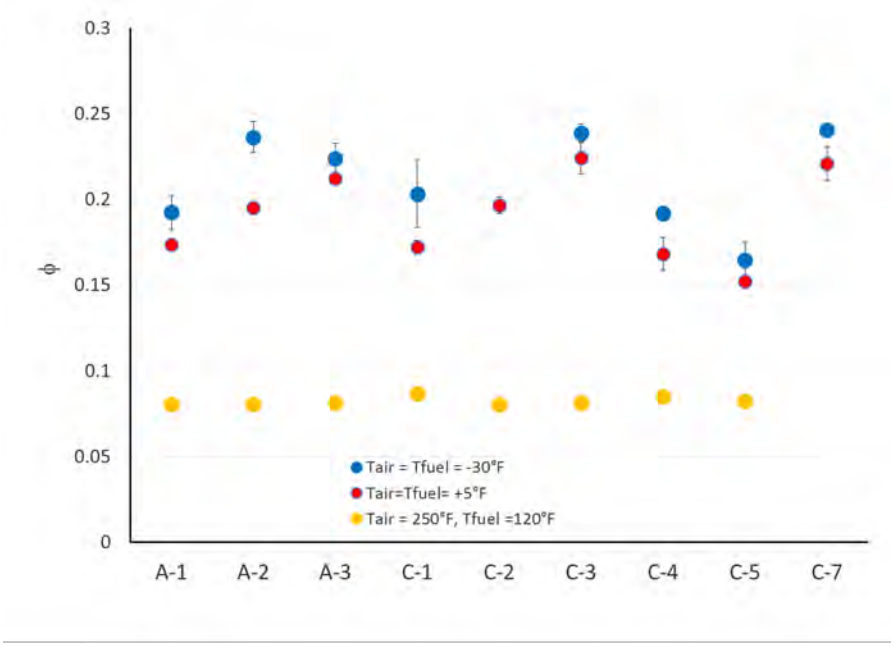

Figure 8. ϕ at LBO for Hot and Cold Experiments

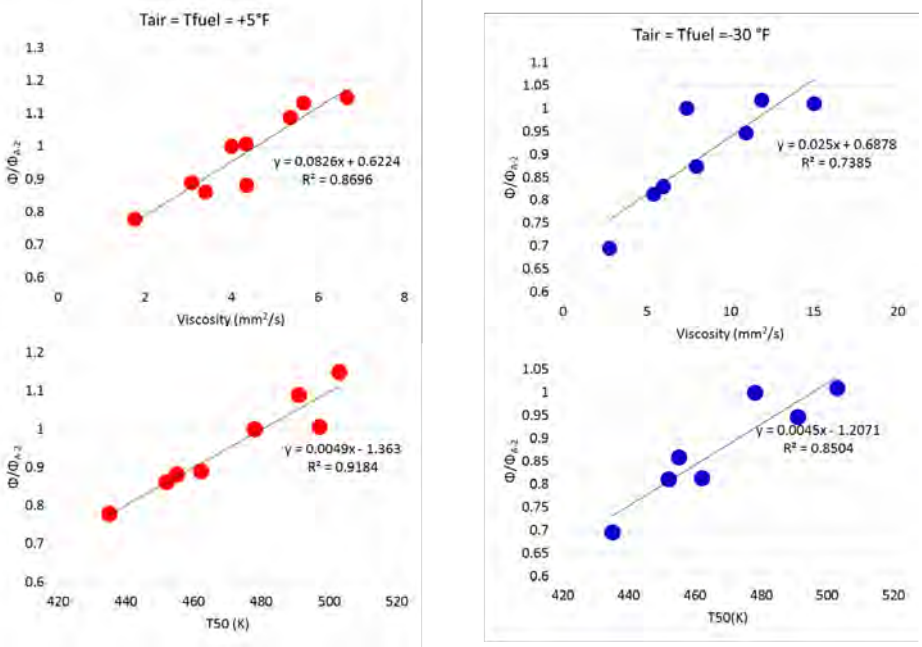

Figure 9. LBO Equivalence Ratio Relative to the LBO Equivalence Ratio for the Baseline A2 Fuel plotted vs T50 and Viscosity

C. Configuration for High Altitude Relight

The Referee Rig was modified in the past year to facilitate high altitude relight experiments. The ability to conduct altitude relight experiments at sub-atmospheric pressures was added to the facility by the addition of an air ejector and associated subsystems to the rig. The ejector was installed in the downstream side of the rig as shown in Figure 10. The control of the combustor back pressure for ignition experiment was set by maintaining a steady pressure at the ejector motive flow port. The pressure within the combustor was then controlled control valves to bleed room air at atmospheric pressure into the duct upstream of the suction port of the ejector. The hazard of unburnt fuel downstream of the combustor was eliminated

by sucking fuel through several ports on the exhaust stack, while the pressure on the exhaust was temporarily increased by stalling the ejector with air from additional ball valves.

In general, the altitude relight experiments required much more effort and time than the atmospheric cold start due to the low mass fuel mass flows which led to excessive heat gain between ignition attempts. Most of the sub-atmospheric experiments were conducted at a temperature of -30 ℉ and a combustor pressure of 5.45 psia (0.37 atm) which corresponds to the pressure at 25,000 ft. Initial experiments attempted to use the same nozzle that was used for the atmospheric experiments, however it was not possible to ignite either A2 or C5 fuel at the desired conditions at equivalence ratios up to 1.3. It should be noted that the low air flow rates at high altitude resulted in low fuel flows which, in turn, resulted in low fuel pressures resulting in poor atomization. After the initial experiments with the larger flow number nozzle, a small flow number nozzle, was selected for the rest of the studies. With the low flow number (higher pressure drop) nozzle it was possible to ignite all of the fuels at the imposed temperatures and air flow rates.

Figure 11 shows a bar chart of the sub atmospheric ignition experiments over 5880 sparks leading to 456 successful ignitions. Figure 12 shows the regression curves reduced from all of the data points for the altitude relight experiments. The rankings of the fuels were similar to those at atmospheric pressure, shown in Figure 3a above, with the same fuel and air temperature (-30 ℉) with the exception of C5 and C1. At atmospheric pressures the C1 performed better than the A1 and A2, however, for the altitude case the C1 was shifted to the right (worse performance) of the A2 fuel. The C5 fuel which was the easiest to light under all conditions explored in the atmospheric cold start experiments exhibited odd ignition characteristics. At altitude C5 was the easiest to light at low ignition probabilities. However, the ignition probability curve for C5 crossed that for the other fuels leading to lower performance (higher ignition ϕ) at higher ignition probabilities. In addition, the confidence intervals for the C5 fuel were much wider than the other fuels. The reasons for these differences is under examination.

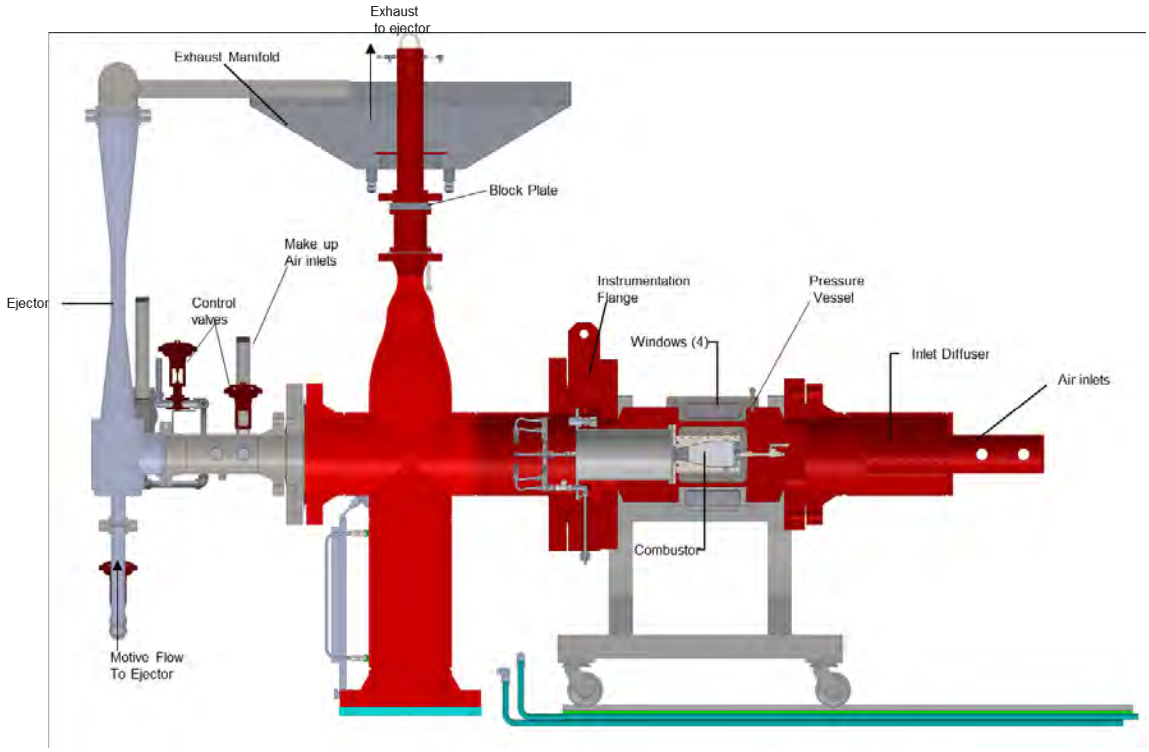

Figure 10. Referee Rig Configured for High Altitude Relight Studies

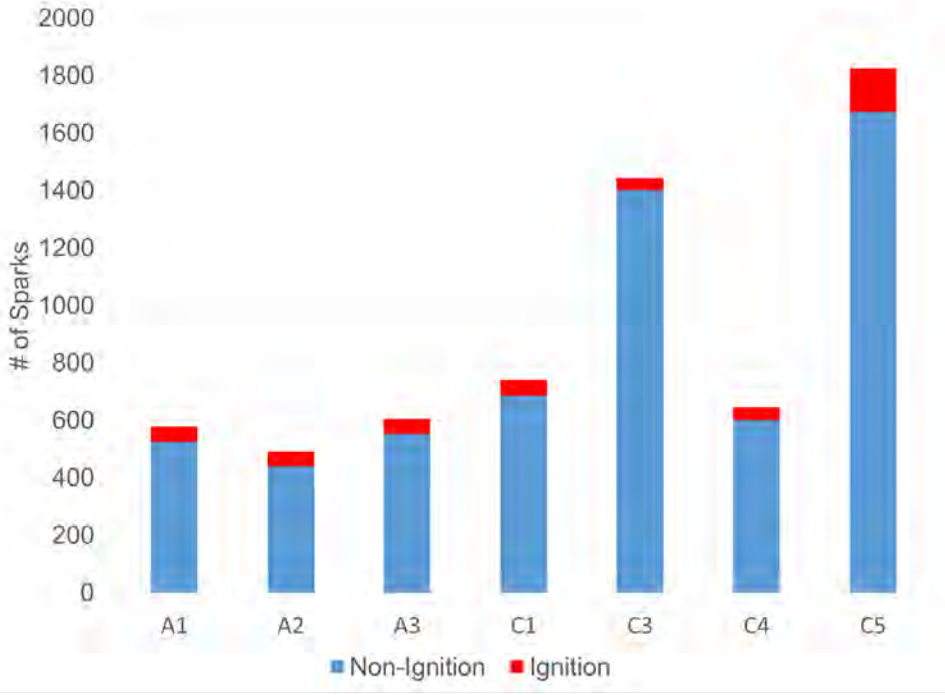

Figure 11. Summary of Sparks Resulting in Ignition and Non-Ignition for the High Altitude Ignition Experiment. 5881 Sparks total, 456 Successful Ignitions

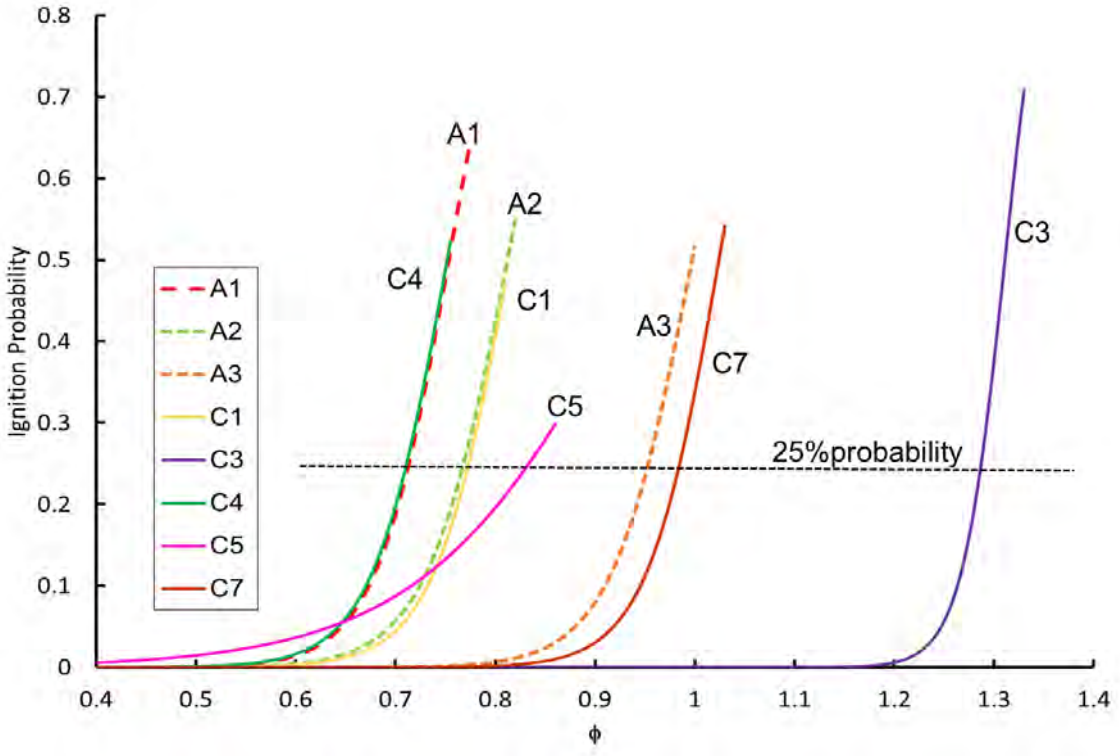

Figure 12. Ignition Probability Curves for Pcmb =5.45 psi, ΔP = 2%, T = -30°F.

The effect of the various physical properties verses the equivalence ratio at 25% ignition probability is examined in Figure 13 - Figure 14. The best correlations were found with the viscosity and the distillation properties. The ignition performance showed poor correlation with DCN and vapor pressure. It was noted that the C3 fuel, which had the lowest viscosity, showed high sensitivity to temperature change. Figure 15 shows the ignition probability at different fuel and air temperatures for C3 fuel. The viscosity curve for the C3 is also plotted. The results were obtained by 10 separate ignition attempts of up to 40 sparks at each temperature. The results show a large drop in ignition performance between -18 and -30 ℉. This range is also the range in which the viscosity exceeds 12 cSt.

After noting that fuel viscosity seemed to be a major driver of ignition performance, an experiment was conducted to determine if three fuels of the same viscosity (created by heating the more viscous fuels to higher temperatures) would have the same ignition performance. Figure 16 shows the results for C1 at -30 ℉, A3 at -16 ℉ and C3 at 4 ℉. For reference, the 25% probability line is shown along with the crossing points marked by x's. It can be seen that increasing the temperature shifted the curves for the C3 and A3 to the left (improved performance) however, the effect was not enough to overlap the curves showing that the viscosity, while important, is not the only driver of ignition performance.

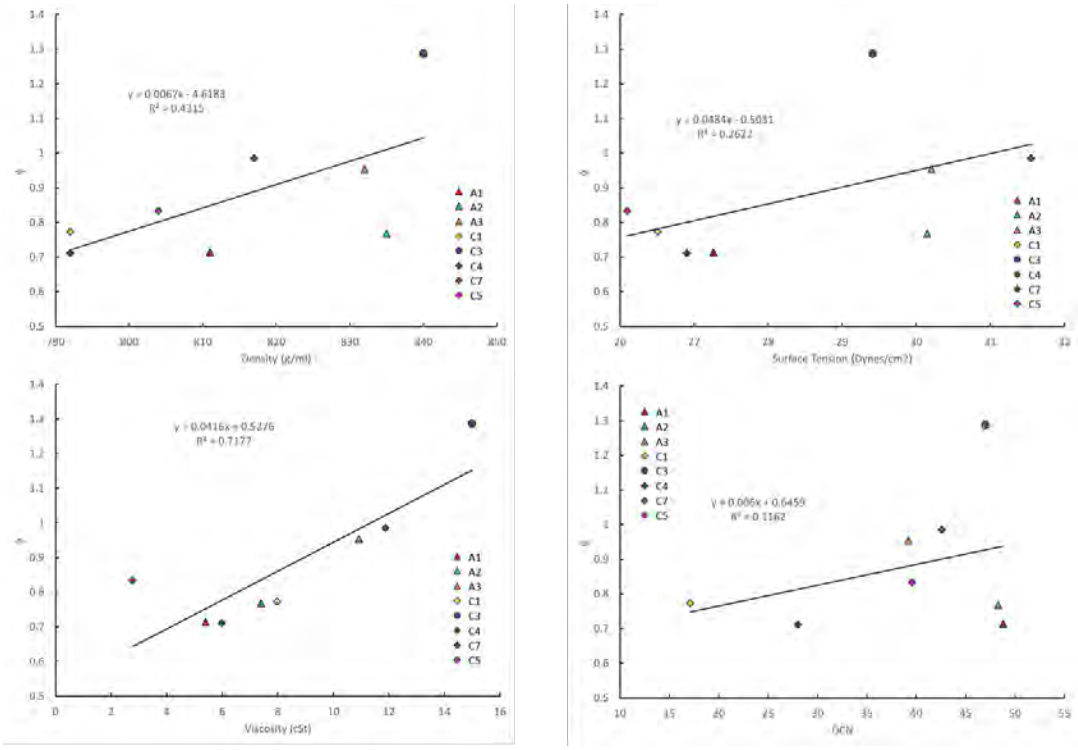

Figure 13. ϕ at 25% ignition Probability vs Atomization and Chemical Properties

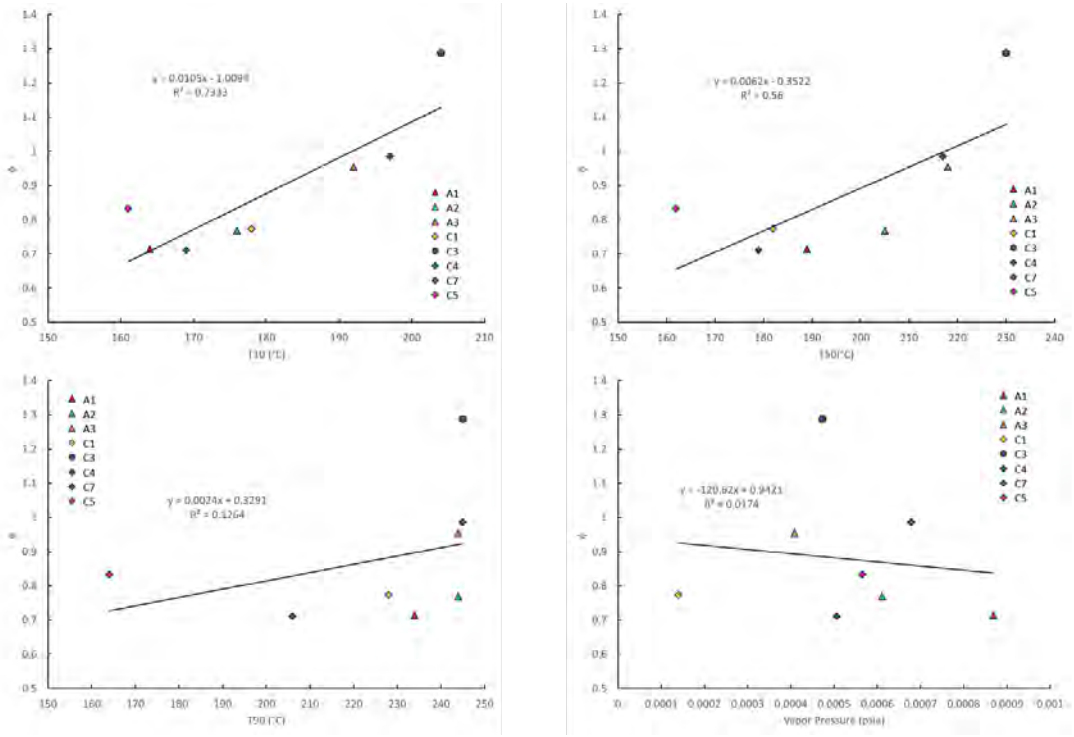

Figure 14. ϕ at 25% ignition Probability vs Atomization Properties

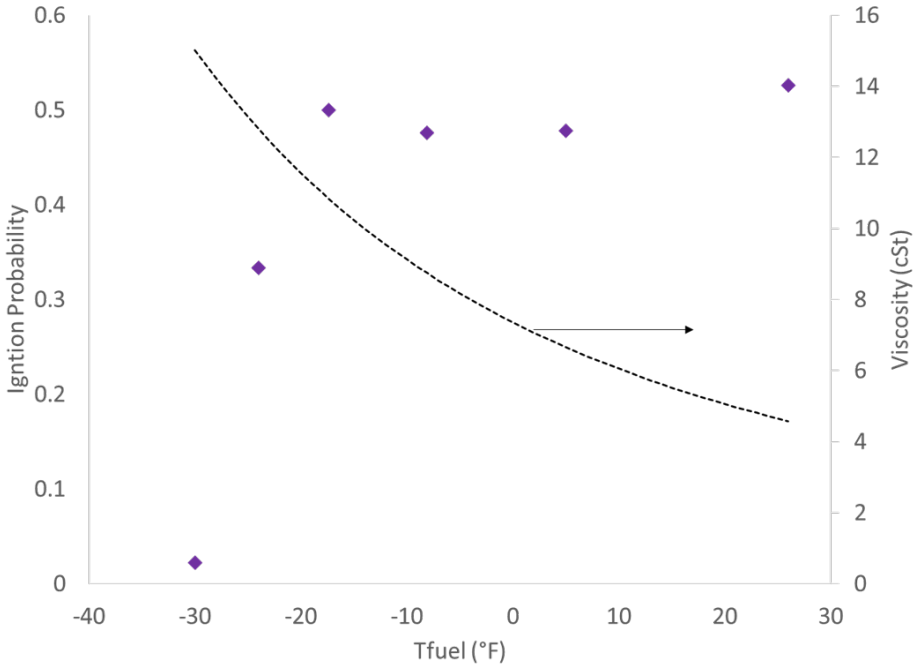

Figure 15. Ignition probability of C3 at Various Fuel and Air Temperatures ΔP =2%, Pcmb=5.45 psia.

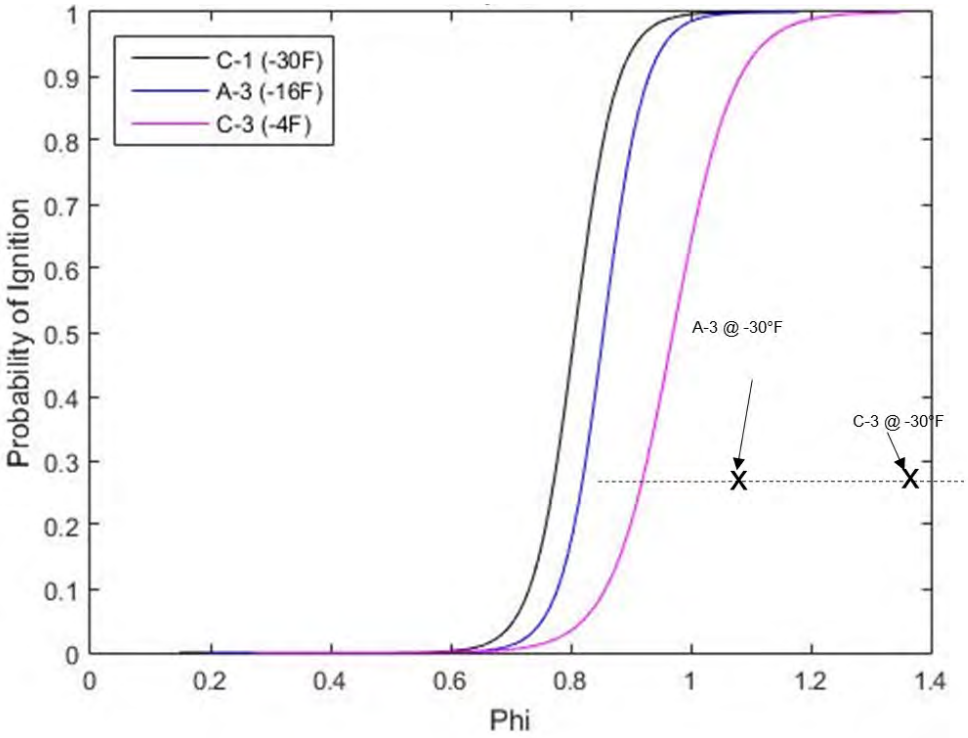

Figure 16. Ignition Probability Curves for Three Fuels at the Same Viscosity

The results from these experiments are under further analysis and will be presented at an upcoming AIAA meeting [2].

References

[1] T. H. Hendershott, S. Stouffer, J. R. Monfort, J. Diemer, K. Busby, E. Corporan, P. Wrzesinski and A. W. Caswell, "Ignition of Conventional and Alternative Fuel at Low Temperatures in a Single-Cup Swirl-Stabilized Combustor," in *2018 AIAA Aerospace Sciences Meeting*, 2018.

[2] Stouffer, S.D., Hendershott, Colborn, J.T.H.,Monfort, J.R., Corporan, E., Wrzesinski, P., Caswell, A.W., "Altitude Relight Performance of Conventional and Alternative Fuels", paper under preparation to be presented at SCITECH 2019, Jan 2019

Milestone(s)

The generation of cumulative distribution functions for the various conventional and alternative jet fuels in the Referee Rig at cold conditions for ignition.

Major Accomplishments

Demonstrating significant fuel sensitivity in ignition probability for various fuels.

Outreach Efforts

Presentation and poster at 2018 ASCENT Spring and Fall meetings.

Student Involvement

Jennifer Colborn, Undergraduate Research Assistant.

Task 9 - Development of Operability Surrogate Fuels

University of Dayton

Objective

The objective was the development of surrogate fuels for operability testing.

Research Approach

Introduction

Increases in global ambient temperature and mean sea level have had negative effects on marine ecosystems, fish productivity, agriculture, and the human population on coastal zones. These factors, paired with the increase in natural disasters, have led to increased volatility of the environment indicative of climate change due to anthropogenic carbon emissions (Neumann et al., 2015). The reduction of these carbon emissions has great potential in the transportation sector, where aviation contributes approximately 9% of these emissions (Office of Transportation and Air Quality, 2019). Commercial aviation must significantly reduce its greenhouse gas (GHG) impact to continue to support global mobility and commerce as NASA is predicting a 2-fold increase in passenger flights in the next decade (NASA, 2018). Through the ICAO, the commercial aviation industry has adopted and defined a method to reduce the global environmental impact of air travel through CORSIA, which sets the voluntary standards to reduce carbon emissions during Phase 1 (through 2026) and mandatory standards during Phase 2 (2027 and beyond) (IATA, 2018). By the year 2050, under a CORSIA-type domestic emission policy, the demand for SAF will need to increase to more than 10% of total jet fuel consumption (Chao et al., 2019).

Any commercial deployment of SAF relies on the approval and evaluation of the fuel via ASTM D4054. This specification ensures the safe usage, fungibility, performance, and compatibility of the SAF under standard usage and severe operability conditions. Specifically, Tier 3 engine operability tests focus on fuel effects under the so-called FOM limit phenomena; namely, LBO, high-altitude relight, and cold-start ignition (Lefebvre, 1983; Rock et al., 2019; Stachler et al., 2017). Because of the broad range of potential physical and chemical properties of a new SAF, extensive combustor testing is typically needed to eclipse uncertainty and ensure safety for FOM operability issues. Estimations for the direct testing for a candidate SAF in cost and volume are said to be in the range of $5 million and 28,000 to 115,000 gallons (Ruzimen, 2018). This estimate does not include overhead costs for all parties involved in the process or the cost of supplying large quantities of potentially expensive test fuel (Colket et al., 2017). Because of the nature of this costly and volume-intensive testing process, the NJFCP's mission is to streamline the SAF approval process and, in turn, reduce the carbon intensity of aviation transportation by ensuring a broad and diverse portfolio of SAF fuels, feedstock, and processing technologies (Colket et al., 2017; Heyne et al., 2017; Heyne et al., 2018).

Recent work on LBO of SAFs in four combustor rigs showed that DCN is the most significant feature importance using RFRA in both the Referee Rig and TJSR, and the second most significant feature importance in the Sheffield rig (Peiffer & Heyne, n.d.; Peiffer et al., n.d.). These three rigs show dominance of chemical timescales near LBO, where chemical timescales are a function of the fuel's chemical properties and accompanying thermodynamic conditions. However, experiments using the Honeywell APU show no sign of DCN affecting LBO (Peiffer et al., 2019). Lack of a swirler and presence of a small pressure atomizer attribute to this difference and enhance the dominance of evaporative timescales near LBO, where evaporative timescales are a function of fuel physical properties and distillate properties.

Recent efforts into gas turbine combustor ignition and the relative impact of spray and volatile fuel properties indicate that the down-selected properties of viscosity, density, surface tension, vapor pressure, and specific heat capacity nearly capture the variance in ignition probability (Opacich et al., 2019). Ignition probability, a metric to determine successful ignitions, is used in gas turbine combustion where turbulence and stochasticity exist. Furthermore, viscosity, density, and surface tension have a larger impact than vapor pressure and specific heat capacity on ignition behavior for both the Referee Rig and Honeywell APU (Opacich et al., 2019). At higher fuel temperatures, surface tension is the most important property to predict relative ignitability in the Honeywell APU. The current certification process for SAF via ASTM D4054 has no specification limit for surface tension. However, surface tension is strongly and positively correlated with density, and there is a specification limit for density in all Category A fuels (Heyne et al., 2017; Heyne et al., 2018).

Historically, surrogates have been used for the manipulation or prescription of fuel properties to mimic the properties of target fuels. Surrogates have been used to mimic autoignition, ignition delay, extinction strain rate, and emissions. The usage of surrogate formulation to understand combustion phenomenon has been explored by Dooley et al. (2010) and Kim et al. (2014; 2017). Dooley *et al.* outlined a method for fuel-specific surrogate formulation through empirical correlation.

The surrogates were designed to emulate chemical kinetic behavior of a target real fuel. Kim *et al.* developed two surrogates with empirical correlations to emulate chemical and physical properties that affect spray and ignition within the diesel combustion process. While these surrogate studies have transformed, confirmed, and in some cases transcended fundamental understandings, combustion theory and SAF approvals could benefit from the manipulation, instead of mimicking, of properties to illustrate complex physical competitions between properties at limit points; namely, LBO and ignition.

This work combines the work of Bell et al. (2017) with recent surface tension and NJFCP reference fuels to report fuels with orthogonal spray break-up properties to illuminate these spray break-up physics via scalable surrogates, which can stress limit theory and competitions between density, surface tension, and viscosity. Here, we report a method and specific orthogonal surrogate compositions on an *N*-dimensional Pareto front concerning the total property space. These compositions and properties represent a near-maximum variance that can be associated with hydrocarbon molecules in the jet fuel distillation range. No previous works have reported results of comparable fuel properties, number of fuels, and the broader implication of their results at once. Moreover, we report the maximum variance in key properties relative to the subset of fuels used here. This fuel property variance, in turn, facilitates both practical and theoretical efforts. Practically, experimental results can illustrate the maximum FOM sensitivity, aiding in the prescreening and formal evaluation of novel SAFs (Colket et al., 2017; Peiffer et al., 2019; Raun, 2019). Theoretically, tests of these fuels can be used to confirm or reject hypotheses regarding the competition of spray break-up, fluid dynamics, chemistry, and heat-mass transfer, elevating both theory and computational fluid dynamics validation test data.

Materials and methods

Materials

Thirteen fuels were used as the basis for maximizing fuel property variance. Three conventional, or Category A, fuels representing a "best" (A-1, POSF 10264), "average" (A-2, POSF 10325), and "worst" (A-3, POSF 10289) were used. Ten fuels composed of blends or neat alternative fuels were available with the relevant properties under the desired condition. The fuels utilized here were the basis of the NJFCP to investigate a wide range of chemical and physical fuel characteristics. Edwards (2013; Edwards et al., 2017) contains explanations of the specified reference fuels. Table S1 of the supplemental information contains property information about the fuels. In Figure 7, a plot presents the fuels used in this work with normalized key properties, revealing the variance of these properties among these neat blend components.

Blending rule

The blending rules used to predict the properties of the optimized SAF blends were molecular weight (MW), atomic hydrogen-to-carbon ratio (H/C), DCN, density (ρ) at −30°C, kinematic viscosity (μ) at −30°C, distillation curve (T10, T50, T90), and surface tension (σ) at −30°C. Blending rules were incorporated from the efforts of Bell et al. (2017) from the general surrogate calculator. Validation methods were additionally performed in the work of Bell et al. to ensure proper usage (Bell et al., 2017). However, a surface tension blending rule was seldom considered and never included in the surrogate calculator. Therefore, for this effort, a surface tension blending rule will be integrated into the surrogate calculator.

Surface tension

The surface tension of the fuel blends was calculated using the Macleod-Sugden correlation as indicated in Equation (1) (Poling et al., 2000). In the equation, σ_m is the surface tension of the mixture, where ρ_{Lm} and ρ_{Vm} are the liquid and vapor mixture density, respectively. $[P_{Lm}]$ and $[P_{Vm}]$ are the parachor of the liquid and vapor mixture. At low pressures, the term P_{Vm} involving vapor density could be neglected (Poling et al., 2000). For this study, all jet fuels were blended at ambient conditions; thus, P_{Vm} is neglected. With this simplification to Equation (1), the equation can be rewritten as shown in Equation (2). Equations (3) and (4) are used to calculate the parachor of the liquid. $[P_{ij}]$ is the parachor of the mixture, where $[P_i]$ and $[P_j]$ are the parachor of pure component *i* and *j*. λ_{ij} is the binary interaction coefficient determined from experimental data; in the absence of experimental data, λ_{ij} could be set to be 1.

$$\sigma_m = \left[[P_{Lm}]\rho_{Lm} - [P_{Vm}]\rho_{Vm}\right]^n \quad (1)$$

$$\sigma_m = \left[[P_{Lm}]\rho_{Lm}\right]^n \quad (2)$$

$$[P_{Lm}] = \sum_i \sum_j x_i x_j [P_{ij}] \quad (3)$$

$$[P_{ij}] = \lambda_{ij} \frac{[P_i] + [P_j]}{2} \quad (4)$$

When *n* in Equation (2) is set to 4, the equation can be reduced to the Weinaug-Katz equation (Weinaug & Katz, 1943). In this study, λ_{ij} in Equation (4) is given a value of one with supporting experimental material provided in the Figure 8. Although previous application of this blending rule were used for pure component mixing, here it was used for complex jet fuels mixtures with supporting material provided in Figure 8.

Jet fuel blend optimizer

The Bell *et al.* general surrogate calculator (Bell et al., 2017) is shown to be effective with the current blending methods, where it only minimizes overall error rather than reducing the error of each property relative to their targets individually. The jet fuel blend optimizer (JudO) can optimize user-defined properties at an *N*-dimensional scale. The goal of this optimization is to keep other user-specified properties constant and stress certain properties to create orthogonal surrogate fuels. Blending rules are integrated into objective functions to achieve desired property values.

Figure 9 presents a schematic of the optimization approach, which is based on the framework of JudO (Kosir et al., 2019; Flora et al., 2018). JudO uses mole fractions of the fuel set as inputs to the optimization. All initial guesses are randomly generated, where each fuel has a chance to be assigned a value for mole fractions between 0 and 1. This strategy aids in the optimization technique to investigate a wide range of potential compositions with accompanying potential local minima, rendering a "unbiased" optimization final solution.

Once the initial guess is determined, a Mixed Integer Distributed Ant Colony Optimization (MIDACO) solver (Schlueter et al., 2013) will start to optimize the mole fractions based on the given random initial guess with supplied objective and constraint functions. The objective functions were evaluated on the l^2 norm and normalized to A-2 values. MIDACO is a commercially available numerical high-performance solver that uses ant colony optimization with multiple objective functions to obtain a near-global optimum solution. An advantage to using this solver is the derivative-free, evolutionary hybrid algorithm that treats the objective and constraint functions as a "black-box which may contain critical function properties like non-linearity, non-convexity, discontinuities or even stochastic noise" solver (Schlueter et al., 2013).

When the optimization is complete with the supplied compositions, functions, and thus, fuel mixture properties, JudO will output possible best mole fractions, enabling a Pareto solution. Those possible best solutions are then compiled to form the cumulative Pareto front, which is a combination of all the solutions obtained from the initial guesses; 10,000 initial guesses were used for each run in this study. Orthogonal surrogate fuels are then determined via down selection from the compiled solutions presented in the cumulative Pareto front. Orthogonality in this study was focused only on the three properties of interest (surface tension, density, viscosity). Additionally, other objective functions were added to increase the variance in values of the three interesting properties during down selection to obtain the largest variance in results during the combustor FOM testing.

Results and discussion

Fuel blending optimization is performed over four scenarios involving three variables (surface tension, viscosity, density) and two levels for each variable (larger than A-2 value, smaller than A-2 value). Orthogonal array testing is then generated for the four scenarios in Table 2, according to the appropriate variable and level. Orthogonal array testing was then used to maximize variance across several critical properties for combustor testing and minimize the number of tests (Tsui, 1992).

With each scenario, 10,000 random initial compositional guesses to unbiased solutions and the corresponding Pareto solutions were used to generate the cumulative Pareto front. Figures 10, 11, 12, and 13 consists of scatterplots and histograms of Pareto front solutions, illustrating converged probability densities and relative opportunities for property variance. Each scatterplot consists of calculated properties. Each dot on a scatterplot represents one of the possible best solutions found by JudO. The purple dashed line represents the properties of A-2. Using orthogonal array testing, a surrogate was selected and represented by the orange star. The surrogates were selected to minimize or maximize the properties of density, viscosity, and surface tension, relative to A-2, according to the four scenarios. Other properties were intended to be as close to the A-2 values as possible using the other objective functions in this optimization. The properties considered here were MW, H/C, DCN, σ, μ, and ρ. Although the selected surrogate might not have the absolute minimum values of the solution space, the multi-dimensionality concerning all properties suggests the largest variance happens at that point. Down-selected surrogate fuels and their respective properties for each of the scenarios are presented in Table 3, and Figures 10, 11, 12, and 13 identify the mole fractions and volume fractions of each surrogate. Four surrogate fuels were then blended and measured at −30°C for viscosity and density. There was no error between measured and calculated density at −30°C for the four surrogate fuels. Viscosity measurements also showed good results with reasonable error. This could be due to viscosity having an exponential relationship with temperature, whereas density has a linear relationship with temperature.

Figure 10 displays the total of 3,047,039 results of scenario 1, where the intention of surrogate 1 was to have the lowest surface tension, viscosity, and density; surrogate 1 consists primarily of 68% A-1 and 28% C-4, where A-1 is the "best" jet fuel, with all three properties lower than that of A-2, and C-4 has the second-lowest surface tension and relatively low viscosity and density. C-1 has the lowest surface tension; however, with relatively high viscosity, it was not considered in the solution of surrogate 1. Figure 12 illustrates scenario 2, which minimizes surface tension and maximizes viscosity and density. Each of the 3,336,938 possible best solutions is shown on the scatterplots. The orange star represents surrogate 2, which was the best solution for this scenario. This mixture consists of 29% A-1 and 68% C-3, where C-3 has the highest viscosity and relatively high density. Figure 13 shows 2,201,505 solutions for scenario 3, and, like the previous figures, indicates the best solution for surrogate 3 by the orange star. The goal of surrogate 3 was to minimize viscosity and maximize surface tension and density. Surrogate 3 consists of 53% A-1 and 46% A-2, where A-2 is the target fuel of this study. Figure 14 reports 3,937,813 solutions for scenario 4, and the objective for surrogate 4 was to minimize density and maximize surface tension and viscosity. The selected surrogate consisted of a six-component mixture, much different from the other solutions: 3% A-2, 2% C-4, 59% C-7, 5% C-9, 5% Syntroleum S-8, and 21% Camelina HEFA. Minimizing density while maximizing surface tension was difficult with the fuels selected for this work. Because the majority of the fuels selected here had positive correlations between surface tension and density, it was challenging to minimize density while maximizing surface tension. If larger variance needs to be achieved, then more novel fuels, solvents, and neat molecules need to be integrated into JudO. This is also a limitation of JudO; the surrogate properties can only be as high or low as the highest or lowest fuel used in JudO. After generation of these four surrogates, ignition probability can be further characterized on a fuel basis by the three variables in the orthogonal array testing (Opacich et al., 2019).

Conclusion

Previous efforts from the NJFCP program have shown that certain fuel properties (σ, μ, and ρ) have the most on predicting ignition probabilities (Heyne et al., 2019; Opacich et al., 2019; Peiffer et al., 2019). Current ASTM D4054 and D1655 specifications set bounds on viscosity and density; however, surface tension does not have a bound on any values at any given temperature. Surface tension has been validated and incorporated into JudO, a fuel blending optimization tool. These fuel properties, along with other pertinent properties important in combustion testing of novel fuels, were then integrated into JudO as objective functions to create surrogate fuels to further understand the effect on key properties relative to ignition probability. With these enhancements to JudO, more surrogates can be designed based on key properties of other combustor FOMs and accompanying hypotheses on performance parameters. In this work, four orthogonal surrogate fuels were created using JudO and orthogonal array testing to maximize variance in the specified fuel properties above. This work and supporting experimental evidence could lower the barrier for SAF approval and facilitate the achievement of the carbon reduction goals. In future research, more properties need to be added to JudO to cover more FOMs, and more novel fuels, solvents, and neat molecules need to be considered for integration in this tool to achieve greater variance in properties than currently estimated.

Table 2. Orthogonal array testing.

Scenarios	σ(-30°C), mN/m	μ(-30°C), cSt	ρ(-30°C), kg/L	Surrogate
Reference	30.0	6.1	0.837	A-2
1	⬇	⬇	⬇	1
2	⬇	⬆	⬆	2
3	⬆	⬇	⬆	3
4	⬆	⬆	⬇	4

Table 3. Properties of orthogonal fuels for all scenarios.

Property	A-2 Reference	Scenario Surrogate 1 min(σ, μ, ρ)	Surrogate 2 min(σ),max(μ, ρ)	Surrogate 3 min(μ),max(σ, ρ)	Surrogate 4 min(ρ),max(σ, μ)
MW, g/mol	159	156	172	156	169
σ (−30˚C), mN/m	30.0	26.7	28.1	28.5	29.4
ρ (−30˚C), kg/L	0.837	0.806	0.832	0.824	0.827
ν (−30˚C), cSt	6.1	4.8	9.1	5.3	8.9
DCN	48	41	48	48	48
H/C	1.91	2.04	1.98	1.95	2.05
T10, ˚C	160	151	175	154	173
T50, ˚C	209	186	231	201	218
T90, ˚C	260	241	254	254	262
ρ (−30˚C),* kg/L	[redacted]	0.806	0.832	0.824	0.826
ρ % error		0%	0%	0%	0%
ν (−30˚C),* cSt		4.5	10.3	5.2	8.5
ν % error		-6%	13%	2%	5%

*Properties are measured at −30˚C.

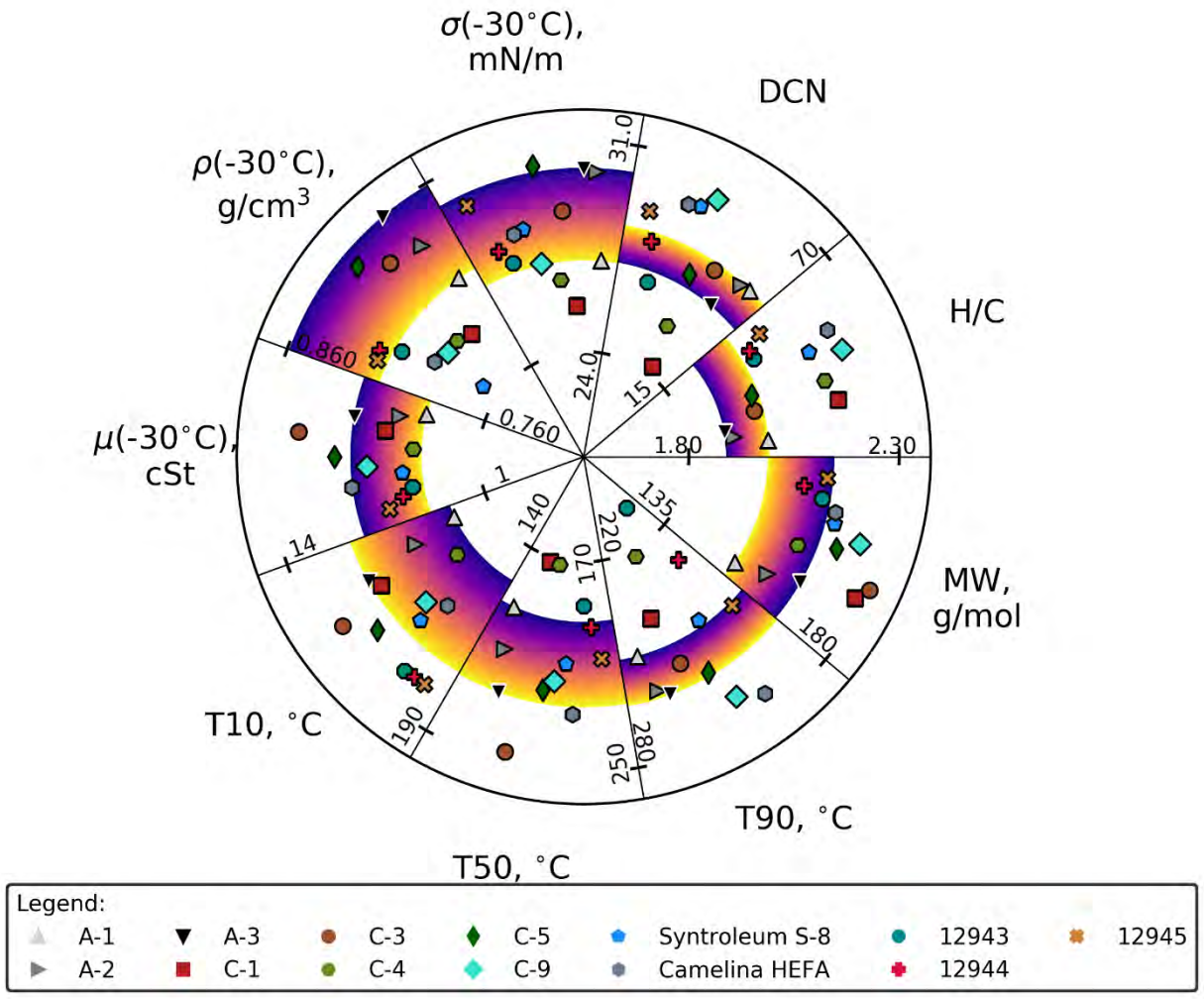

Figure 7. A plot of the 13 fuels and their respective normalized properties. Category A fuels are shown in the color gradient on the map, where yellow is the "best" case and purple is the "worst" case for each property. The rest of the fuels are plotted according to their normalized properties and respective to their marker.

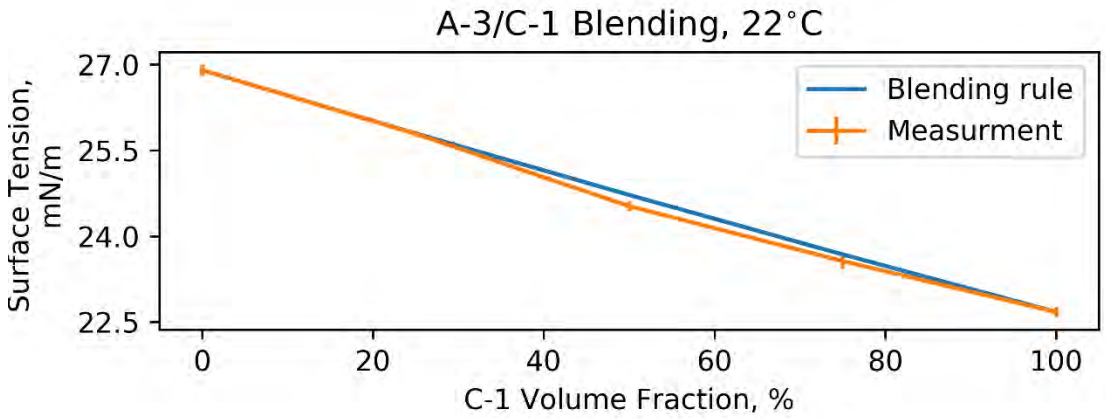

Figure 8. Surface tension blending rule validation. Error bar represent 95% confidence interval.

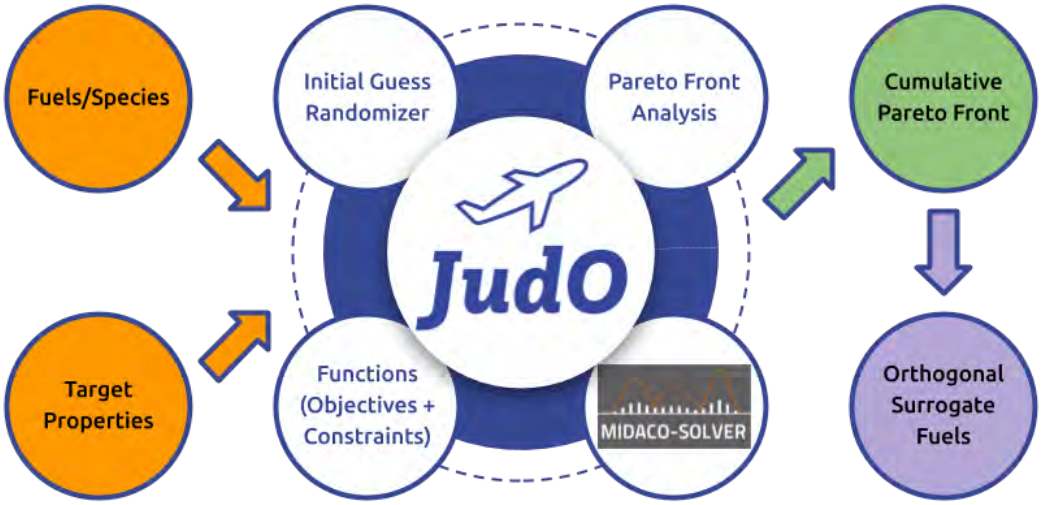

Figure 9. Schematic of the jet fuel blending optimization tool JudO, a suite centered around a computational tool called Mixed Integer Distributed Ant Colony Optimization (MIDACO) (Schlueter et al., 2013), which is implemented to optimize a user-specified fuel set (conventional and alternative jet fuels) of varying properties with specific design parameters and target properties (MW, H/C, DCN, density, kinematic viscosity, distillation curve, and surface tension) to illuminate Pareto front compromises for the fuels considered here.

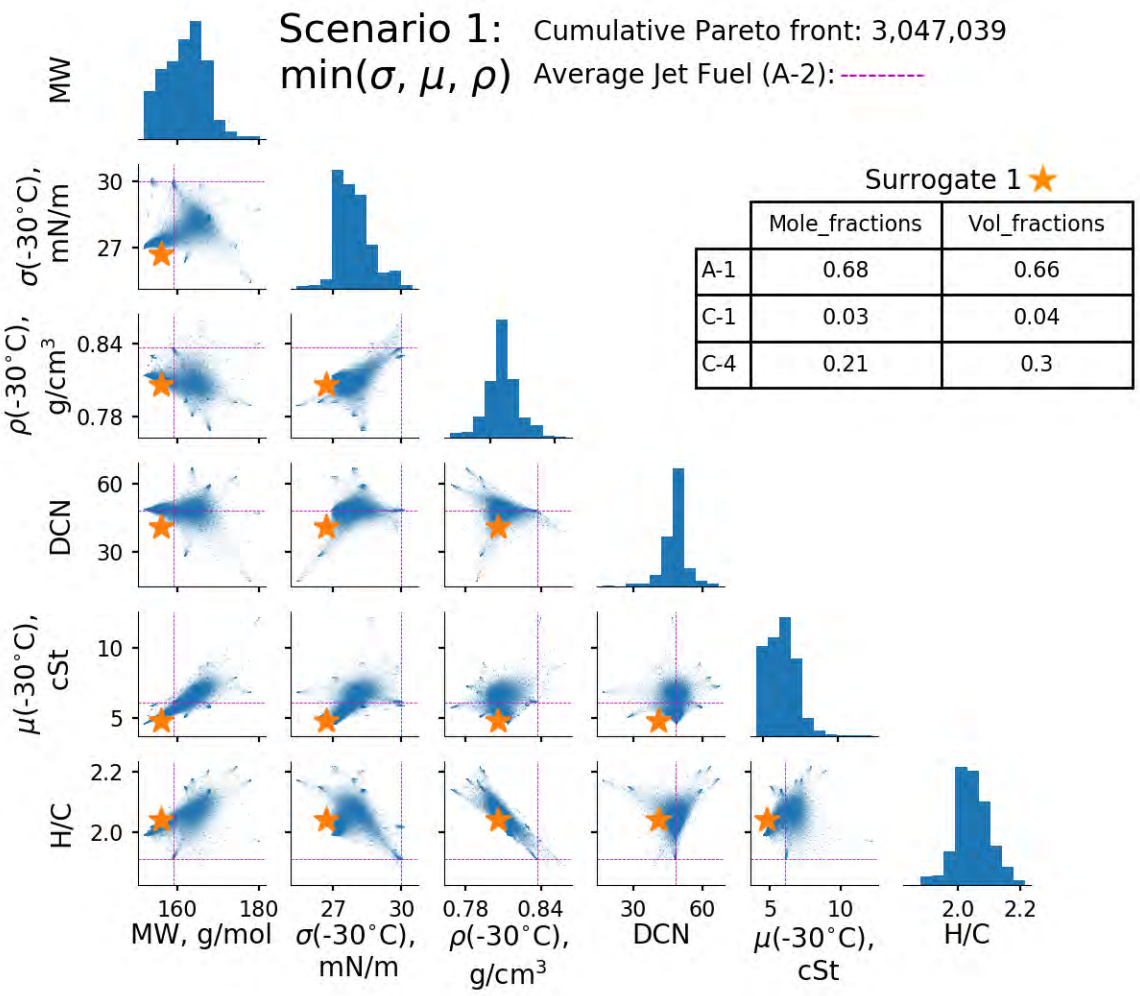

Figure 10. Cumulative Pareto solutions for scenario 1 with combinations of optimized properties on histograms and scatterplots with other properties. Scatterplots consist of calculated properties with respect to each other. Each dot on a scatterplot represents one of the possible best solutions found using the jet fuel blending optimization tool JudO. The dashed line indicates the properties of A-2, and the orange star represents the properties of surrogate 1 with respect to the cumulative Pareto solutions.

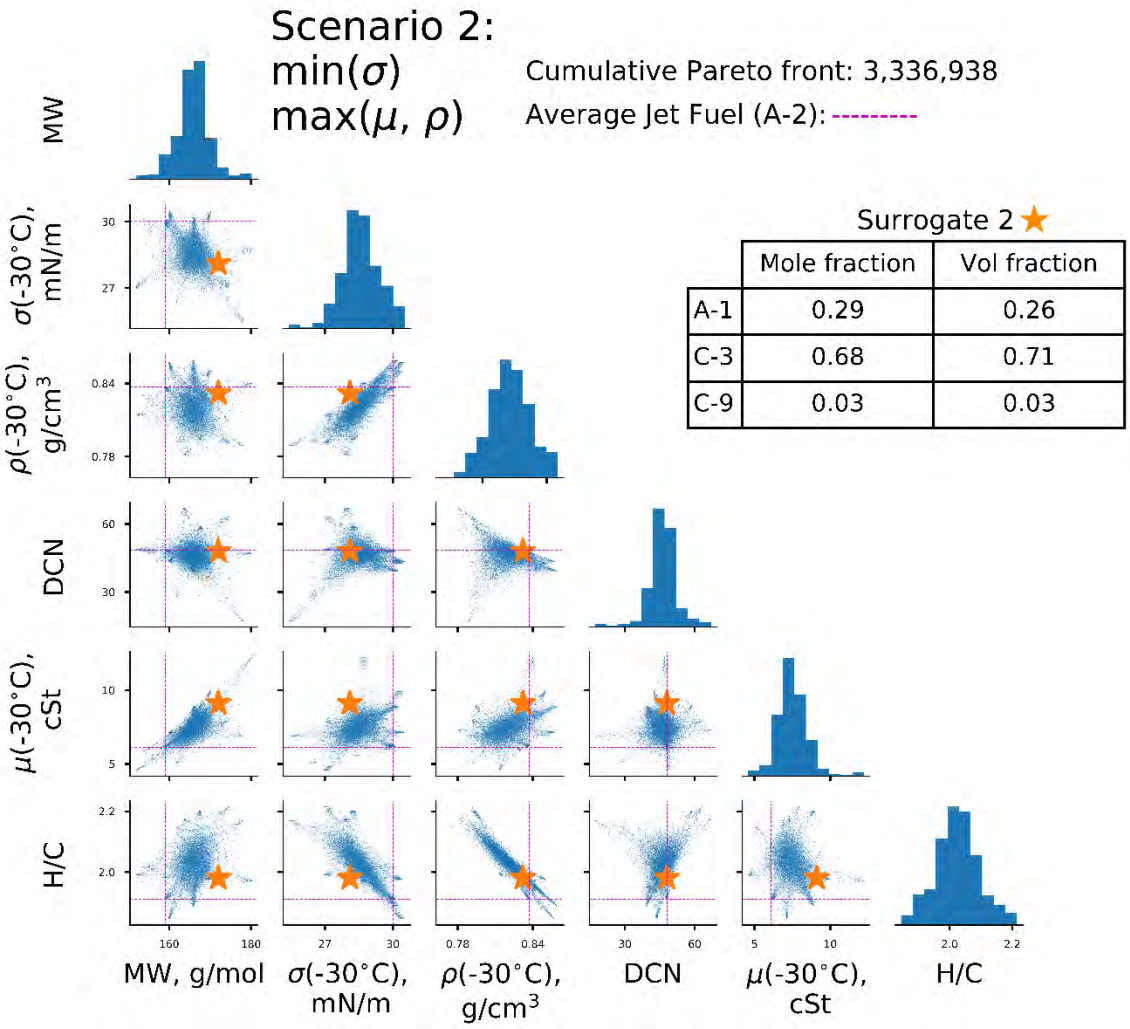

Figure 11. Cumulative Pareto solutions for scenario 2. Scatterplots consist of calculated properties with respect to each other. Each dot on a scatterplot represents one of the possible best solutions found using the jet fuel blending optimization tool JudO. The dashed line indicates the properties of A-2, and the orange star represents the properties of surrogate 2 with respect to the cumulative Pareto solutions.

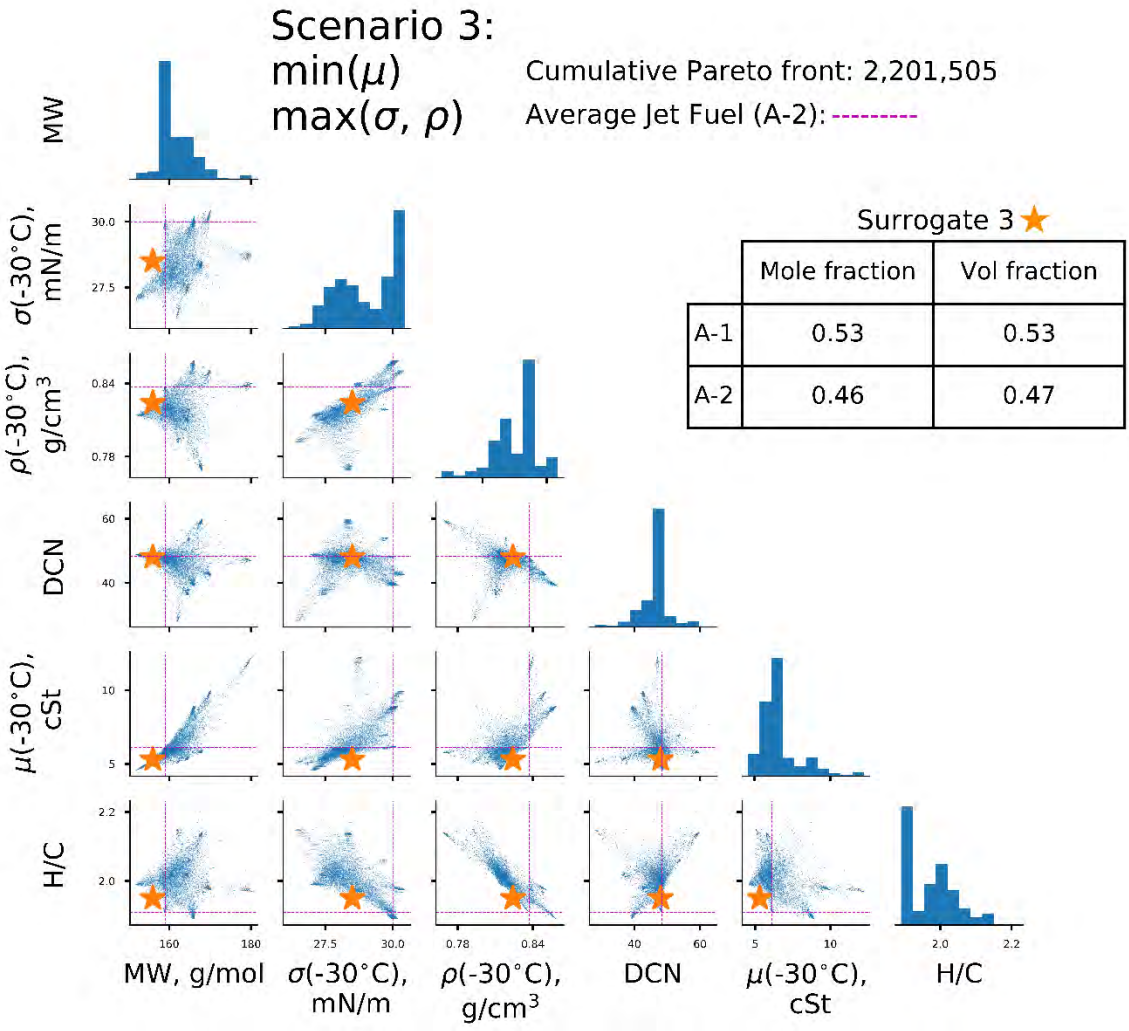

Figure 12. Cumulative Pareto solutions for scenario 3. Scatterplots consist of calculated properties with respect to each other. Each dot on a scatterplot represents one of the possible best solutions found using the jet fuel blending optimization tool JudO. The dashed line indicates the properties of A-2, and the orange star represents the properties of surrogate 3 with respect to the cumulative Pareto solutions.

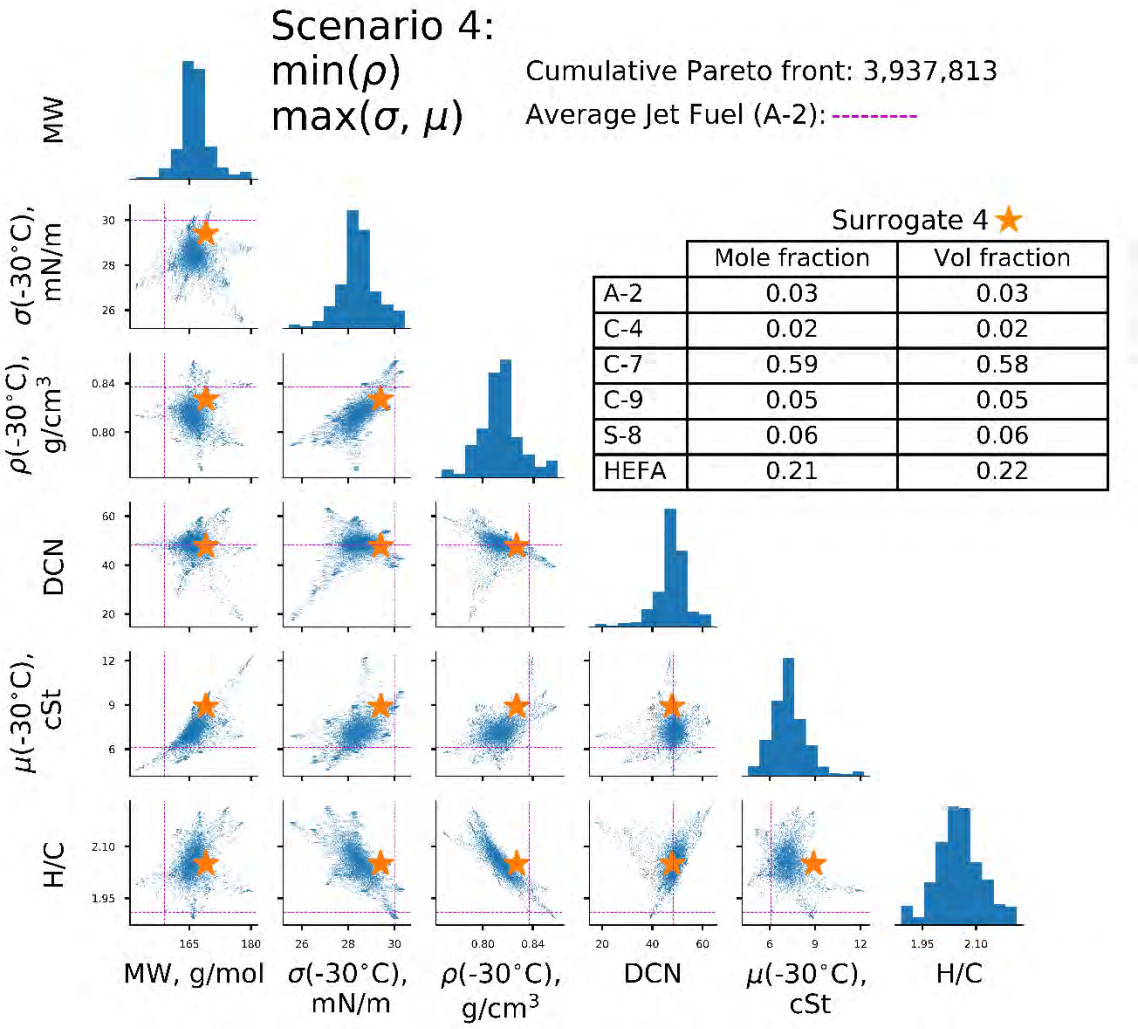

	Mole fraction	Vol fraction
A-2	0.03	0.03
C-4	0.02	0.02
C-7	0.59	0.58
C-9	0.05	0.05
S-8	0.06	0.06
HEFA	0.21	0.22

Figure 13. Cumulative Pareto solutions for scenario 4. Scatterplots consist of calculated properties with respect to each other. Each dot on a scatterplot represents one of the possible best solutions found using the jet fuel blending optimization tool JudO. The dashed line indicates the properties of A-2, and the orange star represents the properties of surrogate 4 with respect to the cumulative Pareto solutions.

References

Bell, D., Heyne, J.S., Won, S.H., Dryer, F., Haas, F.M., & Dooley, S. (2017). On the development of general surrogate composition calculations for chemical and physical properties. 55th AIAA Aerospace Sciences Meeting, 1–5. doi:10.2514/6.2017-0609

Chao, H., Buyung, D., Delaurentis, D., & Stechel, E.B. (2019). Carbon off setting and reduction scheme with sustainable aviation fuel options: Fleet-level carbon emissions impacts for U. S. airlines. Transportation Research Part D: Transport and Environment, 2020;75:42–56. doi:10.1016/j.trd.2019.08.015

Colket, M.B., Heyne, J., Rumizen, M., Gupta, M., Edwards, T., & Roquemore, W.M. et al. (2017). An overview of the national jet fuels combustion program. AIAA J.

Dooley, S., Won, S.H., Chaos, M., Heyne, J., Ju, Y., & Dryer, F.L. et al. (2010). A jet fuel surrogate formulated by real fuel properties. Combustion and Flame, 157:2333–9. doi:10.1016/j.combustflame.2010.07.001

Edwards, T. (2017). Reference jet fuels for combustion testing. 55th AIAA Aerospace Sciences Meeting, 1–58

Edwards, J.T., Shafer, L.M., & Klein, J.K. (2013). U.S. Air Force hydroprocessed renewable jet (HRJ) fuel research

Flora, G., Kosir, S., Heyne, J., Zabarnik, S., & Grupta, M. (2018). Properties calculator and optimization for drop-in alternative jet fuel blends. AIAA, 1–14. doi:10.2514/6.2019-2368

Heyne, J.S., Colket, M.B., Gupta, M., Jardines, A., Moder, J.P., & Edwards, J.T. et al. (2017). Year 2 of the national jet fuels combustion program: Towards a streamlined alternative jet fuels certification process. 55th AIAA Aerospace Science Meeting, 1–13

Heyne, J.S., Peiffer, E., Colket, M.B., Jardines, A., Shaw, C., Moder, J.P., et al. (2018). Year 3 of the National Jet Fuels Combustion Program: Practical and scientific impacts of alternative jet fuel research. 56th AIAA Aerospace Science Meeting

Heyne, J.S., Opacich, K.C., Peiffer, E.E., & Colket, M. (2019). The effect of chemical and physical fuel properties on the approval and evaluation of alternative jet fuels. 11th U.S. National Combustion Meeting, p. 1–10

IATA. (2018). Carbon Offsetting and Reduction Scheme for International Aviation (CORSIA): Fact sheet

Kim, D., Martz, J., Abdul-Nour, A., Yu, X., Jansons, M., & Violi, A. (2017). A six-component surrogate for emulating the physical and chemical characteristics of conventional and alternative jet fuels and their blends. Combustion and Flame, 179:86–94. doi:10.1016/j.combustflame.2017.01.025

Kim, D., Martz, J., & Violi, A. (2014). A surrogate for emulating the physical and chemical properties of conventional jet fuel. Combustion and Flame, 161:1489–98. doi:10.1016/j.combustflame.2013.12.015

Kosir, S.T., Behnke, L., Heyne, J.S., Zabarnick, S., Flora, G., & Denney, R.K. et al. (2019). Improvement in jet aircraft operation with the use of high-performance alternative drop-in fuels in conventional fuels. AIAA SciTech Forum 2019:1–27

Lefebvre, A.H. (1983). Fuel effects on gas turbine combustion. Wright-Patterson AFB, Dayton, OH

NASA. (2018). NASA update FAA ASCENT meeting 2018

Neumann, B., Vafeidis, A.T., Zimmermann, J., & Nicholls, R.J. (2015). Future coastal population growth and exposure to sea-level rise and coastal flooding - a global assessment. PLOS ONE 2015; doi:10.1371/journal.pone.0118571

Office of Transportation and Air Quality. (2019). Fast facts U.S. Transportation sector greenhouse gas emissions 1990-2017

Opacich, K.C., Heyne, J.S., Peiffer, E., & Stouffer, S.D. (2019). Analyzing the relative impact of spray and volatile fuel properties on gas turbine combustor ignition in multiple rig geometries. AIAA Scitech 2019 Forum

Peiffer, E.E. & Heyne, J.S. (n.d.). Characteristic timescales for lean blowout of alternative jet fuels in four combustor rigs.

Peiffer, E.E., Heyne, J.S., & Colket, M. (2019). Sustainable aviation fuels approval streamlining: Auxiliary power unit lean blowout testing. AIAAJ, 1–9. doi:10.2514/1.J058348.

Poling, B., Prausnitz, J., & O'Connell, J. (2000). The properties of gases and gas mixtures. doi:10.1036/0070116822

Rock, N., Emerson, B., Seitzman, J., & Lieuwen, T. (2019). Liquid fuel property effects on lean blowout in an aircraft relevant combustor.141. doi:10.1115/1.4042010.

Ruan. H., Qin, Y., Heyne, J., Gieleciak, R., Feng, M., & Yang, B. (2019). Chemical compositions and properties of lignin-based jet fuel range hydrocarbons. Fuel, 256:115947. doi:10.1016/j.fuel.2019.115947

Rumizen, M. (2018). D4054 Clearinghouse. (Personal communication)

Schlueter, M., Erb, S.O., Gerdts, M., & Kemble, S. (2013). MIDACO on MINLP Space Applications, 1–25.

Stachler, R.D., Heyne, J.S., Stouffer, S.D., Division, E.E., Miller, J.D., & Roquemore, W.M. et al. (2017). Investigation of combustion emissions from conventional and alternative aviation fuels in a well-stirred reactor. 1–28. doi:10.2514/6.2017-0382.

Tsui, K.L. (1992). An overview of Taguchi method and newly developed statistical methods for robust design. IIE Transactions, 24:44–57. doi:10.1080/07408179208964244.

Weinaug, C.F. & Katz, D.L. (1943). Surface tensions of methane-propane mixtures. Industrial Engineering Chemistry, 35:239–46. doi:10.1021/ie50398a028

Milestone(s)

- Surrogate fuels were formulated to exacerbate or ameliorate properties of a given fuel, rather than to mimic the properties.
- Orthogonal reference surrogate fuels were generated to identify the effect of specific properties on combustor operability testing.
- Surface tension blending was incorporated into a currently used fuel blending optimization tool, where this property was not previously considered.

Major Accomplishments

Reporting operability surrogate fuels.
Fuel blending optimization tool updated with surface tension and incorporation of NJFCP fuels.
Experimental results from testing surrogate fuels can illustrate the maximum FOM sensitivity, aiding in the prescreening and formal evaluation of novel SAFs.

Publications

Peer-reviewed publications

Yang, Zhibin, Robert Stachler, and Joshua S. Heyne. "Orthogonal reference surrogate fuels for operability testing" Energies 13, no. 8 (2020): 1948 https://doi.org/10.3390/en13081948

Outreach Efforts

Yang, Z.: Presentation at 15th Dayton Engineering Sciences Symposium

Student Involvement

Zhibin Yang, graduate research assistant. Zhibin developed surrogates to match fuel properties.
Robert Stachler, PhD student. Robert helped with surrogate fuel formation.

Task 10 – Investigation of Chemical and Physical Effects on LBO

University of Dayton

Objective

The objective of this Task is to investigate chemical and physical effects on LBO in a swirl-stabilized single-cup combustor.

Research Approach

Introduction

The lower stability limit of gas turbine engines, or lean blowout (LBO), is an important limit phenomenon for safety, the approval of novel sustainable aviation fuels, and identifying transitions between competing physics [1]. LBO is a complex process that can be impacted by engine design, operating conditions, or any number of fuel properties.

Combustor configuration strongly influences LBO limits. Recirculation zones, air velocity, and combustor dome pressure drop (ΔP) are all influenced by the combustor, nozzle, and swirler design. These different features can impact fuel spray and mixing quality. Nozzle atomization technique and cone angle have been found to influence the equivalence ratio at LBO (φ_{LBO}) [2,3]. The presence of a swirler, as well as the number of vanes, swirl angle, and swirl direction impact the spray quality which will influence φ_{LBO} [4–8].

Fuel properties have also been found to impact φ_{LBO} strongly. Lefebvre found that varying fuel atomization and evaporation properties strongly influenced φ_{LBO} in a variety of engine geometries [9]. Physical properties have been shown to strongly impact LBO due to their influence on atomization [9–12]. Fuel property variance can be found within petroleum-derived fuels, impacting LBO limits regardless of engine configuration [9,13].

Changes in operating conditions can also heavily influence φ_{LBO}. Variances in combustor pressure (P) and ΔP can lead to differences in air velocity, which can affect fuel atomization. Fuel and air temperatures highly influence evaporation as well as droplet breakup, since the physical properties that control fuel atomization are highly temperature dependent [3].

Increased temperatures cause less required energy from the combustion process to vaporize the fuel, leading to an improved LBO limit.

Aircraft engines must operate over a wide range of pressures and temperatures where LBO performance is important. Combustor conditions vary throughout flight, which can influence LBO limits. Fuels must be able to perform acceptably under these varying conditions. Lefebvre described φ_{LBO} with Eq. 1, where combustor design parameters, thermo-fluid effects, and fuel-dependent properties demonstrate the multi-property dependency of LBO [9].

$$\phi_{LBO} = \underbrace{\left[\frac{f_{pz}}{v_{pz}^{(1+x)}}\right]}_{Geometry} \underbrace{\left[\frac{\dot{m}_A^{(1+x)}}{p_3^{(1+nx)}\, exp(x\, T_3/b)}\right]}_{Thermofluids} \underbrace{\left[\frac{D_0^2}{\lambda_{eff} LHV}\right]}_{\substack{Fuel \\ Effects}} \tag{1}$$

Burger, Plee, and Mellor have extended the work of Lefebvre, evaluating LBO by considering the effects of chemical kinetics, operating conditions, and combustor geometry [14–16]. Through a combination of relevant fuel parameters and combustor geometries, the chemical, evaporative, and mixing timescales can represent autoignition and extinction, fuel volatility, and combustor properties, respectively, as shown in Eq. 2. Peiffer utilized this method to compare the variance of φ_{LBO} in experimental rigs with varying geometries and operating conditions to explain the relative importance of fuel properties [17]. Dependence on physical properties was noted in rigs without swirlers, which hinders atomization [18].

$$\phi_{LBO} \sim \left(\frac{1}{\tau_{chem}} + \frac{1}{\tau_{evap}} + \frac{1}{\tau_{mix}}\right)^{-1} \tag{2}$$

Recent LBO investigations have also shown high sensitivity to fuel properties [19,20]. A swirl-stabilized, single-cup combustor showed strong correlation to derived cetane number (DCN) at relatively high temperature and increased pressure conditions (T_{air} = 394K, T_{fuel} = 322K, P = 207kPa, ΔP/P = 3%) [19]. In contrast, Peiffer demonstrated that at relatively low temperatures and pressures physical properties, such as distillation temperatures and density were important for describing φ_{LBO} in an auxiliary power unit (APU) [17,18]. The difference in physical and chemical property dependence between different operating conditions implies competition between spray characteristics and autoignition stabilization.

While the extreme operational conditions detailed above demonstrated a difference in property importance, the transition between the physical and chemical regime has not been thoroughly investigated. This study seeks to investigate a transition from LBO performance physical property dependence (spray characteristics) to chemical property dependence (autoignition characteristics) with varying ΔP/P as well as air and fuel temperatures.

Test article

A swirl-stabilized single-cup combustor designed with turbine engine OEM input to simulate key characteristics of actual turbine engine combustors was used for LBO limit investigation (Figure 1). Referred to as the "Referee Combustor, it features effusion cooling and dilution holes as well as an injector and swirler that allow for the reproduction of important turbine engine combustor features [21]. The combustor is housed in a pressure vessel surrounded with fused silica windows to allow for optical access. The reduced combustor scale allows for ignition and LBO experiments with reduced fuel quantities for both elevated and cold fuel and air temperatures. Fuel impact assessments on these performance metrics in this combustor have shown similar trends to actual engines [19,21,22].

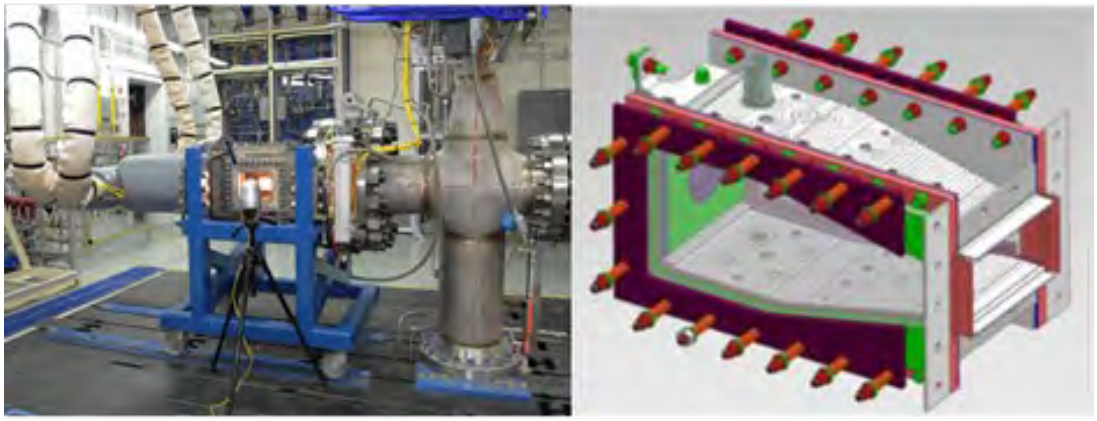

(a) (b)

Figure 1. (a) Referee Combustor rig at the Air Force Research Laboratory (AFRL). (b) Swirl-stabilized (Referee) Combustor design.

Air mass flow to the combustor is metered using two Coriolis meters and pressure was regulated upstream of the control valves. Approximately 15% of the total air flow passes through the swirler, 22% through the dilution holes, and the other 63% through the effusion holes. The volume between the combustor dome and first stage dilution holes is 617 cm^3. Pressure transducers along the combustor wall measured ΔP at 15 Hz and a high-frequency response transducer at 150 kHz detected any pressure oscillations via semi-infinite tube technique. K-type thermocouples positioned on the outside of the combustor as well as the pressure vessel and surrounding supports allow for temperature monitoring to prevent structural damage. When required, fuel is heated using a heat exchanger with water supplied by a process fluid heater to deliver fuel at the nozzle at the desired fuel temperature. The fuel mass flow is measured using Coriolis meters upstream of the heat exchanger, before the nozzle. The fuel and air temperature were typically maintained within ±1.5K of the desired value. Two syringe pumps allow for fine control of the fuel flow.

Combustor LBO is very sensitive to fluctuations in the test conditions such as flow rate, pressure, temperature, and ΔP. Due to an emphasis on repeatability, control of these parameters was imperative. Proportional-Integral-Derivative (PID) loops were used extensively for fine control of various parameters. Pressure drop across the control valves was enough to choke the valves, keeping the mass flow supplied to the combustor independent of any downstream pressure fluctuations. In order to prevent fuel contamination from the previous test fuel, it was paramount to properly purge the fuel lines. Prior to each test, a fuel sample was collected near the fuel nozzle and tested for fuel purity via chemical analysis (GC-FID).

Experimental procedures

LBO tests were conducted by establishing pressure, air temperature, air mass flow, and ΔP. Fuel flow was then introduced and ignited. Adjustments were then made to the fuel temperature and flow rate until the desired condition was reached. After steady conditions were established within the combustor, the LBO test was initiated by slowly decreasing the fuel flow rate via syringe pumps at a rate of 0.25 mL/min every two seconds. For each condition, the LBO test was initiated from the same fuel mass flow rate, approximately 10% above the LBO limit. A slow ramp rate was important for achieving an unbiased LBO. Too fast a ramp rate may lead to a lower φ_{LBO} due to higher wall temperatures. Previous experiments determined that this rate allowed for a repeatable, smooth ramp, wall temperatures to adjust during experimentation, and maximized the number of experiments performed [19]. The LBO limit was determined by a rapid drop in the photodiode signal, which was directed at the primary combustion region. A sufficient number of LBO tests, usually between ten and fifteen, were conducted to ensure that agreement in values was achieved before moving to a different condition. Statistics were updated with each LBO test, and when the 95% confidence interval for the mean φ_{LBO} dropped below 0.75%, agreement was considered to be reached. This estimated φ_{LBO} was usually within a percent of the actual φ_{LBO} determined from more thorough post-test analysis of the 15 Hz photodiode signal. Experiments were performed at the conditions included in Table 1.

Table 1. Test Conditions Evaluated

P	T_{air} = T_{fuel} [K]	ΔP/P [%]
107kPa	338	2,3,3.5,4,5, 6
	305,322,338, 355	3.5

Fuels

Four fuels were tested to study physical or chemical property influence (Table 2) on combustor LBO performance. The fuels were selected due to their wide range of physical and chemical properties. For reference, these were designated either A or C type fuels within the NJFCP [13]. A-type fuels are conventional petroleum fuels commercially available and C-type fuels are research fuels meant to highlight potential sensitivity to varying fuel properties.

Table 2. Fuels Evaluated and Corresponding Selected Physical and Chemical Properties Including 20 and 90% Recovered Temperatures (T_{20} and T_{90}, respectively, Molecular Weight (MW), and Lower Heating Value (LHV)

Property	ASTM Standard	A-2 Jet A	C-1 Alcohol-to-Jet	C-3 64% JP-5, 36% Farnesane	C-7 75% RP-2, 23% JP-5, 2% Decalin
DCN	D6890	48.3	17.1	47	42.6
Kinematic Viscosity, ν (253K, mm^2/s)	D445	4.5	4.9	8.3	6.53
Surface Tension, σ (295K, dynes/cm)	D1331	24.8	23.4	26.1	26.1
Density, ρ (288K, kg/m^3)	D4052	0.803	0.76	0.808	0.817
T_{20} (K)	D2887	447	445	478	464
T_{90} (K)	D2887	533	513	528	534
MW	n/a	159	178	180	170
LHV (MJ/kg)	D4809	43.06	43.8	42.39	43.3

A-2, a nominal Jet A with average properties, was selected as a baseline fuel. C-1 is an alcohol-to-jet, which features a very low DCN to test for chemical property dependence. To study physical property effects, C-3 was selected due to its high viscosity (ν). C-7 is a high cycloparaffin fuel (~62% cycloparaffins) with a high surface tension. Figure 2 displays the relative values of several physical and chemical properties for the tested fuels.

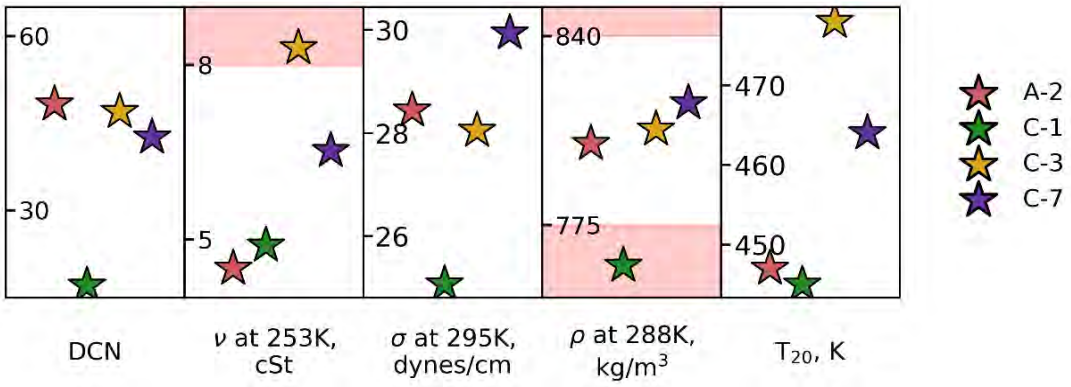

Figure 2 Physical and chemical properties of tested fuels. Red regions denote current specification limits.

Results and discussion

Combustor LBO performance is based on the φ_{LBO} as in previous studies [9,19,23]. The lower the φ_{LBO}, the less fuel is required to maintain the flame, indicating better LBO performance. Figure 3 shows φ_{LBO} response with varying ΔP/P and constant air and fuel temperature.

Increasing ΔP/P resulted in a non-monotonic φ_{LBO} ranking response across all fuels except C-3 were seen to collapse at 3.5% ΔP/P, at which point φ_{LBO} began to increase with increasing ΔP/P. As observed, the LBO limits for C-3 consistently decreased with increasing ΔP/P. Unfortunately, LBO tests for C-3 were not conducted at 6% ΔP/P due to heavy soot formation on the combustor liner and windows. At 2% ΔP/P, C-1 had the lowest (i.e., best) stability limit (φ_{LBO}) among fuels tested. In contrast, at ΔP/P=5 and 6% C-1 was observed to have the highest (i.e., worst) stability limit. The data for A-2 and C-7 diverge above 3.5% ΔP/P, below which they had almost identical performance.

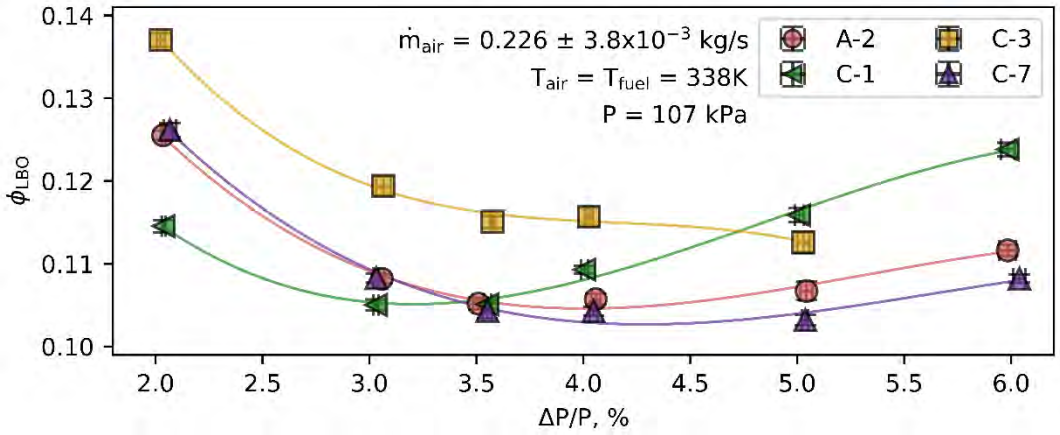

Figure 3. LBO limits (φ_{LBO}) as a function of combustor ΔP/P. Error bars denote the 95% confidence interval for φ_{LBO} and two standard deviations for ΔP/P.

At 2% ΔP/P, the LBO performance ordering of the fuels corresponded to physical property impacts. C-1, which possesses the lowest φ_{LBO}, had beneficial physical properties (lower surface tension, viscosity, and density) relative to other fuels, thus, promoting fuel atomization. Conversely, C-3 had less favorable physical properties (e.g., very high viscosity) which were detrimental to fuel atomization resulting in higher φ_{LBO}. The physical properties of A-2 and C-7 between the more extreme C-1 and C-3, resulting in φ_{LBO} between the two fuels. Low combustor ΔP/P consequently led to poor fuel atomization due to decreased aerodynamic forces acting upon the fuel droplets. With low aerodynamic forces, physical properties highly influenced fuel atomization and droplet size.

When considering the high ΔP/P cases of 5% and 6%, fuel performance changed dramatically compared to the 2% condition. At ΔP/P=5%, C-3 had a lower φ_{LBO} than C-1, which cannot be accounted for when only considering physical properties. C-1 had more favorable physical properties than C-3, which would result in better LBO performance if only physical properties were affecting LBO limits. It is clear that some other property or properties impacted fuel LBO performance at higher ΔP/P. In previous higher temperature and pressure studies (T_{air} = 394K, T_{fuel} = 322K, P = 207kPa, ΔP/P = 3%), DCN was identified as the dominant property for LBO performance due to its strong inverse correlation to φ_{LBO} [19,24,25]. The lower DCN of C-1 could account for its higher φ_{LBO} relative to C-3, indicating that chemical properties were beginning to impact φ_{LBO}. Once ΔP/P was high enough to minimize physical property impact, chemical properties began to dominate the lean stability limit. At 3.5% ΔP/P, A-2, C-1, and C-7 all demonstrate the beginning of a transition from physical property to chemical property dependence due to the collapse of their LBO limits at 3.5% ΔP/P and the increase in LBO limit above 3.5% ΔP/P. However, since C-3 did not attain a lower φ_{LBO} than C-1 at ΔP/P less than 5%, physical properties still had an influence between these two conditions. These trends indicated a transition regime rather than a single point, wherein fuels with very poor atomization characteristics shift the minima (improved LBO) to higher ΔP/P.

Random forest regression analysis was leveraged in similar techniques as those used by Peiffer [17]. Random forest analysis is a machine learning technique that utilizes random sampling and replacement, or bagging, to evaluate how different

variables (e.g., fuel properties) impact a particular result (e.g., fuel performance). Around twenty data points are required for a normal pattern to appear [26]. For this analysis, a minimum of thirty data points were considered at each condition. By using bagging techniques, random forests can evaluate and predict importance values for given properties without bias and with lower error than other statistical techniques with small sample sizes [27,28]. Each parameter in the selected regression was evaluated against φ_{LBO}. Linear regression analyses to correlate LBO performance to fuel properties were attempted, but no correlations could be discerned because of the non-monotonic trends. Since only four fuels and relatively small data sets (between 30–40 data points per condition) were used, a more robust statistical analysis method was required.

Weber number (We), defined in Eq. 3, was selected to evaluate physical property and operating condition effects on the fuel spray. Weber number is a dimensionless spray parameter which considers the disruptive aerodynamic forces (ρv^2) and the fuel binding forces (σ/l). It is the ratio between fluid inertial and surface tension forces. By considering the competition between breakup inhibiting and promoting forces, fuel spray quality can be evaluated [3].

$$We = \frac{\rho\, v^2\, l}{\sigma} \tag{3}$$

For the present study, the fuel velocity (v) was unknown so the pressure drop across the nozzle (ΔP_{noz}) was used, due to ΔP_{noz} scaling with v^2. Since the same fuel nozzle was used for all experiments, the characteristic length (l) was equivalent for all fuels tested, which allowed for approximation of Weber number (We_{apr}) as shown in Eq. 4. Density (ρ) and surface tension (σ) were calculated based on the fuel temperature at each point. Random forest analysis was also performed using all three properties considered in We_{apr}, as well as substituting each property individually for We_{apr}, and it was found that the inclusion of only We_{apr} resulted in higher adjusted R^2 (R_{adj}^2) values.

$$We_{apr} = \frac{\rho(T)\,\Delta P_{noz}}{\sigma(T)} \tag{4}$$

The Ohnesorge number (Oh) was additionally considered to evaluate physical property effects on LBO performance. As shown in Eq. 5, the Ohnesorge number only considers physical properties and was able to be fully evaluated [3].

$$Oh = \frac{\mu(T)}{[\rho(T)\,\sigma(T)D]^{0.5}} \tag{5}$$

When $\Delta P/P$ was set at 2%, We_{apr}, as well as viscosity, were shown to be the most influential parameters to φ_{LBO} (Figure 4a). At the low $\Delta P/P$ conditions, atomization was strongly controlled by physical properties such as viscosity and those included in We_{apr}. These physical properties affected fuel atomization, which in turn impacted φ_{LBO}. For the range of $\Delta P/P$, ΔP_{noz} was found to be between 48 and 200 kPa. Lefebvre [3] calls out 100 kPa being the minimum ΔP_{noz} required to produce a cone-shaped spray in pressure-swirl nozzles like the one used in this study. This value was not reached for most fuels with $\Delta P/P$ below 3.5%, because the fuel mass flow was low enough that the spray was most likely tulip or onion-shaped rather than a conical sheet, meaning physical properties strongly influenced the LBO limit Interestingly, DCN was also observed to have measurable impact at 2% $\Delta P/P$. However, it is not near the collective impact that We_{apr} and μ have at low $\Delta P/P$, allowing low $\Delta P/P$ to be considered physical property-dominated.

At higher $\Delta P/P$, fuel chemical property influence is observed (Figure 4a) where DCN is the most important property, followed by molecular weight (MW) and We_{apr}. The improved atomization at higher $\Delta P/P$ caused physical properties to have a lesser impact on fuel performance once the 100kPa ΔP_{noz} atomization threshold was surpassed. With comparable atomization characteristics between the fuels, regardless of physical properties, fuel chemical properties evidently impact the LBO limit.

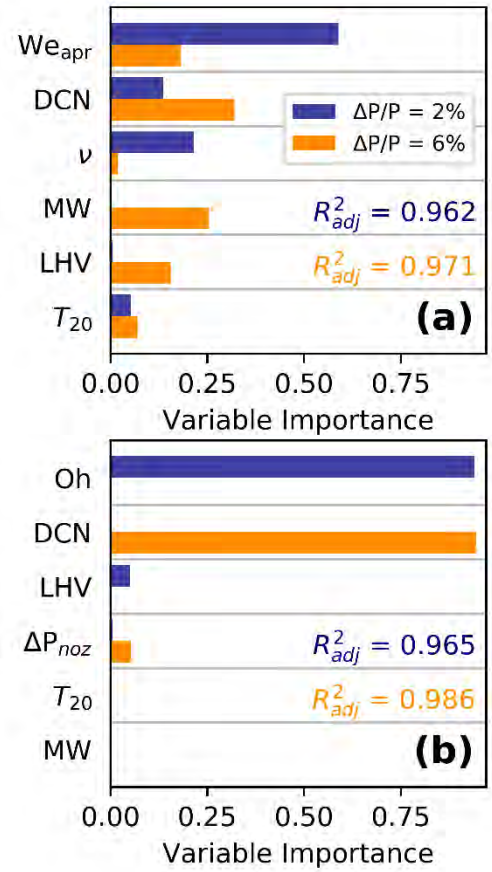

Figure 4. (a) The random forest regression including approximated Weber Number for ΔP/P of 2% and 6%, and (b) random forest results for ΔP/P of 2% and 6% for Ohnesorge number. The Ohnesorge regression results show higher adjusted R2 values than the approximated Weber number.

As shown in Figure 4, the Ohnesorge number clearly illustrates the transition from physical to chemical property dependency with increasing ΔP/P. In Fig. 4b, at 2% ΔP/P, the Ohnesorge number, which considers only physical properties, is observed to be the most important parameter. Because of the low ΔP/P, atomization will be poor, allowing physical properties to dominate LBO performance. In contrast, at 6% ΔP/P, the Ohnesorge has no impact on LBO due to improved atomization, thus, transition to a DCN dominated effect.

Fuel and air temperature was varied at constant ΔP/P=3.5% to examine potential physical-to-chemical transitions via temperature impacts (Figure 5). The fuel performance variance over the temperature range reported here was modest compared to previous studies [27]. Experimental limitations at this configuration required temperatures below 360K. To first order, φ_{LBO} decreased with increasing temperatures, as all break-up and vaporization rates increased at higher temperatures. While most of the fuels were closely grouped, C-3 did not overlap with any of the other fuels, most likely due to its higher viscosity and relatively high distillation temperatures. Together, these properties would account for poorer atomization and vaporization, which led to worse LBO performance for C-3. The φ_{LBO} for C-1 was unaffected by increases in temperature from 34 –355K, which suggests a transition to chemical property transition. Conversely, fuels A-2 and C-7 continued to have a decreased φ_{LBO} at similar conditions. The effect of fuel l and air temperature on the C-3 φ_{LBO} was more pronounced than for the other fuels as evident by its steeper slope.

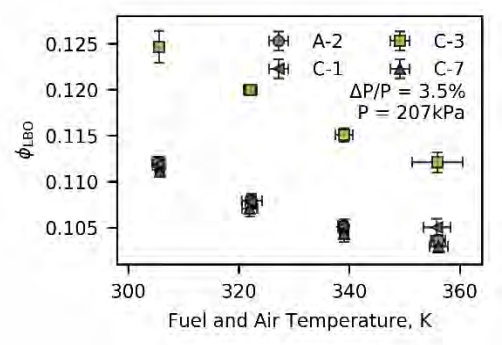

Figure 5. Impact of varying fuel and air temperature on equivalence ratio.

Conclusion

LBO experiments were conducted in a single-cup swirl-stabilized combustor (Referee Combustor) to study the impacts of fuel chemical and physical properties under varying pressure drops across the dome and at varying fuel and air temperatures. The Referee Combustor was designed with turbine engine OEMs input to simulate key characteristics of actual turbine engine combustors. LBO has previously been found to correlate with chemical properties (i.e. DCN) at relatively high air and fuel temperatures and pressures, while at low fuel and air temperatures and pressures LBO correlates most strongly with physical properties such as viscosity.

Results showed that LBO performance (φ_{LBO}) responded non-monotonically to fuel properties and to combustor ΔP/P, and the relative performance of the fuels was found to change with varying ΔP/P. At lower combustor ΔP/P, LBO dependence on physical properties due to poorer fuel atomization was demonstrated. At higher ΔP/P the trends appear to shift to LBO performance being impacted by chemical properties (i.e., DCN). The changeover from physical to chemical property dependence was found to be a range rather than a single temperature or ΔP/P point. Random forest regression analysis using dimensionless parameters demonstrated that an approximate Weber Number and Ohnesorge number were the most influential parameters at low ΔP/P, while DCN was the most impactful property at high ΔP/P.

References

[1] M. Colket, J. Heyne, M. Rumizen, et al., Overview of the National Jet Fuels Combustion Program, AIAA Journal 55 (4) (2016) 1087-1104.
[2] N. Papanikolaou, I. Wierzba, Effect of Burner Geometry on the Blowout Limits of Jet Diffusion Flames in a Co-Flowing Oxidizing Stream. J. Energy Resour. Technol. 118 (2) (1996) 134–139.
[3] A.H. Lefebvre, D.R. Ballal, Gas Turbine Combustion: Alternative Fuels and Emissions, CRC Press Taylor & Francis Group, Boca Raton, Fl., U.S.A., 2010, p. 221-240.
[4] M.D. Durbin, D.R. Ballal, Studies of Lean Blowout in a Step Swirl Combustor. J. Eng. for Gas Turbines Power 118 (1) (1994) 1–8.
[5] C. Liu, F. Liu, J. Yang, et al., Experimental Investigation of Spray and Combustion Performances of a Fuel-Staged Low Emission Combustor: Effects of Main Swirl Angle, J Eng. Gas Turbines Power 139 (12) (2017) 1–10.
[6] J.F. Bourgouin, J. Moeck, D. Durox, et al., Sensitivity of swirling flows to small changes in the swirler geometry. Comptes Rendus - Mec 341 (1) (2013) 211–219.
[7] A. Ateshkadi, V.G. McDonell, G.S. Samuelsen, Lean blowout model for a spray-fired swirl-stabilized combustor, Proc. Combust. Inst. 28 (2007) 1281-1288.
[8] A. Ateshkadi, V.G. Mcdonell VG, G.S. Samuelsen, Effect of mixer geometry on fuel spray distribution, emissions and stability, American Institute of Aeronautics and Astronautics, 1998.
[9] A.H. Lefebvre. Fuel Effects on Gas Turbine Combustion, Report No. AFWAL-TR-83-2004, Air Force Wright Aeronautical Laboratories, 1983.
[10] J.W. Blust, D.R. Ballal, G.J. Sturgess, Fuel Effects on Lean Blowout and Emissions from a Well-Stirred Reactor, J. Propuls. Power 15 (2) 1999 216–223.
[11] Q. Zhang, D.R. Noble, A. Meyers, K. Xu, T. Lieuwen, Characterization of Fuel Composition Effects in H2/CO/CH4, Turbo Expo (2) (2005) 657–668.
[12] L. Esclapez, P.C. Ma, E. Mayhew, et al., Fuel effects on lean blow-out in a realistic gas turbine combustor. Combust. Flame 181 (2017) 82–99.

[13] J.T. Edwards, Reference Jet Fuels for Combustion Testing, American Institute of Aeronautics and Astronautics, 2017.
[14] V. Burger. The Influence of Fuel Properties on Threshold Combustion in Aviation Gas Turbine Engines, PhD thesis, University of Cape Town, Cape Town, South Africa, 2017.
[15] S.L. Plee, A.M. Mellor, Characteristic Time Correlation for Lean Blowoff of Bluff-Body-Stabilized Flames, Combust. Flame 35 (1979) 61-80.
[16] A.M. Mellor. Semi-Emperical Correlations for Gas Turbine Emissions, Ignition, and Flame Stabilization, Prog. Energy Combust. Sci. 6 (4) (1980) 347–538.
[17] E.E. Peiffer, J.S. Heyne, M. Colket, Sustainable Aviation Fuels Approval Streamlining: Auxiliary Power Unit Lean Blowout Testing, AIAA J 57 (11) (2019) 1–9.
[18] E.E. Peiffer, J.S. Heyne. Characteristic Timescales for Lean Blowout of Alternative Jet Fuels in Four Combustor Rigs, AIAA Prop. Eng. Forum, 2018.
[19] S.D. Stouffer, T.H. Hendershott, J.R. Monfort, et al., Lean Blowout and Ignition Characteristics of Conventional and Surrogate Fuels Measured in a Swirl Stabilized Combustor, American Institute of Aeronautics and Astronautics, 2017.
[20] A.J. Bokhart, D. Shin, N.S. Rodrigues, et al., Spray Characteristics of a Hybrid Airblast Pressure-Swirl Atomizer at Near Lean Blowout Conditions using Phase Doppler Anemometry, American Institute of Aeronautics and Astronautics, 2018.
[21] T.H. Hendershott, S.D. Stouffer, J.R. Monfort, et al., Ignition of Convectional and Alternative Fuels at Low Temperatures in a Single-Cup Swirl-Stabilized Combustor, American Institute of Aeronautics and Astronautics, 2018.
[22] E. Corporan, R. Casselberry, M. Wagner, et al., Fuel Effects on the Lean Operational Limits of a T63 Turboshaft Engine, American Institute of Aeronautics and Astronautics, 2019.
[23] X.F. Wang, A.H. Lefebvre, Influence of Fuel Temperature on Atomization Performance of Pressure-Swirl Atomizers, J. Propuls. Power 4 (3) (1988) 222-227.
[24] J.S. Heyne, N. Glenn, J.T. Edwards, et al., Year 2 of the National Jet Fuels Combustion Program: Moving Towards a Streamlined Alternative Jet Fuels Qualification and Certification Process, American Institute of Aeronautics and Astronautics, 2017.
[25] J.S. Heyne, E.E. Peiffer, M. Colket, et al., Year 3 of the National Jet Fuels Combustion Program: Practical and Scientific Impacts, American Institute of Aeronautics and Astronautics, 2018.
[26] K. Seefeld and E. Liner, Statistics Using R with Biological Examples, University of New Hampshire (2007), Chap. 13.
[26] T. Hastie, R. Tibshirani, J. Friedman, The Elements of Statistical Learning, Data Mining, Inference, and Prediction, Stanford, California: 2008, p. 587-603.
[27] J.G. Colborn, J.S. Heyne, T.H. Hendershott, et al., Fuel and Operating Condition Effects on Lean Blowout in a Swirl-Stabilized Single-Cup Combustor, American Institute of Aeronautics and Astronautics, 2020.
[28] G. Biau and E. Scornet, "A Random Forest Guided Tour," TEST 25 (2016) 197-227.

Milestones

Chemical and physical effects on LBO at various temperature was determined.

Major Accomplishments

Reported the LBO results at various temperature for various fuels.

Publications

Peer-reviewed journal publications

Colborn JG, Heyne JS, Stouffer SD, Hendershott TH, Corporan E. (2021) Chemical and physical effects on lean blowout in a swirl-stabilized single-cup combustor. Proc Combust Inst 38(4), 6309-6316. https://doi.org/10.1016/j.proci.2020.06.119

Student Involvement

Jen Colborn, graduate research assistant, led this effort.

Task 11 - Investigation of Alternative Jet Fuel Dependencies Between Combustors of Different Size and Mixing Approaches

University of Dayton

Objective

The objective of this task is to investigate alternative jet fuel dependencies between combustors of different sizes and mixing approaches.

Research Approach

1. Introduction

As global fuel demand increases, various environmental, economic, and security interests have led to the investigation of SAFs for broader use. Due to differences in composition between SAFs and petroleum-derived fuels, SAFs must undergo a certification and qualification process before being deployed. The process for SAF qualification, known as ASTM D4054, focuses on developing "drop-in" hydrocarbon fuels, meaning that no changes need to be made to engine, aircraft, or airport infrastructure for a fuel to be compatible. Unless a candidate fuel qualifies for fast-track approval, this evaluation is an extensive process that takes years to complete, millions of dollars, and thousands of gallons of fuel (Oldani [1]). As shown in Figure 1, the approval process for non-fast-track jet fuel qualification involves four levels of testing as well as two stages of research reports with comprehensive stakeholder review. Fuel is first tested for general specifications and fit-for-purpose properties before the Phase 1 report is released to the stakeholders, who then complete a technical review of the data before the fuel can proceed to Tier 3 and Tier 4 testing. Both rig and engine testing are then conducted in Tiers 3 and 4. The amount of fuel required for testing increases about 10-fold with every tier in the qualification process.

A renewable jet fuel called RediJet, which was produced through catalytic hydrothermolysis, was recently submitted to ASTM subcommittee J for aviation fuels for approval. According to Coppola [2] , approximately 72,000 gallons of RediJet was required to complete the test plan. Component and rig tests were performed by three different engine manufacturers across nine different test conditions. Engine testing was completed by two engine manufacturers and included a flight test with a twin-engine Falcon 20. Three fuel mixtures were used for each test condition: neat Jet A as a baseline, neat RediJet, and a 50:50 blend. Overall, 144,000 gallons of jet fuel were used for full qualification of the new "drop-in" SAF. Reducing the volume of fuel required for the qualification process would be advantageous for both fuel manufacturers and the sponsors who have a vested interest in SAF.

The aim of the NJFCP was to shorten and redirect the process for jet fuel qualification (Colket et al. [3]). By developing predictive models for fuel behavior and adding some tailored, low-volume testing prior to the phase I research report, additional feedback would be provided to the ASTM evaluation committee and fuel manufacturers to guide early fuel development. The scope of tier 3 and tier 4 testing could then be directed toward a narrower range of potential concerns, thereby reducing the total amount of fuel required. Alternatively, the candidate fuel could be reformulated into a product that has a higher probability of achieving qualification. Importantly, there is a need to understand how fuel effects in small-scale rigs compare with engine observations. Validating small-scale rigs against full-scale engines is also essential for developing predictive models and testing methodology.

At the program level, we identified a range of operating conditions where lean blowout (LBO) or ignition is most likely to be impacted by differences in fuel composition and properties (Colket & Heyne [4]). The most sensitive LBO conditions involve (i) a throttle-chop from cruise to flight idle and (ii) a start transient where the increase in fuel flow rate may not sufficiently keep up with the increase in airflow rate if the control schedule is improperly set for the fuel being used. Fuel impacts on ignition are most important at cold conditions such as a cold-soaked auxiliary power unit (APU) at altitude or a cold-soaked main engine on the ground. Figure 2 shows operating conditions for the typical temperatures (T_{cmb}) and pressures (P_{cmb}) in the combustion chamber. In this figure, "altitude relight" and "cold start" both refer to ignition cases. These conditions were selected because they are some of the most extreme conditions that can exist within an engine and are consistent with the tests required by ASTM D4054 (Coppola [2]; Colket et al. [3]). Similar fuel dependencies have been noted for cold ground start and altitude relight (Hendershot et al. [5]; Stouffer et al. [6]).

Nine experimental rigs within the NJFCP, featuring a wide range of geometries and time scales, were used to observe fuel effects (Colket & Heyne, 2021). As shown in Figure 3, eight of the nine rigs showed a correlation between the derived cetane

number (DCN) and the relative equivalence ratio at LBO (Φ_i). The parameter Φ_i is defined as the LBO performance of fuel (i) relative to the LBO performance of the reference fuel (A2) and is expressed as a percentage (see Equation 1).

$$\Phi_i = \frac{\phi_i - \phi_{A2}}{\phi_{A2}} \quad (1)$$

The only rig that did not show a correlation between DCN and Φ_i was the Honeywell 131-9 APU combustor rig (APU-CR), one of the two industry combustors used in the program. This result appears to be incongruent with the goal of the NJFCP; namely, to reduce tier 3 or tier 4 testing. However, closer examination of results from both the Referee Rig (RR) and a GE9X full annular combustor rig (GE9X-FAR) showed that fuel dependencies vary with operating conditions.

Colborn et al. [7] showed that the relative LBO in the RR at an air temperature and pressure of 65 °C and 107 kPa, respectively, is dominated by the Ohnesorge number (Oh) at 2% DP/P. In contrast, the DCN dominates at 6% DP/P, with a smooth transition from one extreme to the other. At 3.5% DP/P and 107 kPa, the fuel with the lowest DCN and most favorable atomization properties (hereafter labeled as C1) showed no sensitivity to air temperature between 65 °C and 83 °C. Boehm et al. [8] found this same fuel (C1) had measurably worse LBO performance in a GE9X combustor than the other three fuels tested at three of their four test conditions. At a lower air temperature, C1 showed the same LBO performance as the reference petroleum-derived fuel when the two fuels were heated to 60 °C, which was the reference fuel temperature for this set of tests. These results are summarized in Figure 4. Overall, the data suggest that the physical and chemical properties of the fuel are both important near the low-temperature boundary of the GE9X engine operating range at conditions important to the aircraft engine LBO margin, whereas only chemical properties are important at higher air temperatures and loadings.

In this report, we show that the results introduced above are consistent with LBO theory (Plee & Mellor [9]; Mellor [10]) and that the RR, in concert with a well-thought-out test plan, can show the same fuel dependencies as the APU-CR and the GE9X-FAR. The timescales of evaporation and chemical reactions are impacted significantly by fuel and air temperature, suggesting that the range of operating conditions being tested is critical to a thorough investigation of fuel dependencies. We assert that commercial combustor geometry does not need to be matched with specific operating conditions if the test combustor is tested over a sufficiently wide range of operating conditions to sweep through the range of timescale ratios that are relevant to commercial combustor operability.

2. Background

2.1 Previous work

Several investigations of how fuel affects LBO have already been completed. For example, Rock et al. [11] measured the LBO threshold in an un-cooled flame tube using 18 different fuels and three different inlet air temperatures. They noted a correlation to DCN, T10, T90, or surface tension, dependent depending on the inlet air temperature. Using the same set of 18 fuels, Casselberry et al. [12] demonstrated a correlation between pyrolysis products at 625 °C and the LBO threshold in the RR when the RR was operated at chop-like (warm) conditions. Won et al. [13] investigated the role of preferential vaporization and suggested that the DCN of the front end of the distillation may be a better indicator of LBO than the DCN of the fully vaporized fuel. They also observed that LBO is more strongly correlated with fuel physical properties than with fuel chemistry at low temperature operation. Grohmann et al. [14] similarly observed that both physical and chemical properties of a fuel influence combustor LBO. In a study of the effects of atomization, Muthuselvan et al. [15] related atomization quality with timescales relevant to LBO.

Many experiments and analyses of the ignition characteristics of hydrocarbon fuels have focused on either pre-vaporized and premixed fuel or other fuels and conditions that depart significantly from the most extreme start-up requirements for gas turbines used in aviation. Excellent reviews on these topics have been published by Aggarwal [16] and, more recently, by Colket and Heyne [4]. Mayhew [17] observed correlation between ignition probabilities at cold altitude relight conditions in a derivative of the RR and each of four fuel properties: viscosity, surface tension, 20% recovered temperature (T_{20}), and flash point. Opacich et al. [18] observed similar correlations within datasets derived from both the RR and the APU-CR, although they represented volatile properties using vapor pressure and heat capacity instead of T_{20} and flash point. Part of this work directly follows up on the work introduced by Opacich et al. [18].

2.2 LBO Theory

A common theme in several of the works cited above is that LBO performance can be evaluated by considering three timescales that impact LBO limits, as shown in Equation 2: chemical, mixing and evaporative timescales (Plee & Mellor, 1979; Mellor, 1980). This theory is further illustrated in Figure 5.

$$\frac{1}{\phi_{LBO}} \sim \left(\frac{1}{\tau_{chem}} + \frac{1}{\tau_{mix}} + \frac{1}{\tau_{evap}} \right)^{-1} \quad (2)$$

Fuel physical properties, along with aerodynamic shear forces, flow field, fuel nozzle design, and fuel pressure all affect fuel spray atomization, including droplet size distribution and spray distribution. While combustor design and operating conditions are important to atomization, fuel properties are also an important factor for some commercial combustors at relevant, in-service operating conditions.

Fuel vapor pressure (and/or thermal conductivity), spray characteristics, and combustor aerodynamics all influence the evaporation timescale. From the perspective of fuel dependencies on LBO, it is important to note that the evaporation timescale of some commercial combustors will be impacted significantly by vapor pressure, which varies not only with droplet surface temperature but also with the time-varying composition of the liquid fuel throughout the evaporation process. In systems that are evaporation-limited, fuels with a higher vapor pressure at a given temperature are expected to ignite more readily than fuels with a lower vapor pressure.

The mixing of fuel vapor with air depends on the flow field, turbulence intensity, and the spatial relationship between the fuel spray, the eddies within the flow field, and the flame. Because turbulence is overwhelmingly more important than laminar diffusion in most commercial combustors, there is ample technical justification for neglecting this term when considering fuel effects. Moreover, the characteristic mixing time of a given commercial combustor at any well-defined operating condition is likely to be kept proprietary by the engine companies.

The specifics of fuel-air mixing also influence the gaseous mixture residence time and reactant concentration. These two variables, along with species reactivity, determine the fuel chemistry of combustion and blowout. The chemical timescale is relevant to the physics and may be comprised of different pieces, such as autoignition and extinction.

2.3 Cold Ignition

At extremely low fuel temperatures, the fuel vapor pressure is low. When the inlet air temperature is equally low, fuel droplets are not heated until they reach a heat source, which could be either a plasma discharge or the kernel of a previously ignited fuel/air mixture. The size and spatial distribution of liquid fuel droplets within the combustor flow field at extremely cold conditions is expected to be critical for most, if not all, combustors in aviation service. Very little evaporation occurs outside of the domain of the plasma discharge (spark), and it must therefore supply enough energy to both evaporate the fuel and overcome the critical kernel radius (Kim et al., 2013). Each kernel must release enough heat to both sustain the flame and sufficiently evaporate enough surrounding liquid fuel droplets to replenish the fuel consumed by combustion within the kernel. Only under these conditions can the flame kernel grow, propagate upstream to an anchor point, and transition to a self-sustaining flame. This process can be influenced significantly by fuel volatility, thermal properties, and the physical properties that influence atomization.

2.4 Atomization

Atomization is affected by the viscosity, density, and surface tension of the fuel [(Guildenbecher et al., 2019; Lefebvre & McDonnell, 2017). Increased surface tension inhibits fuel breakup, increased viscosity dampens the instabilities that allow for breakup, and increased density drives lower flow rates in engines that are controlled to deliver a scheduled enthalpy flux or equivalence ratio. This in turn reduces the gage pressure, which supplies the energy that drives atomization.

3. Experiments, Data and Methods

3.1 Referee Rig Experiments

Experiments performed in the RR were completed at the Air Force Research Laboratory (AFRL) located at Wright-Patterson Air Force Base and have previously been published (Henderschott et al., 2018; Colborn et al., 2020). The RR is a non-proprietarty, single-cup, swirl-stabilized combustor designed by GE (this article's corresponding author) with input from four other leading engine manufacturers. The rig simulates representative aerodynamic characteristics of both legacy and emerging swirl-stabilized combustors (Colket & Heyne, 2021). It is a classic rich-quench-lean combustor with effusion-cooled liners, a flat dome protected by an impingement-cooled heat shield, primary dilution holes located at ½ the dome height downstream from the dome, and seconday dilution holes located just aft of the primary reaction zone. The rig features a modular construction to facilitate swapping of fuel injectors and swirlers, which allows researchers to evaluate different swirler effective areas, swirl numbers, spray angles and flow numbers. However, most of the data collected from the RR to date has come from just one design configuration. The AFRL modified the rig's original four-cup design to a single-cup

design, and the University of Dayton Research Institute (UDRI) custom-buillt a thryatron-based exciter to achieve better control over spark energy and frequency relative to jet engine exciters. Readers interested in fabricating a copy of this combustor should contact the authors for information on where to find a copy of the drawings.

In this study, we analyzed four operating conditions of the RR (Table 1). Fuel and air temperature were matched in each condition, and LBO was determined after each successful ignition. For all test conditions, the normalization described by Equation 1 was reset so that its value, corresponding to the fuel sample designated as A2, was always zero. This normalization reduces the dependencies on operating conditions and highlights fuel dependencies.

3.2 APU-CR Experiments

The APU-CR experiments were performed in the combustor component test facility at Honeywell Aerospace. For all experiments, the APU-CR was operated at simulated engine conditions (Culbertson & Williams [22]). APUs are small gas turbine engines used to provide power to spool-up the main engine during starter-assisted air starts. APUs are particularly sensitive to the physical properties that influence atomization and vaporization (Pfeiffer et al. [23]) because of their small volume and correspondingly low combustor residence time ($t_{cmb} = r_{air} V_{cmb} / W_{air}$). The 131-9 combustor is swirl-stabilized and relies on a rich-quench-lean combustion process, like many of the much larger, main engine combustors. A standard 131-9 ignition system was used with the igniter located at approximately the eight o'clock position of the combustor (Culbertson & Williams [22]). Readers who wish to reproduce any of the data presented in the noted publications should contact Honeywell Aerospace.

The warm ignition (T_{fuel} = 15 °C) light-off boundary was determined at a baseline air temperature (-35 °C) and pressure (1.05 atm) along with single-point derivatives to higher temperature or lower pressure, as listed in Table 1. The cold ignition (T_{fuel} = -37 °C) light-off boundary was determined at each of the conditions used for warm ignition, plus two additional points at a colder air temperature and low pressure (also listed in Table 1). The LBO data set included six operating conditions. As with the RR data, the equivalence ratios for all test conditions were normalized using Equation 1.

3.3 GE9X-FAR Experiments

The GE9X-FAR experiments were performed in the GE's combustor component test facility. The combustor was operated at simulated engine conditions; although these conditions are proprietary information, sanitized data are publicly available through reference (Boehm et al., 2020), and readers who wish to reproduce this data may contact GE. Unlike the RR and the APU-CR, the GE9X is a large combustor that achieves lean combustion for low NOx emissions using a twin annular premixing swirler. Limited details about this combustor design have been published by Dhanuka et al. [24]. The understandable restrictions around sharing proprietary test data, procedures, and combustor designs from fuel evaluation tests such as these remain one of the prime motivators behind the development of the RR.

The GE data was not available in a format appropriate for the statistical analyses used in this study. The LBO data shown in Figure 4 was normalized at the baseline operating condition using an equation like Equation 1, but it was not reset at each operating condition because dependence on operating condition was part of the story GE communicated. The un-disclosed constant denoted by 'Δ' in the axis label of Figure 4 represents the difference between the actual and displayed equivalence ratio at the reference condition, which disguises proprietary engine LBO performance. However, the original source indicates that the tested points track along a reference velocity, which scales with the log of air flow multiplied by the square of air temperature and occurs in the same order presented in Figure 4 with roughly equal spacing.

3.4 Fuel Property Data

The RR and APU-CR experiments were directly or indirectly part of the NJFCP, and the fuels used in this study were distributed to affiliated labs by a control center led by Tim Edwards at the AFRL. Dr. Edwards was also responsible for acquiring and publishing fuel property data (Edwards, [25]), which is available through the National Alternative Jet Fuels Test Database ([26]. The fuel samples designated as A1, A2, A3, C1, C2, and C5 were tested in both the RR and APU-CR, whereas the fuel samples designated as C3, C4, and C7 were only tested in the RR. The GE9X experiments were part of a different program but included one fuel (C1) provided by the AFRL. Various properties of the fuels used by GE are provided in Table 2.

The fuel densities used in the analyses of the LBO datasets were as measured at 15 °C. For analyses of the ignition datasets, all fuel properties were transformed into their respective values at the tested fuel temperature following the approach described by Opacich et al. (Opacich et al . [18). Fuel properties that were measured over a range of temperatures that bounded the tested fuel temperature (e.g., density) were interpolated to the test temperature. Temperature-dependent fuel properties that were not measured over a sufficient temperature range to warrant interpolation (e.g., vapor pressure) were determined as outlined here. First, we derived a surrogate fuel composition by matching measured fuel property data and

GCxGC-determined hydrocarbon class concentration data, using published blending rules (Flora et al. [27]) to relate molecular properties and compositions to mixture properties. Next the molecular properties over a range of temperatures were calculated based on using the models provided in the molecular properties database published by the National Institute of Standards and Technology (Kroenlein et al. [28]), and the blending rules were applied at each modeled temperature. The resulting temperature-dependent mixture properties were then curve-fitted, and those models were used to estimate the fuel properties at each tested fuel temperature.

3.5 Analysis

The previously described random forest statistical analysis (Colborn et al. [7]; Pfeiffer et al. [23]) was used for this investigation. In summary, the method uses random sampling and replacement to decrease overfitting and allows for one dependent variable (e.g. LBO or ignition performance) to be evaluated against multiple independent variables (e.g. fuel properties) (Hastie et al. [29]). Standard Monte Carlo methods were used to simulate uncertainties in each independent variable based on measurement reproducibility, as quoted in the relevant ASTM standard with an assumed Gaussian distribution. These distributions represent the uncertainty domain within the random forest method. We used the same regression approach as Peiffer et al. [18] and Opacich et al. [23]. The simulation included numerous trials to capture the full distribution of possible values within the reproducibility domain of each measured value. The relative importance values of each independent variable were recorded during each trial. Using this approach, we estimated confidence bands around each relative importance value.

One set of random forest analyses was used to assess the relative importance of atomization, evaporation rate, autoignition and extinction in each of two LBO datasets. Because none of these fundamental processes were clearly known or regressable for all the fuels used in both test articles, it was necessary to choose a set of four independent, orthogonal properties that are known to strongly correlate with each of these four fundamental processes. Primary and secondary droplet breakup at incipient LBO conditions were represented by fuel density at 15 °C. T_{20} was selected to represent the evaporation rate. Extinction was represented by the radical index (RI), and autoignition was represented by the DCN. The idea here was to compare these two analyses and assess how well one dataset (i.e., LBO in the RR at cold conditions) represents the other (i.e., LBO in the APU-CR at normal operating conditions).

A second set of random forest analyses was used to assess the relative importance of five independent variables in each of three cold ignition datasets. We represented atomization dependencies using the Ohnesorge Number, which combines dynamic viscosity (μ), density, surface tension (σ), and the nozzle diameter, *D*, into a single dimensionless parameter (Equation 3):

$$Oh = \frac{\mu(T)}{[\rho(T)\sigma(T)D]^{0.5}} \quad (3)$$

Fuel dependency on the evaporation rate was represented by vapor pressure, and fuel dependency on droplet heating was represented by specific heat. The definition of the dependent variable, representing ignition performance, was somewhat different between the RR dataset and the APU-CR datasets. In the APU-CR datasets, the ignition variable was defined by the minimum equivalence ratio required to achieve ignition within a Honeywell-standard duration of time, during which the ignitor is firing periodically as it would in a commercial APU. In the RR dataset, the ignition variable was defined by the equivalence ratio corresponding to a 10% ignition probability per spark along a binomial regression fitted curve to the equivalence ratio and light/no-light data corresponding to each spark. Details of this binomial regression have been published by Hendershot et al. (2018).

4. Results

4.1 LBO Results

Although several laboratory rigs showed a strong correlation between LBO and the DCN (Figure 3), the APU-CR did not. Instead, it showed a strong correlation to physical and volatility properties such as viscosity (ν), and 20% recovered temperature (T_{20}) as shown in Figure 6. At cold conditions, in contrast to the results at warm conditions, the RR also showed a correlation to physical and volatility properties, but not the DCN. Due to the relatively low fuel temperatures at cold start, temperature-dependent physical properties such as density, viscosity, and surface tension trend higher, which is detrimental to fuel atomization. In addition, vapor pressure trends lower, which is detrimental to evaporation. It is therefore not surprising that the effects of such properties would be more observable at these conditions. In essence, the cold temperature

in the cold LBO experiments with the RR serves to prolong the time scale of the physical processes necessary for combustion (namely, evaporation) and drive this time scale closer to the combustor residence time.

Main effects plots of Φ versus fuel properties, shown in Figure 6, suggest that both the RR and the APU-CR show a correlation between Φ and fuel physical properties when the time scale of evaporation is on the same order as the combustor residence time. To further analyze this fuel property dependency, we repeated a random forest statistical analysis 100 times. The results of the random forest analyses are summarized in Figure 7.

Overall, three important results were observed from the random forest analysis. First, each rig showed nearly the same relative importance of T_{20} (representing evaporation rate) and density (representing atomization) on LBO, which suggests that the RR, when operated at cold conditions, adequately represents the relevant physics that largely determine LBO performance in the APU-CR operated at representative engine conditions. Second, the fuel properties that influence evaporation rate are clearly more important than those that correlate strongly with chemical reactivity. This result suggests that the LBO performance of the RR and APU-CR, as operated in these tests, is affected by evaporation more than chemical reactivity. Data collected in this way should therefore be used to evaluate the impact of variation in fuel physical properties, not fuel chemistry, on LBO. Third, the relative importance of the DCN and RI at these conditions was not equal between the RR and the APU-CR, which suggests that the RR is not a good surrogate for the APU-CR in this context. However, that is not a requirement because the LBO performance in the APU-CR is not determined by the DCN or RI. In contrast, the LBO performance of the GE9X-FAR was more strongly determined by the fuel chemical properties. A useful surrogate laboratory combustor for the GE9X-FAR should therefore produce similar relative importance values for influential fuel chemical properties.

With respect to the data from the GE9X-FAR, Table 2 documents the notable differences between the petroleum-derived reference fuel and the SAF blend component (designated as C1). Sample C1 is 6.3% lighter, has 1.7% higher specific energy, and has a much lower DCN than the reference fuel. The lower density and higher specific energy of C1 are expected to push LBO toward a lower (and more favorable) Φ_{C1}. The lower density leads to a higher volumetric flow rate, which leads to higher fuel pressure and, consequently, finer atomization, whereas the higher LHV leads to a higher flame temperature for a given equivalence ratio. Conversely, the lower DCN of C1 is expected to lead to a higher (i.e., less favorable) Φ_{C1} based on the empirical trends shown in Figure 3. The data shows higher Φ_{C1} at three of the four test conditions, which is consistent with the much lower DCN of C1 relative to the reference fuel. However, at the lowest air temperatures that were tested, Φ_{C1} and Φ_{Ref} were essentially the same, presumably because the favorable density and specific energy of C1 compensate for its unfavorable DCN.

GE also provided LBO data for Jet A fuel at two different temperatures. Although these two tests did not employ fuel from a quarantined tank dedicated for such tests, the commercial jet fuel was acquired from the same supplier, and we therefore assumed that the properties of the two fuels are comparable. The colder fuel had higher density, viscosity, and surface tension and lower initial vapor pressure, but the chemical properties of the fuel vapor were the same. These differences in physical properties were reflected in the data: at the lowest air temperatures, $\Phi_{Ref,32C}$ was higher than $\Phi_{Ref,60C}$. At the three conditions where C1 showed measurably worse LBO performance than the reference fuel, the colder reference fuel performed as well as the warmer reference fuel. Together, these trends suggest that the LBO phenomenon in the GE9X-FAR is governed by fuel chemistry at three of the four test conditions, but evaporation becomes important when the air temperature is reduced. The two SAF fuels that were partially derived from hydrogenated esters and fatty acids (HEFA) showed similar results to each other at all conditions and outperformed the reference fuel at the lowest-temperature test condition, as expected based on their lower viscosity and density relative to the reference fuel.

4.2 Ignition Results

Main effects plots of Φ versus fuel properties, shown in Figure 8, suggest that both the RR and APU-CR showed a correlation between Φ and both fuel physical properties (viscosity) and volatile properties (T_{20}). To further analyze this property dependency, we performed a random forest statistical analysis with 2,000 iterations. Figure 9 provides a summary of the random forest results. As noted in section 3.1, $Oh(T_{fuel})$, $C_p(T_{fuel})$ and $P_{vap}(T_{fuel})$ were used to represent atomization, droplet heating, and droplet evaporation rate, respectively, for the random forest analyses.

The three fuel properties we selected were of similar importance in the RR at cold conditions and in the APU-CR at both cold and warm conditions. Each property accounted for about 27% of the observed variation in ignition performance. The random forest analysis suggested that 4-5% of the observed variation in ignition performance within each of the three datasets could be attributed to variation in combustor air temperature and pressure, and the remaining ten percent of the variation could not be accounted for.

Ideally, the ignition performance data would be normalized, and the datasets would be selected in such a way as to remove all dependencies on combustor operating conditions. However, data are collected prior to the analysis, and pre-test predictions are not yet capable of informing the researchers with enough information to make this possible. Moreover, the highly non-linear dependencies of ignition performance on operating conditions are difficult to completely obscure using any straightforward normalization. Although the unexplained variation in our results (~10% for each dataset) is not as low as some may like it to be, it is nevertheless excellent for a one-dimensional ignition model that does not resort to overfitting. Machine learning analyses, such as the random forest regressions used here, could be integrated with a physical two- or three-dimensional model, but further development of such an approach is still needed.

Overall, the main result of our ignition analysis is that the fuel property dependencies within each of the three datasets are nearly the same, which suggests that a small, standardized set of test articles can be used to characterize fuel dependencies on ignition within the industry-wide fleet of combustors. This result has important practical implications for the evaluation of potential SAFs. From a more fundamental perspective, our observation that two fuel properties were required to account for the evaporation timescale suggests a need for more detailed data relating to fundamental heat and mass transfer processes within the intersecting region of cold fuel droplets and plasmas or pre-existing flame kernels. Such data could lead to an even better understanding of the fundamental processes that govern fuel property dependencies on kernel initiation and growth.

5. Conclusion

In this study, we suggested that combustor operating conditions can be used to vary the relative importance of the evaporation, chemical, and mixing timescales that are characteristics of combustion phenomena. By adjusting the operating conditions of the LBO experiments the ratio of the evaporation time to residence time can be matched. For example, we demonstrated that the RR, when operated at cold fuel and air conditions, exhibits the same fuel property dependencies on LBO (i.e., density and the 20% recovered temperature) as the APU-CR at normal operating conditions in spite of large difference in residence time between these two combustors. Furthermore, when operated at representative flight idle conditions, the RR exhibits the same LBO dependencies on fuel properties (i.e., DCN) as the GE9X-FAR at similar operating conditions. We additionally observed that when the GE9X-FAR is operated at lower temperatures, the LBO phenomenon is governed by a combination of chemical and physical fuel properties rather than by the DCN. This result is consistent with previous work in the RR [7] exploring the transition in operating condition space between evaporation- and chemistry-governed LBO.

Analysis of data from cold ignition in the RR and both standard-day and cold ignition in the APU-CR, shows that the Ohnesorge number (which represents atomization), specific heat (which represents heat absorption from a nearby plasma or flame kernel into a fuel droplet), and vapor pressure (which represents evaporation from the surface of a droplet that has been transported into the path of the plasma or flame kernel) were all equally important to the ignition phenomenon. This was true, independent of the large differences in combustor cup volume between the RR and APU-CR and in the operating conditions being tested.

Collectively, our data indicate that results from the RR are strongly correlated to those from real engines in tests designed to gage the fuel dependencies of combustor operability. The RR therefore shows potential as a standard, laboratory-scale test article for representing swirl-stabilized combustors in the ASTM fuel evaluation process for SAFs.

References

1. Oldani, A. (2020). FAA ASCENT & clearinghouse programs [Presentation]. PNNL HTL Workshop, Pacific Northwest National Laboratory
2. Coppola, E. N. (2018). CHJ pathway readijet renewable jet fuel produced by catalytic hydrothermolysis (CH) [Presentation]. ASTM Committee D02 on Petroleum Products and Lubricants, Subcommittee D02.J0.06 on Emerging Turbine Fuels.
3. Colket, M., Heyne, J. Rumizen, M., Gupta, M., Edwards, T., Roquemore, W. M., Andac, G., Boehm, R., Lovett, J., Williams, R., Condevaux, J., Turner, D., Rizk, N., Tishkoff, J., Li, C., Moder, J., Friend, D., & Sankaran, V. (2017). Overview of the national jet fuels combustion program. AIAA Journal, *55*(4), 1087-1104.
4. Colket, M., & Heyne, J. (2021). *Fuel effects on operability of aircraft gas turbine combustors*. Manuscript submitted for publication.
5. Hendershott, T. H., Stouffer, S., Monfort, J. R., Diemer, J., Busby, K., Corporan, E., et al. (2018). Ignition of Conventional and Alternative Fuels at Low Temperatures in a Single-Cup Swirl-Stabilized Combustor [Presentation]. AIAA Aerospace Sciences Meeting. Kissimmee, FL.

6. Stouffer S D, Hendershott T H, Colborn J, Monfort J R, Corporan E, Wrzesinski P, et al. Fuel Effects on Altitude Relight Performance of a Swirl Cup Combustor. In: AIAA Scitech 2020 Forum. Orlando, Florida; 2020.
7. Colborn, J. G., Heyne, J. S., Stouffer, S. D., Hendershott, T. H., & Corporan, E. (2020). Chemical and physical effects on lean blowout in a swirl-stabilized single-cup combustor. Proceedings of the Combustion Institute, *38*(4), 6309–6316.
8. Boehm, R., Thomsen, D. D., & Andac, M. G. (2020). GE-Aviation program update [Public plenary presentation], FAA CLEEN II Consortium.
9. Plee, S. L., & Mellor, A. M. (1979). Characteristic time correlation for lean blowoff of bluff-body-stabilized flames. Combustion and Flame, *35*, 61–80.
10. Mellor, A. M. (1980). Semi-empirical correlations for gas turbine emissions, ignition, and flame stabilization. Progress in Energy and Combustion Science, *6*(4), 347–58.
11. Rock, N., Chterev, I., Emerson, B., Won, S. H., Seitzman, J., & Lieuwen, T. (2019). Liquid fuel property effects on lean blowout in an aircraft relevant combustor. Journal of Engineering for Gas Turbines and Power, *141*(7).
12. Casselberry, R. Q., Corporan, E., & DeWitt, M. J. (2019). Correlation of combustor lean blowout performance to supercritical pyrolysis products. Fuel, *252*, 504–511.
13. Won, S. H., Rock, N., Lim, S. J., Nates, S., Carpenter, D., Emerson, B., et al. (2019). Preferential vaporization impacts on lean blow-out of liquid fueled combustors. Combustion and Flame, *205*, 295–304.
14. Grohmann, J., Rauch, B., Kathrotia, T., Meier, W., & Aigner, M. (2018). Influence of single-component fuels on gas-turbine model combustor lean blowout. Journal of Propulsion and Power, 97–107. 10.2514/1.B36456
15. Muthuselvan, G., Suryanarayana, R. M., Iyengar, V. S., Pulumathi, M., Thirumalachari, S., & Srinivasan, K. (2020). Effect of atomization quality on lean blow-out limits and acoustic oscillations in a swirl stabilized burner. Combustion Science and Technology, *192*(6), 1028–1052. https://doi.org/10.1080/00102202.2019.1607846
16. Aggarwal, S. K. (1998). A review of spray ignition phenomena: Present status and future research. Progress in Energy and Combustion Science, *24*(6), 565–600.
17. Mayhew, E. K. Impact of alternative jet fuels on gas turbine combustion systems [Ph.D. thesis, University of Illinois at Urbana-Champaign]. IDEALS. https://www.ideals.illinois.edu/handle/2142/101653
18. Opacich, K. C., Peiffer, E., & Heyne, J. S. (2019, January 1-10). Analyzing the relative impact of spray and volatile fuel properties on gas turbine combustor ignition in multiple rig geometries [Presentation]. AIAA Scitech 2019 Forum, San Diego, CA.
19. Kim, H. H., Won, S. H., Santner, J., Chen, Z., & Ju, Y. (2013). Measurements of the critical initiation radius and unsteady propagation of n-decane/air premixed flames. Proceedings of the Combustion Institute, *34*(1), 929–936. https://doi.org/10.1016/j.proci.2012.07.035
20. Guildenbecher, D. R., López-Rivera, C., & Sojka, P. E. (2009). Secondary atomization. Experiments in Fluids, *46*(3), 371–402. https://doi.org/10.1007/s00348-008-0593-2
21. Lefebvre, A. H, & McDonell, V. G. (2017). Atomization and sprays (2nd ed.) [Internet]. CRC Press Taylor & Francis Group.
22. Culbertson, B., & Williams, R. (2017). Alternative aviation fuels for use in military APUs and engines: Versatile affordable advanced turbine engine (VAATE), Phase II and III (Report No. 0007 : AFRL-RQ-WP-TR-2017-0047). Honeywell International, Inc.
23. Peiffer, E. E., Heyne, J. S., & Colket, M. (2019). Sustainable aviation fuels approval streamlining: Auxiliary power unit lean blowout testing. AIAA Journal, *57*(11), 4854–4862. https://doi.org/10.2514/1.j058348
24. Dhanuka, S. K., Temme, J. E., & Driscoll, J. F. (2011). Unsteady aspects of lean premixed prevaporized gas turbine combustors: Flame-flame interactions. Journal of Propulsion and Power, *27*(3), 631–641. https://doi.org/10.2514/1.B34001
25. Edwards, J. T. (2017). Reference jet fuels for combustion testing [Presentation]. 55th AIAA Aerospace Sciences Meeting. Grapevine, TX.
26. Home | AJF:TD | U of I [Internet]. [cited 2021 Jun 5].
27. Flora, G., Kosir, S., Behnke, L., Stachler, R., Heyne J, Zabarnick S, & Gupta, M. Properties calculator and optimization for drop-in alternative jet fuel blends [Presentation]. AIAA Scitech 2019 Forum. https://doi.org/10.2514/6.2019-2368
28. Kroenlein, K., Muzny, C., Kazakov, A., Diky, V., Chirico, R., & Magee, J. (2019). *NIST standard reference 203: TRC web thermo tables (WTT)* [Internet]. National Institutes of Standards and Technology.
29. Hastie, T., Tibshirani, R., & Friedman, J. (2008). *The elements of statistical learning, data mining, inference, and prediction* (2nd ed.). Stanford University.

Figures and Tables

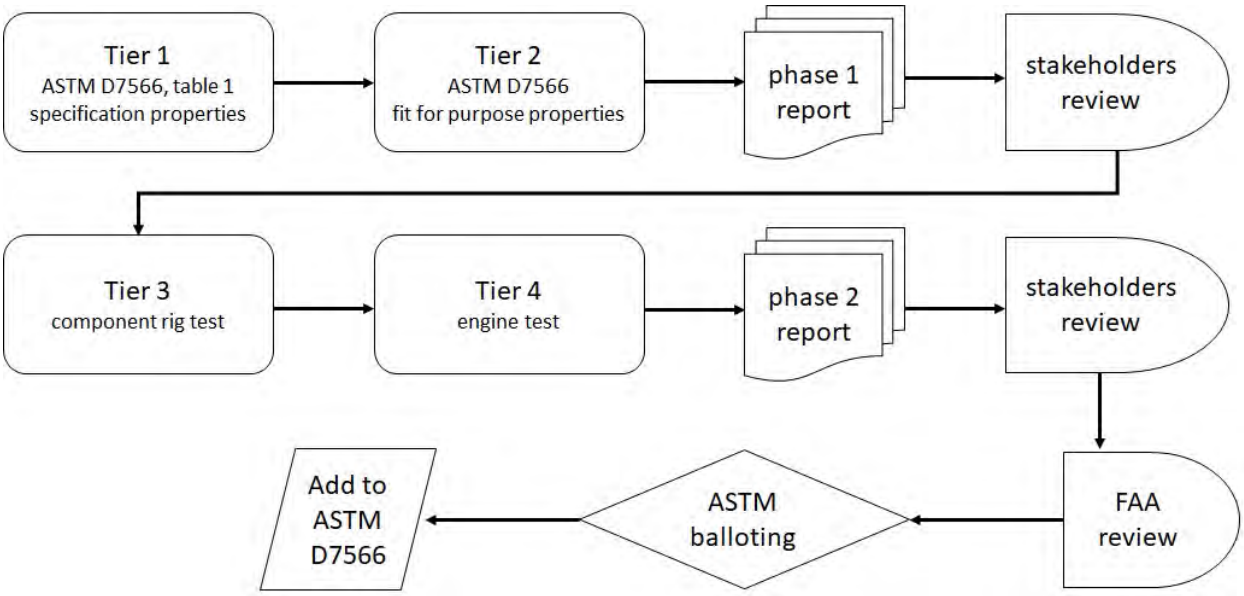

Figure 1. ASTM D4054 fuel evaluation process.

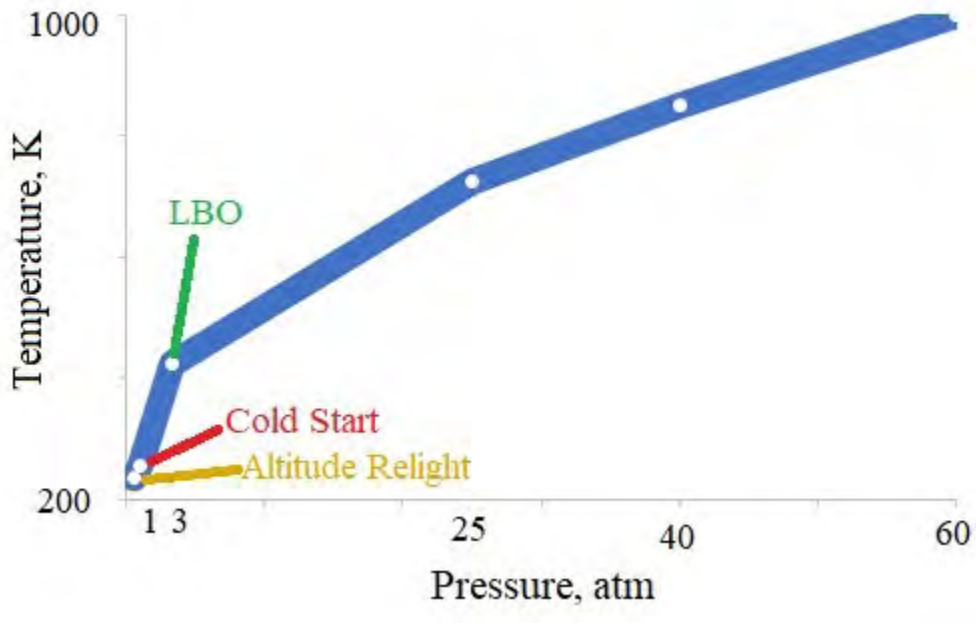

Figure 2. Visual representation of operating conditions relevant to combustion figures of merit.

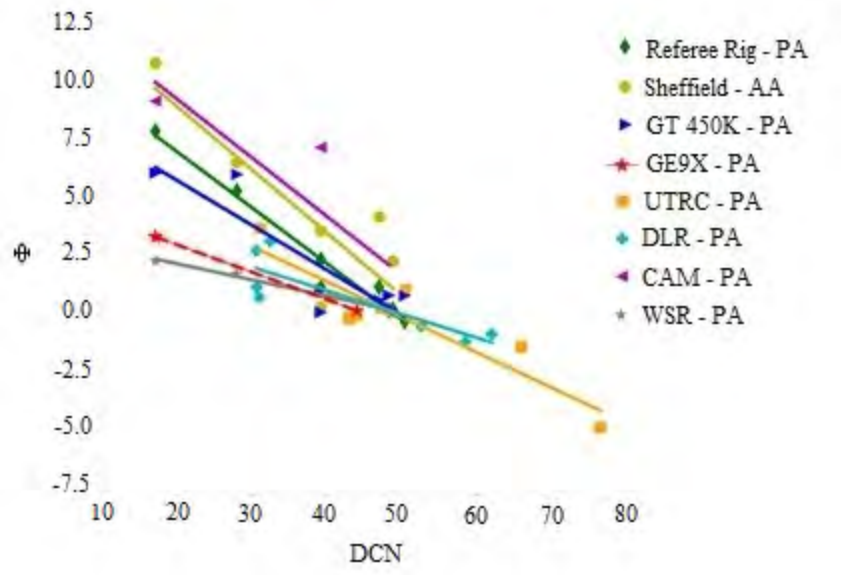

Figure 3. Lean blowout limit as a function of derived cetane number (DCN) for eight different rigs used within the National Jet Fuels Combustion Program.

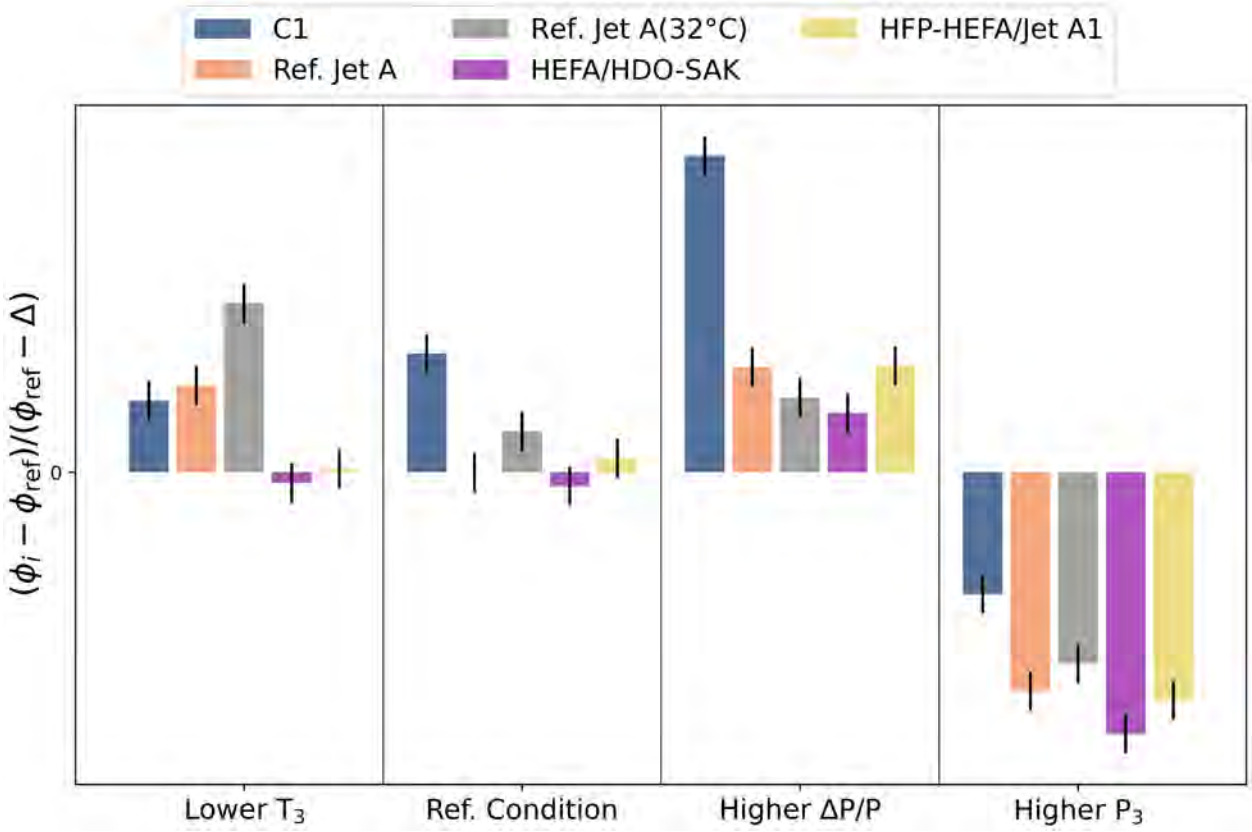

Figure 4. Relative lean blowout at four operating conditions in the GE9X full annular combustor rig. This figure was redrawn using data that was digitally extracted from the GE report to the FAA, which was part of the CLEEN II Consortium Program Update Public Plenary.

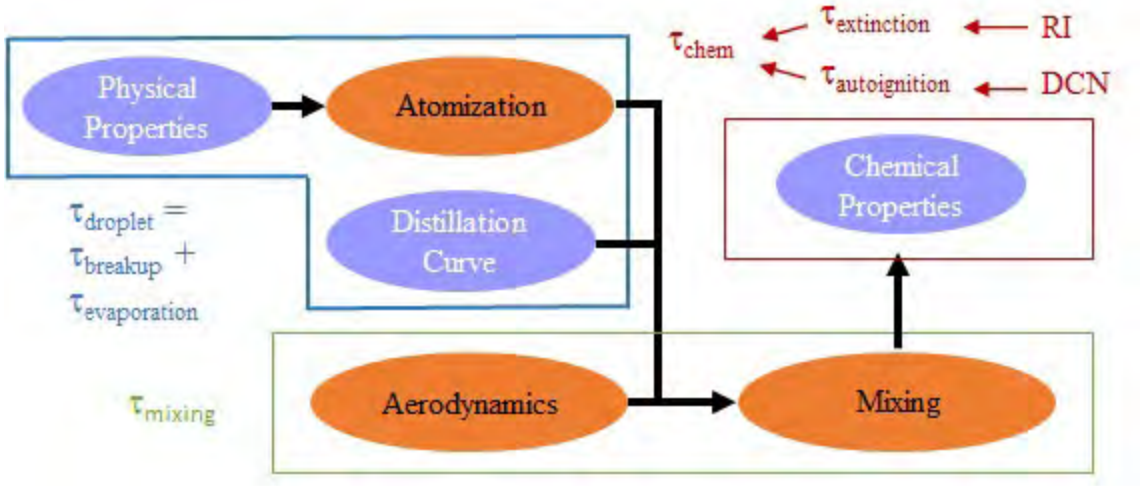

Figure 5. Available lean blowout pathways. Orange ovals represent combustor-specific characteristics and purple ovals show any fuel-dependent properties that can impact lean blowout limits.

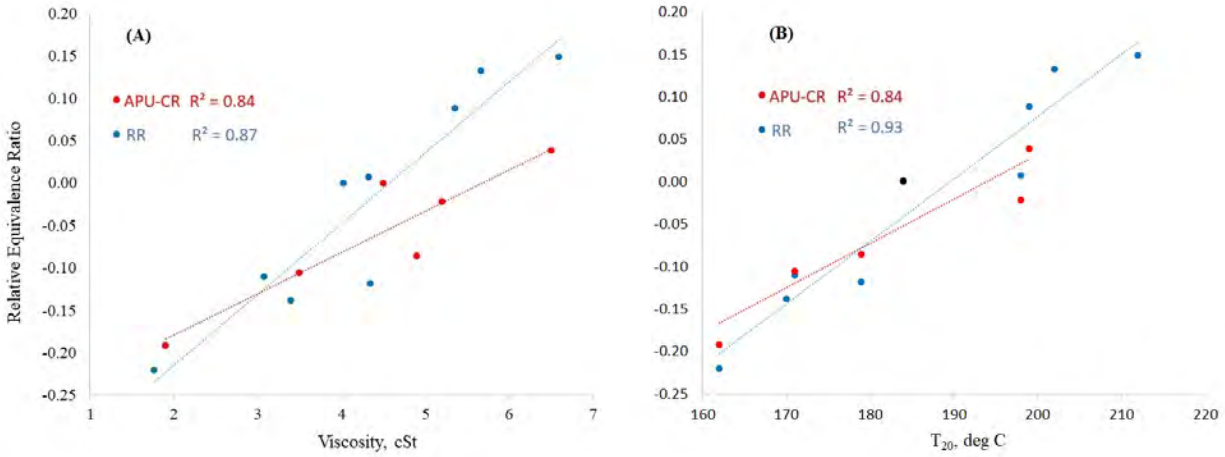

Figure 6. APU combustor rig (APU-CR) and Referee Rig (RR) LBO performance correlation with (a) viscosity (ν) and (b) 20% recovered temperature (T_{20}). Data is from Colborn et al. [OBJ].

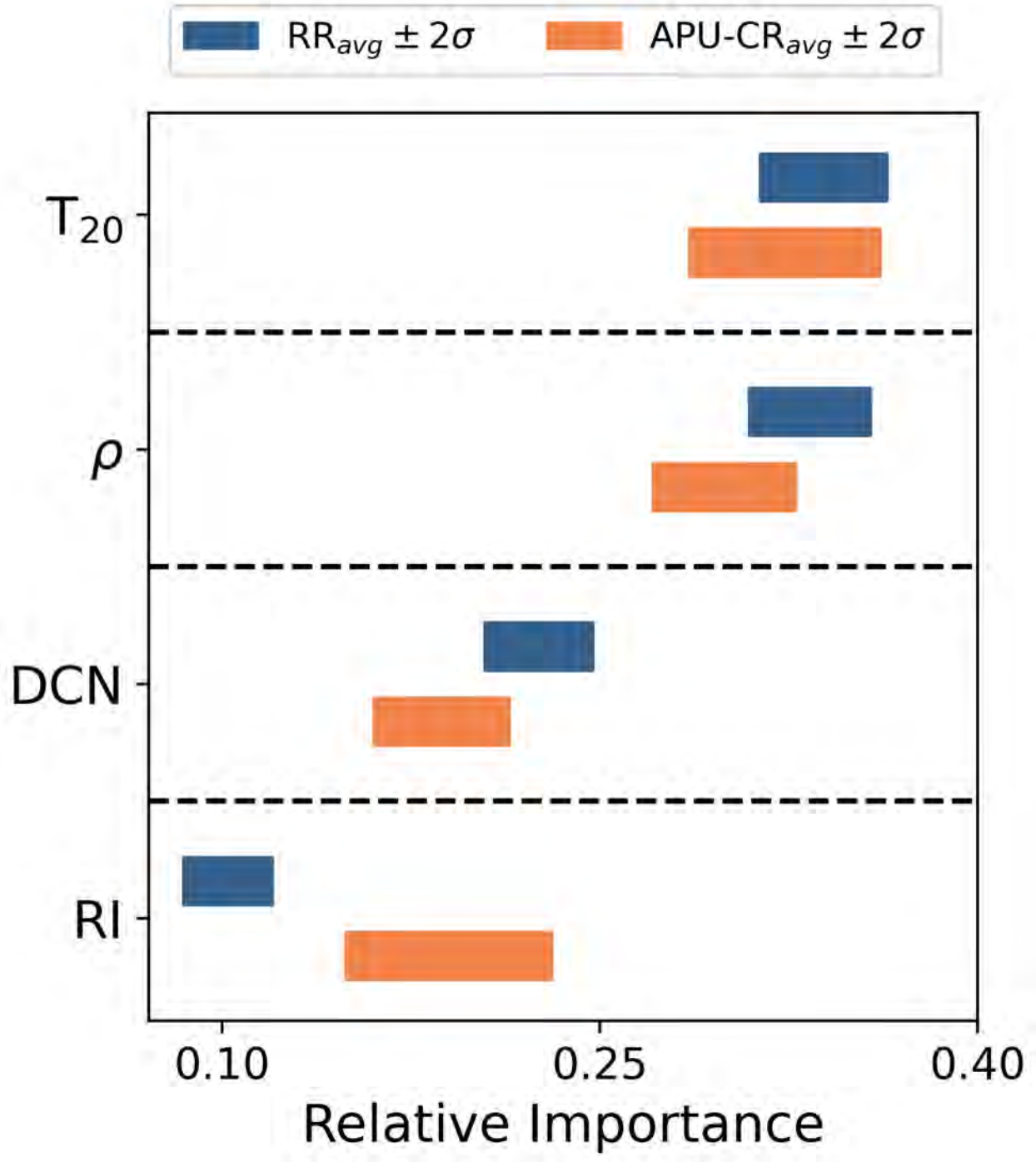

Figure 7. LBO determinants importance values for the RR at cold conditions and the APU-CR at normal operating conditions. On average, 98.6% of the LBO performance variance in the RR is explained by the chosen independent variables, while 91.8% of the LBO performance variance in the APU-CR is explained. Abbreviations: T20, 20% recovered temperature; ρ, density; DCN, derived cetane number; RI, radical index.

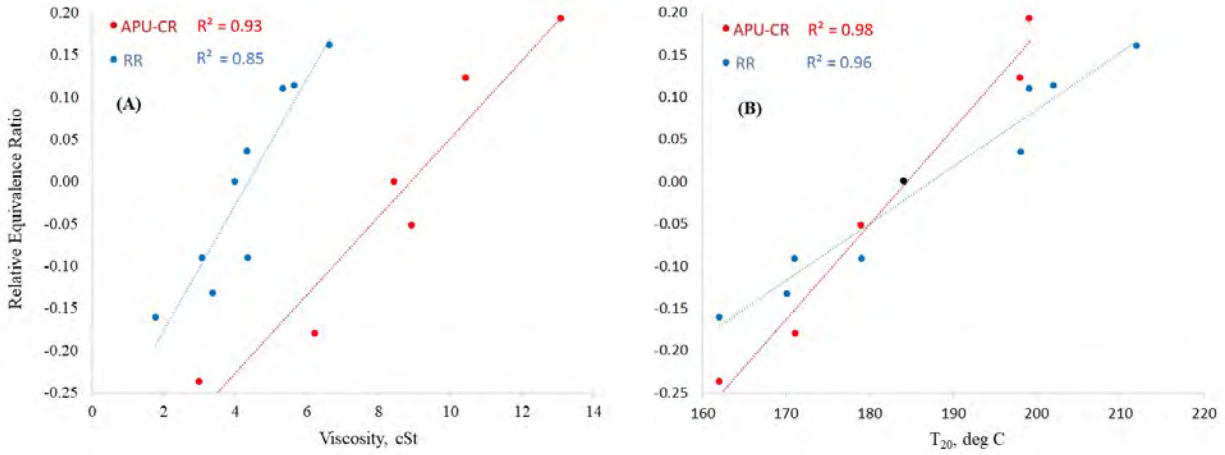

Figure 8. RR and APU-CR ignition equivalence ratio as a function of (a) Viscosity and (b) 20% recovered temperature (T_{20}). Data is from Hendershot et al. [5].

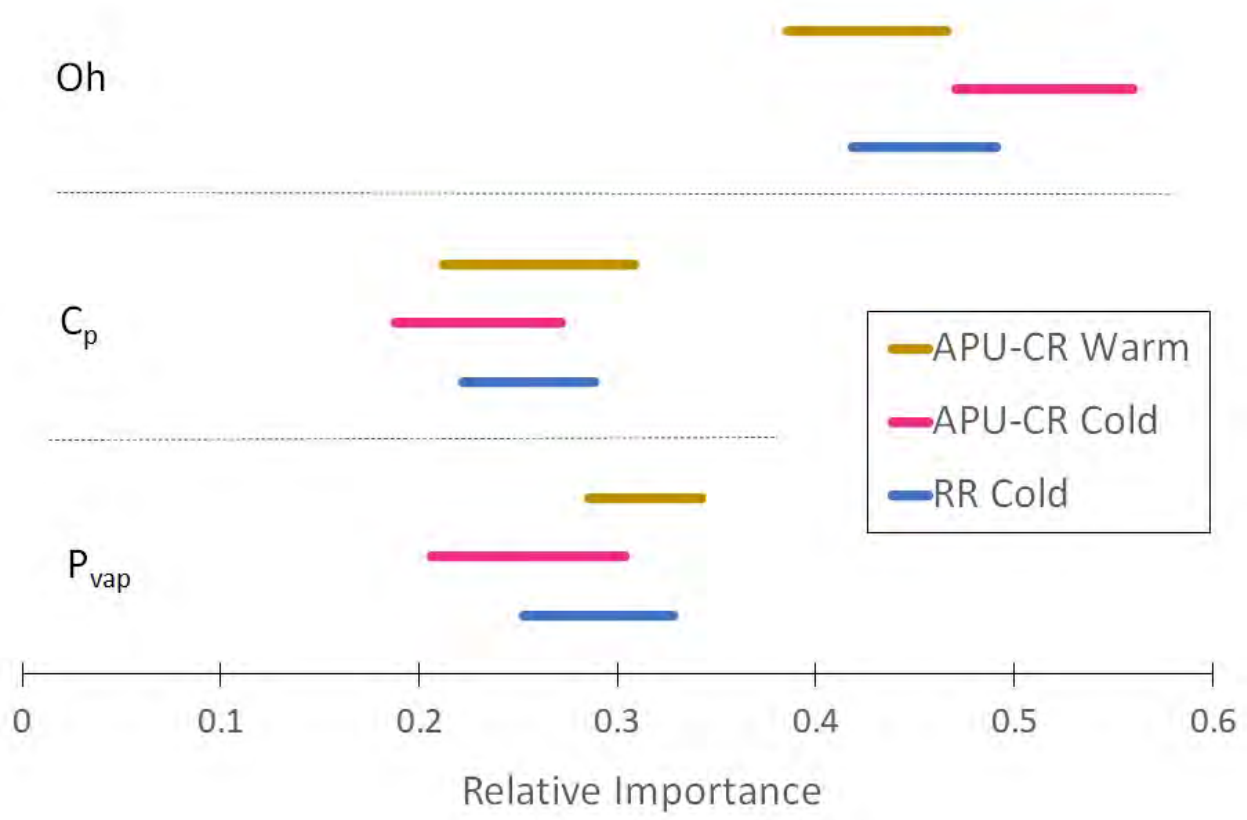

Figure 9. Ignition equivalence ratio determinants importance values for the RR at cold conditions and the APU-CR at both cold and warm conditions. On average, 89% of the ignition performance variance in the RR is explained by the chosen independent variables, 91% of the ignition performance variance in the APU-CR at cold conditions is explained, and 87% of the ignition performance variance in the APU-CR at warm conditions is explained.

Table 1. Operating conditions for the APU combustor rig (APU-CR) and Referee Rig (RR).

Rig	Operating Condition	Fuel Temperature [°C]	Air Temperature [°C]	Pressure [atm]	$\Delta P/P_{cmb}$ [%]
RR	Cold Lean Blowout [7]	-34, -15	-34, -15	1.02	2%
	Cold Start [5]	-34, -15	-34, -15	1.02	2%, 3.5%
APU-CR	Lean Blowout [22]	15	51 to 314	1.0, to 5.7	
	Cold Ignition [22]	-37	-44, -35, 15	1.05, 0.2, 0.3	
	Warm Ignition [22]	15	-38, 15	1.05, 0.2	

Table 2. Properties of fuels used in GE9X-FAR testing

Property	Jet A	C1	HFP-HEFA / Jet A1	HEFA / HDO-SAK
Density@15.6C (g/ml)	0.809	0.758	0.786	0.789
LHV (MJ/kg)	43.3	44.0	43.4	43.2
Hydrogen (wt%)	13.91	15.25	14.23	13.90
Viscosity@37.8C (cSt)	1.49	1.53	1.16	1.21
Viscosity@-20C (cSt)	5.02	4.99	3.15	
Viscosity@15.6C (cSt)		2.41 (curve fit)		1.66
DCN	~48	17.1		

Milestone(s)

- Determined alternative jet fuel dependencies between combustors of different sizes and mixing approaches.

Major Accomplishments

- Reported the alternative jet fuel dependencies between combustors of different sizes and mixing approaches.

Publications

Peer-reviewed journal publications

Boehm, R.C., Colborn, J. G., & Heyne, J. S. (2021). Comparing alternative jet fuel dependencies between combustors of different size and mixing approaches. Frontiers in Energy Research, *13*. https://doi.org/10.3389/FENRG.2021.701901.

Student Involvement

Jen Colborn, graduate student research assistant, led this effort.